**DYFP**

**2022**

**18th International Conference on Deformation, Yield and Fracture of Polymers, April 10 to 14, 2022. Rolduc Abbey, Kerkrade, NL**

# Book of Abstracts

Edited by: A.R. Studart & L.E. Govaert

# DYFP2022, the 18th International Conference on Deformation, Yield and Fracture of Polymers

## April 10 –14, 2022
## Rolduc Abbey, Kerkrade, the Netherlands

Welcome to the 18th edition of the International Conference on Deformation, Yield and Fracture of Polymers. This is a conference that has a tradition dating back more than 50 years to an origin at Churchill College in Cambridge, UK. In 2006 the conference changed venues to Rolduc Abbey in Kerkrade, NL.  The conference is internationally regarded as one of the mayor events related to the mechanics of polymeric materials and we have a long tradition of mixing young with old presenters, oral with poster presentations and technical excellence with a great venue so that the participants can get to know each other more casually outside of the lecture hall.

With the 2021 edition postponed as a result of the world-wide COVID pandemic, we are very pleased that it was finally possible to organize a live DYFP-event again with over 120 delegates attending. The Pandemic left its scars, as many overseas colleagues will not be able to attend due to various regulations.

We are proud to present a program that includes 19 invited speakers, in a hybrid online/live set-up, allowing colleagues who cannot attend live to be present as well. Of course, the program is greatly strengthened by the contributed talks and the large poster sessions.  The International Advisory Committee provided great input to the program and their interests and sense of important fields in polymer mechanics is very diverse as shown by the session topics:

- *Molecular Modelling*
- *Soft Matter & Rubbers*
- *Additive Manufacturing*
- *Fracture & Toughness*
- *Physics of Polymer Glasses*
- *Biological & Bioinspired*
- *Fatigue & Durability*
- *Surface, Contact & Adhesion*
- *Structure Development & related Properties*

We are looking forward to this 2022 edition of the DYFP conference and are enthusiastic about the conference and anticipate enthusiastically the chance to meet the new and the old as well as to seeing exciting new results from both.

André Studart and Leon Govaert

**Organizing Committee of DYFP2022:**

Program Chair : André Studart
Organising Chair : Leon E. Govaert
Co-Chair : Tom A.P. Engels
Treasurer : Ans van der Pasch
Technique : Leo H.G. Wouters
Secretariat : Alice J.J.T. van Litsenburg

Secretariat DYFP2022:
Materials Technology Group,
Eindhoven University of Technology
Gem-Z, 4.139, P.O. Box 513, NL-5600 MB Eindhoven,
The Netherlands

Phone:    +31 40 2472851
Fax:       +31 40 2447355
Email:    dyfp-conferences@tue.nl
Web:      www.DYFP-Conferences.org

**International Scientific Committee of DYFP2022:**

A.J. Crosby (UMass, US)
A.J. Lesser (UMass, US)
R.A. Pearson (Lehigh, USA)
S. Castagnet (Pprime, FR)
C. Creton (Paris, FR)
L. Laiarinandrasana (Mines Paris Tech, FR)
D. Long (CNRS, FR)
J.P. Gong (Hokkaido, JP)
T.A. Tervoort (ETHZ, CH)
T. Peijs (Warwick, UK)
G. Cross (TCD, IE)
D.N. Theodorou (Athens, GR)
C. Marano (Polimi, IT)
Liangbin Li (USTC, CN)

**18th International Conference on Deformation, Yield and Fracture of Polymers**
April 10-14, 2022 Rolduc Abbey, Kerkrade, NL

**Sunday April 10, 2022**

16.00          Registration open

18.00          Welcome reception & buffet

**Monday April 11, 2022**

08.30          Registration open

10.00          Welcome by André Studart and Leon Govaert

page

| 15.15 | *Mapping deformation and dissipation during fracture of soft viscoelastic hydrogel* | 13 |
| | Rong Long (Invited, USA) *(hybrid)* | |

| 15.40 | Tea | |

**Session 3:** **Additive Manufacturing**
Chair: Lambert van Breemen (NL)

| 16.10 | *Epoxy-based core-shell hybrid materials and low-density foams via material extrusion additive manufacturing* | 14 |
| | Brett Compton (Invited, USA) | |

| 16.35 | *Advances in light-assisted volumetric additive manufacturing* | 15 |
| | Antoine Boniface (Invited, CH) | |

| 17.00 | *Aligning molecular and structural dynamics in additive manufacturing by molecular engineering; towards enhanced thermoplastic weld mechanics and geometrical stability* | 16 |
| | Jules Harings (NL) | |

| 17.25 | *Experimental investigation and material modelling of the photopolymers for DLP additive manufacturing process* | 17 |
| | Kubra Sekmen (FR) | |

| 17.50 | End of oral session | |

| 18.00 | Happy hour | |

| 19.15 | Dinner | |

| 21.00 | Poster session I | |
| | *Wine & cheese for the poster session are kindly sponsored by Sabic* | |

**Tuesday April 12, 2022**

**Session 4:** **Physics of Polymer Glasses**
Chair: Clive Siviour (UK)

| 09.00 | *Non-linear Viscoelastic Response of Polymer Glasses: From Holeburning to LAOS* | 18 |
| | Greg McKenna (Invited, USA) | |

| 09.25 | *The Toughness of a Single Weld Formed by Fused Filament Fabrication* | 22 |
| | Vicky Nguyen (Invited, USA) | |

| 09.50 | *Evidence of large densification of polymer glass under combined high pressure and shear flow* | 23 |
| | Graham Cross (IE) | |

| 10.15 | *Plasticity of glassy polymers at the mesoscale: implementation of a finite element model based on shear transformation zone dynamics* | 24 |
| | Frederik Van Loock (NL) | |

| 10.40 | Coffee | |

| 11.10 | *Modelling the tensile deformation and yielding of amorphous glassy polymers using "TS2-SL" theory* | 25 |
| | Valeriy Ginzburg (USA) | |

| 11.35 | *Elasticity, plasticity and fracture toughness at ambient and cryogenic temperatures of epoxy systems used for the impregnation of high-field superconducting magnets* | 26 |
| | Andre Brem (CH) | |

| 12.00 | *Entanglements and mobility in ultrathin polymer film mechanics* | 27 |
| | Cynthia Bukowski (USA) *(hybrid)* | |

| 12.25 | Lunch | |

**Session 5:** **Fracture & Toughness**
Chair: Claudia Marano (IT)

| 14.00 | *How moving cracks in brittle solids choose their path …* | 28 |
| | Jay Fineberg (Invited, IL) | |

| 14.25 | *Nonlinear elastic effect on interacting crack paths in PDMS films* | 29 |
| | Loic Vanel (FR) | |

| 14.50 | *Embrittlement of Short Fiber Reinforced Thermoplastic Systems Under Multiaxial Loading Conditions* | 30 |
| | Martijn Wismans (NL) | |

| 15.15 | *Revisiting the fracture-mechanical behaviour of unfilled and filler reinforced elastomers by advanced experimental techniques* | 31 |
| | Eric Euchler (DE) | |

| 15.40 | Tea | |

| 16.10 | *Effect of temperature, time and molecular weight on the fracture behavior of soft thermoplastic elastomers* | 35 |
| | Simone Sbrescia (BE) | |

| 16.35 | *Microrheometric study of damage and rupture of capsules in simple shear flow* | 37 |
| | Chaymea El Mertahi (FR) | |

**Session 6:** **Biological & Bioinspired**
Chair: André Studart (CH)

| 17.00 | *Composites for sustainable development based on wood, wood fibers or nanocellulose fibrils – strain field data and mechanical properties* | 41 |
| | Lars Berglund (Invited, SE) | |

| 17.25 | *Embracing Complexity for Enduring and Adaptive, Organic Robots via Autonomous Materials* | 42 |
| | Robert Shepherd (Invited, USA) *(hybrid)* | |

| 17.50 | End of oral session | |

| 18.00 | Happy hour | |

| 19.15 | Dinner | |

| 21.00 | Poster session II | |
| | *Wine & cheese for the poster session are kindly sponsored by Sabic* | |

**Wednesday April 13, 2022**

**Thursday April 14, 2022**

**Poster Contributions – Session I – Monday April 11, 2022**　　　page

# Oral contributions

# Nonlinear mechanics of physically crosslinked polymer elastomers: from molecular simulations to network models

Amanda J. Parker[1) 2)] and Jörg Rottler [2)]

1) College of Engineering and Computer Science, Australian National University, Canberra ACT 2600, Australia

2) Department of Physics and Astronomy and Quantum Matter Institute, University of British Columbia, Vancouver BC V6T 1Z1, Canada

We present molecular simulations of uniaxial deformation of a generic model **triblock copolymer elastomer** that is physically crosslinked by microphase separation in order to elucidate microscopic mechanisms responsible for strain hardening and toughness. Our simulations show that triblocks exhibit significant increase of strain hardening compared to homopolymer elastomers. We analyze trends of several molecular parameters such as global chain deformation and local monomer motion, number and shape of spherical domains, and the evolution of the fraction of chains bridging between domains [1]. We then introduce an **entropic network model** that accounts for the distinct stress contributions arising from the physical crosslinks as well as entanglements by coupling analytical expressions for an entropic strain energy density directly with chain deformations obtained from the molecular dynamics simulations [2]. The model requires only one elastic modulus to describe both physically cross-linked triblock networks and uncrosslinked homopolymers. Our theory quantitatively reproduces the macroscopic stress response of simulated linear [2] and star [3] block copolymer elastomers well into the nonlinear regime. The simulations reveal the evolution of entanglements and how the breakup of physical crosslinks contributes to additional strain hardening.
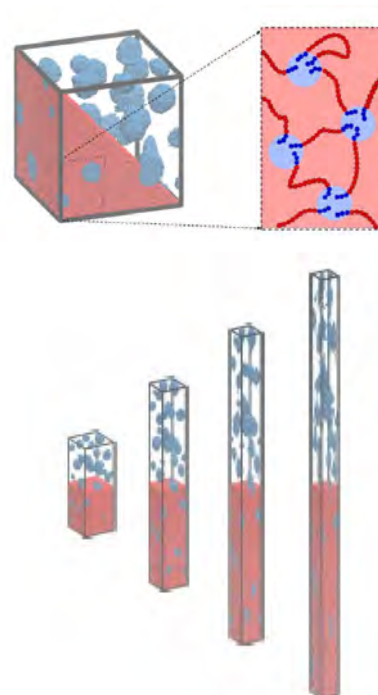


*Figure 1: Top: Linear sphere-forming ABA triblock copolymer, with glassy A domains physically crosslinking a rubbery B midblock. Bottom; simulation of uniaxial deformation.*

[1] A. J. Parker and J. Rottler, Molecular Mechanisms of Plastic Deformation in Sphere-Forming Thermoplastic Elastomers, Macromolecules 48, 8253 (2015).
[2] A. J. Parker and J. Rottler, Nonlinear Mechanics of triblock copolymer elastomers: from molecular simulations to network models, ACS Macro Letters 6, 786 (2017).
[3] A. J. Parker and J. Rottler, Entropic network models for Star Block Copolymer Thermoplastic Elastomers, Macromolecules 51, 10021 (2018).

# A Molecular Model for Creep in Oriented Polyethylene Fibers

## Prof. Thomas C. O'Connor

*Carnegie Mellon University | Materials Science & Engineering.*

Highly oriented and crystalline polyetheylene (PE) fibers have a large failure stress under rapid tensile loading but exhibit significant creep at much smaller stresses that limits their applications. The mechanisms of PE fiber creep have long been debated – with both chain scission and chain slip within crystals being considered. Our recent studies have identified a possible microscopic mechanism for chain slip and fiber creep due to stress-enhanced, thermally activated nucleation of dislocations at chain ends in crystalline regions. We observed 1D dislocations nucleation to be the strength-limiting failure mechanism of PE crystals in rapid tensile loading and the anticipate it to also be the dominate mechanisms of tensile creep.

In this study, we establish a microscopic theory for how chain slip mediated by dislocation nucleation at chain ends couples to macroscopic tensile loading in PE fibers. Molecular dynamics simulations are used to parameterize a Frenkel–Kontorova model that provides analytic expressions for the ultimate strength and activation energy for dislocation nucleation as a function of stress. Results from four commonly used hydrocarbon potentials are compared to show that the qualitative behavior of our model is robust and to estimate quantitative uncertainties. In all cases, the results can be described by an stress-activated Eyring model with values of the zero-stress activation energy $E_{0a} \approx 1.5$ eV and activation volume $V* \approx 45$ Å3 that are consistent with the experimental results for increasingly crystalline materials. The limiting yield stress is $\sim 8$ GPa.

Our results provide a first microscopic theory relating the molecular energy landscape of a polymer crystal directly to the macroscopic strength and stress-activated creep measured in fiber tensile tests. Our results suggest that activated dislocation nucleation at chain ends is an important mechanism of creep in highly oriented PE fibers, and our simple model provides a framework for developing microscopic theories for other crystalline polymers.

# Bond Orientation-Assisted Retractive Stress in Polymer glasses

Tingyu Xu, Liangbin Li

*National Synchrotron Radiation Lab, CAS Key Laboratory of Soft Matter Chemistry, University of Science and Technology of China, Hefei, China*
*Email: lbli@ustc.edu.cn*

After cold drawing and sufficient relaxation by storage below glass temperature Tg, the polymer glasses are shown to display considerable retractive stress when warmed up above the storage temperature but still below Tg. The emerging so-called "elastic yielding stress" is around one order of magnitude higher than that comes from entropic elasticity [1, 2]. With molecular dynamics simulation, current results show that four elements are necessary for the emergence of elastic yielding, including i) particles with high energy and ii) high mobility, iii) energy dissipation during annealing, and iv) bond orientation. Whilst intra-chain tension is demonstrated to not be the determinant origin of elastic yielding [3]. The retractive elastic yielding stress in pre-deformed polymer glasses can also emerge by oscillatory shear. During small-amplitude oscillatory shear, the emergent retractive stress decreases with the decrease of bond orientation. We propose a theoretical model to correlate elastic yielding stress with bond orientation parameter and dissipated energy, which is in a good agreement with the simulation results. The bond-orientation assisted retractive stress is also expected to play a crucial role in mechanical stress during deformation.

**References**

[1] Cheng S, Wang S Q. Elastic yielding in cold drawn polymer glasses well below the glass transition temperature[J]. Physical review letters, 2013, 110(6): 065506.
[2] Cheng S, Wang S Q. Elastic yielding after cold drawing of ductile polymer glasses[J]. Macromolecules, 2014, 47(11): 3661-3671.
[3] T. Xu, C. Nie, F. Peng, J. Sheng, L. Li. Bond Orientation-Assisted Retractive Stress in Polymer glasses: A Simulation Study on Elastic Yielding. (to be published)

# Molecular modeling of flow-induced crystallization of polypropylene

Nikolaos I. Sigalas[1] and Alexey V. Lyulin[1,2]

[1]*Soft Matter and Biological Physics, Department of Applied Physics, Technische Universiteit Eindhoven, 5600 MB, Eindhoven, The Netherlands.*
[2]*Center for Computational Energy Research, Department of Applied Physics, Technische Universiteit Eindhoven, 5600 MB, Eindhoven, The Netherlands.*

Understanding the mechanisms of crystallization of isotactic polypropylene (iPP) under flow is important for designing easily recyclable and efficient packaging products in the future. Current experiments cannot fully predict how the flow-induced crystallization (FIC) is affected by temperature and molecular-weight distribution. Molecular simulations can be used to provide useful insights on this phenomenon. To tackle the long spatial and temporal scales of crystallization, a mesoscopic model which captures the essential characteristics of iPP crystallization was developed. The model was developed for high temperatures above the melting point and at these temperatures statistical and structural properties were compared against experimental and simulation results.

## Introduction

Nowadays, in the modern circular economy, there is a trend towards designing easily recyclable and energy-efficient products. One growing segment of such products is the packaging industry. Polypropylene is widely used for this purpose and its performance in packaging applications is a strong function of its semicrystalline morphology that develops during processing.

In order to understand the crystallization mechanisms, we perform computer simulations of pure bulk isotactic polypropylene (iPP) at different temperatures and molecular weight distributions. A challenge is to span the large spatial and temporal scales govern iPP crystallization, from coil-helix transitions to lamella formation. For this reason, two strategies are employed: flow-induced crystallization and coarse-graining. Regarding the latter strategy, the coarse-grained models, where a number of atoms is considered as one interaction site, encode the key physics of systems studied and reduce drastically the computational time.

In the present manuscript, using the Single Chain Monte Carloand molecular dynamics (MD) techniques, we simulate one single iPP chain at the united-atom level at temperatures above melting and we use it as a reference to develop a new coarse-grained model for iPP. The key characteristic of the model is that it preserves the helical behavior of iPP and distinguishes the helices into right-handed (RH) and left-handed (LH).

## Simulated Models

For the development of a coarse-grained (CG) model for iPP, a united-atom (UA) single chain iPP of 2000 monomers was used as a reference. At the UA representation carbons and hydrogens are fused into one single atom (Figure 1a). At CG representation, a single interaction site comprises a methyl, a methine and two half methylenes groups that are shared between adjacent beads (Figure 1b). The center of the CG site is placed at the center of the mass of these groups. It is essential that both levels display a helical behavior (Figure c,d). The UA single chain was created using MAPS [1] and simulated using the Single Chain Monte Carlo algorithm [2] at 500K. Then it was mapped from the UA to the CG level and all the bonded and non-bonded interactions were extracted for the CG model.

The Single Chain Monte Carlo [2] is a fast and efficient algorithm which samples a single unperturbed chain (**Figure 2b**) and produces representative results for the whole polymer. This is feasible based on Flory's random coil hypothesis [3] which suggests that a chain in a melt behave as if it is subject to local interactions only. Commonly, in a full melt simulation (**Figure 2a**), non-bonded interactions would be calculated for atoms both along the same chain (intramolecular) and between different chains (intermolecular). For the purpose of sampling single unperturbed chain conformations

representative of the melt, non local intramolecular interactions between topologically distant segments and all intermolecular interactions can be omitted and only local interactions are taken into account.
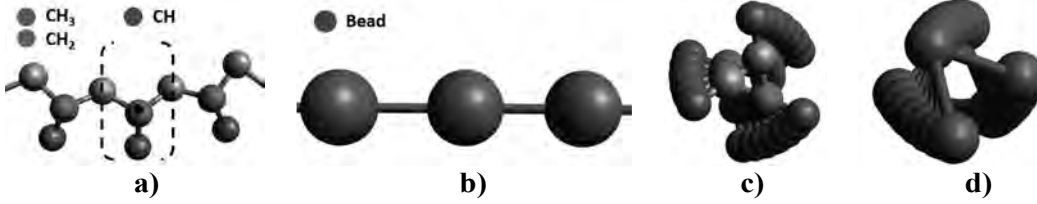


**Figure 1.** All-trans configuration of iPP **a)** at the united-atom level and **b)** at the coarse-grained level. Right-handed helical configuration of iPP **c)** at the united-atom level and **d)** at the coarse-grained level. The center of mass of the iPP monomer parts which comprise a coarse-grained bead (dashed line) is indicated by a black dot in **a)**.
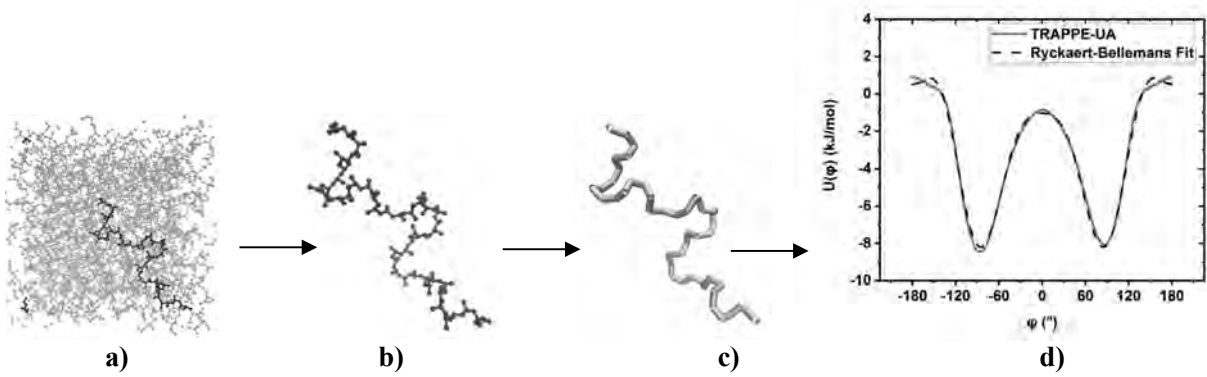


**Figure 2: a)** An iPP melt at the UA level. A single iPP chain is highlighted with blue color **b)** A single UA iPP chain. This representation can serve as input for single unperturbed chain MC simulations **c)** A single CG iPP chain produced by mapping the single UA iPP chain. From this representation the interactions for the new CG force field can be extracted. **d)** Dihedral effective potential $U(\varphi)$ vs CG effective dihedral angles. The red curve represents the mapped CG trajectory from TraPPE-UA [4]. A Ryckaert-Bellemans function was fitted to the potential of mean force $U(\varphi)$, and is shown by the black dashed curve.

## Results and Discussion

A UA single chain of 2000 iPP monomers was simulated using Single Chain Monte Carlo at 500K for $10^9$ steps with TraPPE-UA force field [4]. TraPPE-UA force field has been extensively used in melt [5] and crystallization [6] simulations of iPP. A sequence of different UA configurations (Figure 2b) was produced and then mapped at the CG level (Figure 2c). From this CG trajectory, the probability distributions $P(l)$, $P(\theta)$ and $P(\varphi)$ for the CG bond length $l$, bending angle $\theta$ and dihedral angle $\varphi$, respectively, were extracted and, subsequently, were converted to the corresponding potential energy $U$ using $U = -RT\ln(cP)$. Here, we present the coarse-graining scheme for the dihedral interactions which is the essential part of the force field for capturing the helical behavior. In Figure 2d, the red curve represents the dihedral potential energy $U(\varphi)$ extracted from the mapped CG trajectory from TraPPE-UA force field [4]. A Ryckaert-Bellemans function $U(\varphi) = \sum_{n=0}^{5} a_n (\cos\varphi)^n$ was fitted (black dashed curved), where $a_n$ is a constant. It should be noted that each potential well in Figure 2d, corresponds to different handedness, either LH or RH. The new CG force field comprises effective stretching, bending, torsional and non-bonded interactions. For the stretching interactions a harmonic potential was used, for the bending interactions a restricted bending potential [7], while non-bonded interactions were parametrized by using a geometrical approximation. The new CG potential was named HELIPP for HELical Isotactic Polypropylene Potential.

For the validation of HELIPP at high temperatures, a single unperturbed CG chain of 2000 chemical monomers was simulated with HELIPP by Single Chain Monte Carlo for $10^9$ steps. The characteristic ratio $C_n$

with respect to the number of real chemical bonds $N_b$ is plotted in Figure 3a. It is obvious that $C_n$ has clearly reached a plateau value for Nb > 3000. The plateau value of $C_n$ calculated by HELIPP equals 5.7, slightly lower than the value measured using TraPPE-UA (6.4). By performing single chain MC simulation using the existing MARTINI force field [8], the estimate was 8.9. So, HELIPP reproduces better the stiffness of the iPP chain than the existing MARTINI CG model and yields a characteristic ratio comparable to the experimental results [9]. All the simulations of the characteristic ratio were carried out at 500 K, while the reference temperature for the experimental measurements was 463 K .



a)                                        b)
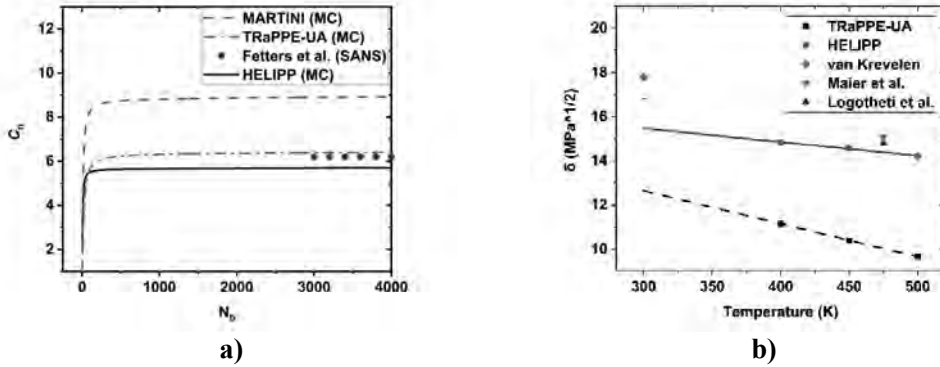
**Figure 3. a)** The characteristic ratio $C_n$ vs the number $N_b$ of real chemical backbone bonds from Monte Carlo simulations for a single chain of 2000  monomers on both UA and CG levels at 500K. At the UA level the TRaPPE-UA [4] was used, plotted with a red dash-dot line, while at the CG level the new HELIPP potential was used, plotted with black line. Results obtained with the existing MARTINI force field [8] at 500 K are also shown as a green dashed line. Experimental values [9] at 463K are shown with the blue dots. **b)** The solubility parameter plotted at different temperatures for an iPP of 40 chains of 50 monomers per chain. The solubility was calculated both at the UA level with TRaPPE-UA (black square) and at the CG level with HELIPP (green dot) using molecular-dynamics simulations. The experimental values obtained from Maier et al. [14] and from van Krevelen [15] are plotted with a magenta inverse triangle and a red rhombus, respectively, while atomistic simulation results obtained by Logotheti et al. [5]  are plotted with a blue triangle.

Furthermore, we performed molecular dynamics simulations of a CG melt of 40 chains of various chain lengths  (50,500,1000 monomers per chain). The density was measured as 730 kg/m$^3$, in good agreement with experimental results (710-674 kg/m$^3$) [10]. Subsequently, the entanglement molecular weight $M_e$ was calculated using the CReTA algorithm [11]. $M_e$ was computed equal to 4.432±121g/mol, whereas in experiments carried out for iPP melt,  Me was estimated between 5.100-5.500 g/mol [12].

Finally, we have calculated the cohesive energy of the iPP melt which can be expressed by the Hildebrand solubility parameter $\delta$ [13]. The temperature dependence of the solubility parameter is plotted in Figure 4b. It can be seen that at T = 475 K, $\delta$ = 14.2 MPa$^{1/2}$ obtained from HELIPP and $\delta$ = 10 MPa$^{1/2}$ from TRaPPE-UA force field. Comparing with other experimental  ($\delta$ = 15.2 MPa$^{1/2}$) [14] and simulation data ($\delta$ = 14.8 MPa1/2) [4] at T = 475 K, HELIPP seems to reproduce the solubility parameter much better than TRaPPE-UA. At T = 298K, the experimental value [15] varies from 16.8 to 18.8 MPa$^{1/2}$, while the present estimation with HELIPP is 15.5 MPa$^{1/2}$ showing a larger deviation at this temperature.

To show the potential of HELIPP to be used on crystallization, a system of 20 chains of 1000 CG monomers each was simulated with non-equilibrium MD. Specifically, it was cooled down from 500K to 380K, then stretched at the same temperature to 5 times its initial length and annealed isothermally at 380K. The formation of lamellae can be seen in Figure 4.
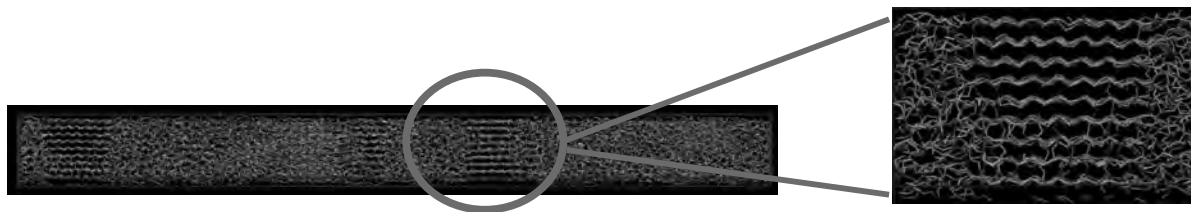
**Figure 4.** A lamella snapshot of a CG system of 20 chains of 1000 CG monomers each using the HELIPP after a stretch-induced crystallization simulation.

## Conclusions

- HELIPP reproduces  structural properties at high temperatures sufficiently well and most importantly is able to capture the different handedness of the iPP helices

- A new coarse-graining method is proposed by employing the single chain Monte Carlo algorithm

- HELIPP can be extended to study crystallization

- HELIPP performs 40 times faster than a typical UA force field

## References
[1]     D. N. Theodorou, U. W. Suter, *Macromolecules*, 2002, **18(7)**, 1467-1478.
[2]     P. N. Tzounis, S. D. Anogiannakis,  D. N. Theodorou, *Macromolecules*, 2017, **50(11),** 4575-4587.
[3]     P. J. Flory, *Principles of Polymer Chemistry*, (Ithaka, NY), 1953.
[4]     M. G. Martin, J. I. Siepman, *J. Phys. Chem.*, 1999, **103(21)**, 4508-4517.
[5]     E. G. Logotheti, D. N. Theodorou, *Macromolecules*, 2007, **40(6)**, 2235-2245,
[6]     T. Yamamoto,  Macromolecules, 2014, 9, 3192-3202
[7]     M. Bulacu, N. Goga, W. Zhao, G. Rossi, L. Monticelli, X. Periole, D. P.Tieleman, S. J. Marrink, *J. Chem. Theory Comput.*, 2013, **9(8)**, 3282-3292.
[8]     E. Panizon, D. Bochicchio, L. Monticelli, G. Rossi, *J. Phys.Chem. B*, 2015, **119(25)**, 8209-8216.
[9]     J. L. Fetters, D. J. Lohse, A. G. F. César, P. Brant,  D. Richter, *Macromolecules*, 2002, **35(27)**, 10096-10101.
[10]   H. M. Freischmidt, R. A. Shanks, G. Moad, A. Uhlherr,  *J. Pol. Sc., B, Pol. Phys.*, 2001, **39(16)**,1803-1814.
[11]   C. Tzoumanekas, D. N. Theodorou, Macromolecules, 2006, **39(13)**, 4592-4604.
[12]   A. Eckstein, J. Suhm, C. Friedrich, R. D. Maier, J. Sassmannshausen, M. Bochmann, R. Mülhaupt, *Macromolecules*, 1998, **31(4)**,1335-1340.
[13]   M. Belmares, M. Blanco, W. A. Goddard, R. B. Ross, G. Caldwell, S. Chou, J. Pham, P. M. Olofson, C. Thomas, *J. Comp. Chem.*, 2004, **25(15)**, 1814-1826.
[14]   R. D. Maier, R. Thomann, J. Kressler, R. Mulhaupt, B. Rudolf, *J. Pol. Sc., B, Pol. Phys.*, 1997, **35**, 1135-1144.
[15]   D. W. Van Krevelen, K Te Nijenhuis. *Chapter 1 - Polymer Properties. Properties of Polymers*, 4th Edition, 2009.

# Crazing reveals an entanglement network in glassy ring polymers

Jiuling Wang and Ting Ge[*]

*Department of Chemistry and Biochemistry, University of South Carolina,
Columbia, South Carolina 29208, USA*

[*]*Email: tingg@mailbox.sc.edu*

Molecular simulations [1] are used to show that an entanglement network exists in non-concatenated ring polymers of sufficiently long contour length when they are cooled down well below the glass transition temperature. The entanglement network consists of only a fraction of the topological constraints that force ring polymers to be in self-similar globular conformations [2]. The entanglement network can support stable craze formation in ring polymer glass under tensile loading. The structural features of the ring polymer craze and the drawing stress during the craze formation are related to the underlying entanglement network by generalizing traditional models for the crazing in linear polymer glass. The computer simulations and theoretical analysis demonstrate tuning polymer topology as a promising way to manipulate the mechanical properties of traditional plastic materials.

**References**
[1] Wang, J.; Ge, T., *Macromolecules* **2021**, *54*, 7500-7511.
[2] Ge, T.; Panyukov, S; Rubinstein, M., *Macromolecules* **2016**, *49*, 708-722.

# Mapping and quantifying covalent bond scission during fracture of elastomers with mechanosensitive molecules

Juliette Slootman, C. Josh Yeh, Victoria Waltz, Matteo Ciccotti, Jean Comtet and <u>Costantino Creton</u>

*Laboratoire SIMM, ESPCI Paris, PSL University, CNRS, Sorbonne Université, Paris - F*

Elastomers find many applications in the engineering and biomedical field for their ability to stretch reversibly to large deformations. Yet their maximum extensibility is limited by the occurrence of fracture which is currently still poorly understood. Due to a lack of experimental evidence, current physical models of elastomer fracture describe the rate and temperature dependence of the fracture energy as being solely due to viscoelastic friction in the bulk, with chemical bond scission at the crack tip contained in the fracture plane and assumed to remain independent of strain rate.

By coupling new fluorogenic mechanochemistry with quantitative confocal microscopy mapping, we are for the first time able to quantitatively detect, with high spatial resolution and sensitivity, the scission of covalent bond as ordinary elastomers fracture at different strain rates and temperatures[1]. Our measurements reveal that in simple networks, bond scission, far from being restricted to a constant level near the crack plane, can be both delocalized over up to hundreds of micrometers and increase by a factor of 100, depending on temperature and stretch rate.

Because of that, simple unfilled elastomers suffer from poor fracture resistance at high temperature where viscoelastic dissipation is low. A recently introduced molecular design based on multiple interpenetrating networks composed of a brittle filler network isotropically prestretched to a value $\lambda_0$ by swelling it in an extensible matrix leads to a dramatic increase of fracture energy $\Gamma_c$ relative to simple elastomers and this is particularly true at high temperature where viscoelasticity is low. This toughening is typically attributed to sacrificial bond scission creating a dissipative damage zone ahead of the propagating crack[2, 3].

However, the molecular mechanisms controlling the *size* of the damage zone when the crack propagates and the relation between damage and fracture energy for this new class of materials are currently unknown. We fractured samples with variable degrees of prestretch $\lambda_0$ at different stretch rates and temperatures and used the same fluorogenic mechanochemistry combined with quantitative confocal mapping and mechanical testing to characterize both $\Gamma_c$, and the extent of bond scission occurring in the sacrificial network by post-mortem observations near the fracture surfaces.[4]

We find that increasing the prestretch of the filler network leads to a higher increase in $\Gamma_c$ coupled. We show also that, while qualitatively larger concentration of bond scission in the bulk of the elastomer lead to a higher value of $\Gamma_c$, there is no direct linear relation between the extent of bond scission in the filler network and $\Gamma_c$ .

We propose that the large increase in $\Gamma_c$ is due to the dilution of highly stretched strands in the entangled and unstretched matrix, which effectively delocalizes stress redistribution upon bond scission, and protects the neighboring covalent bonds of the matrix network from scission in a way that a composite material does. This mechanism protects the material from crack growth by avoiding localization of bond scission at the crack tip.

## Conclusions

In summary we draw two main conclusions from these observations, permitted by the high fluorescence and stability of the mechanophore:

There is an intricated coupling between strain rate dependent viscous dissipation and strain dependent irreversible network scission which paint an entirely novel picture of fracture in soft materials, where energy dissipated by covalent bond scission accounts for a much larger fraction of the total fracture energy than previously believed.

Delaying the localization of bond scission by the interpenetrated network design is a promising strategy to toughen elastomers even in the absence of viscoelastic dissipation.

More generally these results point to the fundamental difference between strain rate dependent dissipation (due to molecular friction) and strain-dependent dissipation (due to force-triggered catastrophic and fast molecular reaction).

## References

[1] J. Slootman, V. Waltz, C.J. Yeh, C. Baumann, R. Göstl, J. Comtet, C. Creton, Quantifying Rate- and Temperature-Dependent Molecular Damage in Elastomer Fracture, Physical Review X 10(4) (2020) 041045.
[2] P. Millereau, E. Ducrot, J.M. Clough, M.E. Wiseman, H.R. Brown, R.P. Sijbesma, C. Creton, Mechanics of elastomeric molecular composites, Proceedings of the National Academy of Sciences 115(37) (2018) 9110-9115.
[3] E. Ducrot, Y. Chen, M. Bulters, R.P. Sijbesma, C. Creton, Toughening Elastomers with Sacrificial Bonds and Watching them Break, Science 344(6180) (2014) 186-189.
[4] J. Slootman, C. J. Yeh, P. Millereau, J. Comtet, C. Creton, A molecular interpretation of the toughness of multiple network elastomers at high temperature, PNAS, in press (2022)

# Macroscale Double Networks: From the Molecular- to Macro-scale

D. R. King,[1] T. Okumura,[2] J. P. Gong[3]

1. Faculty of Advanced Life Science, Hokkaido University; dking@sci.hokudai.ac.jp
2. Graduate School of Life Science, Hokkaido University; okumura.t@sci.hokudai.ac.jp
3. Faculty of Advanced Life Science and WPI-ICReDD, Hokkaido, University; gong@sci.hokudai.ac.jp

The double network concept has been revolutionary in its ability to turn soft, brittle hydrogels into tough, robust materials.[1] Double network hydrogels consist of two interpenetrating networks, where each network has a specific mechanical response: the "first network" acts as a sacrificial network, consisting of a rigid, extended network with relatively low loading percentage, and the "second network" is a globally percolated, stretchable network. When a double network hydrogel is stretched, covalent, "sacrificial bonds" of the first network break, dissipating energy. Here, we attempt to utilize the essence of this structure at the macroscale, by creating rigid skeletons and embedding them in a stretchy and tough matrix, mimicking the first and second networks, respectively. The goal of this research is to demonstrate that the "double network concept" is applicable at length-scales beyond the molecular scale, which we have termed "Macro-DN". Furthermore, we aim to outline the required properties necessary to optimize the properties of these composites.

We demonstrate the Macro-DN concept using a simple system comprised of a 3D printed plastic grid in a rubber matrix. First, we examine the fracture process of the Macro-DN composites with a rectangular-mesh style skeleton, containing rigid crossbars (Figure 1).[2] During stretching, the grid quickly fractures in one section, and stretch is isolated to that section. When the force exceeds the fracture force of the grid, the grid breaks elsewhere, causing the matrix to relax, and the process repeats. This continues until all fracture regions are exhausted, and the matrix fails critically.

While this method increases the mechanical strength and toughness of soft materials, the increase is limited to about a ~50% increase in toughness, much



Figure 1. Force-stretch curves of a square-grid skeleton (purple), pristine silicone rubber (pink), and their composite (black). The insets (i)-(vii) represent snapshots of the composite sample at the corresponding stretch shown in the loading curves.

less than what is observed in DN gels. To improve upon this result, we have removed the rigid crossbars, to allow for lateral deformation. To maximize the biaxial stress on the matrix, we will incorporate skeletons containing functional structures.[3] We measure the Poisson's ratio of the skeletons, and determine that this value can be modified widely, resulting in composites that have significant Poisson's ratio mismatch between the skeleton and the matrix. Upon testing, we find that Poisson's ratio mismatch results in a significant increase in strength and toughness, especially in the small-strain limit. Because this technique requires only topological interlocking, it can be applied to wide-ranging materials systems.

Finally, we will consider the role of defects in DN systems. We will create simple models that incorporate defects into either the first or second network, or both, and measure the impact these defects have on the mechanical response. Ultimately, we clarify that a unique and important aspect of DN systems is their ability to ignore defects, which is what enables the huge increases in mechanical properties observed in DN gels.

## References

[1]     J. P. Gong, *Soft Matter* **2010**, *6*, 2583.
[2]     D. R. King, T. Okumura, R. Takahashi, T. Kurokawa, J. P. Gong, *ACS Appl. Mater. Interfaces* **2019**, *11*, 35343.
[3]     T. Okumura, R. Takahashi, K. Hagita, D. R. King, J. P. Gong, *Sci. Rep.* **2021**, *11*, 13280.

# Cavitation Mechanisms in Elastomers Exposed to Hydrogen: New insights brought by in-situ tomography and mechanochemistry

Xavier P. Morelle[1,4], Gabriel E. Sanoja[1], Jean Comtet[1], C. Creton[1],
Sylvie Castagnet[2], A. Nait-Ali [2], M. Fazal [2], D. Mellier [2], G. Benoit[2], Y. Pannier [2],
Mario Scheel[3], Timm Weitkamp[3]

[1] *SIMM (UMR CNRS 7615), ESPCI Paris Sciences et Lettres, Paris, France*
[2] *Institut Pprime (UPR 3346 CNRS, ISAE-ENSMA, Université de Poitiers), Poitiers, France*
[3] *Synchrotron SOLEIL, ligne Anatomix*
[4] *Laboratoire IMP (UMR CNRS 5223), Université de Lyon, INSA de Lyon, Villeurbanne, France*
***xavier.morelle@insa-lyon.fr***

## Abstract

Elastomers are used as seals in connecting hardware for gas transport. Upon saturation with a high-pressure gas followed by a fast release of pressure, small cavities may nucleate and inflate inside the elastomer, exhibiting bubbles that progressively disappear over-time, an issue that raises concern over their mechanical integrity and gas barrier properties. This phenomenon, referred to as explosive decompression [1], is one example of cavitation processes that are important for seals as they are well-known to damage elastomers [2, 3] and hamper their lifetime in use.

Cavitation-induced damage, and more generally internal damage in elastomers, is challenging to visualize [4] because elastic restoring forces and surface tension close cracks and flaws in the absence of a load. Moreover, the highly complex and discontinuous loading (coupling gas diffusion, mechanical deformation and fracture processes) endured by an elastomer during cavitation by explosive decompression does not facilitate neither a clear understanding of the mechanisms at play, nor the identification of the critical material parameters needed to improve cavitation resistance. This is essential for extending lifetime as well as in terms of safety for sensible use of seals in storage and transportation of flammable gases such as hydrogen.

Here, we combine the complementary results from two high-resolution techniques, *in situ* micro-tomography and *post mortem* confocal microscopy, to gain a better appraisal of the damage and fracture mechanisms occuring during such cavitation process. While synchrotron-based *in situ* X-ray tomography can provide time-resolved (~4$s$ time laps) and 3D information (~3$\mu m$ spatial resolution) on the kinetics and morphology of cavity growth and deflation; mechanochemistry (by incorporating mechanofluorescent damage probes in a model ethyl-acrylate elastomer network [5]) provides a novel methodology to thoroughly visualize (~1$\mu m$ resolution) the extent of remaining molecular (*i.e* bond-scission) damage in the undeformed configuration.

We examine cavities nucleated by rapid decompression of hydrogen-saturated both in commercial (EPDM) and tailor-made (ethyl-acrylate with different network architectures) elastomers and demonstrate that cavity expansion is an irreversible and multi-step fracture process. The combination of both visualization techniques not only allows to spatially resolve the complex internal damage, but also serves to demonstrate that cavity growth in elastomers occurs through the nucleation and subsequent propagation of randomly oriented and distributed penny-shape cracks [6]. Moreover, we show that cavitation-resistance can be significantly improved through multiple-network architecture and hypothesize that such property gain is related to their improved mode-I fracture toughness as well as their network strain-hardening capability at large stretches.

## References

[1] Gent, A.N. and D.A. Tompkins *Journal of applied physics* **1969**, 40 (6), p. 2520-2525.
[2] Yamabe, J., A. Koga, and S. Nishimura, *Engineering Failure Analysis* **2013**, 35, p. 193-205.
[3] Jaravel, J., et al., *Polymer Testing* **2011**, 30(8), p. 811-818.
[4] Barney, C.W., et al. *Proc Natl Acad Sci USA* **2020**, 117(17): p. 9157-9165.
[5] Slootman, J., Waltz, V., Yeh, C. J., Baumann, C., Göstl, R., Comtet, J., & Creton, C. *Physical Review X* **2020**, *10*(4), 041045.
[6] Morelle, X. P., Sanoja, G. E., Castagnet, S., & Creton, C. *Soft Matter* **2021**,17 (16), p. 4266-4274.

# Mapping deformation and dissipation during fracture of soft viscoelastic hydrogel

Yuan Qi[1,†], Xueyu Li[2,3,†], Sairam Pamulaparthi Venkata[4], Xingwei Yang[1], Tao Lin Sun[5], Chung-Yuen Hui[3,4], <u>Rong Long</u>[1,*], Jian Ping Gong[2,3,6,*]

[1]*Department of Mechanical Engineering, University of Colorado Boulder, Boulder, CO, 80309, USA*

[2]*Faculty of Advanced Life Science, Hokkaido University, Sapporo, 001-0021, Japan*
[3]*Soft Matter GI-CoRE, Hokkaido University, Sapporo 001-0021, Japan*

[4]*Field of Theoretical and Applied Mechanics, Sibley School of Mechanical and Aerospace Engineering, Cornell University, Ithaca, NY 14853, USA*

[5]*South China Advanced Institute for Soft Matter Science and Technology, South China University of Technology, Guangzhou, 510640, China*

[6]*Institute for Chemical Reaction Design and Discovery (WPI-ICReDD), Hokkaido University, Sapporo 001-0021, Japan*

[†]These authors contribute equally to this paper.
*Corresponding authors: Rong Long and Jian Ping Gong.
**Email:** rong.long@colorado.edu, gong@sci.hokudai.ac.jp

## Abstract

Energy dissipation around a propagating crack is the primary mechanism for the enhanced fracture toughness in viscoelastic solids. Such dissipation is spatially non-uniform and is highly coupled to the crack propagation process due to the history-dependent nature of viscoelasticity. Experimental characterization of the viscoelastic dissipation field during crack propagation has been challenging because of the highly amplified deformation around the crack tip. Here we present a method to measure the evolution of deformation fields in a soft viscoelastic hydrogel by tracking randomly distributed tracer particles. The dissipation field is determined by plugging the measured deformation field into a nonlinear constitutive model. The results enable us to separately determine the intrinsic and dissipative components of fracture toughness. Using this approach, we study an anomalous fracture behavior observed in experiments: under a fixed global stretch, the crack first propagates at a low speed and suddenly accelerated to a much higher speed, even in the absence of external energy input. The measured deformation fields reveal that the two stages do not satisfy the steady state condition often assumed in viscoelastic fracture theories. In addition, the two stages are found to share a similar intrinsic toughness, despite the over 30-fold difference in crack extension speed. These findings suggest that the two stages of crack propagation correspond to two branches of non-steady state solutions. More generally, going beyond steady state assumption opens new solution spaces for viscoelastic fracture, which are yet to be explored.

# Epoxy-based core-shell hybrid materials and low-density foams via material extrusion additive manufacturing

## Brett G. Compton

*Mechanical, Aerospace, and Biomedical Engineering Department*

*University of Tennessee, Knoxville*

*bcompto1@utk.edu*

Material extrusion additive manufacturing (AM) technologies – including fused filament fabrication (FFF) and direct ink writing (DIW) – present unique opportunities to create composites and multi-material hybrid architectures that cannot be made using other AM technologies. The direct deposition nature of these processes enable the straightforward deposition of multiple materials though the use of multiple single-material print heads, co-extrusion nozzles, or mixing print heads, while shear stresses in the fluid during the extrusion process can effectively align high aspect ratio filler materials like fibers, whiskers, and platelets, leading to unprecedented control over fiber orientation within a printed part.

Drawing inspiration from natural materials that exhibit elegant multi-material architectures to achieve high stiffness, strength, and buckling resistance with minimal mass, this talk will focus on the use of material extrusion AM to create new epoxy-based hybrid materials with novel core-shell motif. Exemplary materials include porcupine quills and sunflower stalks, both of which are comprised of cylindrical cores of low density foam surrounded by a stiff shell of denser material. In this motif, the stiffer material is positioned further from the neutral bending axis by the presence of the foam, thereby increasing the flexural rigidity of the structure compared to an equivalent mass of the denser stiff material alone. Utilizing similar approaches with 3D-printable materials would enable low relative density honeycombs and lattice materials with higher stiffness and greater resistance to elastic collapse than single-material lattices of comparable mass.

This talk will begin with a brief introduction to AM of thermoset polymer materials that are amenable to formulation with a wide range of structural and functional filler materials. Next, the core-shell coextrusion print head will be described and the core-shell architectural motif will be motivated with a simple mechanics model. For the low-density core material, an epoxy-based syntactic foam utilizing glass microballoons will be described and characterized. At approximately 58 volume percent loading of microballoons, density as low as 0.68 g/cc can be achieved. For the high-stiffness shell material, an epoxy-based composite reinforced with ultra-high modulus short carbon fibers will be described and characterized. Elastic modulus values above 20 GPa are achieved with this ink. The printing behavior and mechanical properties of printed core-shell hybrids will be investigated next, with complementary microstructural analysis via x-ray computed tomography and optical and scanning electron microscopy. The core-shell motif results in up to 20% increase in the specific flexural modulus over either of the constituent materials alone, while rupture of the glass microballoons during extrusion and core eccentricity are found to be the largest printing-related factors limiting mechanical performance. The talk will conclude with a brief discussion of future research directions including graded material transitions and opportunities in new material systems.

# Advances in light-assisted volumetric additive manufacturing

Antoine Boniface and Christophe Moser

*Laboratory of Applied Photonics Devices, EPFL, CH.*

3D printing has revolutionized the manufacturing of volumetric components and structures in many areas. Several fully volumetric light-based techniques have been recently developed thanks to the advent of photocurable resins, reaching print time of a few tens of seconds while keeping sub 100 micron resolution. We will review a variety of materials that have been reported by several groups including ours and that includes soft cell-loaded hydrogels, acrylates, glass, ceramics that have been fabricated with a 3D printer using tomographic projections of light patterns. This recently-developed technique, pioneered in our lab, consists of illuminating a volume of photo-responsive material with a set of light patterns from multiple angles. The cumulative light exposure results in a volumetric energy dose that is sufficient to solidify the material in the desired geometry. However, these new approaches only work with homogeneous and relatively transparent resins.

We will present in the last part of the talk, a method that takes into account light scattering in the resin prior to computing projection patterns. Using a tomographic volumetric printer, we experimentally demonstrate that implementation of this correction is critical when printing objects whose size exceeds the scattering mean free path.

# Aligning molecular and structural dynamics in additive manufacturing by molecular engineering; towards enhanced thermoplastic weld mechanics and geometrical stability

Varun Srinivas[1], Francesca Bertella[1], Catharina S.J. van Hooy-Corstjens[2], Sanjay Rastogi[1,3], Jules.A.W. Harings[1]

[1]*Aachen-Maastricht Institute for Biobased Materials, Maastricht University, P.O. Box 616, 6200 MD, Maastricht, The Netherlands (jules.harings@maastrichtuniversity.nl).* [2]*Zuyd University of Applied Sciences, P.O. Box 413, 6200 AK, Heerlen, The Netherlands,* [3]*King Abdullah University of Science and Technology, Thuwal 23955-6900, Kingdom of Saudi Arabia.*

The entangling of polymer molecules is the origin of the praised intrinsic mechanical properties attained under mild melt (re-)processing conditions, making thermoplastics the sustainable construction material of choice. However, in the emerging field of additive manufacturing (AM), mass adoption of thermoplastics lags behind. Upon temporarily and spatial heating into the liquid state, particles in Selective Laser Sintering (SLS) or filaments in Fused Deposition Modeling (FDM) fuse first in two dimensions and successively in the third dimension, additively realizing unprecedented geometrical freedom. To create mechanically robust weld interfaces, polymer molecules must homogeneously mix and entangle throughout the entire volume of the manufactured part. Low translational diffusivity of polymer molecules, insufficient molecular mixing and re-entangling across the weld interface prevents the expression of the intrinsic mechanical properties in the z-direction [1].

We propose "co-crystallization", specifically stereocomplex crystallization, to physico-mechanically anchoring polymer chains originating from either side of the weld interface across the interfacial region. Using polylactide as a model, we demonstrate that inadequate alignment of chemically controlled diffusion and crystallization time-scales with printing parameters are the cause of internal stresses, inferior mechanical properties, and short- and long-term distortion in geometry (warping) [2]. By means of controlled chemical design, here relative molar masses, enantiomeric purity and plasticization concepts, in alternating spatial positioning of enantiomerically opposite polylactides, and



*Figure 1: Storage modulus following interfacial stiffening by stereocomplexation (SC) and successive nucleation of homocrystallization (HC) visualized by POM and FTIR imaging.*

complementary analytical techniques such as DSC, DMA, tensile testing, rheometry, and FTIR- and synchrotron WAXD imaging, we will (i) highlight the alignment of time-scales from molecular, structural as well as processing perspective (Figure 1), and (ii) its technical implications on enhancing ultimate thermoplastic performance in AM of thermoplastics [3-4].

## References

[1] McIlroy, C.; Olmsted, P. D. *Polymer,* **2017**, *123*, 376–391.
[2] Srinivas, V.; Van Hooy – Corstjens, C.S.J.; Harings, J.A.W., *Polymer* **2018**, *142*, 348-355.
[3] Srinivas, V.; van Hooy-Corstjens, C. S. J.; Vaughan, G. B. M.; van Leeuwen, B.; Rastogi, S.; Harings, J. A. W. *ACS Applied Polymer Materials,* **2019**, *1* (8), 2131–2139.
[4] Srinivas, V.; Bertella, F.; Van Hooy-Corstjens, C.S.J.; Van Leeuwen, B.; Craenmehr, E.G.M.; Cavallo, D.; Rastogi, S.; Harings, J.A.W. *Additive Manufacturing* **2020**,*36*, 101655.

# Experimental investigation and material modelling of the photopolymers for DLP additive manufacturing process

Kubra Sekmen[1], Thomas Rehbein[2], Alexander Lion[2], Michael Johlitz[2], Andrei Constantinescu[1]

[1]*Laboratoire de Mécanique des Solides, CNRS, École Polytechnique, Institut Polytechnique de Paris, 91128 Palaiseau, France*
[2]*Department of Aerospace Engineering, Institute of Mechanics, Bundeswehr University Munich, Werner-Heisenberg-Weg 39, 85577 Neubiberg, Germany*
*Email: kubra.sekmen@polytechnique.edu*

Digital light processing (DLP)-based additive manufacturing is one of the innovative fabrication methods that builds 3D objects with complex geometry in a layer-by-layer fashion, via simultaneous in-plane photopolymerization [1]. During the UV curing process, the material properties and final product geometries change considerably due to the process parameters. Therefore, reliable and experimentally validated constitutive models are required for the numerical simulations to predict the material behaviour during and after the printing process [2,3].

This work presents experimental investigations as well as material modelling techniques to predict the influence of process parameters on viscoelastic properties. A commercial acrylate-based photosensitive resin PR48 (Colorado Photopolymer Solutions) is used for material characterization. 3D objects are fabricated by curing in a UV chamber (UVP Crosslinker, Analytik Jena) and printing with an Ember DLP 3D printer (Autodesk). Our interest is focused on the effect of the UV light intensity, temperature and frequency on the degree of cure-dependent viscoelastic properties.

Firstly, differential scanning calorimetry (DSC) tests are carried out for the thermal characterization of the PR48 liquid resin. Besides, the specific heat capacity is determined for the almost completely cured and uncured samples with the DSC measurements. Photo-DSC experiments are performed to investigate the curing reaction and modelling of the evolution of the degree of cure depending on the light intensity and temperature. The change in the degree of cure dependent viscoelastic properties is measured with UV rheometry below the gelation point and dynamic mechanical analysis (DMA) beyond the gelation point. Time-temperature and time-cure superposition principles are applied to the experimental results obtained by the DMA. In addition, chemical shrinkage behaviour is captured as a function of the degree of cure by the high-precision balance setup. UV curing properties of the resin are assessed with the thickness measurement by optical tomography. As a result of our experimental studies, model equations are proposed to describe the material behaviour. The model parameters and the constitutive relations for the reaction kinetics are identified to represent the experimental data.

This experimental work has revealed that the viscoelastic properties of the photopolymer have a strong dependency on both the temperature and the degree of cure during and after the photopolymerization reaction. This presentation will highlight that the assumption of linear-elastic material behaviour is insufficient for the numerical simulations.

## References

[1] Mu, Q.; Wang, L.; Dunn, C. K.; Kuang, X.; Duan, F.; Zhang, Z.; Qi, H. J.; Wang, T.; *Additive Manufacturing* **2017**, *18,* 74-83.
[2] Rehbein, T.; Lion, A.; Johlitz, M.; Constantinescu, A., *Polymer Testing* **2020**, *83*, 106356.
[3] Rehbein, T.; Lion, A.; Johlitz, M.; Sekmen, K.; Constantinescu, A., *Progress in Additive Manufacturing* **2021**, 1-14.

# Non-linear viscoelastic response of polymer glasses: From hole-burning to LAOS

Gregory B. McKenna[1,2] and Satish C.H. Mangalara[2]

[1]*Department of Chemical and Biomolecular Engineering, North Carolina State University, Raleigh, NC 27695*
[2]*Department of Chemical Engineering, Texas Tech University, Lubbock, TX 79409*
*gbmckenn@ncsu.edu; satish.mangalara@ttu.edu*

Mechanical spectral hole-burning (MSHB) is used as a complement to large amplitude oscillatory shear (LAOS) to characterize the non-linear viscoelastic response of polymeric glasses. Similarities and differences with MSHB and LAOS in other soft matter are shown.

## Introduction

The dynamic heterogeneity of glass-forming materials has recently been characterized using non-resonant spectral hole burning dielectric spectroscopy[1,2]. In systems with relatively weak dielectric response such as polymers mechanical spectral hole-burning (MSHB) offers an alternative approach[3,4]. However, unlike the dielectric hole burning, the MSHB suggests that dynamic heterogeneity may be related to dynamic regime rather than to a specific spatial heterogeneity[5]. The prior work MSHB work was carried out well above the glass transition. Here we describe a new series of results in which MSHB experiments were performed deep in the glassy state[6,7] and show that the response is related to the strength of the sub-glass β-transition and that the energy dissipated in the test is insufficient to explain the hole burning events in terms of changing fictive temperature due to glassy heterogeneities. Furthermore, because the MSHB experiment requires a large amplitude sinewave "pump" prior to the hole-burning probe, we show results from analysis of the data in terms of the LAOS framework[8-10] and find[11] that the behavior of the glassy polymers does not limit in the same way as is found in soft matter LAOS experiments on polymer melts and solutions[12]. For example, in the glasses the ratio of the third harmonic to the first harmonic $I_3/I_1$ varies much more weakly than the square of the sinewave amplitude. This contrasts with the hole burning results where in both types of system the hole amplitude varies approximately quadratically in the amplitude of the pump sinewave.

## Experimental methods

### Materials

Commercial grade poly(methyl methacrylate) (PMMA) and polycarbonate (PC) were used for the experiments. They were machined into cylindrical form for torsional testing as described elsewhere. Prior to mechanical testing the samples were heated above the glass transition temperature and cooled rapidly to room temperature where they were aged for 9000 s prior to testing for approximately 900 s, thus respecting the Struik [13] protocol that the testing time be less than 10% of the aging time.

### Mechanical spectral hole-burning (MSHB) experiments

In MSHB experiments the sample is made up of three experiments. First, one obtains the small strain linear response to a step strain. Then the material is subjected to a large amplitude sinewave and this is followed by a small step strain. In the third experiment the sample is again subjected to the large amplitude sinewave followed by the small step strain, but in the opposite direction from the second experiment. The small strains are then added together, divided by two and compared to the linear response:

$$G_+(\gamma,t) = G_{pump}(\gamma,t) + G_{mod}(\gamma,t) \qquad \textbf{(1)}$$

$$G_-(\gamma,t) = G_{pump}(\gamma,t) - G_{mod}(\gamma,t) \qquad \textbf{(2)}$$

$$G_{mod}(\gamma,t) = \frac{G_+(\gamma,t) - G_-(\gamma,t)}{2} \qquad \textbf{(3)}$$

Where the differences between the modified response $G_{mod}(\gamma,t)$ and the linear response are interpreted as "holes". The definitions are shown in Figure 1 and typical holes are shown in Figure 2.
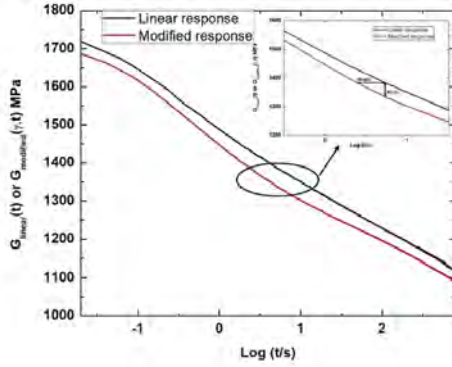


**Figure 1**. Definitions of vertical and horizontal holes. Results for PMMA with 4% pump and 0.6% probe at 0.0728 Hz and T=22 °C. After Mangalara and McKenna [6].
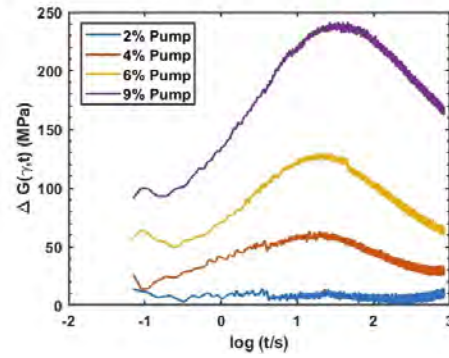
**Figure 2.** Vertical holes for PMMA for a frequency of 0.0189 Hz and different pump strains. T=22 °C. After Mangalara and McKenna [6].

*Large amplitude oscillatory shear (LAOS) experiments*

The LAOS analysis followed the approach provided by the McKinley group with MITLAOS program (McKinley's group; http://web.mit.edu/nnf/) providing either Fourier transform analysis to obtain the harmonics for the large pump sinewave or the Chebyshev polynomials for the data analysis[8-10].

**Results and discussion**

*MSHB*
Figures 1 and 2 provide the fundamental information relevant to making hole-burning measurements. Figure 3 shows the results of the hole magnitudes for PMMA as a function of the pump amplitude squared. We see that, as is typical of hole burning experiments, the square dependence expected[1-4] from other hole-burning experiments is approximately followed. Similar results, but with much lower intensity of the holes, were found in PC [7] which has a much weaker β-relaxation than does PMMA [14,15].

*LAOS*
The LAOS experiments, however, showed surprising results. In many instances, and especially as the sinewave amplitude becomes small, the harmonic ratio $I_3/I_1$ follows the square of the sinewave amplitude. As we see in Figure 4, for the PMMA, this is not the case with the harmonic ratio varying with a power that is close to unity, thus suggesting that the observed square dependence of the harmonic ratio is not universal and, in the glassy polymers is not followed. In addition, the absolute intensities of the harmonics are not generally reported in the LAOS analysis. When we look at the strain dependence of the intensity of the first harmonic for the PMMA we see that $I_1$ is not linearly dependent on the strain magnitude, thus suggesting that the first harmonic is not related to the linear viscoelastic response of the

material, i.e. as a modulus it would decrease with increasing strain. This is shown in Figure 5 where we see that $I_1$ varies approximately as $\gamma^2$.
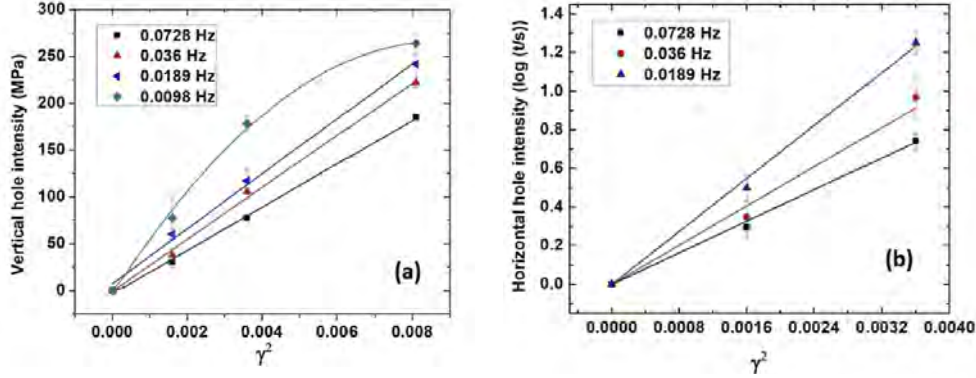


**Figure 3.** **(a)**Vertical holes intensity and **(b)** horizontal hole intensity for PMMA as a function of pump amplitude squared for different pump frequencies, as indicated. T=22 °C. After Mangalara and McKenna [6].
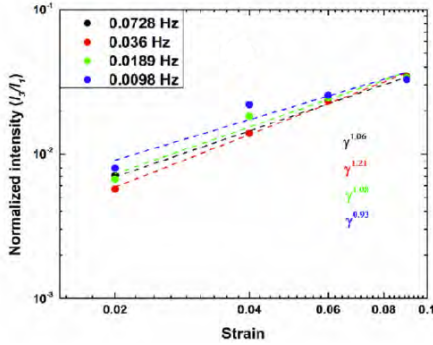


**Figure 4.** LAOS Fourier harmonic ratio $I_3/I_1$ for PMMA as a function of strain at different frequencies, as indicated. T=22 °C. After Mangalara and McKenna [11].
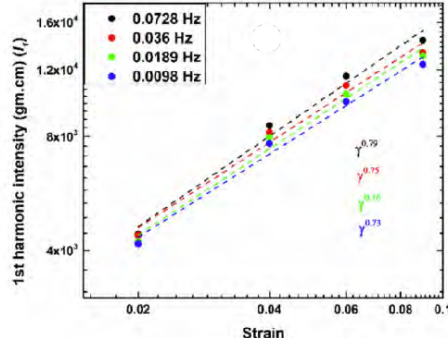
**Figure 5.** LAOS Fourier first harmonic $I_1$ for PMMA as a function of strain at different frequencies, as indicated. T=22 °C. After Mangalara and McKenna [11].

## Summary and conclusions

The use of MSHB and LAOS to fingerprint the response of material non-linearity has proven valuable in the mechanics of soft matter such as polymer melts and solutions as well as in colloidal dispersions. The work reported here represents some of the first results for the use of these powerful tools to characterize the response of polymer glasses. We find that the MSHB response is related to the β-relaxation intensity, thus, similar to melts and solutions to the type of dynamics rather than to an explicit measure of spatial heterogeneity. For the LAOS measurements we have found that the response of the glassy polymers differs significantly from that of the softer materials in that the ratio of the harmonic amplitudes does not vary quadratically with strain and we find that the first harmonic itself varies sub-linearly with strain, thus indicating that it is not related to the linear viscoelastic modulus. Future work should examine induced heterogeneity in polymer glasses to examine how the non-linear responses vary with such heterogeneity.

## Acknowledgements

## References

[1] Schiener, B.; Böhmer, R.; Loidl, A.; Chamberlin, R.V., *Science* **1996**, *274*, 752-754.

[2] Schiener, B.; Chamberlin, R.V.; Diezemann, G.; Böhmer, R., *J. Chem. Phys.* **1997**, *107*, 7746-7761.

[3] Shi, X.; McKenna, G.B., *Phys. Rev. Lett.*, **2005**, *94*, 157801.

[4] Shi, X.; McKenna, G.B., *Phys. Rev. B.*, 2006, *73*, 014203.

[5] Qin, Q.; Doen, H.; McKenna, G.B., *J. Polym. Sci., Part B: Polym. Phys.*, **2009**, *47*, 2047-2062.

[6] Mangalara, S.C.H.; McKenna, G.B., *J. Chem. Phys.*, 2020, *152*, 074508.

[7] Mangalara, S.C.H.; Paudel, S.; McKenna, G.B., *J. Chem. Phys.*, **2021**, *154*, 124904.

[8] Wilhelm, M.; Maring, D.; Spiess, H.-W., *Rheol. Acta*, 1998, *37*, 399-405.

[9] Hyun, K.; Wilhelm, M.; Klein, C.O.; Cho, K.S.; Nam, J.G.; Ahn, K.H.; Lee, S.J.; Ewoldt, R.H.; McKinley, G.H., *Prog. Polym. Sci.*, **2011**, *36*, 1697-1753.

[10] Ewoldt, R.H., *J. Rheol.*, **2013**, *57*, 177-195.

[11] Mangalara, S.C.H.; McKenna, G.B., *Mechanics of Time-Dependent Materials*, **2022**, https://doi.org/10.1007/s11043-021-09529-6.

[12] Shamim, N.; McKenna, G.B., *J. Rheol.*, **2014**, *58*, 43-62.

[13] Struik, L.C.E., *Physical Aging in Polymers and Other Amorphous Materials,* Elsevier, Amsterdam, 1978.

[14] Guerdoux, L.; Duckett, R.A.; Froelich, D., *Polymer*, **1984**, *25*, 1392-1396.

[15] Flory, A.; McKenna, G.B., *Macromolecules,* **2005**, *5*, 1760-1766.

# The Toughness of a Single Weld Formed by Fused Filament Fabrication

Thao D. Nguyen

*Department of Mechanical Engineering, Johns Hopkins University, Baltimore, MD 21210, USA*

The tear and peel tests have been widely applied to measure the toughness properties of thin rubber sheets, adhesives, and polymer films. Recently, the tear test has been applied to characterize the Mode III toughness of a single weld in polymers produced by melt extrusion additive manufacturing. In addition, our groups have developed a peel test to measure the Mode I toughness of a single weld. In this presentation, I will present finite element modeling studies of the tearing of a weld between two printed filaments and the peeling of a single printed filament from a printed wall to investigate the effects of the geometry of the printed filament and material properties on the measured tear and peel energies. The mechanical behavior of the printed filaments was described by a viscoplastic model for glassy polymers and the weld was represented using cohesive surface elements and the Xu-Needleman traction-separation relationship. The geometric model and the material parameters were chosen based on experimental measurements. As expected, the peel and tear energies varied with the specimen dimensions, the curvature of the printed filaments, the yield stress relative to the cohesive strength of the weld, and the post-yield stress drop. The effects of the hardening modulus were small. These factors altered the viscoplastic dissipation in the material ahead of the propagating crack tip. The results showed that viscoplastic dissipation can constitute a large fraction of the tear and peel energies and is strongly affected by the specimen dimensions and the geometry and material properties of the printed filament. There was also considerable mode mixty in the tear energy. The findings can be used to design tear and peel tests to measure the intrinsic fracture toughness of the weld.

# Evidence of large densification of polymer glass under combined high pressure and shear flow

Graham L. W. Cross[1], Owen Brazil[2], H. Özgür Özer[3], Benjamin Watts[4], John B. Pethica[5]

[1]*School of Physics, CRANN & AMBER, Trinity College Dublin, Ireland, crossg@tcd.ie*
[2]*School of Physics, CRANN & AMBER, Trinity College Dublin, Ireland, crossg@tcd.ie*
[3]*Department of Physics Engineering, Istanbul Technical University, 34469, Maslak, Istanbul, Turkey*
[4] *Laboratory for Synchrotron Radiation, Paul Scherrer Institute, 5232 Villigen, Switzerland*
[5]*School of Physics, CRANN & AMBER, Trinity College Dublin, Ireland, crossg@tcd.ie*

It is generally thought that shear of disordered matter leads to rejuvenation, including a reverse of densifying effects of thermal ageing reported for metallic glasses. Here we report the opposite effect for a polymer glass. We used the high aspect ratio geometry of the layer compression test to measure the uniform and homogeneous accumulation of plastic strain during isothermal confined compression of a deeply quenched film of polystyrene glass [1]. Combined scanning transmission X-ray microscopy (STXM) and atomic force microscopy confirmed defect-free deformation leaving up to 1.2% residual densification under conditions of confined uniaxial strain. At higher peak strain, plastic shear flow extruded glass from below the compressing punch under conditions of a high background pressure. A further density increase by 2% was observed by STXM for a highly thinned residual thickness of polymer (Fig. 1). While the uniaxial densification can be accounted for by a simple elastic-plastic constitutive model, the high pressure extrusion densification cannot. This compactification of polymeric glass stands in contrast to recent findings for bulk metallic glasses under deep notch triaxial compression, indicating rejuvenation under compressed shear flow.
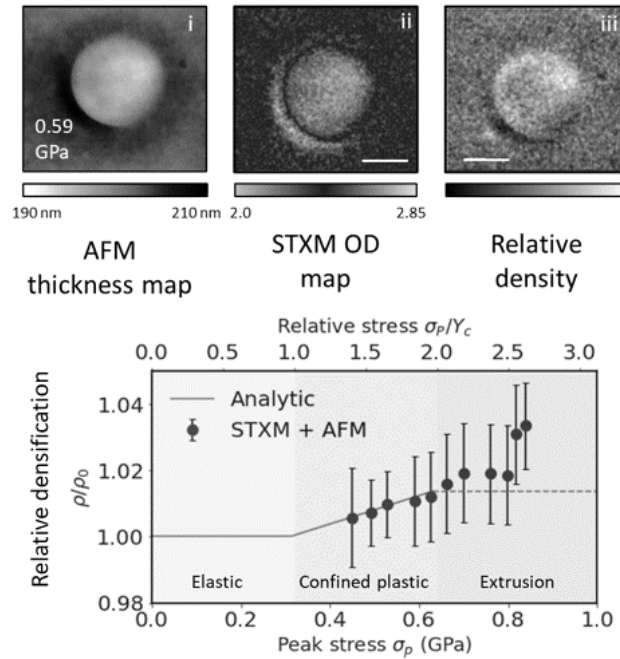
**Fig. 1.** (a) Large densification (iii) in polystyrene films via combined AFM height map (i) and STXM (ii) measurements. (b) Residual density increase for a 203 nm polystyrene film as a function of peak compressive stress $\sigma_p$ in the layer compression test. Densification up to 3.4% is observed under extrusive shear flow at high peak stress far exceeding elastic residual stress prediction (dotted line).

[1] Brazil, O, et. al, *submitted to Physical Review Letters*, **2021**

# Plasticity of glassy polymers at the mesoscale: implementation of a finite element model based on shear transformation zone dynamics

F. Van Loock[1,2], N. Klavzer[1], J. Chevalier[3], L. Brassart[4] and Thomas Pardoen[1]

[1]*Institute of Mechanics, Materials and Civil engineering (iMMC), UCLouvain,*
*B-1348, Louvain-la-Neuve, Belgium*
[2]*Polymer Technology group, Eindhoven University of Technology, PO Box 513,*
*5600, MB, Eindhoven, the Netherlands*
[3] *Solvay, Material Science Application Center (MSAC), B-1120 Bruxelles, Belgium*
[4] *Department of Engineering Science, University of Oxford,*
*OX1 3PJ Oxford, United Kingdom*

## Abstract

Polymeric glasses exhibit complex behaviour when subjected to deformation below the glass transition temperature. Sophisticated continuum models are available to predict this response; they generally give good reproductions of the measured monotonic stress-strain data of bulk material systems. However, they require a large number of mostly phenomenological parameters and struggle to accurately predict the response for more complicated (e.g. confined) loading states.

The use of a mesoscale numerical model based on shear transformation zone (STZs) activations offers an attractive method to bridge standard continuum modelling approaches and atomistic simulations which are typically limited to small length and time scales. Plastic deformation is dictated by conformational changes of molecular clusters (STZs) and their interaction with the linear, elastic matrix. The model sheds light on the role of processing conditions on the stress-strain response of amorphous polymers with only a few physical fitting parameters. In addition, model predictions give insight to the degree of heterogeneity of the stress and strain distribution of an amorphous polymer at the mesoscale, see Fig. 1.

The scope of this contribution is to introduce the theoretical framework of the STZ model and its implementation in a commercial FE software package [1]. Emphasis is placed on the effect of time and space discretisation on the predicted macroscopic stress-strain response. The dependence of the predicted yield strength upon the values of the model parameters is analysed via a mean-field approximation. In addition, we explore possible routes to calibrate the model based on measurement data.
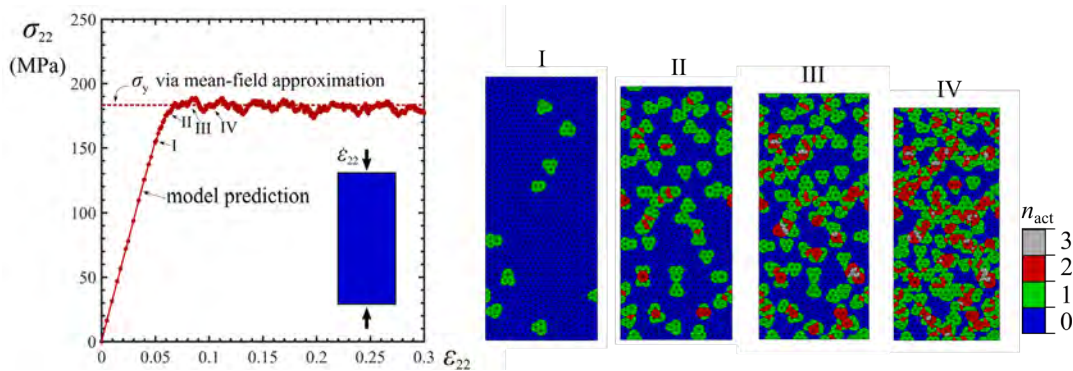
**Fig. 1** – Predicted stress-strain response of a model polymeric glass material element in plane strain compression at $T = 293$ K and for $\dot{\varepsilon} = 10^{-2}$ s$^{-1}$ . The estimated value of the yield strength via the mean-field approximation is included. Snapshots show the number of cumulative STZ activations, $n_{act}$, of each finite element close to yield. See the work of Van Loock et al. for simulation details [1].

## References

[1] Van Loock, F.; Brassart, L.; Pardoen, T., *International Journal of Plasticity* **2021**, 145, 103079.

# Modelling the tensile deformation and yielding of amorphous glassy polymers using "TS2-SL" theory

Valeriy V. Ginzburg

*Chemical Engineering and Materials Science, Michigan State University, 428 S. Shaw Lane, Room 2100 East Lansing, Michigan 48824-1226*
*Email: vvg851966@gmail.com*

Modeling tensile deformation of amorphous glassy polymers at temperatures close to their $T_g$ (above the brittle-ductile transition) is an important problem relevant to many industrial applications. Here, we utilize a recently-developed "Two-state, two-(time)-scales dynamic model with Sanchez-Lacombe equation of state" ("TS2-SL") [1] to predict tensile stress-strain curves for amorphous PS and PMMA as function of temperature, strain rate, and – in a semi-quantitative fashion – the polymer molecular weight. Within this approach, we split the uniaxial tension into two parts – dilation and shear. The effect of dilation is to reduce the density of the material, leading, in turn, to the reduction in the α-relaxation time. Shear, then, is modelled as a single Maxwell element, with the stress-dependent relaxation time as discussed above. At high stress, the relaxation time approaches its lower limit which roughly corresponds to the entanglement relaxation time. With this approach, we calculated stress-strain curves for PS and PMMA at various temperatures and strain rates (see example in Figure 1a). Based on this analysis, we also calculated yield stress as a function of temperature and compared it with experimental data [2] (Figure 1b). Next steps include the implementation of the model in a Finite Element Analysis tool, the description of the stress "overshoot", and the calculation of the brittle fracture stress and the brittle-ductile transition.
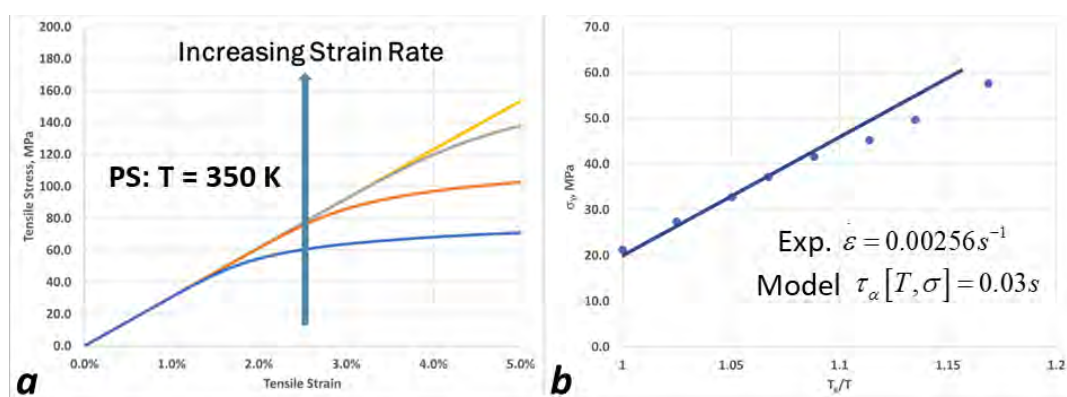


Figure 1. (a) Calculated stress strain curves with strain rates (bottom to top) $10^{-3}$, $10^{-1}$, $10^1$, and $10^3$ s$^{-1}$; (b) Yield stress for PS, model (line) vs. experiment (circles).

## References

[1] Ginzburg, V. V., *Soft Matter* **2021** (in press)
[2] Wang, S. Q.; Cheng, S.; Lin, P.; Li, X., *J. Chem. Phys.* **2014**, *141*, 094905.

# Elasticity, plasticity and fracture toughness at ambient and cryogenic temperatures of epoxy systems used for the impregnation of high-field superconducting magnets

André Brem[1], Barbara J. Gold[1], Bernhard Auchmann[2], Davide Tommasini[2],
Theo A. Tervoort[1]

[1]*Department of Materials, ETH Zurich, Zurich, Switzerland*
[2]*CERN TE-MPE, Geneva, Switzerland*

The emergence of new generations of superconducting magnets in high-energy physics applications have intensified the search for improved epoxy systems to be used as encapsulating materials at cryogenic temperatures [1, 2]. The prime function of these epoxy systems is to provide electrical insulation, adhesion and mechanical support for the magnet coils that typically contain a highly brittle ceramic phase, and to prevent any energy-release mechanisms that might lead to heating effects, resulting in a loss of the superconductive state [3].

The study evaluates the thermal expansion coefficient, as well as the elastic-, plastic- and fracture behaviour, at ambient and cryogenic (liquid nitrogen) temperatures, of four different epoxy systems that are used in high-field superconducting magnets. As expected, both the elastic and plastic behaviour of the epoxy systems at room temperature depend strongly on their distance to the glass transition temperature, but become similar at cryogenic temperature. The rate dependency of the yield stress at room temperature of the four epoxy systems was similar and is well described by the Eyring model. At cryogenic the temperatures the rate dependency disappears. The fracture toughness remained equal or even increased upon cooling to cryogenic temperatures for each of the four epoxies. However, the fracture toughness values of the four epoxies tested were quite different from each other, see Figure 1, suggesting that fracture toughness not only depends on the van der Waals interactions between the segments but is also determined by other molecular characteristics, such as the network structure.
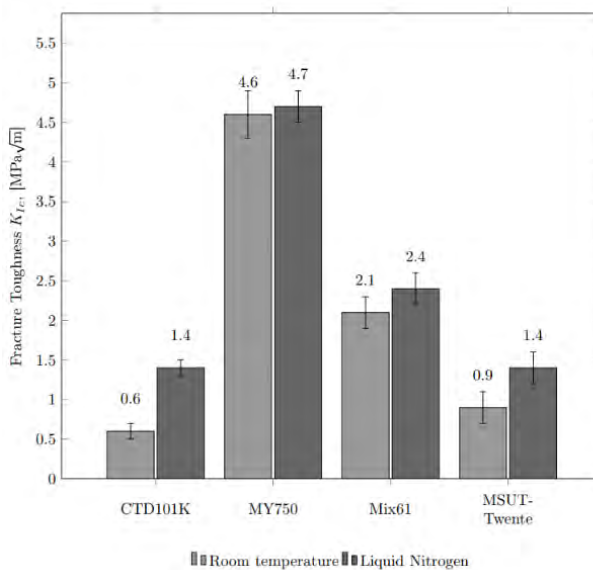


*Figure 1: Fracture toughness values for the various epoxy systems measured at room temperature and in liquid nitrogen.*

## References

[1] Yang, J. P.; Chen, Z. K.; Yang, G.; Fu, S. Y.; Ye, L.; *Polymer* **2008**, 49, 3168
[2] Chen, Z.K. Yang, G. Yang, J. P.; Fu, S. Y.; Ye, L.; Huang, Y.G., *Polymer* **2009**, 50, 1316
[3] Iwasa, Y.; *Cryogenics* **1985**, 25, 304$

# Entanglements and mobility in ultrathin polymer film mechanics

Cynthia Bukowski[1], Tianren Zhang[2], Robert A. Riggleman[2], Alfred J. Crosby[1]

*[1]University of Massachusetts Amherst, cbukowski@umass.edu, crosby@mail.pse.umass.edu*
*[2]University of Pennsylvania*

Mechanical strength in glassy polymers is dictated by interchain entanglements and molecular mobility. However, at thicknesses below 100 nm, polymer chain behavior differs from bulk materials. Our research provides new insight into controlling entanglements and mobility in thin films and overcoming the intrinsic brittleness that limits mechanical strength. We use a group-built instrument, The Uniaxial Tensile Tester for UltraThin films (TUTTUT) [1, 2], to measure the complete stress-strain response of polymer films down to 15 nm in thickness. This instrument allows measurements to be conducted on liquid-supported or freestanding films. Here, we discuss two recent studies that focus on elucidating the role of entanglements and microstructural domains in determining mechanical strength and ductility for ultrathin films.

To understand the connection between the number of interchain entanglements and the mechanical response, we fabricated polystyrene films using blends of long and short chains to systematically change the number of entanglements. Films of 100 nm in thickness were spin cast from dilute solutions of varying blend concentration. Once a critical number of entanglements was reached, the maximum stress and failure strain decreased with decreasing number of interchain entanglements. We developed an analytical model that connects the average number of load-bearing entanglements per chain in blended systems to a film's mechanical strength by quantitatively comparing experimental results and molecular dynamics simulation results.

A second study measured the uniaxial extensional properties of thin films of poly(styrene-*b*-2-vinylpyridine), where the block copolymer domains have similar elastic modulus, glass transition temperature, and crazing stress. The morphology of the films was altered through solvent vapor annealing prior to uniaxial extension. These results show how relative positioning of phase-separated blocks within a thin film can significantly alter a film's mechanical response. Comparing disordered and ordered lamellar morphology films in a freestanding state, ordered films can withstand higher stresses. Placing these films on a water surface during uniaxial extension caused local domain plasticization, increasing failure strains in comparison to freestanding films. Through this research, we are expanding the knowledge of how molecular entanglements and mobility influence the mechanical response of thin glassy polymer films and developing design principles for creating strong thin materials.

## References

[1] Liu, Y.; Chen, Y.-C.; Hutchens, S.; Lawrence, J.; Emrick, T.; Crosby, A. J., *Macromolecules* **2015**, *48*, 6534-6540.
[2] Bay, R. K.; Shimomura, S.; Liu, Y.; Ilton, M.; Crosby, A. J., *Macromolecules* **2018**, *51*, 3647-3653.

# How moving cracks in brittle solids choose their path …

J. Fineberg[1], L. Rozen-Levy[1], J. Kolinski[2]

[1]*The Racah Institute of Physics, The Hebrew University of Jerusalem, Givat Ram, Jerusalem Israel.*

[2]*École Polytechnique Fédérale de Lausanne, Lausanne, 1015, Switzerland*

## Abstract

While we have an excellent fundamental understanding of the dynamics of 'simple' cracks propagating in brittle solids, we do not fully understand how the path of moving cracks is determined. Here we experimentally study cracks that propagate between 10-95% of their limiting velocity within a brittle material. We deflect these cracks by either allowing them to interact with sparsely implanted inclusions or driving them to undergo an intrinsic oscillatory instability in defect-free media. Both of these deflection mechanisms significantly perturb the otherwise singular fields at the crack's tip. Dense, high-speed measurements of the strain fields surrounding the crack tips obtained via imaging reveal that the near-tip paths selected by these rapid and strongly perturbed cracks are entirely governed by the direction of the maximal strain energy density. Surprisingly, directions minimizing the near-tip shear are not selected. This fundamentally important result may potentially be utilized to either direct or guide running crack or increase material toughness by controlled insertion of inclusions or particles.

*The Strain Energy Density (SED) prediction agrees well with selected propagation directions.* (a–left) Two examples of typical cracks ($v \sim 0.5\ C_R$) whose paths are governed by crack-particle interactions. Paths (particles) are indicated by red lines (yellow diamonds). (a-right) The strain energy density field (SED) in J/$m^3$ ahead of cracks within the dashed red boxes. Diamonds denote the maximal value of the SED for each $x$ in the reference frame. Red dots: current and future tip locations. Linear fits (magenta arrow) to the SED maxima ahead of the tip agree well with the future crack tip locations. Yellow diamonds: particle locations. (b-left) The trajectory of a spontaneously oscillating crack propagating at $\sim 0.95 C_R$ in a homogeneous gel at the onset of the oscillatory instability. The paths of successive crack tips are denoted in red. Two snapshots of the crack tip in the laboratory frame are denoted by yellow dots. Panels on the right present the respective SED fields in J/$m^3$, within the material area just ahead of each crack tip. As in (a), diamonds mark locations of the maximal SED value for each $x$, and lines fitted to these maxima agree well with the propagation direction denoted by the red line connecting the sequential tips (red dots). (c) An ensemble of such experiments: all deflected crack directions are accurately predicted by the maximum strain energy density (SED) condition. Filled circles: predictions for crack-particle interactions with velocities ($v/C_R$) (colors) and particle ensembles (2-6 particles/$mm^2$). Open symbols: the oscillatory instability. Open triangles: sequential data in (b). Dashed line represents perfect agreement.
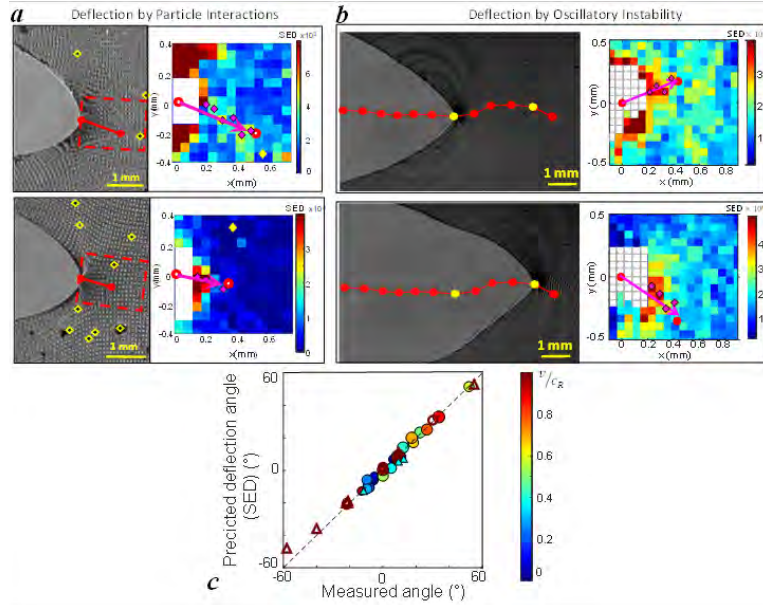
## Reference

[1] Rozen-Levy, L. Kolinski, J. M., Cohen, G., and Fineberg, J.; Phys. Rev. Lett., **2020**, vol. 125, art. number 175501

# Nonlinear elastic effect on interacting crack paths in PDMS films

C. Peretti[1], E. Lindas[1], O. Chaffard[1], T. Biben[1], A. Gravouil[2], O. Ramos[1], S. Santucci[3], L. Vanel[1]

[1]*Université de Lyon, Université Claude Bernard Lyon 1, CNRS, Institut Lumière Matière, France*
[2]*Université de Lyon, LaMCoS, INSA-Lyon, CNRS, France*
[3] *Université de Lyon, Ecole Normale Supérieure de Lyon, CNRS, Laboratoire de physique, France*
*loic.vanel@univ-lyon1.fr*

The observed repulsive behaviour of two initially collinear cracks growing towards each other and leading to a hook-shaped path questioned recently the validity of the Principle of Local Symmetry within Linear Elastic Fracture Mechanics theory [1]. Theoretical and numerical work has solved this dilemma, providing the precise geometric conditions for the existence of the repulsive phase and revealing a multi-scale behaviour of the repulsive/attractive transition [2]. However, in polymer films, the repulsive phase depends strongly on the microscopic behaviour of the material, highlighting the crucial role of the fracture process zone [1]. At interaction distances larger than the process zone size, microscopic shape of the process zone tip controls crack repulsion. The maximum angle of repulsion is then systematically smaller than the one predicted by linear elasticity [2].

Nonlinear elastic materials such as elastomers also depart from the prediction of linear elasticity for interacting cracks. We performed experiments on PDMS film that indeed show a maximum angle of repulsion not only significantly smaller than the one of linear elasticity, but also smaller than the one observed in polymer films with a plastic process zone. Our FEM simulations on a Mooney-Rivlin material confirm that the nonlinear elastic response of PDMS modifies the crack path, reducing the repulsive strength between the two interacting cracks.
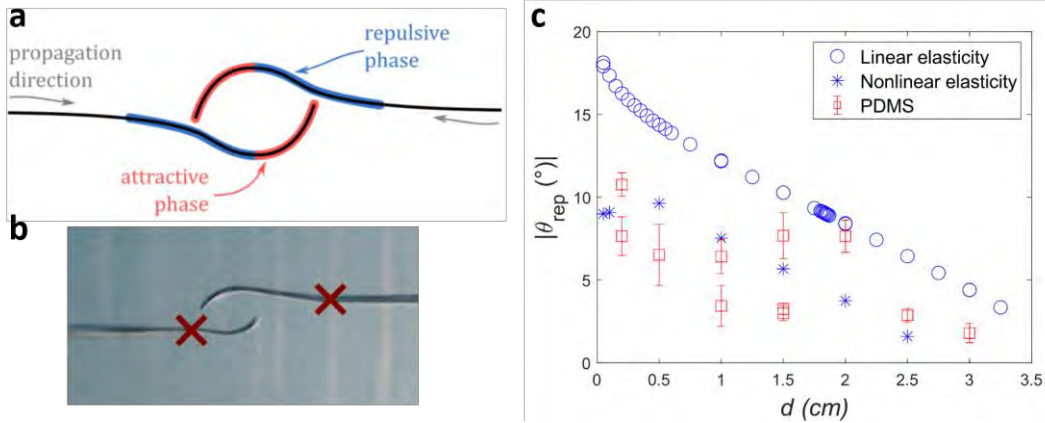


**Figure 1 a.** Repulsive and attractive phase (FEM). **b**. Example in PDMS film. **c**. Maximum repulsion angle in PDMS films and from FEM simulation of Mooney-Rivlin material as a function of the vertical separation of the two cracks (d=0 corresponds to perfectly aligned cracks).

## References

[1] Dalbe, M.-J.; Koivisto, J.; Vanel, L.; Miksic, A.; Ramos, O.; Alava, M.; Santucci, S.; *Phys. Rev. Lett.* **2015** 114, 205501
[2] Schwaab, M.-E.; Santucci, S.; Biben, T.; Gravouil, A.; Vanel, L. ; *Phys. Rev. Lett.* **2018** 120, 255501.

# Embrittlement of Short Fiber Reinforced Thermoplastic Systems Under Multiaxial Loading Conditions

M. Wismans[1,2], T.A.P. Engels[1], L.C.A. van Breemen[1], L.E. Govaert[1]

[1]Eindhoven University of Technology, Department of Mechanical Engineering, Polymer Technology, P.O. BOX 513, 5600 MB, Eindhoven, The Netherlands
[2]DPI, P.O. Box 902, 5600 AX, Eindhoven, the Netherlands

Due to their high stiffness to weight ratio, and the continuous drive to lower weight in the automotive sector, short-fiber reinforced thermoplastics are replacing application-critical, structural parts traditionally made from metallic materials. In these often safety critical applications it is vital to predict the performance of these fiber reinforced thermoplastics quantitatively. Fiber-reinforced thermoplastics with a quasi-brittle matrix show a ductile response in uniaxial tension and a brittle response in a multiaxial stress state. Here, cavitation dominated failure prevails over plasticity dominated failure. Currently, constitutive models are lacking the ability to describe cavitation dominated failure accurately.

In this study, the embrittlement of short-fiber reinforced thermoplastic systems is studied using a hybrid approach, combining numerical and experimental observations. Uniaxial tensile experiments and biaxial experiments via puncture tests are performed for a range of annealing times. Embrittlement is observed for the puncture tests in contrast to the uniaxial tensile tests. The embrittlement shows a gradual decrease in impact energy following a different evolution as compared to unfilled thermoplastics where a step-response is observed.

The trends observed in the experimental study are interpreted using a micro-mechanical model based on a representative volume element (RVE) of the composite. The behaviour of the fiber is modelled as being linear elastic matrix and the matrix by using the Eindhoven Glassy Polymer (EGP) model. The EGP model describes the intrinsic deformation behaviour of polymers and incorporates the effect of annealing time on its behaviour. The geometry of the RVE and the stress distribution throughout the matrix during deformation can be tracked and an example is shown in Figure 1. The high local triaxiality, which is a measure for the stress state, and the increase of regions where the hydrostatic stress is higher as a critical value explain the observation why embrittlement is visible for the biaxial load while not present for the uniaxial load. The observations seem to indicate that macroscopic failure is not triggered when the local stress reaches a critical value but rather by an accumulation of local damage. An energy or volumetric failure criterion is a more suitable failure indicator.
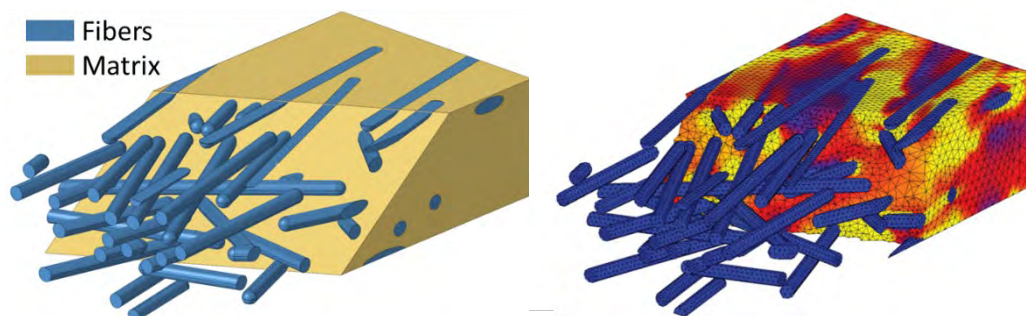


Figure 1: Left: Geometry of the representative volume element RVE. Right: Stress distribution of the matrix during deformation.

# Revisiting the fracture-mechanical behavior of unfilled and filler reinforced elastomers by advanced experimental techniques

Eric Euchler[1], Konrad Schneider[1], Sven Wießner[1,2]

[1]*Leibniz-Institut für Polymerforschung Dresden e.V., Dresden, Germany.*
*euchler-eric@ipfdd.de*
[2]*Technische Universität Dresden, Dresden, Germany.*

Summary: For elastomers, advanced experimental techniques have been applied to better understand the impact of (micro-)mechanical phenomena, such as cavitation and strain-induced crystallization (SIC), on the macroscopic fracture-mechanical properties. In this study, the formation and orientation of SIC in natural rubber have been investigated at non-uniaxial tension using synchrotron X-ray scattering.

## Introduction

Strain-induced crystallization (SIC) is one of the most important factors for the outstanding mechanical properties of natural rubber (NR). The topic of SIC in NR was extensively investigated with a focus on the homogeneous uniaxial strain, e.g. using synchrotron X-ray scattering experiments [1-6]. However, even assuming a homogenous deformation at uniaxial tension, local deviations from the fiber symmetry may occur on a sub-microscopical length scale. For example, in the case of pre-cracked or damaged elastomer samples, the strain field is often highly inhomogeneous [6-8]. As a consequence, the residual crystallinity and crystallite orientation, e.g., around a crack tip, will be inhomogeneous, too, and affect the local material properties, such as strength and stiffness or resistance against crack propagation.

## Experimental

To study deviations from the fiber symmetry, wide-angle X-ray scattering (WAXS) experiments have been performed using (NR) samples sheets of the so-called "pure-shear" geometry leading to plane strain deformation [9-11]. While for samples with small widths the assumption of fiber symmetry is normally valid, here "pure-shear" samples with a high width-to-length ratio were investigated. The samples had dimensions of 80 mm (width) × 10 mm (height) × 1 mm (thickness), while bulges on both sides with a diameter of 5 mm enable a defined clamping. On the free sample length, two lines were applied for optical strain estimation. Due to this geometry, the width of the samples remained mainly constant during tension – closely to the "pure-shear" deformation state. By stretching such NR samples, a non-uniaxial strain field occurs and thus, the orientation of strain-induced crystallites is not homogeneous. By rotating the NR samples around the strain direction perpendicular to the X-ray beam, all structural information on the deviation from fiber symmetry can be collected.

In this study, unfilled NR (NR00) and NR samples reinforced with 20 phr of carbon black (NR20) have been investigated by WAXS experiments at the beamline P03 at *Deutsches Elektronen-Synchrotron* (DESY), Hamburg, Germany [12]. A wavelength of 0.094 nm (energy of 13.2 keV) and a beam size of about 20 μm × 20 μm were used. The general arrangement of the measurements is shown in Figure 1 (left). For the WAXS measurement, a PILATUS 300k detector (DECTRIS AG, Switzerland) with a pixel size of 0.172 mm x 0.172 mm and a sample-to-detector distance of 206 mm was used. The intensities of the incident and the transmitted beam were measured with an ionization chamber and by a beam stop diode, respectively.

The NR samples were investigated at seven different rotation angles of the sample with respect to the strain direction, $\psi$ (Figure 1, right), varying from $-45°$ to $+45°$ with steps of $15°$. At each $\psi$ step, 10 patterns were captured by scanning along the sample in strain direction with a step width of 1 mm and an exposure time of 1 s. Due to the rotation of the sample, the X-ray path through the sample, $(x + b_x)$, depends on $\psi$. As a result, the paths of the two scattered signals at $\pm 2\Theta$ were different from each other. The scattering data pre-processing contained the following phases: (i) estimation of the absorption coefficients (0.418 mm$^{-1}$ for NR00, 0.440 mm$^{-1}$ for NR20); (ii) correction of the scattering intensities considering the background scattering and sample thickness reduction, which was affected by the deformation level and the rotation angle with respect to the strain direction [13, 14].
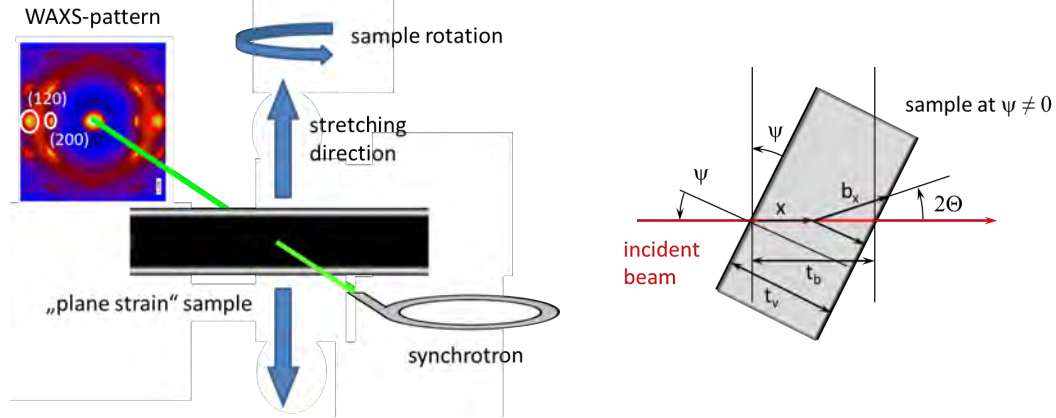


Figure 1: (Left) Arrangement of the stretched sample in the synchrotron X-ray beam. The equatorial peaks have the indices (200) and (120), here a WAXS pattern of a NR sample with fiber symmetry is shown. (Right) Sketch illustrating the top view on a rotated sample according to the strain direction. The correction of different beam paths through the sample is shown: $\psi$ is the angle between the incident beam and sample. Instead of the initial sample thickness $t_v$, the beam passes the thickness $t_b$, while the path of the scattered beam is $(x + b_x)$.

## Results

The crystal structure of NR was intensively investigated, e.g. Takahashi and Kumano [15] gave a comprehensive overview of these investigations. The unit cell is monoclinic with parameters $a = 1.241$ nm, $b = 0.881$ nm, fiber axis $c = 0.823$ nm, and $\beta = 93.1°$. The structure factors $F$ of the crystalline peaks (200) and (120) are $|F_{200}| = 128.91$ and $|F_{120}| = 290.91$, respectively [2]. The geometry is very similar to the orthorhombic cell, as reported by Nyburg [16], and used for further evaluation due to simplification.

Representative WAXS patterns of stretched NR00 at different rotation angles are shown in Figure 2. The experimental data show, that there is a very strong dependence of the intensities of the individual peaks on the rotation angle of the sample. This confirms that there is no fiber symmetry within the samples due to the non-uniaxial deformation. Generally, the $c$-axis of the crystallites was strongly oriented with respect to the tensile axis.



| -45° | -30° | -15° | 0° | 15° | 30° | 45° |
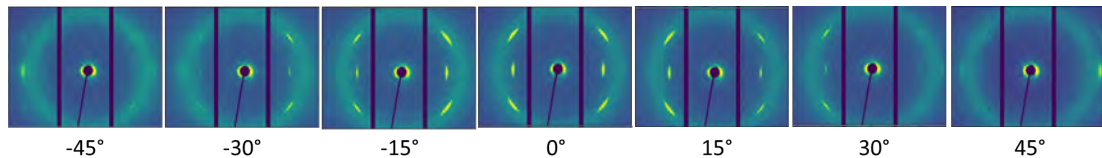
Figure 2: Corrected WAXS patterns of a NR00 sample in dependency of the rotation angle around the strain direction, which is vertical. Rotation angles are $\pm 45°$, $\pm 30°$, $\pm 15°$, $0°$. The strain ratio was 5:1 and the scattering intensities are given in a.u.

The further discussion is focused on the equatorial peaks (200) and (120). The characterization of the crystalline peaks was done via integrating the peak area after subtraction of the underlying amorphous halo. The general alignment of the sample with respect to the beam and a scattering crystallite within the sample are shown in Figure 3.
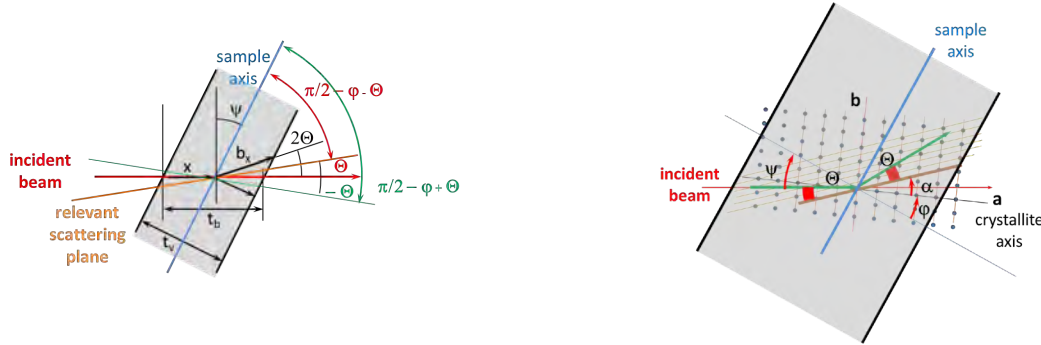


Figure 3: Detailed scattering geometry, here for the crystalline peak (120): The sample is rotated to the beam by an angle $\psi$, the $a$-axis of an individual crystallite has an angle of $\varphi$ within the sample, the scattering crystalline plane has an angle of $\alpha$ to the $a$-axis. The scattering angle $\Theta$ is between the incident beam and the scattering plane as well as between this and the scattered beam.

If the *Bragg* condition is fulfilled, the characteristic peaks of a pattern appear with the scattering angle $2\Theta$ between the incident and the transmitted beam as well as the angle $\alpha$ between the scattering crystalline plane to the $a$-axis. Thus, for the left and right equatorial peak (200) with $2\Theta_{200} = \pm 8.682°$ and $\alpha_{200} = 0°$ always one possible orientation of crystallites ($\psi + \varphi_{1/2}$) is possible. For each of the (120) peaks with $2\Theta_{120} = \pm 12.808°$ and $\alpha_{120} = \pm 70.48°$ always two possible orientations of the scattering crystallites may appear [14].

Assuming a random (uniform) orientation of crystallites, the superimposition with a Gaussian distribution of oriented crystallites is a reasonable approach to fit the crystalline peak intensities as a function of the rotation angle [14]. This enables the estimation of intensity constants and provides a suitable description of the peak intensities in a very pragmatic way. Figure 4 shows experimental data representing the influence of the rotation angle on the crystalline peak intensities for unfilled and CB-filled NR (NR00 and NR20). From the estimated amounts of oriented and randomly distributes crystallites, the relative amounts of oriented crystallites for NR00 and NR20 are 91% and 72%, respectively.
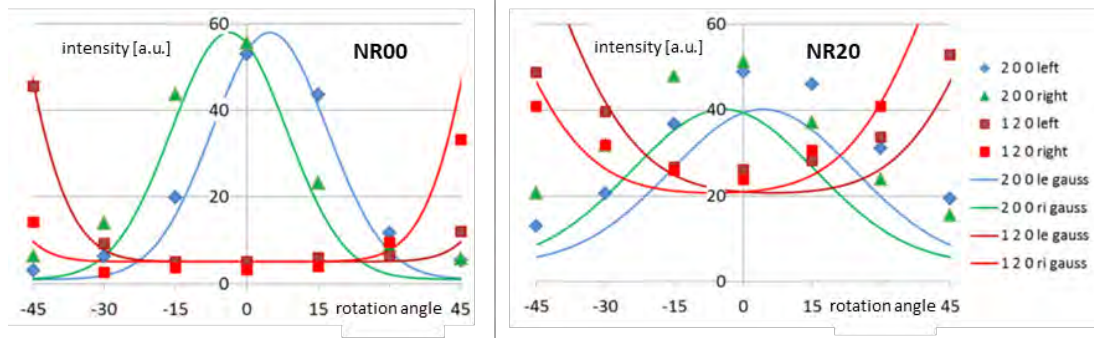


Figure 4: Crystalline peak intensities (symbols) and fitting curves (lines) of the intensities using a *Gaussian* distribution superimposed for NR00 (left) and NR20 (right); for both samples, the strain ratio was kept constant at 5:1 [14].

The *Scherrer* equation [17] enables a rough estimation of crystallite sizes in certain directions. For NR00 mean crystallite sizes have been estimated for (200) and (120) peaks as 25 nm and 9 nm, respectively. For NR20 mean crystallite sizes have been estimated for (200)

and (120) peaks as 20 nm and 8 nm, respectively. In the case of NR20, the number of crystallites oriented with respect to their *a*-axis is remarkably smaller than in the case of the unfilled samples. This is mainly caused by the constraint of crystallization due to the limited space between adjacent filler particles and not only by the inhomogeneous strain due to the constrained sample geometry.

## Conclusions

The experimental results show a clear impact of a constrained geometry on the orientation of strain-induced crystallites in NR (incl. the presence of reinforcing fillers). In fact, the reinforcing potential of SIC has an influence not only on the mechanical behavior of anisotropic loaded elastomer materials but also on their crack growth resistance. The anisotropic load ahead of the crack tip will influence the orientation of crystallites in the vicinity of the crack tip and, thus, the progress of the macroscopic failure.

Systematic tests on the orientation of crystallites due to inhomogeneous deformation are rarely performed, although they are always necessary when the deformation of the material suggests deviations from the SIC fiber symmetry. These deviations can be expected not only in "pure-shear" geometries leading to plane strain deformation but also very locally in the vicinity of crack tips. Spatially resolved investigations of the morphology and microstructure in front of crack tips will be realized within ongoing research activities.

## Acknowledgement

## References

[1] Toki, S.; Fujimaki, T.; Okuyama, M., *Polymer* **2000**, 41, 5423-5429.
[2] Trabelsi, S.; Albouy, P. A.; Rault, J., *Macromolecules* **2002**, 35, 10054-10061.
[3] Huneau, B., *Rubber Chemistry and Technology* **2011**, 84, 425-452.
[4] Brüning, K.; Schneider, K.; Roth, S. V.; Heinrich, G., *Macromolecules* **2012**, 45, 7914-7919.
[5] Rublon, P.; Huneau, B.; Verron, E.; Saintier, N.; Beurrot, S.; Leygue, A.; Mocuta, C.; Thiaudière, D.; Berghezan, D., *Engineering Fracture Mechanics* **2014**, 123, 59-69.
[6] Demassieux, Q.; Berghezan, D.; Cantournet, S.; Proudhon, H.; Creton, C., *Journal of Polymer Science Part B: Polymer Physics* **2019**, 57, 780-793.
[7] Le Cam, J. B., *Rubber Chemistry and Technology* **2010**, 83, 247-269.
[8] Euchler, E.; Bernhardt, R.; Schneider, K.; Heinrich, G.; Wießner, S.; Tada, T., *Polymer* **2020**, 187, 122086.
[9] Stoček, R., Dynamische Rissausbreitung in Elastomerwerkstoffen, Fakultät für Maschinenbau, TU Chemnitz, 2011.
[10] Moreira, D. C.; Nunes, L. C. S., *Polymer Testing* **2013**, 32, 240-248.
[11] Schieppati, J.; Schrittesser, B.; Wondracek, A.; Robin, S.; Holzner, A.; Pinter, G., *Engineering Fracture Mechanics* **2021**, 257, 108010.
[12] Buffet, A.; Rothkirch, A.; Dohrmann, R.; Korstgens, V.; Abul Kashem, M. M.; Perlich, J.; Herzog, G.; Schwartzkopf, M.; Gehrke, R.; Muller-Buschbaum, P.; Roth, S. V., *Journal of Synchrotron Radiation* **2012**, 19, 647-653.
[13] Stribeck, N., X-Ray Scattering of Soft Matter.Springer: Berlin Heidelberg, 2007.
[14] Schneider, K.; Schwartzkopf, M., *Crystals* **2019**, 9, 294.
[15] Takahashi, Y.; Kumano, T., *Macromolecules* **2004**, 37, 4860-4864.
[16] Nyburg, S., *Acta Crystallographica* **1954**, 7, 385-392.
[17] Patterson, A. L., *Physical Review* **1939**, 56, 978-982.

# Effect of temperature, time and molecular weight on the fracture behavior of soft thermoplastic elastomers

S. Sbrescia,[1] J.Ju,[2] C. Creton,[2] T.A.P. Engels,[3] M.E. Seitz[3]

1) Bio and Soft Matter Division (BSMA), Institute of Condensed Matter and Nanosciences (IMCN), Université Catholique de Louvain, Louvain-la-Neuve, Belgium.
2) Laboratoire Sciences et Ingénierie de la Matière Molle, ESPCI Paris, PSL University, CNRS, Sorbonne Université, Paris, France
3) Materials Science Center, DSM, Geleen, The Netherlands.
Simone.sbrescia@uclouvain.be; jianzhu.ju@espci.fr; costantino.creton@espci.fr; Tom.engels@dsm.com; Michelle.seitz@dsm.com

Thermoplastic elastomers (TPEs) are an important class of engineering polymers and are heavily used in many applications like breathable films, surgical products, wire and cable insulation, as well as fatigue resistant ducts, boots, and bellows.[1] However, little is known about their high temperature mechanical performance, including the fracture and fatigue behaviours, and how it is affected by chemistry and structure. Moreover, we evaluate the failure of these systems at different test conditions. We observe similarities, but also non trivial differences, between the effect of temperature and deformation rate, respectively, depending on the testing method, that are important to be aware of when designing with these materials. In this talk we show that:

- The effect of temperature is to decrease the materials toughness,[2,3] irrespective of the testing configuration. Additionally, increasing temperature changes the materials behaviour from highly deformable and notch resistant to extremely notch sensitive.
- The effect of rate shows opposed trends with different test geometry (Fig 1a-b), that can be understood by the strongly localized versus homogeneous deformation that is induced from the testing configuration.
- To improve the toughness of the system we confirm that the observed, strong influence of molecular weight on the failure strength, as shown for standard tensile experiments,[3] translates as well to more complex test geometries.
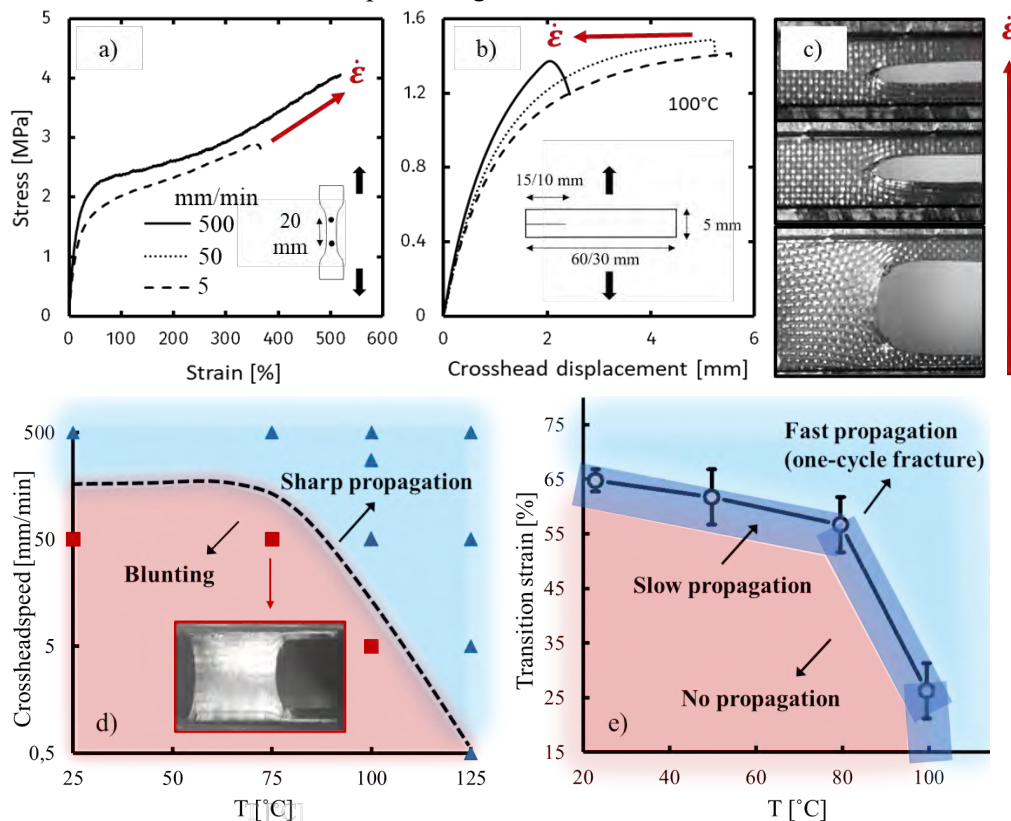
Fig. 1: Unnotched tensile test (a) and fracture test in pure shear geometry (b) at different crosshead speed. c) Snapshot of the blunting crack right before failure for different test speed (100 °C). d) From fracture tests: map presenting the effects of T and crosshead speed on the crack-propagation behavior. e) From fatigue tests: transition strain from a fast crack propagation to no propagation at all depending on applied strain and temperature.

## References

[1] Fakirov, S. In *Handbook of Condensation Thermoplastic Elastomer;* Wiley-VCH Verlag GmbH and Co, Weinheim: 2005.
[2] Aime, S.; Eisenmenger, N. D.; Engels, T. A. P.; *J. Rheol. (N. Y. N. Y)*, **2017**, 61 (6), 1329–1342.
[3] Sbrescia, S.; Ju, J.; Engels, T.; Van Ruymbeke, E.; Seitz, M.;. *J. Polym. Sci.*, **2021**,1-17.

# Microrheometric study of damage and rupture of capsules in simple shear flow

C. El Mertahi[1] , N. Grandmaison[1], C. Dupont[1], R. Jellali[1], D. Brancherie[2]
and A.-V. Salsac[1]

[1] *Biomechanics and Bioengineering Laboratory (UMR 7338), Université de Technologie de Compiègne - CNRS, Compiègne, France - a.salsac@utc.fr*
[2] *Roberval Laboratory, Université de Technologie de Compiègne, Compiègne, France - delphine.brancherie@utc.fr*

## Summary

Capsules under shear flow undergo fatigue phenomena which may lead to rupture. We considered bioartificial microcapsules made of ovalbumin reticulated with terephthaloyl chloride (TC) with the objective to characterize the impact of damage on the mechanical properties of the membrane. Moreover, we conducted a statistical study of the occurrence of rupture depending on the capsule radius. The break-up probability increases with the capsule radius.

## 1. Introduction

Capsules, which are liquid droplets enclosed in a thin elastic membrane, are present in nature (red blood cells, phospholipid vesicles) and in various industrial applications (biotechnology, pharmacology, cosmetics...). They are used to protect and transport active ingredients by isolating them from the external fluid suspension.

When placed in an external flow at high shear rates, capsules undergo deformation and damage. Rupture occurs when the capsule membrane loses its rigidity at some locations, making it incapable to resist any longer. Depending on the applications, capsule damage is to be prevented to preserve the encapsulated substance or on the contrary provoked to initiate the rupture and then the release of the inner fluid. It is thus necessary to understand the mechanisms responsible for damage and the parameters that control rupture initiation.

Numerous numerical studies have been conducted on the deformation of capsules [1, 2] by implementing a fluid-structure interaction model accounting for the membrane large deformations induced on a capsule subjected to an external flow. Recently, a damage model has been developed by Grandmaison et al [3] that accounts for the initiation and growth of microdiscontinuities and subsequently the local initiation of rupture. On the experimental side, very few studies have been carried out on the rupture of capsules. Chang & Olbricht [4] showed the capsule burst in a simple shear flow at high shear by membrane fatigue. In their study, the break up was initiated from one of the major axis tips of the deformed capsule and propagated in the shear plane. Rehage & Koleva [5] also observed the rupture of thin polysiloxane microcapsule under simple shear flow. The rupture occured in the central region, close to the tips of the flow vorticity axis (zones of maximum tension) at small deformations. Rupture was also observed in hyperbolic flow by Xie & al [6] using Chitosan/PFacidYN thin membrane. When the hydrodynamic stress exceeds the limit for breakup, the microcapsule stretches up leading to the formation of two lobs connected by a thin filament which is then destabilized in droplets.

None of the experimental studies carried out have investigated capsule damage phenoma. However, this is a crucial point in order to control rupture and build a reference set to validate the numerical damage models. To fill this gap, the objective of the present work is

dedicated to a rheometric study of the capsule damage and rupture based on an identification of the membrane mechanical properties. A decrease in the capsule surface shear modulus will inform on its damage and upcoming rupture. After having detailed the experimental setup and methods in Section 2, we present the results of the parametric identification of capsule damage in Section 3 and a statistical study of the rupture is presented in Section 4.

## 2. Experimental setup and methods

### 2.1. Capsule fabrication

Microcapsules are prepared by means of interfacial cross-linking of an emulsion of 1 ml of an aqueous solution, consisting of 10 % (w/v) ovalbumin (A5253-250G, Sigma) dissolved in phosphate buffer (P3619-1GA, pH=7.4, Sigma), mixed with 10 ml of vegetable oil (ISIO 4, Lesieur) using a laboratory vortex (Heidolph TopMix 94323). Then, 10 ml of vegetable oil containing 2.5 % (w/v) terephthaloyl chloride (120871-250G, Sigma) is added to the emulsion. The interfacial reticulation time is 15 min. Once prepared, capsules are rinsed before use and suspended in glycerol at a concentration of 2 %. Owing to concentration differences leading to osmotic effects, the capsules are pre-stressed with an inflation ratio $\alpha = \frac{a}{a_o} - 1 = 53$ %, where $a_o$ is the reference capsule radius and a the pre-stressed capsule radius.

### 2.2. Microrheometry

Our study of capsule motion is carried out in a Couette flow using two counter-rotating concentric cylinders as illustrated in figure 1 and between which we introduce a volume of 12 ml of capsules suspended in glycerol. The distance between the two cylinders is about 1 mm. After the capsules are placed in the region between the cylinders and the flow is started for a chosen shear rate, their motion and deformation are recorded by a video camera (model LM165M, Lumenera) mounted below the outer cylinder to provide a bottom view of the capsules. The capsule image is inverted by passing through a 45° mirror (figure 1). To enhance the resolution of the recorded images, a spot light (KL 1600 LED, SCHOTT) is used.
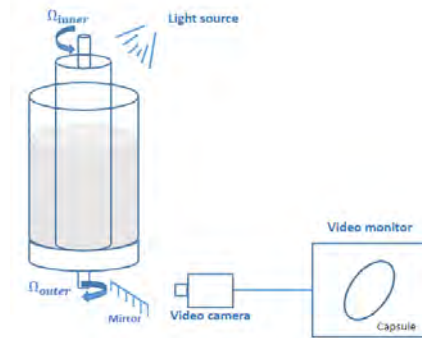


FIGURE 1 – Schematic of the Couette apparatus.

### 2.3. Identification of the membrane elasticity

To identify the surface shear modulus $G_s$ of the capsule membrane, an experimental-numerical strategy is used. From the experience, we know the values of the shear rate $\dot{\gamma}$, the viscosity $\mu$ of the capsule-in-glycerol suspension and the contour of a deformed capsule observed during the shear flow which is obtained manually using ImageJ. A least squares fit of the contour with an ellipse provides the values of the semi-axes $L_1$ and $L_2$ and then the Taylor parameter $D_{12} = \frac{L_1 - L_2}{L_1 + L_2}$. From previous numerical simulations of capsule deformation [1] we exploit the plot of variation of $D_{12}$ with the capillary number ($Ca = \frac{\mu \dot{\gamma} a}{G_s}$) $D_{12} = f(Ca)$ and the plot $L_3/a = g(D_{12})$, where $L_3$ is the third semi-axis of the deformed capsule [7]. From

$D_{12} = f(Ca)$ we obtain Ca. $L_3/a$ is obtained from $L_3/a = g(D_{12})$. The capsule radius a is obtained applying the volume conservation of the capsule : $a = \sqrt[3]{L_1 L_2 L_3}$. Finally the surface shear modulus $G_s$ is obtained through the expression $G_s = \frac{\mu \dot{\gamma} a}{Ca}$.

## 2.4. Probability of rupture

The capsule distribution in glycerol is considered to be homogeneous in this study. To identify the number of ruptured capsules, we quantify their number in a volume of 10 μl of the capsule-in-glycerol suspension, we shear the mixture using the microrheometer and we quantify the number of sheared capsules. We assume that the disappeared capsules are ruptured during the flow. The results of this study are presented in section 4.

# 3. Capsule damage

This section aims at presenting the results obtained in terms of the evaluation of the surface shear modulus $G_s$. We study its dependence on the size of the capsules and its evolution as a function of the exposure time to shear. To this end, we evaluate $G_s$ and the capsule radius following the method presented in 2.3 for different exposure times $t_E$.



(a) $t_E < 4$ min     (b) $5$ min $\leqslant t_E < 6$ min     (c) $t_E \geqslant 8$ min
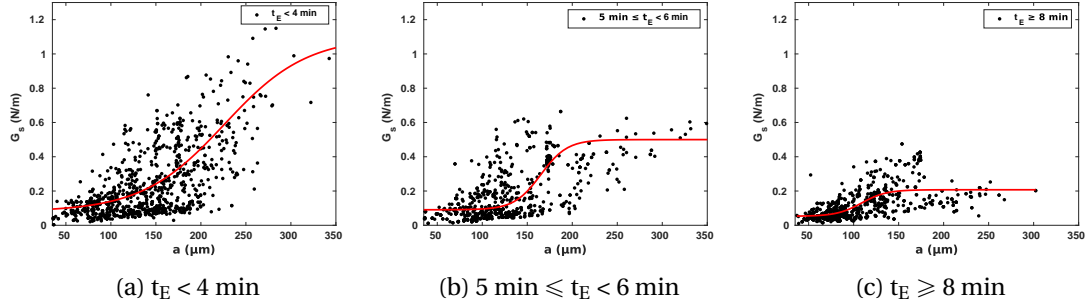
FIGURE 2 – $G_s$ evolution as a function of the capsules radius for different exposure times $t_E$

We present in Figure 2 the evolution of $G_s$ as a function of the capsules radius for different exposure times. We show that $G_s$ increases with the capsule radius and adjusts to a sigmoïd function. When the exposure time to shear $t_E$ exceeds 4 minutes, we observe a progressive decrease of the surface shear modulus for capsules of radius larger than 60 μm. In figure 3, we present specifically the evolution of $G_s$ as a function of the exposure time for capsules of specific sizes. We attribute this decrease in surface shear modulus to the degradation of the mechanical properties of the membrane.



(a) $70$ μm $\leqslant a \leqslant 75$ μm     (b) $120$ μm $\leqslant a \leqslant 125$ μm     (c) $150$ μm $\leqslant a \leqslant 155$ μm
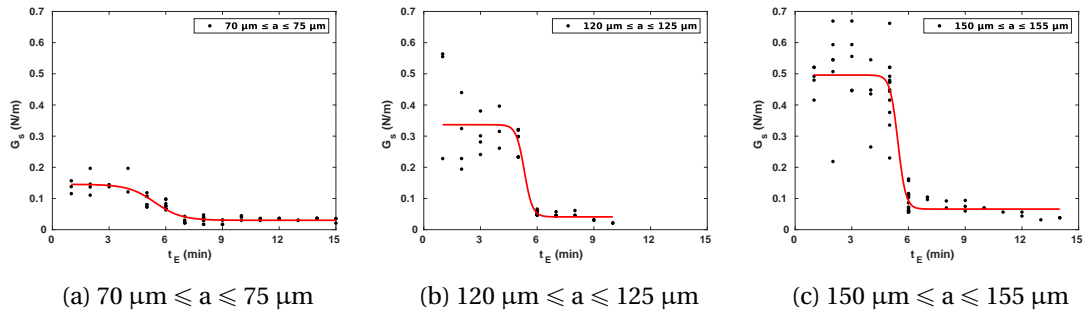
FIGURE 3 – $G_s$ evolution as a function of the exposure time to shear for three sizes of capsules

# 4. Capsule rupture

To obtain the percentage of ruptured capsules, we quantify their number before and after exposure to shear suspending them in simple shear flow for different exposure times $t_E$. In this study, we only present the results obtained for $t_E$ =10 min. The capsules no longer present at time $t_E$ are considered broken. In figures 4 and 5, we present the results obtained for capsules sheared at a rate of 300 s$^{-1}$ for 10 min and a viscosity of 0.95 Pa.s. As shown in figure 5, the percentage of disappeared capsules increases with their radius until their total disappearance for capsules having radius larger than 60 µm. This observation provides information on rupture kinetics. The capillary number of broken capsules (ratio of the viscous to the elastic forces), evaluated using equation (2) ranges from 0.12 to 0.2.
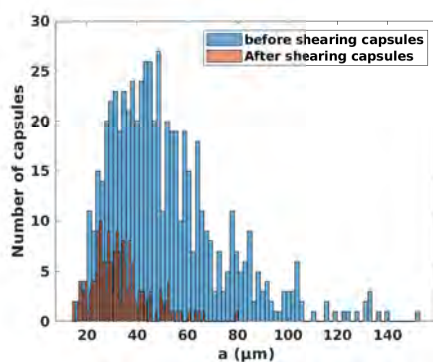


FIGURE 4 – Number of capsules in a volume of 10 µl.
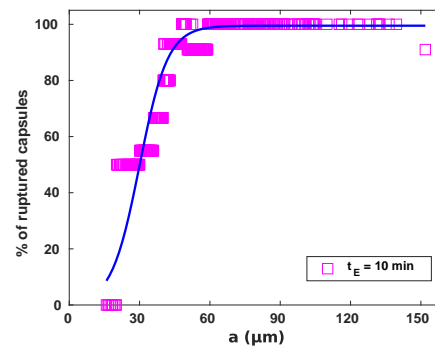


FIGURE 5 – Pourcentage of ruptured capsules as a function of their radius.

## 5. Conclusion

The study of damage is crucial to control and prevent capsule rupture. To be predictive, the damage models used in the simulations [3] must be identified. To this aim, we propose a parametric method based on the membrane mechanical properties evolution. Such an identification is a crucial point for the evaluation of the parameters of the damage models. The second point explored in this work is based on a statistical study of rupture kinetics depending on capsule radius.

## Références

[1] J. Walter, A-V. Salsac, D. Barthès-Biesel, and P. Le Tallec. Coupling of finite element and boundary integral methods for a capsule in a stokes flow. *International journal for numerical methods in engineering*, 83(7) :829–850, 2010.

[2] Z-Y. Luo, L. He, and B-F. Bai. Deformation of spherical compound capsules in simple shear flow. *Journal of Fluid Mechanics*, 775 :77–104, 2015.

[3] N. Grandmaison, D. Brancherie, and A-V. Salsac. Modelling of damage of a liquid-core microcapsule in simple shear flow until rupture. *Journal of Fluid Mechanics*, 914(A25), 2021.

[4] K-S. Chang and W-L. Olbricht. Experimental studies of the deformation and breakup of a synthetic capsule in steady and unsteady simple shear flow. *Journal of Fluid Mechanics*, 250 :609–633, 1993.

[5] I. Koleva and H. Rehage. Deformation and orientation dynamics of polysiloxane microcapsules in linear shear flow. *Soft Matter*, 8(13) :3681–3693, 2012.

[6] K. Xie, C. De Loubens, F. Dubreuil, D. Gunes, M. Jaeger, and M. Leonetti. Interfacial rheological properties of self-assembling biopolymer microcapsules. *Soft matter*, 13(36) :6208–6217, 2017.

[7] X-Y. Wang, A. Merlo, C. Dupont, A-V. Salsac, and D. Barthès-Biesel. A microfluidic methodology to identify the mechanical properties of capsules : comparison with a microrheometric approach. *Flow*, 1, 2021.

# Composites for sustainable development based on wood, wood fibers or nanocellulose fibrils – strain field data and mechanical properties

Lars Berglund

*Wallenberg Wood Sci Ctr*
*Dept of Fiber and Polymer Techn*
*KTH Royal Inst of Technology*
*SE-100 44 Stockholm, Sweden, blund@kth.se.*

Cellulose biocomposites are often described as eco-friendly materials, but this requires some analysis in order to select the best material for a given application. In addition, the mechanical performance needs to be comparable or superior to established materials, such as glass fiber composites. Wood is an interesting material source, since the tree is a renewable resource, mechanical fiber properties are superior to isotropic plastics and there is already an existing infrastructure for production of low-cost wood-based reinforcements and fibers. In addition, lignin and hemicelluloses may in practice improve interfiber or interfibril adhesion so that no polymer matrix or binder is needed.

The intrinsic mechanical cell wall properties of wood fibers appear to be more favorable than previously thought, provided good stress transfer can be ensured between material components. The potential of wood substrates, such as veneer, for multifunctional, load-bearing composites is well illustrated by optically transparent composites, although low transverse fracture toughness is a concern. Mechanisms have been clarified using digital image correlation (DIC) techniques in combination with a finite element updating (FEM-U) method. The limitation of wood substrate composites is in shaping, where molded fiber or nanocellulose materials can form more complex geometries.

Hot-pressed wood fibers are in essence nanocomposites, although failure properties are often controlled at micro- or even larger scales. Both Young's modulus and tensile strength values can be competitive with glass fiber composites, and reasons for this will be discussed. Comparable nanocellulose materials have somewhat better strength and strain to failure, but suffer low values for eco-indicators (eg cumulative energy demand) and the difficulty to control nanocellulose fibril orientation. The combination of DIC and FEM-U also offers insight into differences in deformation mechanisms between wood fiber and nanocellulose materials.

Although nanocelluloses have inferior eco-indicator values to wood fibers, they can be used as films or coatings in the form of multifunctional 2D platelet/nanocellulose composites. They can have very high content (>20vol%) of 2D platelets (eg graphene oxide, MXene, clay) with in-plane alignment as reinforcement for the nanocellulose matrix. Modulus ($\approx 40$GPa) and tensile strength (>500 MPa) can have high values, although modulus data are lower than even conservative theory would predict. The reasons are discussed in terms of stress transfer mechanisms between nanocellulose and 2D platelets.

# Embracing Complexity for Enduring and Adaptive, Organic Robots via Autonomous Materials

Robert F Shepherd, PhD

*Cornell University, College of Engineering*
*Sibley School of Mechanical & Aerospace Engineering, 553 Upson Hall, Ithaca, NY 14853*

Animals are semi-discretized. Systems of organs that perform multiple functions and are spatially discrete from each other, yet interconnected chemically and electrically. The complexity of animals such as vertebrate mammals allow for adaptation within a single generation that has allowed many examples of species that have thrived without genetic modification even during periods of significant environmental change. In the search for generally adaptive robots, useful for far field exploration missions, we believe that a similar model of complex, multifunctional, and interconnected organ systems of animals should be embraced, rather than avoided. Of course, it is not yet that simple to be complex, but we will present approaches we have used to distribute sensing, actuation, energy, and computation in soft robots. The framework we use for guiding our design evolution is Autonomous Materials, where we push the manufacturing of robots towards forming processes, and multifunctional use of material chemistry. The resulting machinery presented will be organic both in chemical makeup and subsystem analogy to organisms.



*Bio*:

Rob Shepherd is an associate professor at Cornell University in the Sibley School of Mechanical & Aerospace Engineering. He received his B.S. (Material Science & Engineering), Ph.D. (Material Science & Engineering), and M.B.A. from the University of Illinois in Material Science & Engineering. At Cornell, he runs the Organic Robotics Lab (ORL: http://orl.mae.cornell.edu), which focuses on using methods of invention, including bioinspired design approaches, in combination with material science to improve machine function and autonomy. We rely on new and old synthetic approaches for soft material composites that create new design opportunities in the field of robotics. Our research spans three primary areas: bioinspired robotics, advanced manufacturing, and human-robot interactions. He is the recipient of an Air Force Office of Scientific Research Young Investigator Award, an Office of Naval Research Young Investigator Award, and his lab's work has been featured in popular media outlets such as the BBC, Discovery Channel, and PBS's NOVA documentary series. He is an advisor to the American Bionics Project (americanbionics.org) which aims to make wheelchairs obsolete. He is also the co-founder of the Organic Robotics Corporation (ORC; lightlace.io), which aims to digitally record the tactile interactions of humans and machines with their environment.
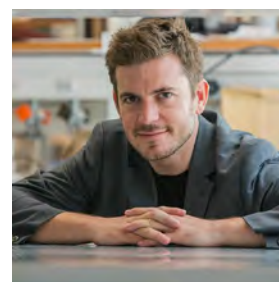
# Molecular stress and strain sensors for polymers

Christoph Weder[a]

*[a] Adolphe Merkle Institute, University of Fribourg, Chemin des Verdiers 4, 1700 Fribourg, Switzerland. christoph.weder@unifr.ch*

Mechanochemical transduction processes are omnipresent in nature. An emerging approach to exploit this general principle in artificial materials relies on the integration of so-called "mechanophores" – motifs that transduce mechanical forces into structural changes or chemical reactions – into polymers. Typical mechanophores are activated by cleaving weak covalent bonds, and the ensuing chemical reactions are harnessed to elicit an ideally useful property change. An alternative approach is the use of dynamic, weak, non-covalent interactions. Supramolecular motifs are particularly useful design elements for mechanophores that can impart polymers with reversible mechanochromic behavior. Several types of mechanophores that rely on this general design approach will be discussed, including motifs that rely on a combination of hydrogen-bonding and pi-pi stacking, rotaxanes, and "loopy" structures containing two interacting fluorophores. The solid-state mechanoresponsive characteristics of polymers containing these elements will be discussed.
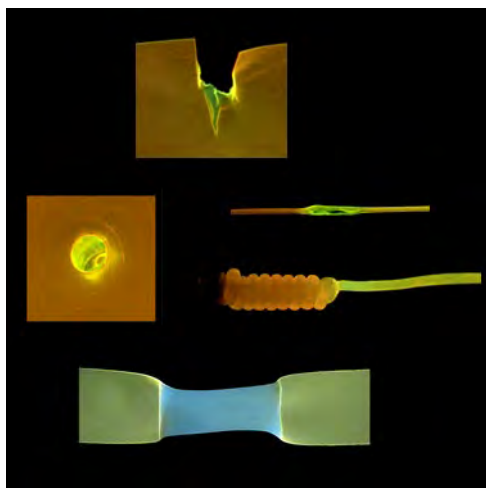
**References:**

Traeger, H.; Kiebala, J.; Schrettl, S.; Weder, C.; Folded Perylene Diimide Loops as Mechanoresponsive Motifs; Angew. Chem. Int. Ed. 2021, 60, 16191-16199.

Muramatsu, T.; Okado, Y.; Traeger, H.; Schrettl, S.; Tamaoki, N.; Weder, C.; Sagara, Y.; Rotaxane-based Dual Function Mechanophores Exhibiting Reversible and Irreversible Responses; J. Am. Chem. Soc. 2021, 143, 9884–9892.

Sagara, Y.; Traeger, H.; Jie, L.; Okado, Y.; Schrettl, S.; Tamaoki, N.; Weder, C.; Mechanically Responsive Luminescent Polymers Based on Supramolecular Cyclophane Mechanophores; J. Am. Chem. Soc. 2021, 143, 5519-5525.

# Modulation of supramolecular interactions in biomimetic fibrillar collagen hydrogels

J. Brun[1], N. Narshad-Iqbal[1], J. Perez[2], N. Pantoustier[1], A. Marcellan[1]

[1]*Soft Matter Science and Engineering Laboratory – (UMR7615), ESPCI Paris PSL - CNRS - Sorbonne Université, 10 rue Vauquelin Paris 75005, France – Email : julie.brun@espci.psl.eu*
[2] *Synchrotron Soleil, L'Orme des Merisiers, Saint-Aubin BP48, 91192, Gif-sur-Yvette Cedex, France.*
.

By using the self-assembly of collagen type I biopolymer, physical hydrogels were prepared *in vitro* to mimic biological tissues. Fibrillar dynamics is governed by supramolecular interactions which can be advantageously tuned to control the non-linear mechanical response while ensuring a good stability in aqueous media.

## Introduction

Among soft materials, hydrogels have very low rigidity (E < 100 kPa) and bear low deformation state (< 100%). Despite their high water content (> 80 wt%), recent artificial networks are now able to reach better mechanical properties such as rigidity and toughness.

Yet, it often implies the use of toxic crosslinking agents with tedious multistep process. Interestingly, hydrated biological materials reach exceptional performances exhibiting various ultrastructures with specific properties relying mainly on supramolecular interactions. By using the self-assembly only type I collagen, the major protein found in ExtraCellular Matrices (ECM), we aim to synthesise *in vitro* fibrillar hydrogels. Tuning the assembly of such polyampholyte proteins enables to reach good stability in physiological medium together with advanced mechanics, approaching the behaviour of biological tissues. We investigated the effect of conditioning parameters, such as anisotropy and chemistry with the objective to improve the final mechanical properties. We studied the effect of alignment in extruded collagen filament in comparison with bulk hydrogels. A chemical modulation of the supramolecular interactions in the collagen assembly was conducted by changing the nature of the aqueous bath. This work contributes to rationalize the effect of the conditioning (medium and mechanical history) on collagen assembly to help elaborating reinforcement strategies.

## Synthesis of biomimetic collagen hydrogel

The collagen is extracted in the laboratory from rat tail tendons in acidic solution. Then, a drying process allows to concentrate the collagen content ($\approx$ 5 wt%), as reported elsewhere [1]. This concentration is higher than the overlap concentration leading to a very soft gel (G'= 0.17 kPa, tan$\delta$ = 0.60). The self-assembly is then initiated by a pH-increase to neutralize the net charge of the collagen molecules resulting in the constitution of a periodic assembly presenting a fibrillar structure (0.5 - 5$\mu$m diameter). After this fibrillogenesis step, the final hydrogel is stable in water and has an increased rigidity (G' = 35 kPa, tan$\delta$=0.04) without any addition of crosslinking agent. This gel can either by under the form of a bulk sample after a moulding step (20x10x2 mm$^3$) or a continuous filament obtained by extrusion process (1 - 0.5 mm diameter). All samples are stored in aqueous solution during 4 days before mechanical experiment and its stability is checked after 14 days by swelling and calorimetry measurements.

## Results and discussion

*A biomimetic mechanical response: effect of structure and anisotropy*

Biological tissues are known to display a typical J-shape response under tensile loading. The curve is highly nonlinear with a *toe* and a *linear* region, respectively at small and high strain. This strain hardening behaviour is assigned to the fibrillary structure of collagen in ECM [2]. Depending on their function, tissues have different ultrastructures giving rise to specific mechanical responses. In Figure 1a, one can appreciate the difference of stiffness between a tendon and a cornea. If their hydration level is not similar (from 24 wt% for tendon to 4.5 wt% for cornea), their fibrillar collagen structure is also different in terms of anisotropy and size: tendon have bigger and very aligned fibres while corneas have an orthogonal plywood of smaller collagen fibres.

*In vitro* synthesized collagen hydrogels exhibit similar nonlinear responses, despite lower stress bearing capability (Figure 1b). Collagen hydrogels have a $E_{toe}$ ranging around 140 kPa ($\pm$ 50 kPa) which is relatively good considering the high amount of water (95 wt%) and the absence of chemical cross linking. As a guideline, collagen gels where self-assembly has been suppressed, *i.e* gelatin-like, demonstrates much softer behaviour (Figure 2b). Interestingly, the process can also affect the tensile response: the extruded collagen filament shows higher strain hardening with a $E_{linear}$ approaching 1 MPa. X-ray diffraction assess for a more anisotropic structure (more alignement) in the fibre by comparing the azimuthal profiles in Figure 1c.
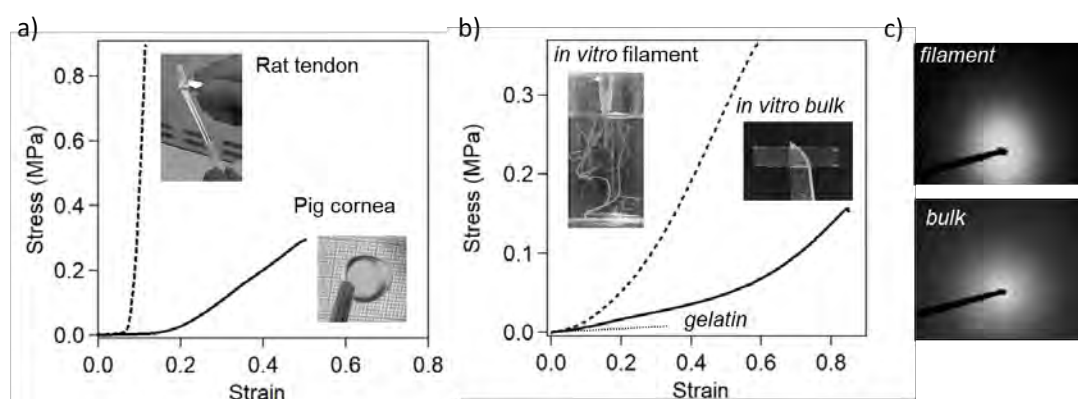


*Figure 1: Effect of structure and anisotropy from biological tissues to in vitro collagen hydrogels. a) Tensile test of a rat tail tendon (24 wt%) and a pig cornea (4.5 wt% from [3]). b) Tensile test of in vitro fibrillar collagen hydrogels (4.5wt%): an extruded filament of 700 μm diameter and a 2 mm-thick a bulk gel. A non-fibrillar gelatin bulk gel at 10 wt% is shown. c) SAXS pattern from SOLEIL beamline.*

*Chemical modulation of supramolecular interactions*

The collagen hydrogels were immersed in deionized water as the reference state. As collagen molecules have 20% of ionisable groups on its backbone, they interact with their aqueous environment depending on pH or ionic strength. The following study investigates the effect of conditioning medium on the hydrogel post gelation (fribrillogenesis). Changing the nature of the bath was found to deeply impact the stability and the mechanics of the hydrogels. As shown in Figure 2a, from pH 5.5 to 10, swelling equilibrium is almost the same with 4wt% collagen content and a rather low effect on hydrogel behaviour is observed, especially in the toe region. In very acidic or basic range (see two dotted curves at pH=4.5 and pH=12), the net charge is too high to neglect electrostatic repulsions leading to a partial destabilization of the structure with a drastic reduction of stiffness. At even more extreme pH, a gel can be completely dissolved demonstrating the full reversibility of the assembly. At constant pH,

ionic strength of the bath is found to induce severe weakening on tensile response, as shown in Figure 2b. With a NaCl content increasing from 0 M to 0.7 M, both rigidity and deformability drops, even for small concentrations of NaCl. When the salt content is higher than 0.15 M (*i.e.* the physiological value), the gels swell linearly with the salt concentration due to osmotic pressure resulting in a sharp drop of the toe modulus. As shown in Figure 2c, $E_{toe}$ scales with the swelling, Q to the power minus 4. The value is high compared to conventional network (n = -1 [4]) demonstrating that the supramolecular assembly is highly salt-sensitive.
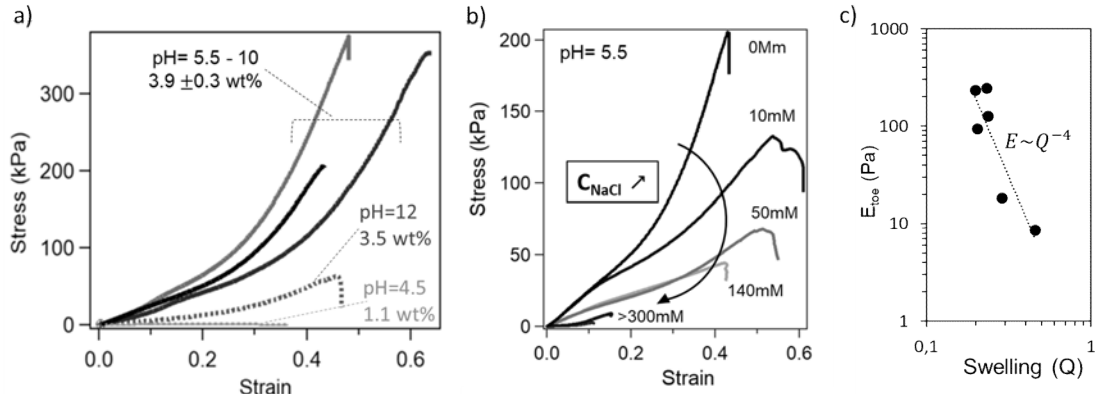


*Figure 2: Effect of the conditioning bath on bulk hydrogels mechanics. a) Tensile behaviour for gels soaked in different pH at low ionic strength. b) Tensile behaviour for various concentrations of NaCl (0 to 0.7 M) in pure water at pH ≈ 5.5. c) Evolution of the toe modulus with respect to swelling induced by salt addition (NaCl at 0 M to 0.7 M ).*

## Supramolecular assembly strengthened by pre-stretching

When the hydrogels were pre-stretched in immersion prior to testing, the resulting tensile response is significantly different from an un-stretched sample (0%). A global stiffening is observed in Figure 3a while conserving the non-linearity of the response. Both modulus in *toe* and *linear* region are increased as the amplitude of the pre-stretching increases. $E_{toe}$ and $E_{lin}$ respectively triple and double from 0% to 40% stretched samples. The influence of stretching is also pronounced in stress relaxation measurements: the more the gel is pre-stretched the higher the amplitude of relaxation is (see exponential decay in Figure 3b). Interestingly, the 40% elongated sample has the highest relaxation amplitude while being the stiffer indicating a high degree of relaxation mechanisms. Besides, the dynamics of the response suggest that the relaxation mechanisms are different.
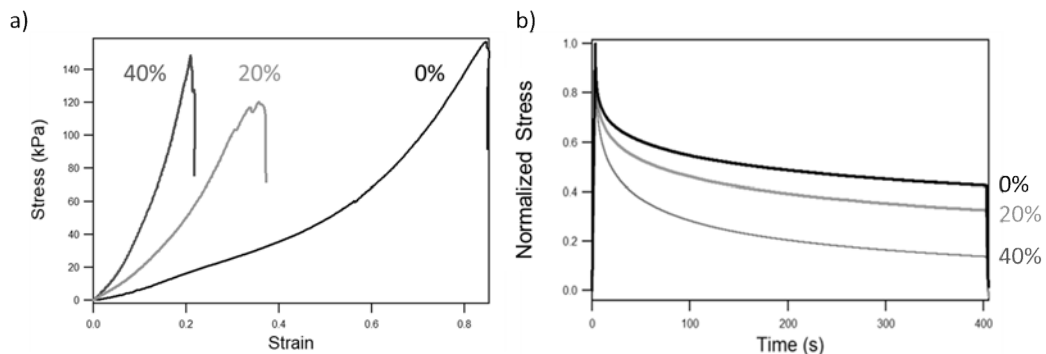


*Figure 3: Effect of the amplitude of pre-stretch on bulk collagen hydrogels after 4 days immersion in water. a) tensile response and b) stress relaxation at various elongations.*

## Conclusions

Dense *in vitro* collagen hydrogels display biomimetic features such as a fibrillar architecture and a nonlinear strain hardening behaviour. The mechanical response is relatively good considering the high amount of water (> 95 wt%) while being fully reversible (no chemical crosslinks). Bulk fibrillar gels have an initial modulus about 100 kPa, which is at least an order of magnitude higher than non-assembled gels. Extruded collagen filament has a more aligned fibrous structure with a higher strain hardening and stiffness, reaching almost 1MPa at high strain.

The final mechanical properties of hydrogels vary significantly depending on their aqueous environment. If pH has a rather low impact in a wide "user friendly" range, salt addition was shown to lead to more drastic swelling and thus lower rigidity. Even at low salt content, the addition of salt affects the intermolecular interaction between collagen fibres (this effect also depends on the type of salts). The mechanical history (pre-stretching) of the fibrillar assembly also impacts deeply the tensile response and the relaxation mechanisms.

To conclude, final properties of supramolecular collagen hydrogels can be tuned using both chemical and mechanical modulations. It contributes to provide a toolbox to improve mechanical properties of soft biomaterials and by analogy, helping to rationalize the behaviour of complex biological tissues.

## References

[1] Lama, M.; Raveendranathan, B.; Brun, J.; Fernandes, F. M.; Boissière, C.; Nassif, N.; Marcellan, A., *Macromolecular Bioscience* **2021**, 21, 2000435.

[2] Fratzl, P.; Misof, K.; Zizak, I.; Rapp, G.; Amenitsch, H.; Bernstorff S., *Journal of Structural Biology*, **1998,** 122, 119-122.

[3] Salameh, C.; Salviat, F.; Bessot, E.; Lama, M.; Chassot, J.-M.; Moulongui, E.; Wang, Y.; Robin, M.; Bardouil, A.; Selmane, M.; Artzner, F.; Marcellan, A.; Sanchez, C.; Giraud-Guille, M.-M.; Faustini, M.; Carminati, R.; Nassif, N., *Proceedings of the National Academy of Sciences of the USA* **2020**, 117, 11947-11953.

[4] Rubinstein, M.; Colby, R. H.; Dobrynin, A. V.; Joanny, J.-F., *Macromolecules* **1996**, 29, 398-406.

# Deformation and Fracture of Soft Collagenous Tissues

Edoardo Mazza[1,2], Serjosha Robmann[1], Eleni Kahle[1], Alberto Stracuzzi[1,2]
Adam Wahlsten[1], Alexander E. Ehret[1,2]

[1]*Department of Mechanical and Process Engineering, ETH, Zurich, Switzerland*
[2]*Empa, Swiss Federal Laboratories for Materials Science and Technology, Dübendorf, Switzerland*

A quantitative determination of the conditions leading to fracture of soft collagenous tissues (SCTs) is important for medical applications involving tissue cutting, perforation or suturing. As an example, premature rupture of fetal membranes is a major reason for neonatal morbidity and death. Although SCTs are generally considered as highly defect tolerant [1,2], fetal membranes can fail as a consequence of perforation for amniocentesis, suturing during prenatal surgery, or "embrittlement" due to influence of biochemical agents. These problems motivated a wide range of investigations aimed at an improved understanding of the deformation mechanisms and the fracture behavior of human amnion, the layer determining stiffness and strength of fetal membranes.

The asymmetric stiffness of collagen fibers, which is very low in compression and high in tension, and their organization as a network cause very large lateral contraction associated with outflow of interstitial fluid for SCTs loaded in uniaxial tension [3]. As a consequence, a strong compaction of the fiber network occurs in the nearfield of a defect, effectively avoiding propagation of cracks. Experiments performed within a multiphoton microscope provided quantitative information on the compaction process at the crack tip: on the one hand the collagen alignment was visualized using second harmonic generation, on the other the local deformation field was characterized based on the kinematics of the stained nuclei of epithelial cells. The "strip-biaxial" configuration was applied to determine the tearing energy of SCTs for a range of sample dimensions and environmental and loading conditions. In order to rationalize the experimental findings, we developed a dedicated computational framework based on a "hybrid" approach that combines a continuum model with a discrete fiber network model (DNM) for the nearfield of the defect [4,5]. The DNM represents collagen fibers as connectors, which are embedded in an isotropic matrix able to bind and release water. The discrete model introduces a length scale, thus avoiding the singularity at the crack tip, and allows implementing a fiber-level failure criterion, which governs material failure. The model confirms experimental observations indicating that the "short crack"-dimension in SCTs is in the *cm* range, despite a very narrow "process zone" (in the sub-*mm* range) and even though the fibres are elastic and brittle.

The present contribution applies and extends previous experimental and computational methods and quantifies the influence of loading rate, bath osmolarity and tissue hydration level on the deformation and fracture behavior of SCTs. For fetal membranes, the results provide useful insights for the development of surgical instruments and procedures in order to reduce the risk of iatrogenic preterm rupture.

## References

[1] Gordon JE. In *Structures or Why things don't fall down*, Plenum Press, New York (1978)
[2] Yang, W.; Sherman, V.R.; Gludovatz, B.; Schaible, E.; Stewart, P.; Ritchie, R.O.; Meyers , M.A.; *Nat Commun*, **2015**, 6, 6649
[3] Ehret, A.E.; Bircher, K.; Stracuzzi, A.; Marina, V.; Zündel, M.; Mazza, E.; *Nat Commun*, **2017**, 8, 1002
[4] Bircher, K.; Zündel, M.; Pensalfini, M.; Ehret, A.E.; Mazza, E.; *Nat Commun*, **2019**, 10, 792
[5] Bircher, K.; Ehret, A.E.; Spiess, D.; Ehrbar, M.; Simões-Wüst, A.P.; Ochsenbein-Kölble, N.; Zimmermann, R.; Mazza, E.; *Interface Focus*, **2019**, 9, 20190010

# Three-dimensional printing of biologically inspired composites from liquid crystal polymers

Kunal Masania[1,2], Silvan Gantenbein[1], Chiara Mascolo[1,2], Caroline Houriet[2], André R. Studart[1]

[1] *Complex Materials, Department of Materials, ETH Zürich, 8093 Zürich, Switzerland*
[2] *Shaping Matter Lab, Faculty of Aerospace Engineering, Delft University of Technology, 2629 HS Delft, Netherlands*

## Abstract

Lightweight biological materials such as bone, silk and wood, which demonstrate complex hierarchically structured shapes with outstanding mechanical properties by utilising directed self-assembly to grow structures. Here[1], we demonstrate a bioinspired 3D printing approach to create lightweight structures with hierarchical architectures, complex geometries and unprecedented stiffness and toughness. By self-assembly of liquid crystal polymer molecules, orienting the molecular domains with the print path, we can reinforce the polymer according to the expected mechanical stresses. The resulting material is recyclable and leads to stiffness, strength and toughness that outperform state-of-the-art 3D printed polymers by an order of magnitude and rival even the high-performance composites.

Thermotropic LCPs form nematic liquid crystalline domains when melted. These domains can be aligned in the FDM nozzle along the extrusion direction. After exiting the nozzle, solidification stops the thermal reorientation of the molecules due to the cessation of flow resulting in a skin-core morphology. The maximal Young's modulus and strength were achieved when printing parallel (0°) to the loading direction (17 GPa stiffness and 400 MPa strength). The dependence of the modulus on the print direction can successfully be predicted using a classical laminate theory approach. It is possible to adapt the local material architecture to the specific loading conditions that are applied to the part by designing the filament deposition direction during 3D printing. We show 3D printed objects with stress-adapted print line architecture with mechanical properties that are much stronger than state-of-the-art 3D printed polymers and rival the highest performance lightweight materials using a readily available polymer and a commercial desktop printer.

In addition, we present a new approach to combine conventional 3D printing with in-situ spinning of fibres. By controlling the volume of molten polymer at the nozzle tip and rapidly translating the printhead, we are able to spin fibres with diameters down to 20 um, reaching tensile strength and Young's modulus as high as 2.6 GPa and 208 GPa, respectively. These values are comparable to those of carbon fibres, which require energy-intensive fabrication processes. By spin-printing complex-shaped structures with unusual fibre-reinforcing architectures, we show that this new manufacturing platform opens new opportunities for the design and fabrication of lightweight parts combining recyclability and high mechanical performance.

## References

[1] Gantenbein, S., Masania, K., Woigk, W., Sesseg, J., Tervoort, T. A. and Studart. A.R. "Three-dimensional printing of hierarchical liquid crystal polymer structures", Nature, 561 (2018): 226-230.

# Molecular Weight Dependence of Crack Growth in Polyethylenes, "Slip Slidin' Away"

Robin R.J. Cerpentier[1], Mark J. Boerakker[2], Theo A. Tervoort[3] and Leon E. Govaert[1]

[1]*Einhoven University of Technology, 5600 MB Eindhoven, the Netherlands, [2]SABIC, Technology Centre Geleen, 6167 RD Geleen, the Netherlands, [3]ETH Zurich, 8093 Zurich, Switzerland.*

Summary: please provide a 50 word summary of the manuscript. Use the alignment set in this manuscript.

## Abstract

In order to find a relation between crack growth resistance and molecular weight of polyethylene, the fatigue crack propagation of polyethylene is studied on a large series of homopolymer grades with substantial variation in the molecular weight distribution. Fatigue crack growth experiments, lasting up to 1 month, were performed at room temperature on compact tension samples, using an optical technique to monitor crack propagation. The experimental results indicate that the crack growth kinetics follow the Paris-Erdogan law with a slope *m* that is identical for all grades, whereas the pre-factor *A* displays a strong dependence on molecular weight. Closer analysis reveals that *A* is predominantly governed by the weight average molecular weight *Mw*, with a small correction for the width of the distribution.

Experiments at different temperatures revealed a somewhat complex temperature dependence, giving evidence of a change in kinetics over the temperature range covered (20-90 °C), indicating the presence of two separate processes contributing to crack propagation. This change in kinetics was observed to be identical for all homopolymer grades, irrespective of the molecular weight distribution. Since the activation energies of both processes are considerably lower than that of chain scission (430 kJ/mol), both processes appear to be related to mechanisms of chain diffusion through the crystalline lamellae. The activation energy of 125 kJ/mol of the high temperature process suggest a relation to the well-known alpha relaxation process (screw-jump diffusion). The low temperature process has a much lower activation energy of 50 kJ/mol. Potential mechanisms will be discussed.
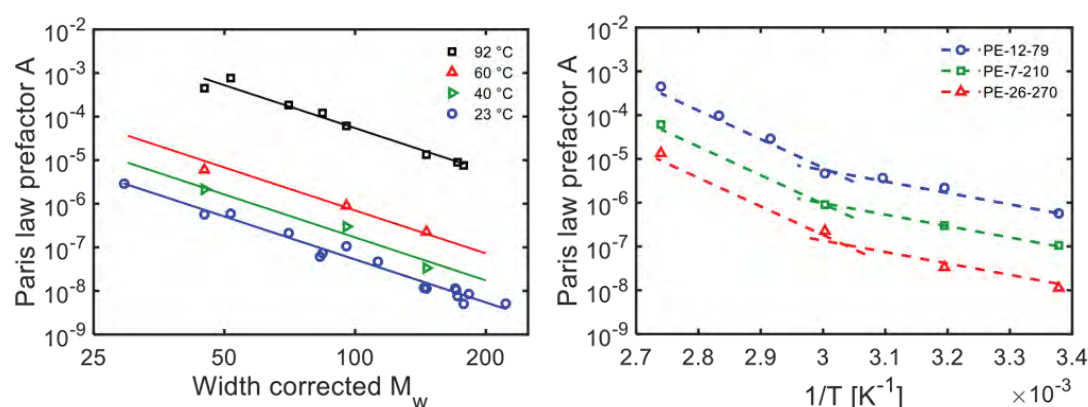


Figure 1. (left) Paris law prefactor *A* versus the width corrected *Mw* for different temperatures. (right) Arrhenius plot showing the temperature dependence of three homopolymer grades.

# Fatigue behaviour of thermoplastic bulk materials under mixed mode loading conditions

Anja Gosch[1], Florian J. Arbeiter[1], Michael Berer[2], Tomáš Vojtek[3,4], Pavel Hutař[3], Gerald Pinter[1]

[1] Materials Science and Testing of Polymers, Montanuniversität Leoben, 8700 Leoben, Austria.
[2] Polymer Competence Center Leoben GmbH, 8700 Leoben, Austria
[3] Institute of Physics of Materials, Academy of Sciences of the Czech Republic, 61662 Brno, Czech Republic
[4] Central European Institute of Technology (CEITEC), Brno University of Technology, 61200 Brno, Czech Republic

## Abstract

The fatigue behaviour of thermoplastic bulk materials under mixed mode I/III loading, a combination of tensile and out of plane shear loading, is scarcely investigated. Nevertheless, it can play a significant role in applications, such as rolling bearing elements. To avoid premature failure of loaded elements in application, the mixed mode contributions have to be accounted for. Therefore, it is necessary to develop both, testing methods, as well as a deeper understanding of the respective materials under mixed mode loading situations.

The current work shows the development of a testing procedure which is suitable to describe the influence of mixed mode I/III loading on thermoplastic bulk materials based on the cyclic cracked round bar specimen. It was shown, that the influence of mixed mode I/III loading can be described using an equivalent stress intensity factor $\Delta K_{eq}$, [1] as long as heat generation due to crack flank friction, as shown in Figure 1 [2], is kept low enough.

To gain a better understanding of the effect of mixed mode loading on thermoplastic materials a mix of technical (polyoxymethylene [1], polyetheretherketone) and commercial (high density polyethylene [2]) polymers were investigated via fatigue tests and accompanying fractographical analysis.
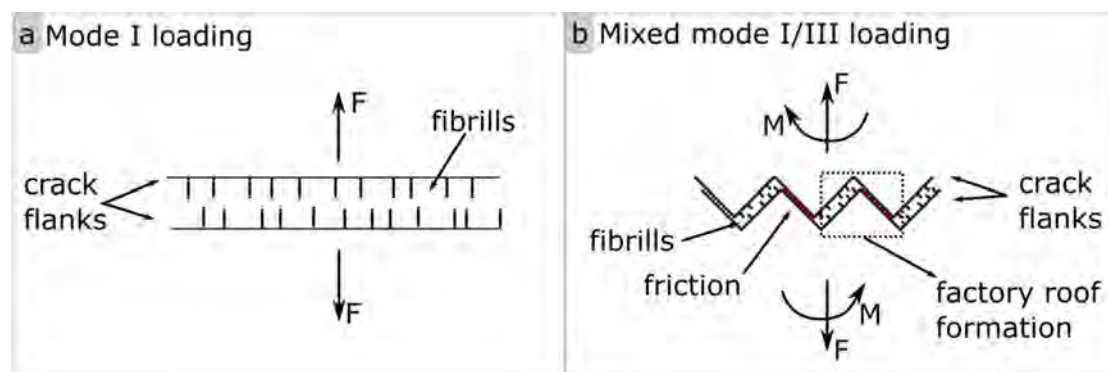
Figure 1: Schematic representation of the influence of pure mode I (a) and mixed mode I/III (b) loading on the local failure mechanism in polyethylene [2].

## References

[1] Gosch A, Berer M, Hutař P, Slavik O, Vojtek T, Arbeiter F, Pinter GG. Mixed Mode I/III fatigue fracture characterization of Polyoxymethylene. International Journal of Fatigue. 2019, vol. 130.2020, no. January, 105269.
[2] Gosch A, Arbeiter F, Berer M, Vojtek T, Hutař P, Pinter GG. Fatigue characterization of polyethylene under mixed mode I/III conditions. International Journal of Fatigue. 2020, vol. 145.2021, no. April, 106084.

# The mechanism behind the impressive fatigue threshold of soft thermoplastic elastomers

Giorgia Scetta[1], Nathan Selles[2], Patrick Heuillet[2], Matteo Ciccotti[1*] and Costantino Creton[1*].

[1]*Sciences et Ingénierie de la Matière Molle, ESPCI Paris, Université PSL, CNRS, Sorbonne Université, 75005, Paris, France.*[2]*Laboratoire de Recherches et de Contrôle du Caoutchouc et des Plastiques , 60, Rue Auber 94408 Vitry-sur-Seine, France*

Thermoplastic polyurethane elastomers (TPU) are a class of polymers characterized by high strength and toughness coupled with large extensibility and reversible elasticity. The origin of this combination of properties, in absence of chemical reticulation and filler particles, is generally associated to TPU's multiphase structure consisting in soft and hard domains physically crosslinked by hydrogen bonds. Despite the ever-increasing interest in TPU, which are often proposed as a sustainable alternative to classical crosslinked elastomers, their behaviour under cyclic fatigue loading, which is crucial for engineering applications,  has not been clarified yet.

Using the classical fracture mechanic approach, slightly modified to account for the viscoelastic character of TPU, we demonstrated that three different commercial TPU (with similar Young modulus close to 10MPa) not only have excellent toughness (50-140kJ/m2)[1], but also present values of fatigue threshold (1000-2000J/m2)[1] almost one order of magnitude higher than those of crosslinked elastomers[2,3] (50-100J/m2).

If the dissipation of energy produced in the fragmentation of hard domains can explain the excellent toughness in TPU, it doesn't explain such a high fatigue threshold. The latter is therefore an intriguing characteristic, common to several TPU and independent of their large-strain behaviour, which requires a different explanation.

By comparing the stress-strain response under cyclic loading between different TPU with a representative crosslinked rubber we discover that, only for TPU the typical strain-induced softening was followed by un unconventional strain-induced stiffening (represented as a permanent increase in the Young modulus). The strain-stiffening takes place only above a critical value of strain and it was associated with the fragmentation of the original hard domains into smaller but more homogeneously dispersed units[4]. Using digital image correlation (DIC) and X-Ray analysis, we proved that such strain-stiffening behaviour, when associated with inhomogeneous strain (as in  the crack tip area of a notched sample under cyclic fatigue), produces a permanent local re-arrangement of the TPU domains. Since the mechanical properties of TPU are intrinsically related to their microstructure, the newly formed inhomogeneous material presents a gradient in stiffness which gradually increases between the bulk and the crack tip area. We argue that the combination of highly deformable material in the bulk (softened during cycles) and hard core at the crack tip (strengthened during cycles) is the key to explain the observed reduction of strain gradient in fatigue material which is responsible for the observed  high fatigue threshold[5] (Figure 1).

We proposed, for the first time, that the strain-induced strengthening in TPU coupled with inhomogeneous strain is the key to explaining the high fatigue threshold of soft TPU. We believe that this mechanism, which in TPU naturally stems from their multi-phase morphology, could be very effective if reproduced by design in other soft polymers where simultaneous high toughness and fatigue threshold are highly desirable.
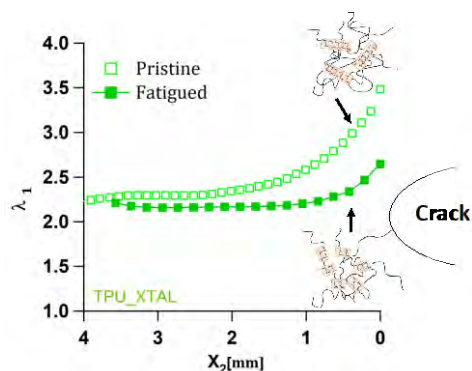
Figure 1: Maximum stretch in the loading direction at different distances from the crack tip. The fragmentation of domains is responsible for the reduction of maximum strain in fatigued sample.

1.    Scetta G, Selles N, Heuillet P, Ciccotti M, Creton C. Cyclic fatigue failure of TPU using a crack propagation approach. *Polym Test*. 2021;97:107140. doi:https://doi.org/10.1016/j.polymertesting.2021.107140

2.    Lake GJ, Thomas AG. The Strength of Highly Elastic Materials. *Proc R Soc A Math Phys Eng Sci*. 1967;300(1460):108-119. doi:10.1098/rspa.1967.0160

3.    Bhowmick AK. Threshold Fracture of Elastomers. *J Macromol Sci Part C*. 1988;28(3-4):339-370. doi:10.1080/15583728808085379

4.    Scetta G, Ju J, Selles N, Heuillet P, Ciccotti M, Creton C. Strain Induced Strengthening of Soft Thermoplastic Polyurethanes Under Cyclic Deformation. *J Polym Sci*. 2021;1(12).

5.    Scetta G, Euchler E, Ju J, et al. Self-organization at the crack tip of fatigue-resistant thermoplastic polyurethane elastomers. *Macromolecules*. 2021;((accepted, in press)).

# Accurate fatigue life prediction of injection moulded short glass fiber reinforced plastics parts

Marc J.W. Kanters, Lucien F.A. Douven

*DSM Engineering Materials, P.O. Box 1066, 6160 BB Geleen, The Netherlands*

Plastics are used in a large variety of applications and the demand for plastics is still increasing. With typical benefits, like freedom in design, ease of processing, reduction in cost, and high specific strength and stiffness, they can offer weight reduction when replacing metals and therefor the upcoming trend is to design load bearing structural parts in reinforced plastics.

Predictability is key when designing load bearing components: to be able to reduce development time, design first time right, and ensure part performance in service. This requires accurate modelling of all relevant performances such as part stiffness, strength, durability, impact, noise, vibration and harshness (NVH), creep deformation, and chemical- and thermal stability. This work focusses on durability, i.e. fatigue lifetime, predictions of injection moulded short glass fiber reinforced plastics (SFRP).

In order to improve the accuracy of fatigue lifetime predictions, a step-by-step approach is taken where the complexity in loading conditions, anisotropy, and stress state is increased systematically. This allows validation of methods, identification of potential gaps, and provides direct leads for improvement [1].

It shows that there are many challenges: First of all it is essential to properly understand and model the mechanisms that lead to failure for a wide range of load amplitudes. Next, it is key to accurately capture the local glass fiber orientation after processing and incorporating it into the stress and failure calculation. The latter comprises features such as describing the microstructure in high detail, using local stresses for material model calibration, comparing approaches based on anisotropic linear elastic or anisotropic elastoplastic material models, applying methods to compensate for local stress concentrations in the cases of highly localized stresses, and incorporating local load amplitudes.

This paper will discuss these key features in more detail, and we will present two application-representative demonstrator parts (a load bracket and a ribbed beam) to demonstrate that this deep-dive has led to a framework that can accurately predict failure of injection moulded short glass fiber reinforced plastics parts.

## References

[1] Kanters, M.J.W.; Douven, L.F.A.; Savoyat, P., *Procedia Structural Integrity,* **2019**, 19, 698

# Combined effect of environment and mechanical loadings on the damage behaviour of reinforced PA 66

Simon Lottier[1,2,3], Nicolas Saintier[1], Bruno Fayolle[2], Guillaume Miquelard-Garnier[2], Laurent Gervat[3]

[1] Arts et Métiers ParisTech, Laboratoire I2M, Espl des Arts et Métiers, 33400 Talence, France
[2] Arts et Métiers ParisTech, Laboratoire PIMM, 151 Bd de l'Hôpital, 75013 Paris, France
[3] Renault Technocentre, 1 Av du Golf, 78280 Guyancourt, France

* simon.lottier@ensam.eu

Composite materials used in engines are subjected to various solicitations which often include coupled mechanical and environmental solicitations. However, these coupling effects are yet poorly understood. This study concerns the combined effect of mechanical fatigue and hydrolysis or oxidation ageing in short glass fibres reinforced polyamide 66 (PA66GF30).

In this work, both weak and strong coupling are investigated. First the effects of pre-oxidation and pre-hydrolysis on the fatigue behaviour is analysed. A detailed analysis of hydrolysis and oxidation on molecular structure is proposed. A particular attention is given to the gradient of molecular changes near the surface in the case of oxidation (molar mass, crystallinity, density) which are found to play a major role in the subsequent fatigue damage mechanisms. Fatigue damage mechanisms are analysed by means of detailed SEM fractography. In addition, high resolution synchrotron micro-tomography was performed to observe the initial damage induced by oxidation and hydrolyses on the virgin material, and the evolution of damage induced by the fatigue loading. The observed damage mechanisms will be compared to the detailed fatigue mechanisms already identified on those materials by a previous study using similar technics [1].

Based on those observations a fatigue criterion will be proposed to take account for the effect of ageing on the fatigue behaviour [2].
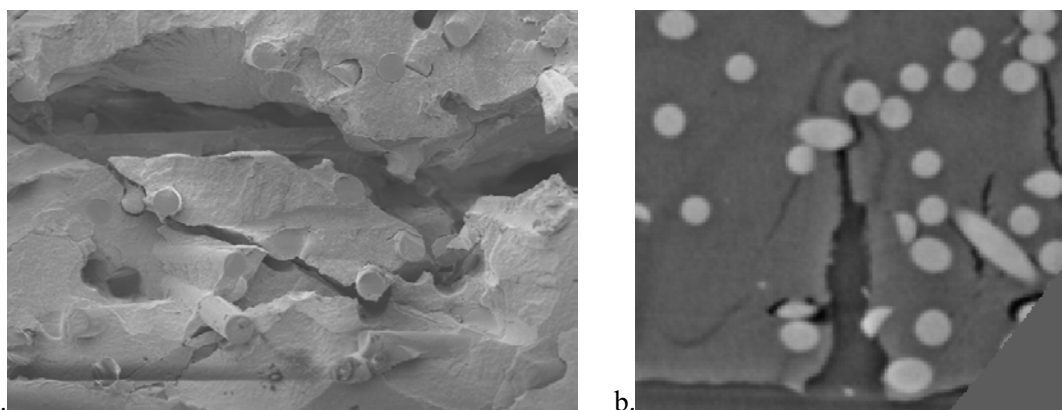


Fig. 1 – Oxidized PA66GF30 after fatigue break, near surface, a. SEM, b. microtomography

## References

[1] Rolland, H.; Saintier, N.; Raphael, I.; Lenoir, N.; King, A.; Robert, G., *Polymer* **2018**, *143*, 217-229
[2] Raphael, I.; Saintier, N.; Rolland, H.; Robert, G.; Laiarinandrasana, L., *International Journal of Fatigue* **2019**, *127*, 131-143

# Tough gels with weak bonds

Alba Marcellan

*Sciences et Ingénierie de la Matière Molle*
*ESPCI Paris, Université PSL, CNRS, Sorbonne Université, 75005 Paris, France*

Wet and soft matter – as synthetic hydrogels – has attracted increasing interest in the materials science community. Significant breakthroughs have been made in the field, especially in terms of mechanical toughening. New gel designs with advanced mechanical responses suggest that gels could be key players in the development of emerging technologies such as soft robotics, electronics, or tissue engineering.

Conventional synthetic gels are mainly made of water – typically above 90% water – and behave like soft elastic solids. Polymer chains are organized into a percolating network at macroscopic scale with mesh sizes of the order of a few tens of nanometers. To prevent the fracture, one option consists of eliminating defects by designing ideal networks with a perfect control of mesh size distribution. However, this method is difficult to carry out and inefficient in practice. We have adopted a different strategy, taking advantage of gel's intrinsic fragility and introducing dynamic heterogeneities. Based on polymer physics principles, we have designed model gels that combine a conventional polymer network and the addition of weak reversible sacrificial interactions. Unlike conventional covalent bonds, these weak interactions have a low selectivity and can readily break and re-form, ensuring topological adaptation of the network under stretch. Working cooperatively, such reversible sacrificial bonds allow the gel to combine paradoxical properties, such as enhanced rigidity and shape recovery together with self-repair abilities. This concept of gel toughening by weak bonds extends to gel adhesion and suggests bridges with living matter.

In a global context of preservation of resources and production of materials with low environmental impact, gels open tracks for the rational and efficient design of high performance synthetic polymers.

Rose, Dizeux, Narita, Hourdet, Marcellan; Time Dependence of Dissipative and Recovery Processes in Nanohybrid Hydrogels, Macromolecules (2013).

Rose, Prevoteau, Elziere, Hourdet, Marcellan, Leibler; Nanoparticle solutions as adhesives for gels and biological tissues, Nature (2014).

Guo, Sanson, Hourdet, Marcellan; Thermoresponsive Toughening with Crack Bifurcation in Phase-Separated Hydrogels under Isochoric Conditions, Advanced Materials (2016).

Hu, Barbier, Li, Ji, Le Blay, Hourdet, Sanson, Lam, Marcellan, Tang ; Hydrophilicity-Hydrophobicity Transformation, Thermoresponsive Morphomechanics, and Crack Multifurcation Revealed by AIEgens in Mechanically Strong Hydrogels, Advanced Materials (2021).

Lama, Raveendranathan, Brun, Fernandes, Boissiere, Nassif, Marcellan ; Biomimetic Tough Gels with Weak Bonds Unravel the Role of Collagen from Fibril to Suprafibrillar Self-Assembly, Macromolecular Bioscience (2021).

# Controlling and studying touch perception through adhesion, friction, and soft matter phenomena

Prof. Charles Dhong

*cdhong@udel.edu*
*Department of Materials Science and Engineering*
*Department of Biomedical Engineering*
*University of Delaware*

Compared to sound or vision, technologies to control sense of touch remain relatively underdeveloped. A key challenge for controlling and understanding touch is that the mechanical interface between the finger and an object is complex[1], yet these spatial and temporally varying mechanical forces ultimately give rise to tactile perception. Therefore, understanding or controlling touch is fundamentally an adhesion and interfaces problem, and well-positioned for innovations from soft matter mechanics and materials. Here, we discuss two areas. First, through silane monolayers on surfaces smoother than discriminable by touch, we showed that humans are sensitive to single atom substitutions in the silane due to transitions in monolayer ordering. Through mechanical testing, we were able to predict which materials which might generate enough differences in friction prior to human testing, thereby generating a library of potential tactile materials.[2] Second, the human sense of softness was thought to depend on indentation depth and contact area.[3] However, due to JKR mechanics of bulk objects, prior studies were not able to decouple the contributions from indentation depth from those of contact area on the human perception of softness. Through thin-film confinement and surface patterning, we were able to create a systematic series of samples which varied in the ratio of indentation depth and contact area. Results from human studies yielded a design equation for the human sense of softness as a function of indentation depth and contact area, which for bulk materials, translated to a 2-fold increase in softness for a 3-fold decrease in elastic modulus. Furthermore, subjects tended to have a consistent ordering of our samples, even though they were presented only two at a time. Consequently, the human sense of softness was found to be transitive, or potentially universal between subjects. Together, these studies demonstrate that materials and mechanics innovations could contribute to new touch technologies for virtual reality, rehabilitation, and basic biology.

## References

[1]   D. J. Lipomi, C. Dhong, C. W. Carpenter, N. B. Root, V. S. Ramachandran, *Adv. Funct. Mater.* **2019**.

[2]   A. Nolin, A. Licht, K. Pierson, C.-Y. Lo, L. V Kayser, C. Dhong, *Soft Matter* **2021**, *17*, 5050.

[3]   C. Dhong, R. Miller, N. B. Root, S. Gupta, L. V Kayser, C. W. Carpenter, K. J. Loh, V. S. Ramachandran, D. J. Lipomi, *Sci. Adv.* **2019**, *5*, eaaw8845.

# Wet Adhesion and Bioadhesive Technology

Xuanhe Zhao

*MIT*

Two dry surfaces can instantly adhere upon contact with each other through intermolecular forces such as hydrogen bonds, electrostatic interactions and van der Waals interactions. However, such instant adhesion is challenging when wet surfaces such as body tissues are involved, because water separates the molecules of the two surfaces, preventing interactions. Although tissue adhesives have potential advantages over suturing or stapling, existing liquid or hydrogel tissue adhesives suffer from several limitations: weak bonding, low biological compatibility, poor mechanical match with tissues, and slow adhesion formation. This talk will discuss how to address these challenges in wet adhesion and bioadhesives with a new dry-crosslinking mechanism and a new class of bioadhesives capable of forming fast, tough and biocompatible adhesion with diverse organs and devices. I will then discuss a set of new applications enabled by the bioadhesive technology, including bioadhesive drug delivery, bioadhesive electronics, coagulation-independent bioadhesive hemostasis, and bioadhesives for robotic surgery.

# Pressure Tunable Adhesion of a Rough Elastomer

Naomi Deneke[1], Jamie Booth[2], Edwin Chan[3], Chelsea S. Davis[1]

[1]*School of Materials Engineering, Purdue University, West Lafayette, IN, USA. chelsea@purdue.edu*
[2]*School of Mechanical Engineering, California State University-Northridge, Northridge, CA, USA*
[3]*Material Science and Engineering Division, National Institute of Standards and Technology, Gaithersburg, MD, USA*

*Introduction*

Control of adhesion strength is important in many applications like wearable adhesives, pressure sensitive adhesives, and robotics. Additionally, achieving multiple adhesion strengths is ideal for applications like pick-and-place manufacturing. A popular method for controlling adhesion is by physically altering the material surface through roughening or patterning. However, these techniques typically result in control of a finite adhesion strength or switchable adhesion. We have developed a material capable of achieving multiple, discrete adhesion strengths by varying the applied load.[1]

*PTA Fabrication*

A pressure tunable adhesive (PTA) is made by thermally annealing a glassy thin film, polystyrene (PS), on a bulk elastomer, polydimethylsiloxane (PDMS) above the glass transition temperature of PS. A schematic is presented in Figure 1.a. Due to differences in surface energy, the PS dewets to form microscopic droplets on the PDMS surface that then solidify when the material is quenched. The size and spacing of the droplets can be controlled by changing the pre-annealing film thickness as seen in Figure 1.b. 5 sample types were fabricated varying in droplet size and spacing.
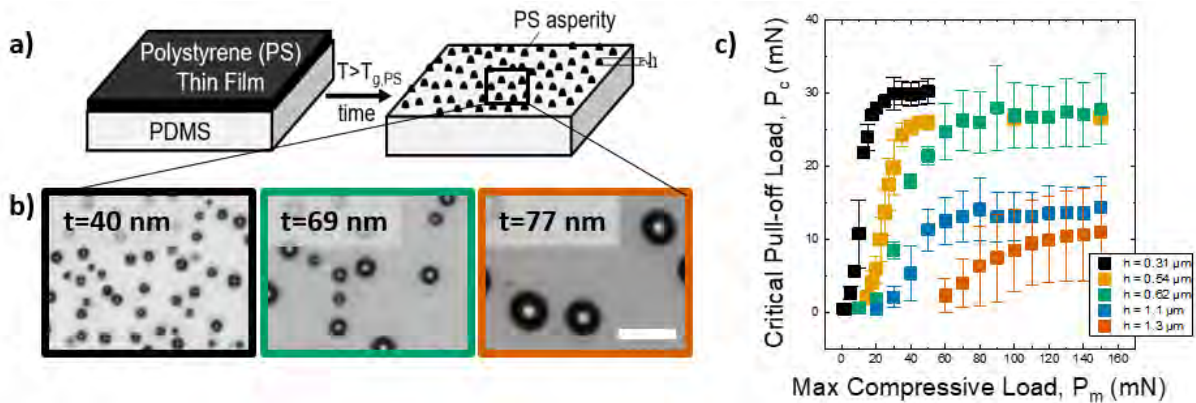


*Figure 1. Schematic of thin film-substrate pre and post thermal annealing (a). Optical images of the PTA surface prepared using different pre-annealing film thicknesses, t, (b). Scale bar is 8 µm. The force required to separate a flat punch probe from the PTA surface as a function of the amount of compressive force applied for various sample types.*

*Pressure Tunable Response*

Flat punch indentation testing was performed to characterize the adhesion strength of the PTA materials as a function of the maximum applied compressive loading, $P_m$. Results of the adhesion tests are presented in Figure 1.c. As $P_m$ increases, the amount of force required to separate the PTA, $P_c$, increases. Additionally, increasing droplet size results in a less sensitive response to applied load and an overall reduction in the adhesive strength of the material. A mechanics analysis is conducted to understand scaling of adhesive strength with applied load. Adhesion strength is found to be dependent on several geometric parameters including droplet height and the characteristic pattern size.

# References

[1]     N. Deneke, A. L. Chau and C. S. Davis, *Soft Matter*, 2020, **17**, 863–869.

# Switchable adhesives for multifunctional interfaces

Michael D. Bartlett[1,2,*]

1- *Mechanical Engineering, Soft Materials and Structures Lab, Virginia Tech, Blacksburg, VA 24060, USA.*
2- *Macromolecules Innovation Institute, Virginia Tech, Blacksburg, VA 24060, USA.*
*\*email: mbartlett@vt.edu*

Emerging and current applications ranging from consumer and medical products to soft robotics and wearable bio-monitoring devices demand strong adhesives which can be easily removed on-demand and subsequently reused. This requires new paradigms in adhesive science and engineering, resulting in the emergence of new classes of multifunctional switchable adhesives [1]. I will introduce some of the key concepts and opportunities in this area and then discuss two approaches for switchable adhesive systems.  First, I will present a framework for designing and rapidly manufacturing materials through kirigami, the Japanese art of paper cutting [2].  I will introduce kirigami-inspired structures for adhesives and show how we can enhance adhesive across a spatially patterned sheet while tuning adhesion in different directions for high capacity yet easy release interfaces. Second, I will show how pneumatically controlled shape and rigidity tuning can be coupled to rapidly switch adhesion (≈0.1 s) across a wide range of programmable adhesion forces with measured switching ratios as high as 1300x [3]. The switchable adhesion system introduces an active polydimethylsiloxane membrane supported on a compliant, foam foundation with pressure-tunable rigidity where positive and negative pneumatic pressure synergistically control contact stiffness and geometry to activate and release adhesion. This approach enables adhesion-based gripping and material assembly, which is utilized to pick-and-release common objects, rough and porous materials, and arrays of elements with a greater than 14 000x range in mass. Third, I will show deterministic control of crack initiation, propagation, and arresting by integrating a granular jamming layer into adhesive films. This process is highly reversible and programmable, allowing for numerous crack initiation, propagation, and arresting cycles at arbitrary selectable locations in a peeling adhesive [4]. These materials and approaches provide model systems to study fundamental adhesive properties while enabling advanced adhesive technologies for both current and emerging opportunities.
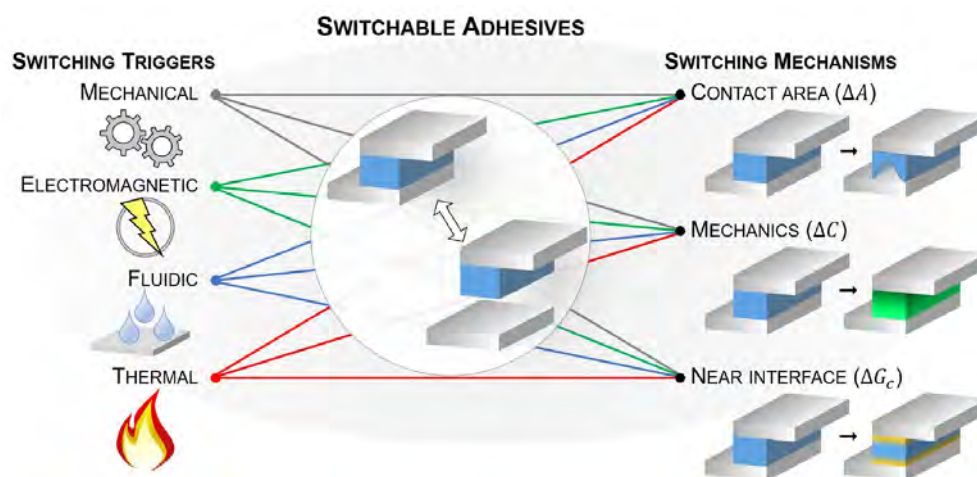


**Figure 1- Triggers and mechanisms of switchable adhesives.**

## References

1.  Croll, A. B., Hosseini, N. & Bartlett, M. D. *Adv. Mater. Technol.* **4**, 1900193 (2019).
2.  Hwang, D. G., Trent, K. & Bartlett, M. D. *ACS Appl. Mater. Interfaces* **10**, 6747–6754 (2018).
3.  Swift, M. D. *et al. Adv. Mater. Technol.* **5**, 2000676 (2020).
4.  Haverkamp, C. B., Hwang, D., Lee, C. & Bartlett, M. D. *Soft Matter* **17**, 1731–1737 (2021).

# SOFT ELECTRONICS FOR DIGITIZING HUMAN BODY AND HUMAN-CENTERED ROBOTICS

## Nanshu Lu

Temple Foundation Endowed Associate Professor
Department of Aerospace Engineering & Engineering Mechanics (ASE/EM)
Department of Electrical and Computer Engineering (ECE)
Department of Mechanical Engineering (ME)
Department of Biomedical Engineering (BME)
The University of Texas at Austin

**Abstract**

Industry 4.0, a.k.a. the cyber-physical systems, point to a future where humans will be more like robots (i.e., digital, computational, connected to the internet, etc.) whereas robots will be more like humans (i.e., soft, human-mimetic actuation and sensation, artificial intelligence, etc.). This talk will introduce my research on the mechanics, materials, bio-integration and functionality of soft electronics based on inorganic but high-performance functional materials such as metals, silicon, carbon nanotubes (CNT), and graphene. In particular, epidermal electronics, a.k.a. electronic tattoos (e-tattoos), represent a class of noninvasive stretchable circuits, sensors, and stimulators that are ultrathin, ultrasoft and skin-conformable. My group has invented a dry and freeform "cut-solder-paste" method for the rapid prototyping of multimodal, wireless, or very large area e-tattoos that are also high-performance and long-term wearable. The e-tattoos can be applied for physiological sensing for healthcare as well as human body digitization for human-robot interaction. While e-tattoos are to be worn by human, e-skins are to be worn by robots. Recently, we have engineered an e-skin based on barely electrically conductive porous nanocomposite laminated with an ultrathin insulating layer. The hybrid piezoresistive and piezocapacitive responses of this novel e-skin have enabled unprecedented pressure sensitivity at large pressures. It therefore could be applied for sensing very subtle surface pulse waves from the temporal artery even under the pressure of a VR headset. A stretchable version of it could be much more sensitive to out-of-plane pressure than in-plane strain, and hence can be mounted on an inflatable manipulator to perform diverse tasks. A perspective on future opportunities and challenges in this field will be offered at the end of the webinar.

**Bio**

Dr. Nanshu Lu is currently Temple Foundation Endowed Associate Professor at the University of Texas at Austin. She received her B.Eng. from Tsinghua University, Beijing, Ph.D. from Harvard University, and then Beckman Postdoctoral Fellowship at UIUC. Her research concerns the mechanics, materials, manufacture, and human / robot integration of soft electronics. She has been named 35 innovators under 35 by MIT Technology Review (TR 35) and iCANX/ACS Nano Inaugural Rising Star. She has received US NSF CAREER Award, US ONR and AFOSR Young Investigator Awards, 3M non-tenured faculty award, and the ASME Thomas J.R. Hughes Young Investigator Award. She has been selected as one of the five great innovators on campus and five world-changing women at the University of Texas at Austin. She is a highly cited researcher identified by Web of Science. For more information, please visit Dr. Lu's research group webpage at https://sites.utexas.edu/nanshulu/ and follow her Twitter: @nanshulu.

# On strain hardening in strain induced crystallization in NR

Laurent Chazeau

*Univ Lyon, INSA Lyon, CNRS, MATEIS UMR 5510, F-69621 Lyon, France*

Since its first observations, strain-induced crystallization (SIC) of natural rubber has been the subject of numerous works. As early as the 1940s, Flory laid the thermodynamic foundations of this phenomenon, and theoretical or experimental publications have never really stopped appearing since then. The SIC has known a very strong revival of interest in the 2000's, inspired by the very large development of synchrotron X-ray diffraction, and of thermal measurement techniques. The decrease of the acquisition time of the detectors allowed characterisations under more and more complex thermomechanical solicitation, with higher and higher solicitation speeds. All these works have fed an extremely rich corpus of data allowing to better define the generic characteristics of the SIC. This has been accompanied by the development of more or less sophisticated models. Theses ones include occasionally a three-dimensional mechanical description. Most of the time, they also contain thermodynamic/physical ingredients, allowing to account for an increasingly large set of experimental data (sometimes at the cost of a large number of parameters). Whatever their quality, it is nevertheless necessary to recognize that, up to now, none of these models allows to describe all the subtleties of the phenomenon. In particular, they often ignore the very strong strain hardening observed under certain experimental conditions; which seems contradictory, in appearance, with the thermodynamic explanation of the SIC. This presentation will therefore be an opportunity to review this issue, based on our own data and those of the literature. We will also discuss the way some authors have chosen to treat it in their modeling, and the questions raised by some experimental data.

# Multiscale characterization of deformation mechanisms of semi-crystalline PolyEtherEtherKetone (PEEK) under tensile loading

H. Willeman[1,3*], J. Bikard[2], O. Lame[3], R. Rinaldi[3], P. Sotta[1]

[1] *Laboratoire Ingénierie des Matériaux Polymères (IMP), UMR CNRS 5223 – INSA de Lyon, Villeurbanne, France (*heloise.willeman-ext@solvay.com PhD student)*
[2] *Solvay Research and Innovation Center, 87 avenue des Frères Perret 69192 St Fons Cedex, France*
[3] *Matériaux, Ingénierie et Sciences (MATEIS), UMR 5510 CNRS - INSA de Lyon, Villeurbanne, France*

We discuss the microscopic deformation mechanisms in PEEK at the scales of lamellar stacks and crystals, obtained by tensile tests combined with in situ, real-time small- and wide-angle X ray scattering (SAXS and WAXS). The onset of plasticity is investigated.

## Introduction

Polyetheretherketone (PEEK) is a semi-crystalline thermoplastic polymer with high mechanical performances over a large temperature range and high resistance to solvents. [1-2] To potentially predict and enhance the material lifetime and its mechanical properties, it is essential to fully understand the PEEK properties at a microscopic scale, from crystal planes to lamellae stacks to spherulites, in relation to its initial structure, itself driven by the process and crystallization conditions [3-6]. In this context, tensile experiments combined with in situ, real-time SAXS and WAXS were performed on PEEK. This approach, based on advanced analysis tools that we have developed, has been successfully applied to polyamides (PA6) [7]. It provides quantitative information on local deformation mechanisms from the elastic regime up to failure, such as stress and strain distributions, lamellae stacks rotation or even damage mechanisms like cavitation. Deformation mechanisms leading to the onset of plasticity are investigated and discussed here.

## Materials and methods

Samples of commercial grades of PEEK were provided by Solvay. Samples were processed by compression-molding plaques of 2 mm thickness at various temperatures between 380 and 420°C to vary the crystallization conditions. Bone-shaped test samples with the narrow part under traction having a square section $2 \times 2$ mm$^2$ were then machined in the plaques. The set-up of tensile tests with combined in situ SAXS and WAXS performed on the Swing beamline at the Soleil synchrotron and on BM02 at ESRF is schematized in Figure 1(a). Tensile tests discussed here were carried out at a constant nominal strain rate $10^{-3}$ s$^{-1}$ at room temperature, i.e. well below the glass transition temperature $T_g = 150$°C. The real-time macroscopic strain at the beam location was determined using optical digital image correlation on the speckled sample surface. The X ray wavelength was $\lambda = 1.03$ Å. The sample to detector distances were 1.51 m for SAXS measurements (scattering vector $q = 4\pi(\sin\theta)/\lambda$ (where $2\theta$ is the scattering angle) from 0.005 to 0.15 Å$^{-1}$) and 0.59 m for WAXS ($q$ from 0.75 to 4.4 Å$^{-1}$).

The long period of lamellar stacks is obtained from SAXS patterns as $L_p = 2\pi/q_{max}$ where $q_{max}$ is the $q$ value at the maximum of the correlation peak in $q^2 I(q)$. The strain at the scale of lamellar stacks is obtained from the variation of the long period $\Delta L_p$ as $\Delta L_p/L_p$. In the same way, the strain within crystal lamellae is obtained from the variation of the distances $d_{hkl} = 2\pi/q_{hkl}$ between crystal planes as $\Delta d_{hkl}/d_{hkl}$, where $q_{hkl}$ denote the positions of diffraction peaks in WAXS patterns. WAXS patterns exhibit 3 main diffraction rings at $q$ values 1.33 Å$^{-1}$, 1.47 Å$^{-1}$ and 1.605 Å$^{-1}$, corresponding to (110), (113) and (200) plane families, respectively [8] (Figure 2(a)). Lamellar stacks scatter along the normal to lamellar planes. The microscopic strain can then be analyzed as a function of the orientation (Figure 1(b)). In SAXS, scattering in the horizontal (tensile) direction (HORI, azimuth angle $\psi = 0$°) comes from lamellar stacks
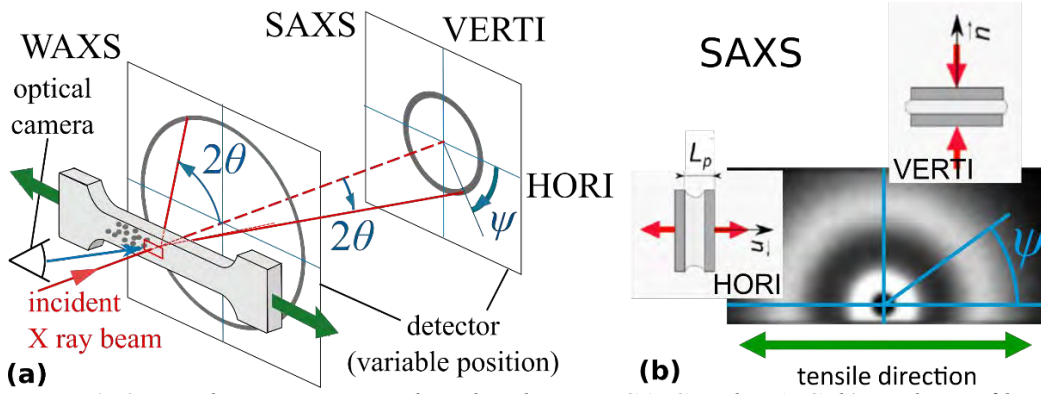
*Figure 1.a) Tensile test set-up combined with in situ SAXS and WAXS. b) analysis of local strain from SAXS pattern.*

whose normal is along the tensile direction. These stacks can only be located in the equator of spherulites and experience tensile stress. Vertical scattering (VERTI, $\psi = 90°$) corresponds to lamellae stacks submitted to compression stress. The same is true in WAXS when families of crystal planes are considered.

## Results and discussion

First, SAXS and WAXS patterns were measured in the initial, unstretched test samples both with the beam perpendicular and parallel to the plane of the compression molded plaques. The patterns show only tiny, negligible deviations from isotropy, which enables assuming the initial morphologies are roughly isotropic.

Representative results obtained in a tensile test conducted at $T = 23°C$ are illustrated in Figure 2. The macroscopic behavior of the sample is described by the stress-strain curve. The onset of plasticity is located at about 5% strain. The local macroscopic strain at beam location is measured using image correlation (black curve in (b)). The microscopic strain is calculated from SAXS and WAXS patterns.

### *Elastic (pre-yield) regime*

In the pre-yield (elastic) regime, the SAXS pattern gradually evolves from a circular, isotropic pattern into an ellipse with more intensity in the HORI direction (Figure 2(a)). In a uniaxially
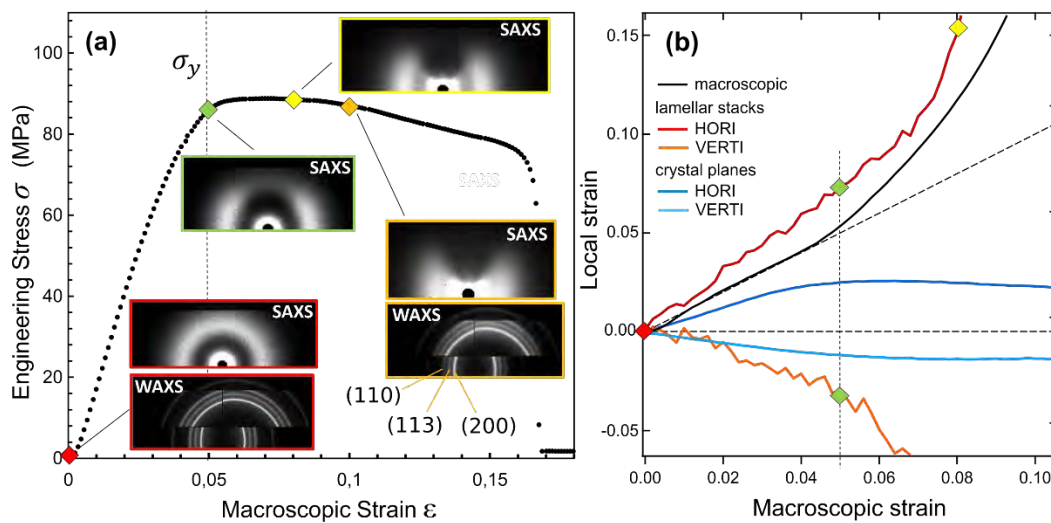


*Figure 2.(a) A representative stress strain curve with corresponding SAXS and WAXS patterns for tensile test at $10^{-3}$ $s^{-1}$;(b) The macroscopic and local strains at the scale of lamellar stacks and (110) crystal planes for $\psi = 0°$ (HORI) and $\psi = 90°$ (VERTI).*
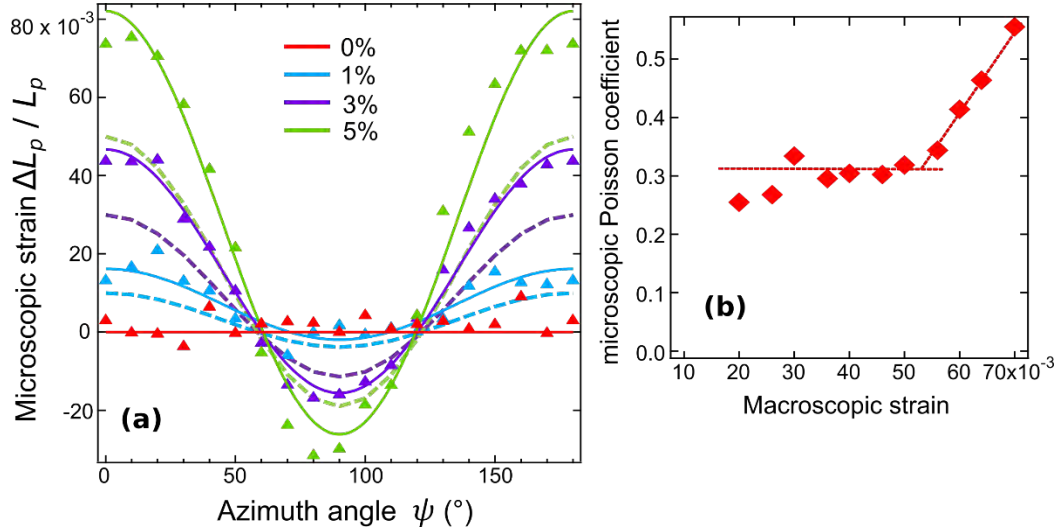
*Figure 3. (a) The local strain in lamellar stacks $\Delta L_p/L_p$ vs the azimuth angle $\psi$ for different values of the macroscopic strain. Symbols: experimental data; full curves: fits using eq 1; dotted curves: eq 1 with $\varepsilon_{micro} = \varepsilon_{macro}$ and $\nu_{micro} = \nu_{macro} = 0.38$. Points at $\psi = 0$ and $\psi = 180°$ correspond to the same data, due to the symmetry of the pattern. (b) Evolution of the fitted $\nu_{micro}$ vs the macroscopic strain. The change of slope at $\varepsilon \cong 5\%$ marks the onset of plasticity.*

stretched homogeneous material, the variation of the long period of lamellar stacks should be expressed as a function of the azimuth angle $\psi$ with the following equation 1:

$$\frac{\Delta L_p}{L_p^0} = \frac{\varepsilon}{3}\left[(1 - 2\nu) + 2(1 + \nu)\frac{3\cos^2\psi - 1}{2}\right] \tag{1}$$

Where $\varepsilon$ is the tensile strain and $\nu$ the Poisson's coefficient of the material. The quantity $\Delta L_p/L_p$, is plotted as a function of the azimuth angle $\psi$ in Figure 3.

Experimental data are relatively well fitted with eq. 1 in the pre-yield regime. The outputs of the fitting process are the local strain $\varepsilon_{micro}$ at the scale of lamellar stacks and an apparent Poisson's coefficient, $\nu_{micro}$., which in fact corresponds to the ratio of the tensile strain in lamellar stacks in compression (which scatter in the VERTI direction) and in those in tension (which scatter in the HORI direction). $\varepsilon_{micro}$ measured in the HORI azimuth direction ($\psi = 0$) and $\nu_{micro}$ are shown as a function of the macroscopic strain in the pre-yield regime in Figure 3. Within experimental uncertainties, $\nu_{micro}$ is roughly constant, equal to 0.31 in the pre-yield regime (up to about 5% strain). The microscopic strain in the HORI azimuth direction is larger than the macroscopic strain by about 30%. Since lamellar stacks which scatter in the HORI direction are necessarily located within the equator of spherulites, this indicates that the equator of spherulites deform more than the whole spherulite. On the other hand, the overall average strain within spherulites, as probed by lamellar stacks which scatter in the VERTI direction, is roughly equal to the macroscopic strain.

The same analysis may be applied to WAXS patterns in order to derive the strain field experienced by crystal planes. Figure 2(b) shows that the strain in crystallites is smaller than the macroscopic strain, which indicates that the modulus of the crystal phase is larger than that of the amorphous phase.

## Onset of the plastic regime

The onset of plasticity at about 5% strain corresponds to an abrupt change in behavior. First, the local macroscopic strain starts to deviate from the overall, average strain. This indicates that strain localization occurs at the location of the X ray beam. The onset of plasticity within the investigated zone coincides with an abrupt increase of the apparent microscopic Poisson's coefficient (Figure 3b), which means that lamellar stacks scattering in the HORI direction, located in the equator of spherulites, start to deform comparatively less than the overall

spherulite. Indeed, in the HORI direction ($\psi = 0$), the microscopic strain $\varepsilon_{micro}$ (as shown in Fig 2b) does not show a significant increase of slope near 5% strain. Also, remarkably, the strain within crystals remain constant in the plastic regime. There is thus a qualitative change in behavior at the onset of plasticity.

The SAXS patterns show qualitative change near 5% strain. The intensity in the VERTI direction ($\psi = 90°$) decreases drastically, indicating that a vast majority of lamellar stacks orient in the HORI direction, which corresponds to polymer chains oriented along the tensile direction. Slightly above the onset of plasticity, the pattern then evolves into a butterfly-shaped pattern, typical of a strongly oriented polymer. The intensity is fully concentrated within a cone of $\psi \cong \pm 35°$ around the $\psi = 0°$ (HORI) direction.

In WAXS patterns, the intensity in diffraction rings becomes concentrated in the VERTI direction. This is true in particular for the (200) ring. This is coherent with the evolution observed in SAXS patterns, as lamellar stacks which scatter in HORI direction correspond to chains oriented in the tensile direction and thus to (200) planes scattering in the VERTI direction. However, changes are more pronounced in SAXS than in WAXS patterns. The intensity in the HORI direction for e.g. (200) planes does not vanish, while it nearly vanishes for lamellar stacks. This indicates that (200) planes parallel to the tensile direction, that is, with chains perpendicular to the tensile direction, are still present in the plastic regime. The corresponding crystallites, however, would not form well-defined lamellar stacks, which would scatter in the VERTI direction.

## Conclusions

In the pre-yield regime, the deformation at the scales of lamellae stacks and crystal lattice is nearly homogeneous, with small but significant deviations however. Beyond yield, the local tensile strain in lamellar stacks and crystal planes in tension (which scatter in the HORI direction) levels off. This is a direct manifestation of the onset of heterogenous modes of deformation, which may be local shear or crystal fragmentation associated to plasticity in the amorphous phase. The final state of the material is quite strongly oriented.

A further evolution in SAXS patterns in the plastic regime is the onset of strong central scattering, indicating that the material is subjected to quite intense cavitation. Note finally that the material behaves differently when stretched at 170°C, that is above $T_g$, with less strain-induced orientation of lamellae and no observed cavitation.

## References

[1] Garcia-Leiner M. et al., Structure-Property Relationships in Commercial Polyetheretherketone Resins, *Polymer Engineering & Science* **2017** *57*,955-64,

[2] Barba D, Arias A., et Garcia-Gonzalez D., Temperature and Strain Rate Dependences on Hardening and Softening Behaviours in Semi-Crystalline Polymers: Application to PEEK, *International Journal of Solids and Structures* **2020** *182-183*, 205-17

[3] Lee Y.; Porter R.S., Effects of Thermal History on Crystallization of Poly(Ether Ether Ketone) (PEEK), *Macromolecules* **1988**, *21*, 2770-76

[4] Hsiao B. S. et al., Time-resolved X-ray study of poly(aryl ether ether ketone) crystallization and melting behaviour: 1. Crystallization, *Polymer* **1993** *34*, 3986-95,

[5] Krueger K. N.; Zachmann H. G., Investigation of the melting behavior of poly(aryl ether ketones) by simultaneous measurements of SAXS and WAXS employing synchrotron radiation, *Macromolecules* **1993**, *26*, 5202-8

[6] Pastukhov L.V et al., Physical Background of the Endurance Limit in Poly(Ether Ether Ketone), *Journal of Polymer Science* **2020**, *58*, 716-36

[7] Millot C. et al., Tensile Deformation of Bulk Polyamide 6 in the Preyield Strain Range. Micro–Macro Strain Relationships via in Situ SAXS and WAXS, *Macromolecules* **2017**, *50*, 1541-53

[8] Wakelyn N. T., On the structure of poly(etheretherketone) (PEEK), *Polymer Communication* **1984**, *25*, 306-308

# Micromechanical modelling of the stress-strain behaviour of isotropic $\alpha$-iPP

H.N. Chávez Thielemann[1†], L.E. Govaert[1] and J.A.W. van Dommelen[1]

[1] *Department of Mechanical Engineering, Eindhoven University of Technology,*
*P.O. Box 513, 5600 MB Eindhoven, The Netherlands.*
[†] *Dutch Polymer Institute (DPI), P.O. Box 902, 5600 AX Eindhoven, The Netherlands.*

## Abstract

The final properties and the underlying microstructure of semi-crystalline polymeric products are strongly affected by the processing conditions. To quantify the actual effect of the microstructure on the macroscopic response, a micromechanical composite inclusion model (CIM) is developed. This method is based on a biphasic inclusion: a material point representation of crystalline lamella and its complementary amorphous domain, in which each phase is handled by a dedicated constitutive law. In specific, the crystalline phase is modelled with crystal plasticity and the amorphous phase with the EGP model [1]. Therefore, the response depends on the characterization of crystallographic slip kinetics, as well as the relaxation spectrum of the isotropic amorphous phase. With this approach it is possible to describe the deformation phenomena and the combined response of both phases, which is finally used to study the macroscopic behaviour, by means of a cluster of inclusions, where the contribution of each biphasic domain is obtained through a hybrid interaction law.

In this work, the CIM is used to describe the elasto-viscoplastic behaviour of initially non-oriented alpha isotactic polypropylene (α-iPP) under uniaxial compression up to the yield point. The unknown intrinsic parameters needed to represent this polymer are identified by assessing the model output with uniaxial compression and tensile experiments at different constant strain rates and temperatures. This includes the elastic modulus, the yield kinetics, the time spectra, and the crystalline texture upon deformation. As a result, the model shows an overall good description of the material behaviour, with yield kinetics in close agreement with experimental results, and a clear relation between the elastic response and the yield stress. Because of the broad range of temperatures and strain rates, it was possible to thoroughly unravel the complex time spectra of the constrained amorphous phase. Based on microstructural analysis, the model is further validated, where the texture evolution upon deformation predicted by the CIM presents some significant matches with the texture obtained with WAXD. The model is then used to better understand the role of the amorphous and crystalline phases in the deformation behaviour. Finally, the long-term response of α-iPP subjected to constant tensile loads is predicted with the CIM and then it is compared with experimental data to demonstrate its suitability.
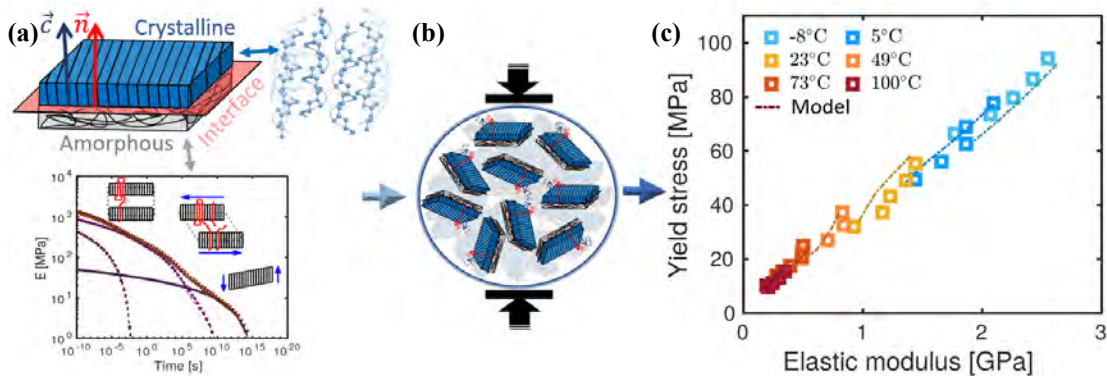
*Figure 1:* (a) biphasic inclusion, (b) inclusion aggregate, (c) yield stress as a function of the elastic modulus, markers indicate experimental results and dashed lines show the CIM simulations.

[1] Poluektov, M.; Van Dommelen, J. A. W.; Govaert, L. E.; Yakimets, I.; Geers, M. G. D., *Journal of Materials Science* **2013**, 48, 3769–3781.

# Mechanisms of strain hardening in polymers; From local conformation to crystalline organisation in PET and PEF

Noëlle Billon[*1], Nicolas Sbirrazzuoli[2]

[1]*MINES ParisTech, Université PSL, Centre de mise en forme des matériaux (CEMEF), CNRS UMR 7635, Sophia Antipolis, France;*
[2]*Institut de Chimie de Nice (ICN), Université Cote d'Azur, CNRS, UMR7272, CEDEX 2, 06108 Nice, France*
*\*(noelle.billon@mines_paristech.fr)*

Since the 20's correlation of strain induced crystallisation of polymers to mechanical behaviour have led to numerous studies. Whatever the polymer is, since natural rubber that was early reported, to new biobased thermoplastic polyesters, this phenomenon induces a drastic mechanical strain hardening. However, it needs specific conditions to be induced. Lot of the studies were devoted to PET due to its great industrial importance. More recently, biobased competitor appeared on the market, the PEF. The variety in chain architectures that was encountered in the literature and the development of fine microstructural analysis now enable to better understand the elementary processes that are involved in Strain Induced Crystallisation (SIC). In parallel the use of well controlled and richly instrumented mechanical protocols analysis of mechanical behaviour (DIC, IR thermography and controlling of strain rates) allows to correlate those processes to the most relevant mechanical data. Present lecture intends to summarise recent results based on in and ex-situ WAXS combined with ex-situ IRFT and mechanical spectrometry comparing two polyesters the PET and the PEF, which enlightens the understanding of relationships between the SIC and chain architecture [1-4]. A schematic of SIC and its consequence on thermomechanical behaviour of polymers will be suggested.

## References

[1] E. Gorlier, J-M. Haudin, Billon N, Polymer, 42(23): 9541-9549,2001.
[2] C Menager, N. Guigo, L. Martino, N. Sbirrazzuoli, N. Billon, et al., Polymer, 158:364-371, 2018.
[3] E. Forestier, C. Combeaud, N. Guigo, G. Monge, J-M. Haudin, N. Sbirrazzuoli, N. Billon, Polymer, 187:122126, 2020. E. Forestier, C. Combeaud, N. Guigo, N. Sbirrazzuoli, N Billon N, Polymer, 203:122755, 2020.
[4] E. Forestier, N. Guigo, C. Combeaud, N. Billon, N., Macromolecules, 53(19):8693-8703, 2021.

# "Tying the knot", ultra-fast entangling across ultra-high molecular weight polyethylene interfaces

Fotis Christakopoulos[1], Enrico M. Troisi[2], Nic Friederichs[2], Jan Vermant[1], Theo A. Tervoort[1]

1. *Department of Materials, ETH Zürich, 8093 Zurich, Switzerland*
2. *SABIC Technology & Innovation, 6160AH Geleen, The Netherlands*

Joining of two solid polymer interfaces of identical monomeric composition has important practical applications, as it directly controls the quality of welding and plays a key role in determining properties of mechanical recycled products. It also has interesting theoretical aspects, e.g. related to adhesion and self-diffusion of macromolecular chains.

Ultra-high molecular weight polyethylene (UHMWPE) is a high-end engineering polymer and is the material of choice in numerous applications ranging from high-performance fibers and bulletproof panels to medical stents and bearing material for joint arthroplasty in hip, knee and shoulder replacements. It combines a low friction coefficient and excellent chemical resistance and in its isotropic form, UHMWPE possesses among the highest values of impact strength and wear resistance of all polymers. However, the very features that lead to its exceptional properties, i.e. ultra-long macromolecular chains, render joining two surfaces of this material a tedious and slow process, leading to long welding times and impeding mechanical recycling of UHMWPE. A special feature of UHMWPE is that it can be produced through dedicated polymerization protocols in a disentangled state. The possibility of accelerating diffusion using these fully disentangled chains is explored and exploited in the present work.

An anomalous fast joining of UHMWPE interfaces, by simply depositing small amounts of nascent disentangled UHMWPE powder at the interface, is observed. The time evolution of build-up of adhesive fracture energy in the molten state and the reduction in interfacial slip between two molten UHMWPE layers, reveal an order of magnitude increase of the rate of interpenetration compared to the dynamics of a regular UHMWPE-melt interface [1]. This ultra-fast self-diffusion mechanism is insensitive to molecular weight, in contrast to reptation-driven diffusion, and provides a direct indication of the entropy-driven "chain explosion" upon melting of nascent disentangled UHMWPE [2].

The usefulness of fast molecular stitching is demonstrated for enhanced recycling of UHMWPE. Knitting recycled UHMWPE together with nascent UHMWPE powder allows for fast recycling of UHMWPE at low processing temperatures with mechanical properties that approach that of the original material.

## References

[1] Wool, R. P; Yuan, B. L.; McGarel, O. J., *Pol. Eng. & Sc,* **1989**, *29*, 1340-1367.
[2] De Gennes, P. G., *C. R. Acad. Sc. Paris Serie 2b* **1995**, *321*, 363-366.

# Dynamic fracture through heterogeneous brittle material

David S. Kammer[1], Gabriele Albertini[2], Mathias Lebihain[3], Laurent Ponson[4]

[1]*Institute for Building Materials, ETH Zurich, Switzerland*
[2]*Harvard University, Cambridge, MA, USA*
[3]*Laboratoire Navier, École des Ponts, Université Gustave Eiffel/CNRS, France*
[4]*Institut Jean le Rond d'Alembert, Sorbonne Université/CNRS, France*

We experimentally and theoretically investigate dynamic fracture of two-dimensional heterogeneous brittle materials. We measure the crack front position and near-tip displacement field to determine the dissipated energy and crack speed changes at material boundaries. We study the link between local crack dynamics and macroscopic fracture toughness.

## Introduction

The microstructure of many biological and engineering materials are a source for remarkable macroscopic mechanical properties. While homogenization theory describes well the link between the microscale and macroscale for elastic properties, its application to fracture and toughness is considerably more challenging as these properties are disorder-driven. In order to develop a homogenized perspective of material failure through fracture, a fundamental understanding of fracture propagation through heterogeneous microstructures is required. Here, we provide experimental observations [1] for dynamic fracture propagation through heterogeneous brittle material and analyse how the crack adapts as it crosses material boundaries.

## Materials & Methods

We run fracture experiments on tapered double cantilever beams made of multi-material 3D-printed polymers, where the crack propagates through a series of periodic stripes of two different brittle materials (matrix and obstacle). We measure the crack front position and near-tip displacement field with integrated digital image correlation. We then determine the rupture speed and the locally dissipated fracture energy during crack propagation.

## Results & Discussion

Our results [1] show that the dynamic rupture abruptly adapts its speed at material interfaces as it enters or exits a stripe of obstacle material. Simultaneously the dissipated energy (i.e., fracture energy) changes; however, more moderately. This is due to rate-dependent fracture energy of the polymeric material. Based on these results, we show that linear elastic fracture mechanics (LEFM) predicts quantitatively well the crack speed jumps at the material interfaces if the rate-dependent fracture energy is taken into account. Further, we demonstrate that the local dynamics of the rupture leads to an apparent toughening of the homogenized macroscopic fracture energy.

## Conclusion

This work shows that classical LEFM describes quantitatively well the equation of motion of cracks in heterogeneous materials and that heterogeneous materials present increased toughness due to high crack speed fluctuations and rate-dependence of local fracture energy.

## References

[1] Albertini, G., Lebihain, M., Hild, F., Ponson, L., Kammer, D. S., *Physical Review Letters* **2021**, 127(3), 035501. https://doi.org/10.1103/PhysRevLett.127.035501

blank

# Poster contributions

# Modelling the Macroscopic Behaviour of Rubber Toughened Glassy Polymers

M. Wismans[1,2], T.A.P. Engels[1], L.C.A. van Breemen[1], J.A.W. van Dommelen[1], L.E. Govaert[1]

[1]*Eindhoven University of Technology, Department of Mechanical Engineering, P.O. BOX 513, 5600 MB, Eindhoven, The Netherlands*
[2]*DPI, P.O. Box 902, 5600 AX, Eindhoven, the Netherlands*

A popular approach to improve the toughness of semi-ductile polymeric material is to add rubber particles resulting in local shear yielding. Representative volume elements (RVEs) are used to study and model the influence of rubber particles on the mechanical response of rubber-toughened polymers. RVEs are micro mechanical models which contain the characteristic of the local morphology, and its mechanical response is *representative* for the heterogeneous material. Studies employing RVEs can provide vital mechanistic insights in the working principles of rubber particles on the toughening behaviour. However, the RVEs are not practically applicable for describing the deformation of structural parts due to the order of magnitude difference in length. A macroscopic model which can describe the effect of rubber particles on the macroscopic deformation behaviour is the modified Gurson model.

In this study, realistic 3D RVEs are employed to provide the reference deformation behaviour for rubber toughened polymers using three different rubber volume fractions. The yield stress of rubber-toughened polymers shows a non-linear dependence with respect to the hydrostatic stress component as shown on the left side of Figure 1 which is due to macroscopic dilatation. Simulations are performed for a range of macroscopic stress states going from pure shear to triaxial. The dependence of the yield stress with respect to the hydrostatic stress can be modelled using the yield function from the modified Gurson model. The yield function is implemented in the Eindhoven Glassy Polymer (EGP) model. The EGP model is a constitutive model which describes the intrinsic deformation behaviour of glassy polymers. Combing both models result in a macroscopic constitutive model which describes the deformation behaviour of rubber-toughened polymers as shown in Figure 1.
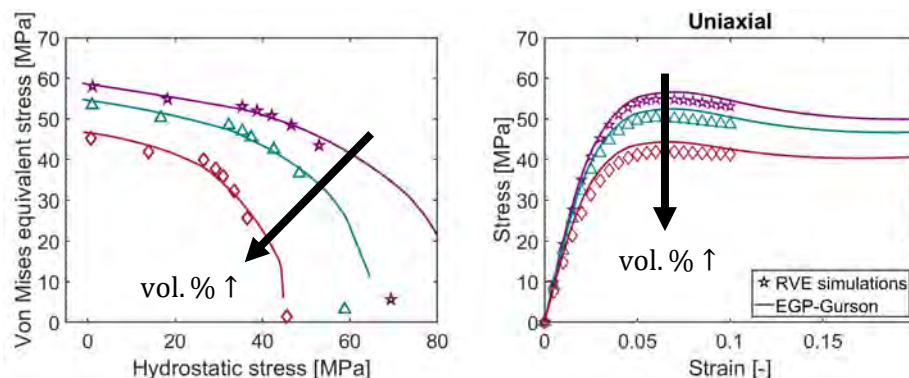


Figure 1: Left: Equivalent stress and hydrostatic yield stress for RVE simulations with various volume fractions and stress states. Right: Stress-strain curve for three different rubber volume fractions in uniaxial tension.

# Structure-property relationships for epoxies at cryogenic temperatures

Pascal Studer and Theo Tervoort

*ETH Zurich, Department of Materials, Zurich, Switzerland*

Our work is concerned with the structure-property relationships of epoxy resins at cryogenic temperatures with the aim of developing new epoxy formulations for use in cryogenic applications. Earlier research has shown that many important properties of epoxy resins such as the elastic modulus, coefficient of thermal expansion and yield stress, converge to similar values at cryogenic temperatures. However, large differences were found in the measured fracture toughness at the temperature of liquid nitrogen, well below the glass transition of the tested resins. In this work, we will present our approach to understand the relationship between the molecular structure of the crosslinked networks and the fracture toughness at cryogenic temperatures. Starting from known chemicals with purity and epoxide equivalent weight quantified by H-NMR, we synthesize our own resin formulations. Through the knowledge of the used monomers and by using theoretical formulas to estimate the crosslink density by assuming full conversion, we compare the predictions for the rubbery modulus obtained from the standard entropic rubber-elasticity theory to empirical measurements on samples obtained by DMTA. This allows us to test the hypothesis which states that the modulus of epoxy resins above the glass transition is not only influenced by entropic elasticity, but also to a significant part by energy elasticity. Furthermore, we develop epoxy formulations with maximized toughness at cryogenic temperature, while still providing rigidity at room temperature, by systematically tuning the amount of aliphatic flexible chain monomers of different molecular weights and chemical composition. DSC reveals the dependence of the glass transition temperature on the weight fraction of these monomers, and formulations are selected for mechanical testing by linear interpolation to obtain a glass transition just above room temperature.

# Ultimate properties of PMMA modified by supramolecular chemistry

M. Rambaud[1]*, L. Trouillet-Fonti[2], C. Vergelati[2], D.Long[1]

[1] *Matéis, Laboratoire INSA, Bât. B. Pascal, 5° étage, 7 Avenue Jean Capelle, 69621 Villeurbanne cedex, France, melissa.rambaud@insa-lyon.fr*
[2] *Solvay, Bât Axel'One, 87 avenue des Frères Perret, CS 70061, 69192 St-Fons Cedex, France*

Ionomers are polymers containing up to 10-15% of ionic groups. These materials show great potential for applications such as shape memory polymers, self-healing polymers, antibacterial polymers and more recently as alternatives to electrolyte batteries [1]. The addition of ionic interactions allows their properties to be controlled, particularly the compromise between glass transitions and melt rheological properties [2 - 3]. Although the properties of ionomers have been extensively studied in this recent decades, the effect of ionic interactions at large strains is not fully understood.

The effects of the presence of ionic salts on the properties of poly (methyl methacrylate) is studied. Sodium and lithium salts are grafted up to a few percent. Glass transition temperatures are studied, as well as relaxation times by rheology. Mechanical properties are studied in the solid state in tension and compression, up to large deformations. Influence of ionic salts on the strain hardening of PMMA is analysed.

The grafting of sodium sulphonate salts on PMMA creates additional interactions between dipoles of the main chain and ions, and between two ions. Thermal stability of PMMA is increased by 25°C with 3% of ion content. The terminal relaxation time is shifted by 5 decades to lower frequency, as can be seen in the figure 1 below.
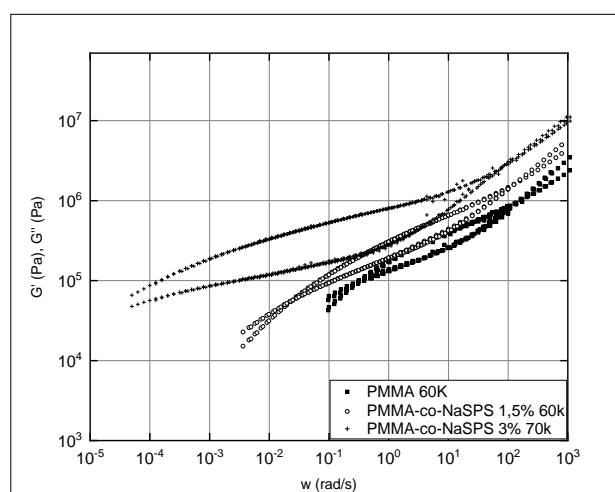


Figure 1 : Time-temperature superpositions of PMMA functionalized with different levels of sodium sulphonate groups. Tref=150°C

# References

[1] Zhang, Longhe, Nicole R. Brostowitz, Kevin A. Cavicchi, and R. A. Weiss. 2014. 'Perspective: Ionomer Research and Applications'. *Macromolecular Reaction Engineering* 8 (2): 81–99

[2] Weiss, R. A., and Hongying Zhao. 2009. 'Rheological Behavior of Oligomeric Ionomers'. Journal of Rheology 53 (1): 191–213.

[3] Martins, Ana Rita, Anthony Bocahut, Marie-Laure Michon, and Paul Sotta. 2019. 'Effect of Intermolecular Interactions on the Viscoelastic Behavior of Unentangled Polyamide Melts'. Journal of Rheology 63 (3): 377–89

# A shear transformation zone mesoscale model for plasticity in polymer glasses with visco-elastic background

N. Klavzer[1], F. Van Loock[1,2], J. Chevalier[3], L. Brassart[4] and T. Pardoen[1]

[1]Institute of Mechanics,Materials and Civil engineering (iMMC), UCLouvain,
B-1348, Louvain-la-Neuve, Belgium
[2]Polymer Technology group, Eindhoven University of Technology, PO Box 513,
5600, MB,Eindhoven, the Netherlands
[3] Solvay,Material Science Application Center (MSAC), B-1120 Bruxelles, Belgium
[4] Department of Engineering Science, University of Oxford,
OX1 3PJ Oxford, United Kingdom

The use of bottom-up multiscale approaches to predict the deformation and failure of fibre-reinforced polymer composites is common nowadays. However, these methods rely on (visco-)elastic-(visco-)plastic continuum models for the matrix, albeit sophisticated, and require a large number of fitting parameters. Still, their predictive capabilities are limited, even in the case of simple unidirectional composites loaded in transverse compression or shear, where the matrix dominates the macroscopic deformation response of the composite, as they inaccurately the strain fields around fibres. To overcome this issue, we make use of mesoscale numerical model based on shear transformation zones (STZ), implemented and calibrated in Van Loock (2021) [1], and formerly applied to thermosets below the glass transition temperature [2].

In this contribution, we extend the STZ model by introducing a visco-elastic (VE) matrix to capture the background VE relaxations. The goal is not only to better represent the behaviour of thermoset polymers with respect to VE effects, but also to address the local couplings between visco-elastic relaxation and STZ activation. The VE matrix is modelled via a Standard Linear Solid and its implementation in the FE model is based on the work of Miled (2011) [3]. The total strain is the sum of the VE strain and the STZ strain (i.e. visco-plastic strain). Emphasis is placed on the impact of the time constant on the model predictions, in particular in the case of pre- and post-yield creep, and the following stress-strain redistribution within the matrix. In addition, the impact on shear banding in confined volumes is studied and compared with previous results using an elastic matrix, as shown in *Fig. 1*. These insights can be used to simulate the time- and temperature-dependent visco-plastic deformation and failure response of a fibre-reinforced polymer composite matrix at the fibre-diameter length scale.
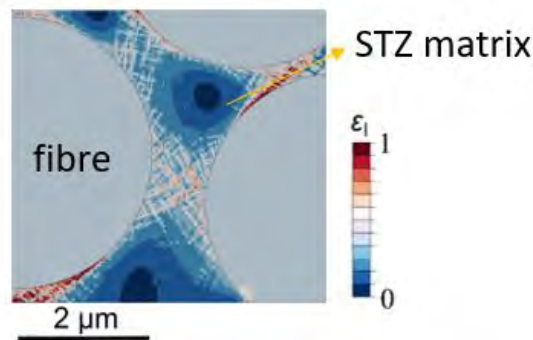


Fig. 1: Principal strain distribution in between fibres of FRP using a STZ enriched matrix. From [4].

## References

[1] Van Loock, F.; Brassart, L.; Pardoen, T., *International Journal of Plasticity* **2021**, 145, 103079.

[2] Chevalier, J.; Brassart, L.; Lani, F.; Bailly, C.; Pardoen, T.; Morelle, X.P., *Journal of the Mechanics and Physics of Solids* **2018**, 121, 432-446.

[3] Miled, B.; Doghri, I.; Delannay, L., *Computer Methods in Applied Mechanics and Engineering* **2011**, 47, 3381-3394.

[4] Chevalier, J., In *Micromechanics of an epoxy matrix for fiber reinforced composites: experiments and physics-based modelling,* Pardoen, T.; Lani, F., UCLouvain, 2018.

# The thermomechanical properties of three different molecular weight polycarbonates and one co-polycarbonate

Peihao Song [1,2*], Akash R Trivedi [1,2], and Clive R Siviour[1]

[1]*Department of Engineering Science, University of Oxford, Parks Road, OX1, 3PJ, UK*
[2]*DPI, P.O. Box 902, 5600 AE Eindhoven, the Netherlands*
*Corresponding author: peihao.song@eng.ox.ac.uk*

Summary: The thermomechanical properties of three different molecular weight polycarbonates and one co-polycarbonate are investigated with Dynamic Mechanical Analysis and compressive tests at different rates and temperatures. This has allowed the small and large strain time-temperature dependent constitutive behaviour of these materials to be characterised and molecular weight and co-monomer effects to be studied.

## Introduction

Polycarbonate (PC) is a typical glassy amorphous polymer whose mechanical behaviour has been extensively studied. Polymers exhibit strong temperature- and rate-dependence, in which strength and stiffness increase as the temperature decreases or the strain rate increases [1-3]. However, measuring the mechanical behaviour of polymers under high rate loading is very challenging because of their low impedance and strength [4]. At the same time, increasing strain rate can change the experimental conditions from isothermal to adiabatic [1, 5]. Under this condition, the heat produced by plastic deformation cannot be dissipated into the environment during high rate loading, and the increase of temperature can induce a qualitatively different constitutive response to that observed in low rate tests [2]. In this paper, the response of polycarbonate to loading at different strain rates is characterised, and the time-temperature equivalence theory [3] is applied to interpret the experimental results. A comparison between low temperature and high rate tests is carried out to understand adiabatic heating effects on large strain deformation. Lastly, the molecular weight and co-monomer effects on mechanical properties are studied.

## Material information and preparation

Table 1 lists the four different grades of injection moulded PCs used in this study. Three different homo-PCs with different melt flow rates (MFR, low MFR implies high molecular weight) and one co-PC were characterised. The PC sheets were annealed to minimise residual stresses from the manufacturing process.

Table 1: Grades of PC used in this study.

| Polymer (LEXAN™ RESIN) | Code | Melt Flow Rate (MFR) at 300 °C/1.2 kg | $T_g$ (°C) |
|---|---|---|---|
| 103R | PC1 | 6 | 145 |
| 500R | PC2 | 10 | 145 |
| HF1110 | PC3 | 25 | 145 |
| HFD 1014 (co-PC) | PC4 | 6 | 130 |

## Experimental characterisation and results

### Dynamic Mechanical Analysis (DMA)

Temperature and frequency sweep DMA tests were performed on a TA Q800 in a three point bend configuration. Figure 1 (a) shows that the moduli obtained from the three point bending mode and the results obtained here are consistent with a standard tensile test (ISO 527 1A) result shown in Figure 1 (b).
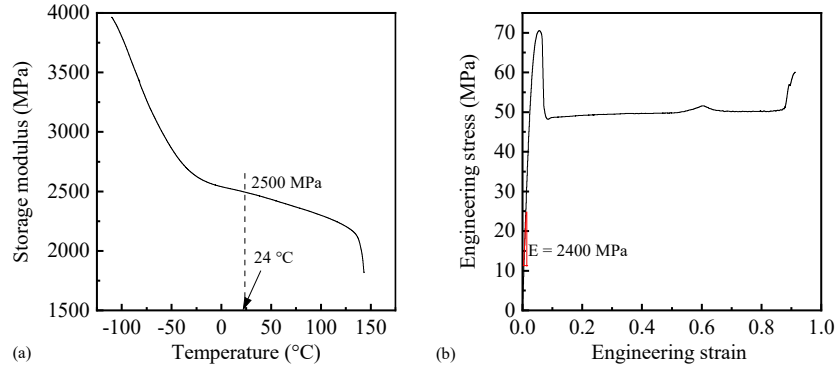
Figure 1 (a) Temperature sweep DMA test; (b) Standard tensile testIsothermal
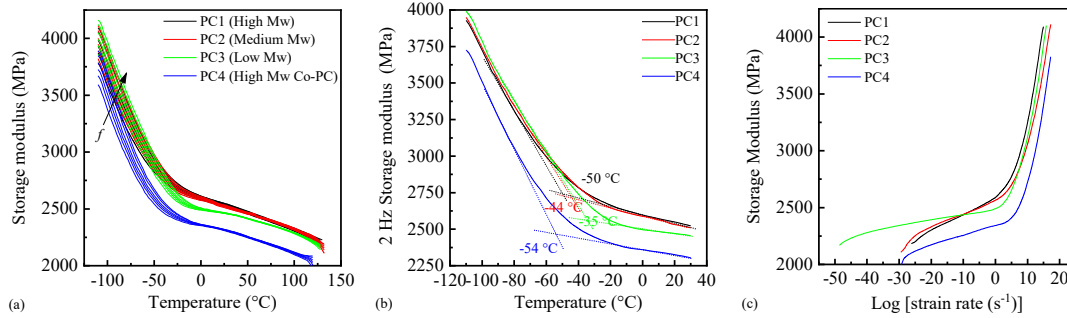


Figure 2. (a) Varying temperature and frequency storage moduli (b) Detail of $\beta$-transition region (c) Master curves obtained from time-temperature superposition.

In Figure 2 (a), it can be observed clearly that the moduli are affected by both temperature and frequency in isothermal frequency sweep DMA tests. It is well known that the $\beta$-transition governs the high-rate performance. In this region (from -110 to -40 C), the modulus of PC3 shows more frequency-dependence than that of PC1 compared with the temperature region from -20 to 120 °C. The inflection point (Figure 2 (b), (c)) reflects the onset of this transition, and for the PC4 starts at a lower temperature (or higher rate) than for the other materials.

*Varying rate and temperature compression tests*

The compression responses from 0.001 s$^{-1}$ to 0.1 s$^{-1}$ were characterised using an Instron 5980 universal test machine. Medium rate experiments at between 1 s$^{-1}$ to 60 s$^{-1}$ were conducted on a hydraulic machine, and a split Hopkinson pressure bar was used for the high rate compression tests. See [6] and [7] for more details about high rate experimental techniques.
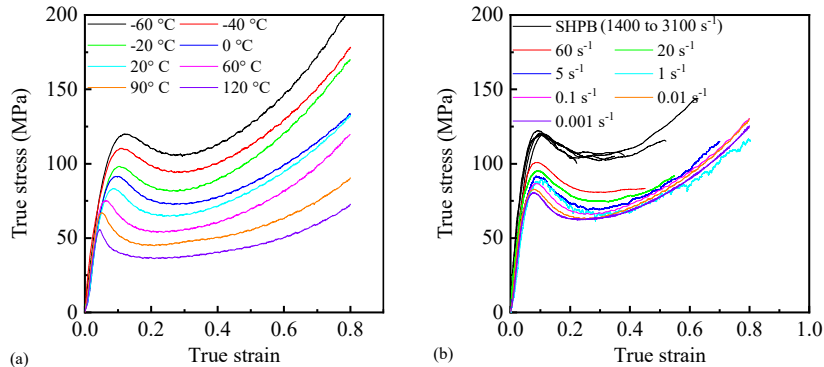


Figure 3 Stress-strain curves at (a) different temperatures, strain rate is 0.01 s$^{-1}$ (b) different strain rates at 20 °C

Figure 3 presents the compressive response of PC1 conducted at varying temperatures from -60 °C to 120 °C and a constant true strain rate of 0.01 s$^{-1}$, and the rate-dependent response at 20 °C for the same material.

## Discussion

The temperature- and rate-dependent yield stresses of the PCs are in Figures 4 (a) and (b). Moreover, the yield stresses of PC1 are higher than the PCs with a lower molecular weight and the co-PC.
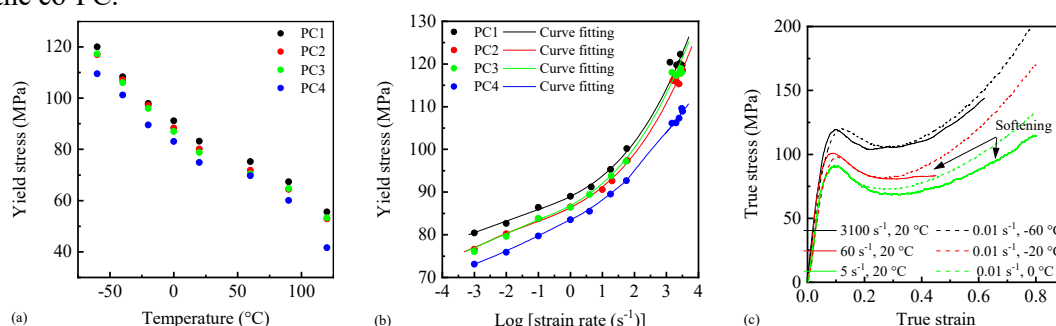


Figure 4 (a) Temperature-dependent yield stress (b) Rate-dependent yield stress (c) Comparing low-temperature and high rate performances of PC1

For the large strain behaviour, the effects of adiabatic heating are considered for high rate loading. Using the method described in our previous work [1, 3], the transition from isothermal to fully adiabatic conditions occurs at a rate of 0.6 s-1. Comparisons between low-temperature low rate data and room temperature high rate data for PC1 are shown in Figure 4 (c). The low-temperature and high-rate data agree well for strains lower than 0.3, whilst softening processes are more evident at a medium rate (5 and 60 s-1) than the high rate (3100 s-1).

The rate- and temperature-dependent strain softening and hardening behaviours of PC were investigated in [8, 9], and the consequence implied was that the secondary transition only affected the strain hardening rather than the strain softening. However, the highest rate and lowest temperature used in these compression tests were 0.01 s$^{-1}$ and -20 °C, respectively. The rate is neither high enough nor the temperature low enough to understand the effects of $\beta$-transition on the high rate performance. In this current work, Figure 4 (c) shows that the constitutive behaviour of the low-temperature QS test and room temperature high rate test is similar to each other at strains up to 0.6. This is consistent with the results of Kendall and Siviour [2], but is still surprising. Significant temperature rises in high rate loading of PC have been reported in the literature [10], but the data here imply that the temperature rise does not qualitatively affect the stress-strain relationship in the material.

## Conclusions

In this study, information about the constitutive behaviour of four different grades of polycarbonates was obtained in low-rate experiments and then compared with the high-rate response. A master curve of storage modulus constructed from Dynamic Mechanical Analysis data was employed to understand the viscoelastic response under small-strain loading at various frequencies and temperatures. For the large-strain constitutive response, experiments at strain rates from 0.001 s$^{-1}$ to 3000 s$^{-1}$ were performed using a conventional crosshead device, hydraulic device, and split-Hopkinson pressure bar. Moreover, experiments at strain rates of 0.01 s$^{-1}$ and temperatures from -60 to 120 °C were also performed, and their results were compared. Although it is known from the literature that the temperature significantly rises in high rate loading, the strain softening and strain hardening behaviours are not significantly affected compared to the quasi-static results. These softening processes were more obvious in medium-rate tests. This indicates that the low-rate low-temperature data might be used to represent high strain rate behaviours; however, further work is needed to fully understand the mechanisms that govern post-yield responses and this apparent lack of sensitivity.

## Acknowledgements

## References

[1] Kendall, M.J. and C.R. Siviour, *Polymer*, **2013**. 54(18). 5058-5063.

[2] Kendall, M.J. and C.R. Siviour, *Philos Trans A Math Phys Eng Sci*, **2014**. 372(2015). 20130202.

[3] Song, P., A.R. Trivedi, and C.R. Siviour. in *DYMAT 2021 - 13th International Conference on the Mechanical and Physical Behaviour of Materials under Dynamic Loading*. **2021**. 250(06013): EDP Sciences.

[4] Trivedi, A.R. and C.R. Siviour, *Mechanics of Time-Dependent Materials*, **2020**.

[5] Furmanski, J., C.M. Cady, and E.N. Brown, *Polymer*, **2013**. 54(1). 381-390.

[6] Siviour, C.R. and J.L. Jordan, *Journal of Dynamic Behavior of Materials*, **2016**. 2(1). 15-32.

[7] Siviour, C.R. in *AIP Conference Proceedings*. **2017**. 1793: AIP Publishing LLC.

[8] Senden, D.J.A., S. Krop, J.A.W. van Dommelen, and L.E. Govaert, *Journal of Polymer Science Part B: Polymer Physics*, **2012**. 50(24). 1680-1693.

[9] Van Breemen, L.C.A., T.A.P. Engels, E.T.J. Klompen, D.J.A. Senden, and L.E. Govaert, *Journal of Polymer Science Part B: Polymer Physics*, **2012**. 50(24). 1757-1771.

[10] Rittel, D., *Mechanics of Materials*, **1999**. 31(2). 131-139.

# The temperature rise in polycarbonate at varying temperature and rate compression tests during large strain deformation

Peihao Song[1, 2*], Akash R Trivedi[1,2], and Clive R Siviour[1]

[1]*Department of Engineering Science, University of Oxford, Parks Road, OX1, 3PJ, UK*
[2]*DPI, P.O. Box 902, 5600 AE Eindhoven, the Netherlands*
*Corresponding author: peihao.song@eng.ox.ac.uk*

Summary: The temperature rise in polycarbonate during compression tests at varying rate and temperature are measured using a thermocouple. The conversion ratio of plastic work to heat during large strain deformation in these loading scenarios are estimated.

## Introduction

It is well known that the mechanical response of most polymers is highly rate and temperature-dependent, and that the mechanical work of plastic deformation can be converted to heat, which can cause observable temperature rises under adiabatic conditions during large strain deformation [1-4]. Moreover, the low-temperature and high rate mechanical performances of many polymers are affected by the secondary ($\beta$)-transition, which occurs around -40 °C for polycarbonate [5, 6]. Safari *et al.* [7, 8] performed expeiments in compression at rates up to order $10^4$ s$^{-1}$; the resulting data indicate that the large strain softening process of PC at a high strain rate is affected by thermal softening. This is partially affected by the $\beta$-transition, and it can lead the strain hardening occurred at lower strains in high rate tests compared with tests under lower strain rates. The rate- and temperature-dependent strain softening and hardening behaviours of PC were also investigated in [9, 10], the data implied that the secondary transition only affected the strain hardening rather than the strain softening. However, the highest rate and lowest temperature used in these experiments were 0.01 s$^{-1}$ and -20 °C, respectively, thus, the effects of $\beta$-transition on the high rate and low temperature performance of PC cannot be entirely understood. In this work, the compression tests were performed at temperatures from -60 to 20 °C, and rates between 0.001 and 0.1 s$^{-1}$. Thermocouples (TC) were used to measure the temperature rise during large strain deformation at 0.1 s$^{-1}$. Finally, the ratios of plastic work to heat were estimated. The ultimate aim of this research is to link performance at low temperatures and high strain rates; however, only the low temperature data are reported here.

## Experimental characterisation and results analysis

LEXAN$^{TM}$ RESIN 500R injection moulded polycarbonate (PC) sheets were kindly supplied by Saudi Basic Industries Corporation (SABIC). The cylindrical compression samples were cut with 5 mm diameter and 3 mm thickness from the centre of these sheets. The sheets were annealed before machining to minimise residual stresses from the manufacturing process.

### *Varying temperature and rate uniaxial compression tests*

Uniaxial compression tests were performed from -60 to -20 °C, at strain rates of 0.001, 0.01 and 0.1 s$^{-1}$ to investigate the rate-dependent mechanical performance around the β-transition region. As expected, Figure 1, the yield stress increases with increasing strain rate at each temperature. Moreover, the stress-strain curves at the rate of 0.01 s$^{-1}$ overlap the curves obtained at 0.1 s$^{-1}$. This is consistent with the experimental environment changing from isothermal to adiabatic between these rates, which results in the thermal softening at large strains. To investigate the temperature-dependent behaviour around the β-transition, the stress-strain curves obtained at the same strain rate and different temperatures are plotted in Figure 2.
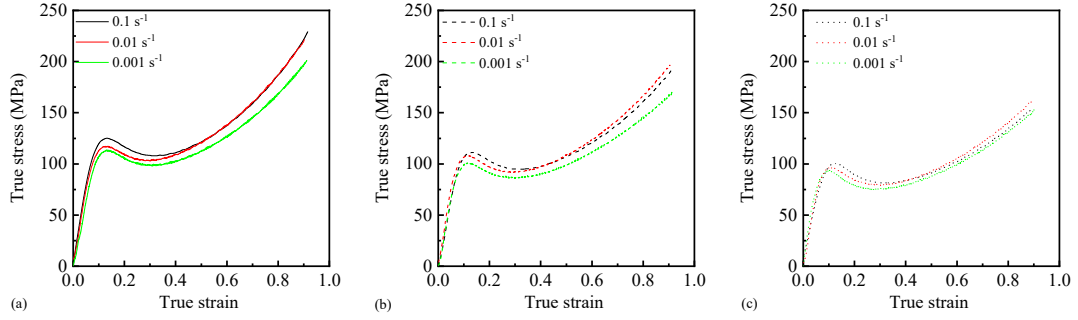
Figure 1 Rate-dependent stress-strain curve at (a) -60 °C, (b) -40 °C, (c) -20 °C
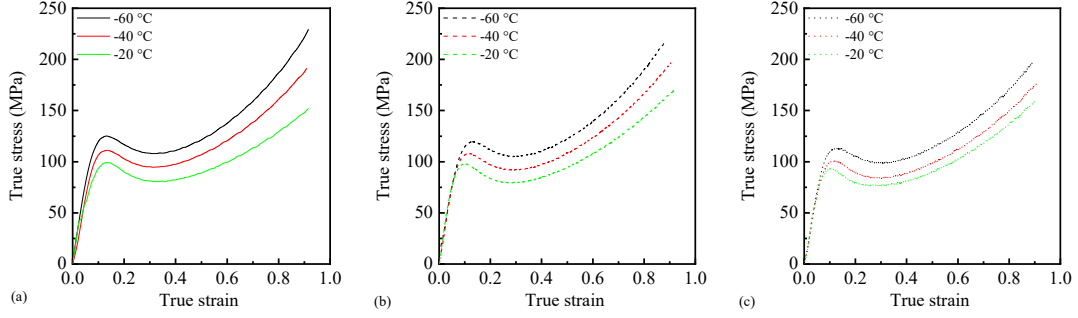


Figure 2 Temperature-dependent stress-strain curve at (a) 0.1 s$^{-1}$, (b) 0.01 s$^{-1}$, (c) 0.001 s$^{-1}$

*Temperature rise measurement at varying temperatures and strain rates*

Thermocouples were employed to measure the temperature rise during the large strain deformation at the rate of 0.1 s$^{-1}$ to quantify the self-heating effects. Analytical temperature rises are estimated using

$$\Delta T\left(\varepsilon\right)=\frac{\beta}{\rho C_p}\int_{\varepsilon_y}^{\varepsilon}\sigma d_\varepsilon \tag{1}$$

where $\beta$ is the fraction of plastic work converted to heat, often called the Taylor-Quinney factor (TQF), the density $\rho$ is 1200 kg/m$^3$, and the temperature-dependent specific heat capacity $C_p$ is taken from Modulated Differential Scanning Calorimetry (MDSC) experiments, which give values of 0.77, 0.88, 0.98 and 1.18 J/(g °C) at -60, -40, -20 and 20 °C respectively.
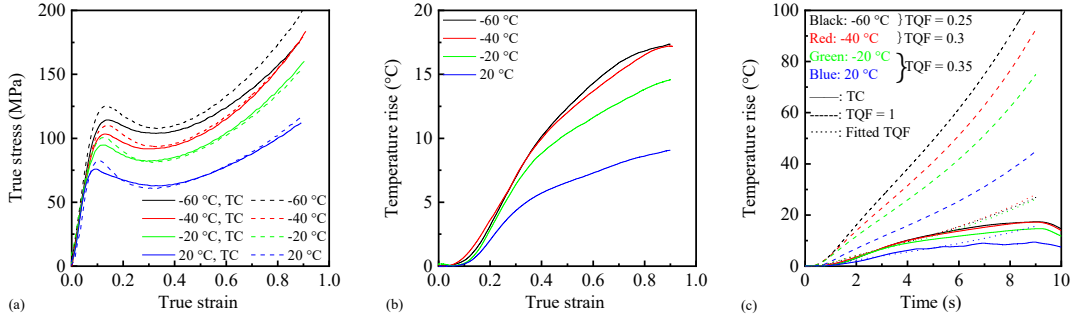


Figure 3 Varying rate tests at 0.1 s$^{-1}$ (solid line and dash line show experiments with and without a thermocouple, respectively), (b) The temperature rise against true strain, (c) Analytical temperature rise versus time

Figure 3 (a) shows a comparison between the stress-strain curves tested with and without thermocouples. The yield stresses of the experiments with TC are lower than the tests without TC for all temperatures. However, the experiments carried out with and without TC from -40 to 20 °C overlapped well in the plastic region. Concerning the plastic region of the -60 °C experiment, the stress-strain curves were not consistent between tests with and without TC, thus, when calculating the analytical temperature rise the stress-strain curves with the thermocouples were used. Whilst we would expect a higher temperature rise at -60 °C

compared to -40 °C, a similar rise is observed, Figure 3 (b). The analytical solutions for temperature rises are plotted in Figure 3 (c): 1) assuming plastic work is fully converted heat (TQF = 1); 2) assuming the plastic work is partially converted to heat with the most suitable TQF. For -20 and 20 °C, the analytical temperature rise overlaps with the value provided by the TC when TQF equals 0.35. However, the TQF were assigned as 0.3 and 0.25 at -40 and -60 °C. This difference might be due to the restrictions in the secondary motions below -40 °C. It is noted that the temperature rise versus strain curves showed a bilinear relation in Figure 3(b). This might be a result of increased heat conduction as the specimens become thinner, or indicate thatsome energy is used to make microstructure evolution during the large strain deformation so that the generated heat is decreased. It should be noted that the fitted TQFs probably include some contribution from thermal losses (i.e. the experiments are not completely adiabatic), and this is the subject of further investigation.

## Conclusion and outlook

This paper describes the rate- and temperature-dependent stress-strain curves from -60 to -20 °C. In the small strain region, increasing the strain rate and decreasing the temperature have similar effects that can increase the yield stress of the material, which is consistent with the time-temperature equivalence principle. However, the stresses at the large strain regime of experiments performed at the rate of $0.1 \text{ s}^{-1}$ were lower than expected compared with lower rate tests because of the thermal softening. Temperature rises from -60 to 20 °C at a rate of $0.1 \text{ s}^{-1}$ were measured using an embedded thermocouple. The temperature rises present an increasing trend with decreasing initial temperature, consistent with the stress-strain curves. The Taylor-Quinney factors obtained from the -60 and -40 °C tests are lower than tests with the temperature above the secondary transition. This may be because energy is required to enable secondary motions when the temperature is lower than -40 °C. Further experiments are needed to verify the effects at a temperature lower than -60 °C. At the same time, temperature rise measurements at medium- and high-rate will be carried out.

## Acknowledgements

## References

[1] Kendall, M.J. and C.R. Siviour, *Polymer*, **2013**. 54(18). 5058-5063.
[2] Kendall, M.J. and C.R. Siviour, *Philos Trans A Math Phys Eng Sci*, **2014**. 372(2015). 20130202.
[3] Regev, A. and D. Rittel, *Experimental mechanics*, **2008**. 48(5). 675-682.
[4] Rittel, D., *Mechanics of Materials*, **1999**. 31(2). 131-139.
[5] Song, P., A.R. Trivedi, and C.R. Siviour. in *DYMAT 2021 - 13th International Conference on the Mechanical and Physical Behaviour of Materials under Dynamic Loading*. **2021**. 250(06013): EDP Sciences.
[6] Siviour, C.R., S.M. Walley, W.G. Proud, and J.E. Field, *Polymer*, **2005**. 46(26). 12546-12555.
[7] Safari, K.H., J. Zamani, F.J. Ferreira, and R.M. Guedes, *Polymer Engineering & Science*, **2013**. 53(4). 752-761.
[8] Safari, K.H., J. Zamani, R.M. Guedes, and F.J. Ferreira, *Mechanics of Time-Dependent Materials*, **2015**. 20(1). 45-64.
[9] Senden, D.J.A., S. Krop, J.A.W. van Dommelen, and L.E. Govaert, *Journal of Polymer Science Part B: Polymer Physics*, **2012**. 50(24). 1680-1693.
[10] Van Breemen, L.C.A., T.A.P. Engels, E.T.J. Klompen, D.J.A. Senden, and L.E. Govaert, *Journal of Polymer Science Part B: Polymer Physics*, **2012**. 50(24). 1757-1771.

# Experimentally simulating the adiabatic self-heating observed in polymers under high rate loading

Akash R. Trivedi[1,2]*, Peihao Song[1,2] and Clive R. Siviour[1]

*[1] Department of Engineering Science, University of Oxford, Parks Road, OX1 3PJ, UK*
*[2] DPI, P.O. Box 902, 5600 AX Eindhoven, the Netherlands*
* Corresponding author: akash.trivedi@eng.ox.ac.uk

## Abstract

Polymers are widely used in engineering applications where they may be subjected to dynamic or impact loading, leading to high rate deformation, at a variety of temperatures. The mechanical response of these materials is highly rate and temperature dependent, and as such, they must be well characterised and understood. One observation that is common in the post-yield, large strain deformation of polymers under high rate loading is adiabatic self-heating. This is the thermal softening that occurs in the sample as the mechanical energy is converted to heat, which cannot diffuse out of the sample on the timescale of the high rate experiment.

In previous research [1], it was shown that it was possible to predict the compressive high rate response of (plasticised) poly(vinyl chloride) using a model calibrated using simple, low rate experiments. This is consistent with experimental observations by Kendall and Siviour [2], in which high rate deformation was experimentally replicated using low rate experiments with heating profiles.  In both cases, details of this adiabatic self-heating were included by assuming a full conversion of the mechanical energy to heat. However, Kendall and Siviour [3] showed that this assumption does not produce consistent results for polycarbonate.

In this paper, a novel experimental apparatus is presented, which allows the adiabatic self-heating to be simulated with a programmed temperature profile. This is applied to polycarbonate samples during quasi-static experiments, and the results are compared to medium and high strain rate experiments on the same material. This enables the mechanical-heat conversion to be investigated systematically and gain a better understanding with which to improve our predictive models.

## References

[1] Trivedi, A.R. and Siviour, C.R., 2020. *Mechanics of Time-Dependent Materials*. (in press) https://doi.org/10.1007/s11043-020-09450-4
[2] Kendall, M.J. and Siviour, C.R., *Polymer* **54** 5058-5063 (2013)
[3] Kendall, M.J. and Siviour, C.R., *Philos. Trans. A. Math. Phys. Eng. Sci.* **372**, 20130202 (2014)

# A continuum-micromechanical model for crazing in glassy polymers under cyclic loading

Tobias Laschütza, Thomas Seelig

*Institute of Mechanics, Karlsruhe Institute of Technology, Germany*
*tobias.laschuetza@kit.edu; thomas.seelig@kit.edu*

Shear yielding and crazing are the key deformation and damage mechanisms which govern the inelastic behaviour of glassy polymers. Much research has been devoted to modeling and understanding their occurrence and eventual competition under monotonic loading conditions; e.g. [1-3]. However, theoretical studies concerning the interaction of crazing and shear yielding under cyclic loading are still rare to date. State-of-the-art constitutive models for the bulk deformation behaviour of glassy polymers account for non-monotonic loading phenomena such as the Bauschinger effect (e.g. [4]). Yet, existing crazing models are so far primarily applicable to monotonic loading.

The present work focuses on the development of a continuum-micromechanical model for crazing that realistically describes the response under cyclic loading. That is, in addition to the non-linear viscoelastic-viscoplastic stretching of the fibrillated craze matter under loading, the model accounts for fibril growth due to drawing in of bulk material as well as creep-recovery when unloaded (e.g. [5]). With a parameter study, the model capabilities are investigated and subsequently the model is applied to a boundary value problem of a mode I crack under cyclic small scale yielding loading conditions.

## References

[1] Estevez, R.; Tijssens, M. G. A.; van der Giessen, E., *Journal of the Mechanics and Physics of Solids* **2000**, 48(12), 2585-2617.
[2] Gearing, B. P.; Anand, L., *International Journal of Solids and Structures* **2004,** 41(12), 3125-3150.
[3] Socrate, S.; Boyce, M.C.; Lazzeri, A., *Mechanics of Materials* **2001**, 33(3), 155-175.
[4] Holopainen, S., *Mechanics of Materials* **2013**, 66, 35-58.
[5] Kambour, R. P.; Kopp, R. W. S., *Journal of Polymer Science Part A-2: Polymer Physics* **1969**, 7(1), 183-200.

# Modelling viscoelasticity(plasticity) in polymers from networks theory and time temperature superposition principle

Noëlle Billon

*MINES ParisTech, Université PSL, Centre de mise en forme des matériaux (CEMEF), CNRS UMR 7635, Sophia Antipolis, France.*

The potential of the development of mechanical approach based on the physics of polymers is well accepted. In that field, the time temperature superposition principle has proved its interest [1-3].

In parallel, a revisited constitutive model [1,4] was proposed that models the complex mechanical behaviour of amorphous and semi crystalline polymers close to glass transition temperature. This model accounts for the elastic contribution of an equivalent network which experiences inelastic mechanisms coming from the evolution of internal state variables when the polymer is deformed.

The experimental database included non-monotonic tensile and shearing tests at targeted "equivalent strain rate at reference temperature" coupled with DIC for obtaining local boundary conditions.

Model exhibited good capabilities to capture the mechanical response of the material at different temperatures and strain rates corresponding to material state ranging from the end of the glassy state to near-liquid state going through viscoelastic and rubbery regime.

Recent improvements allow well reproducing the monotonic and cyclic behaviour of PMMAs as well as PA66 from rubbery like domains to their glassy state with one unique formalism and one unique (and of reduced number) set of parameters.

Conference deals at summarising potential and limitations of such approaches.

## References

[1] Billon, N., J Appl Polym Sci 2012, 125, 4390-4401.
[2] Diani, J.; Gilormini, P.; Arrieta, I.S., Polymer 2015, 58, 107–112.
[3] Federico, C.E.; Bouvard, J.L.; Combeaud, C.; Billon, N., Polymer 2018, 139, 177 – 187.
[4] Maurel-Pantel, A.; Baquet, E.; Bikard, J.; Bouvard, J.L.; Billon, N., Int J Plast 2015, 67, 102-126.

# Full-field micromechanical simulations of semi-crystalline polymers using the FFT method on RVEs obtained by an enhanced phase field model

Amine Bahloul [12], Issam Doghri[1], Laurent Adam[2]

*1 Université Catholique de Louvain, Institute of Mechanics, Materials and Civil Engineering (IMMC), Bâtiment Euler, 4 Avenue G. Lemâitre, B-1348 Louvain-la-Neuve, Belgium*
*2 e-Xstream engineering | Hexagon, 5 rue de Bommel, Z.A.E. Robert Steichen, 4940, Luxembourg*
*(amine.bahloul@student.uclouvain.be, issam.doghri@uclouvain.be, laurent.adam@hexagon.com).*

*An enhanced phase field model proposed by the authors enables to model polymer crystallization and to predict spherulite growth and representative semi-crystalline micro-structures in 2D or 3D* **[1].** *After solidification, the value of the phase field variable in each subcell (2D pixel or 3D voxel) indicates whether the material is amorphous or crystalline. In a recent work proposed by the authors* **[2]**, *full-field micromechanical simulations are performed on the microstructures generated by the enhanced phase field model in order to predict the effective mechanical properties. A Fast Fourier Transform (FFT) method with periodic boundary conditions is used. Care is taken to obtain representative volume elements (RVEs) by computing the number of subcells in each spherulite and the number of spherulite nucleations in each RVE. Numerical FFT predictions of elastic properties for a range of crystallinity ratios are validated against experimental data and compared to simpler composite inclusion models Fig.1. Finite element simulations of thermal shrinkage can be also provided. The conductivity of the RVE can be obtained when a temperature gradient is applied to it in a thermal simulation. The approach was numerically implemented in a research version of the Digimat software. In this work, the polyethylene (PE) was used to validate the model in linear elasticity, whose orthotropic elastic properties of its crystal phase were determined by Choy and Leung* **[6]**. *The amorphous phase is isotropic thanks to the random location of the polymer chains.*

*Currently, the authors are trying to introduce a behaviour more consistent with the physics of polymers for each amorphous and crystalline phase. Generally, an elasto-viscoplastic (EVP) model is used for the crystalline phase, where the elastic part is characterized by an orthotropic tensor and the viscoplastic part is modelled using a slip system model. It is possible to experimentally prove that the viscoelastic criterion of the polymer comes mainly from the amorphous phase by comparing the loss factor for different degrees of crystallinity. The viscoelastic parameters of the amorphous phase are calculated by fitting the macro response of RVE to the experimental data by using Digimat MX software Fig.2. In the context of the SLS process, the evolution of the porosity is a very important factor in the final behaviour of the RVE. Among the objectives is to find its law of evolution and to simulate its impact on the behaviour of the RVE.*
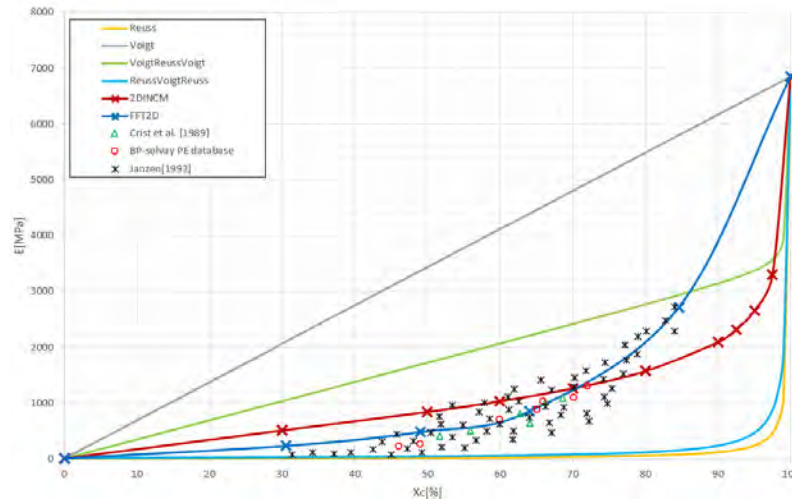
Figure 1: Young's modulus of Polyethylene as a function of the crystallinity ratio. Comparison between experimental data [3], [4] and [5], the proposed phase field based FFT model (FFT2D),a composite inclusion based plane strain RVE model (2DINCM) and 4 simple models.
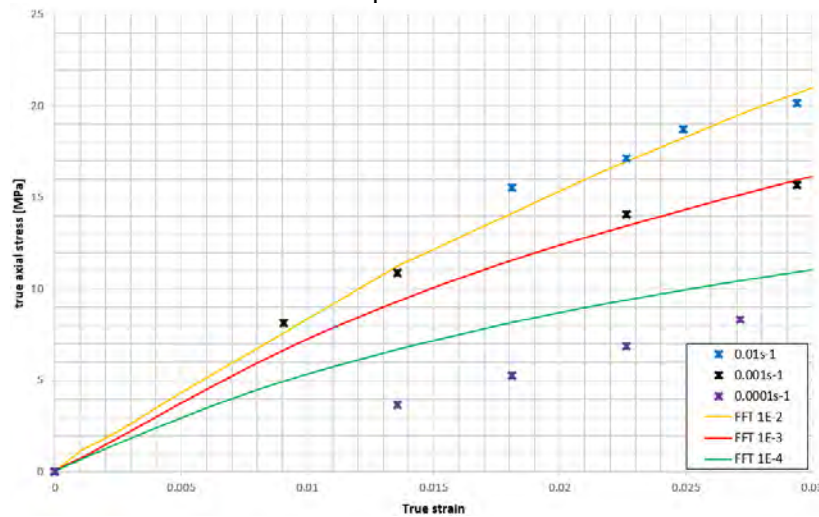


Figure 2: HDPE tensile curve at different strain rates (Exp vs Model).

# References

[1] A.Bahloul, I.Doghri, L.Adam. Polymer crystallization, 2020, 3, e10144.

[2] A.Bahloul, I.Doghri, L.Adam. Computational Materials Science, 2021, 199, 110685.

[3] F. Bédoui, J. Diani, G. Régnier, W. Seiler. Acta Materialia,2006, 54, 1513 - 1523.

[4] Janzen, Jay. Polymer Engineering & Science, 1992, 32, 1242-1254.

[5] Crist Buckley, Fisher Christopher, Howard Paul. Macromolecules,1989, 22, 1709-1718.

[6] Choy, Leung. Journal of Polymer Science: Polymer Physics Edition, 1985, 23, 1759-1780.

# Constitutive Modelling of Amorphous Polymers at High Strain Rates

Grace M. Owen, Davide S.A. De Focatiis

*Department of Mechanical, Materials and Manufacturing Engineering, Faculty of Engineering, University of Nottingham, NG7 2RD, UK. Email: davide.defocatiis@nottingham.ac.uk*

This work presents advances to a physically based constitutive model based on the Oxford Glass-Rubber model for the simulation of the mechanical response of amorphous polymers at high rates of strain. Considerations of adiabatic heating, structural evolution and the presence of the $\beta$-transition are applied to experimental data on polycarbonate.

## Introduction

Polymers and their composites are frequently used in components that may be exposed to high strain rate loading, such as impact events, in a wide variety of fields from automotive to aerospace to medicine. Examples of such products include car bumpers, aircraft fuselages and bone repair supports. However, their behaviour can vary significantly between quasi-static conditions and impact events, as well as at low and high temperatures. A lack of a sufficient understanding of these differences and their underlying physical origins can inhibit optimisation of the material properties with respect to the structural design of the polymer and composite components. A constitutive model that can simulate a very broad range of rates and temperatures is a major challenge, but is essential to describe the full spectrum of the mechanical behaviour of polymers. The objective of this work is to contribute to the development of such a physically based model, focusing here on the particular challenges present in amorphous polymers at high rates of strain.

## Materials and Methods

Although the constitutive model described herein is more generally applicable to glassy polymers, the process of parameterisation is focused on polycarbonate and based on data obtained at the University of Oxford on LEXAN PC 103R (MFR ~6, DBT = -30°C) kindly provided by Sabic. Quasi-static experiments were conducted using screw-driven test machines primarily in compression at a range of temperatures and constant true strain rates to provide input data for the constitutive model. Medium strain rate experiments made use of servo-hydraulic testing, and high strain rate experiments employed the split Hopkinson bar technique. The linear viscoelastic response was measured using dynamic mechanical analysis to obtain isothermal frequency sweeps that were shifted in the frequency domain to produce both viscoelastic mastercurves and shift factors. This was supplemented by linear shear rheology for temperatures above the glass transition.

Our constitutive model is fundamentally based on the Oxford glass-rubber constitutive model [1], inspired by the one-dimensional model first proposed by Haward and Thackray [2], and later developed into a fully 3-dimensional implementation [3,4]. Two contributions are ascribed to the free energy and hence the stress, arising from perturbation of interatomic potentials, relaxed by isotropic segmental flow, and from perturbation of conformational entropy of the entangled molecular network, represented in the glassy state as a crosslinked network. The crosslinked network is modelled here by an Edwards-Vilgis function [5], although other functions have been successfully used in the literature.

The constitutive model describes the material response to a deformation gradient tensor $F$ in terms of the Cauchy stress tensor $\sigma$. The volumetric parts of $F$ and $\sigma$ are separately dealt with assuming linear elasticity such that the mean stress can be defined by $\sigma_{\mathrm{m}} = \frac{1}{3}\mathrm{tr}\,\sigma = K \ln J = K \ln(\det F)$ and $S = \sigma - \sigma_m I$ where K is the bulk modulus.

The deviatoric part of the deformation gradient, $\bar{F} = J^{-\frac{1}{3}}F$ , is used to determine the deviatoric stress $S = S^{\mathrm{b}} + S^{\mathrm{c}}$ from the separate contributions of bond-stretching and conformational stresses, and mirrors previous approaches [1,3]. The deviatoric rate of deformation tensor $\bar{D}$ , obtained in the classical way, is the sum of a linear elastic bond stretching part, and a viscous flow part, and, using an $N$-mode spectrum [4],

$$\bar{D} = \frac{\hat{S}_j^{\mathrm{b}}}{2G_{\mathrm{b}}} + \frac{S_j^{\mathrm{b}}}{2G_{\mathrm{b}}\tau_j} \quad \text{and} \quad S^{\mathrm{b}} = \sum_{j=1}^{N} \upsilon_j S_j^{\mathrm{b}}, \quad \sum_{j=1}^{N} \upsilon_j = 1$$

where $G_b$ is the shear modulus, and $\tau_j$ and $\upsilon_j$ are the $j$-th relaxation time and modal fractions respectively. Here as previously $\hat{S}_j^b$ is the material rate of stress and implemented as the Jaumann rate. The linear viscoelastic shear relaxation spectrum is used to obtain the modes as shown in Figure 1a.

Each relaxation time is referred back to an unstressed relaxation time $\tau_{j,0}^*$ at a reference temperature $T^*$ and structural state $T_f^*$ such that $\tau_j = a_T a_s a_{\sigma,j} \tau_{j,0}^*$ through shift factors for temperature, structure and stress respectively, which are defined as

$$a_T = \exp\left[\frac{\Delta H}{R}\left(\frac{1}{T} - \frac{1}{T^*}\right)\right], \quad a_s = \exp\left[\frac{C}{T_f - T_\infty} - \frac{C}{T_f^* - T_\infty}\right] \quad \text{and} \quad a_\sigma = \frac{V_s \tau_{\text{oct},j}^b}{2RT}\exp\left(-\frac{V_p \sigma_m}{RT}\right)\left[\sinh\left(\frac{V_s \tau_{\text{oct},j}^b}{2RT}\right)\right]^{-1}$$

## Results and Discussion

### *Model parameterisation*

Parameters $\Delta H$, $C$ and $T_\infty$ can be obtained by optimisation on the experimental data, but care needs to be taken to, at this stage, ignore data past the $\beta$–transition and in the proximity of the $\alpha$-transition (where $T_f$ is known to be ill-defined). A comparison of the combined effect of the temperature and structure shift factors, otherwise known as the classical Macedo-Litovitz (ML) equation in viscosity terms, is shown in Figure 1b vs experimental data.
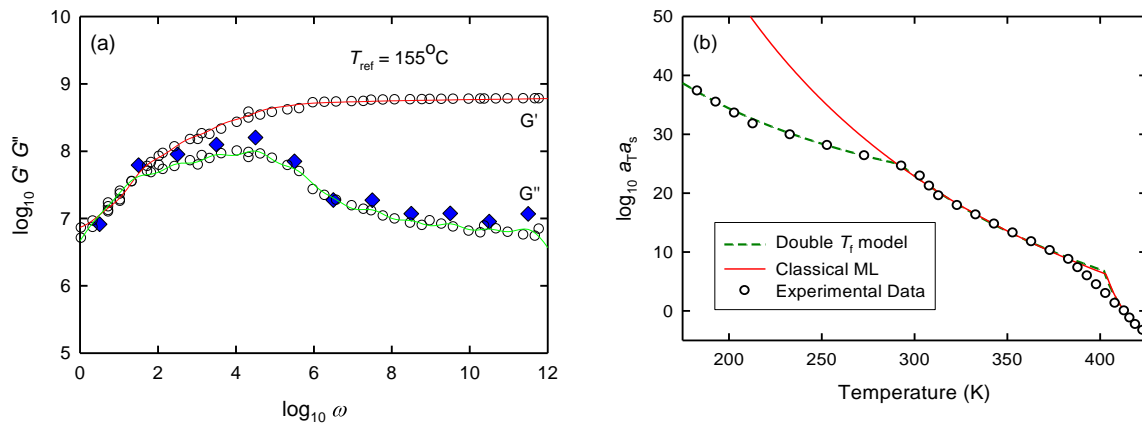


Figure 1 (a) The experimental linear shear viscoelastic relaxation spectrum (circles), the Maxwell modes (diamonds) and the constitutive model response (lines); (b) the shift factors obtained experimentally (circles), the classical ML model (solid line), and the double $T_f$ model (dashed line).

Now to focus on analysis of the quasi-static experimental constant true strain rate data. Measurements of the compressive yield stress as a function of strain rate are used to determine the shear activation volume $V_s$. We then consider that, in a constant true strain rate experiment and following saturation of the yield process, the flow stress remains constant. This means that data for compressive strains $\varepsilon > 36\%$ can be used to obtain the conformational stress. Optimised parameters $N$, $\alpha$ and $\sigma_{\text{flow}}$, corresponding to the network constraint density, the finite extensibility parameter, and the constant flow stress respectively, are determined on the range of data available. As shown for four selected temperature examples in Figure 2a, there is remarkable agreement between this simple model and the broad range of data. The finite extensibility parameter $\alpha$ was found to remain approximately constant at a value of 0.27±0.02, while both $N$ and $\sigma_{\text{flow}}$, are dependent on rate and temperature, but in a manner consistent with the shift factors obtained earlier, as shown for the example in Figure 2b. Unfortunately, it is not possible to obtain conformational parameters with confidence in high strain rate experimental data.
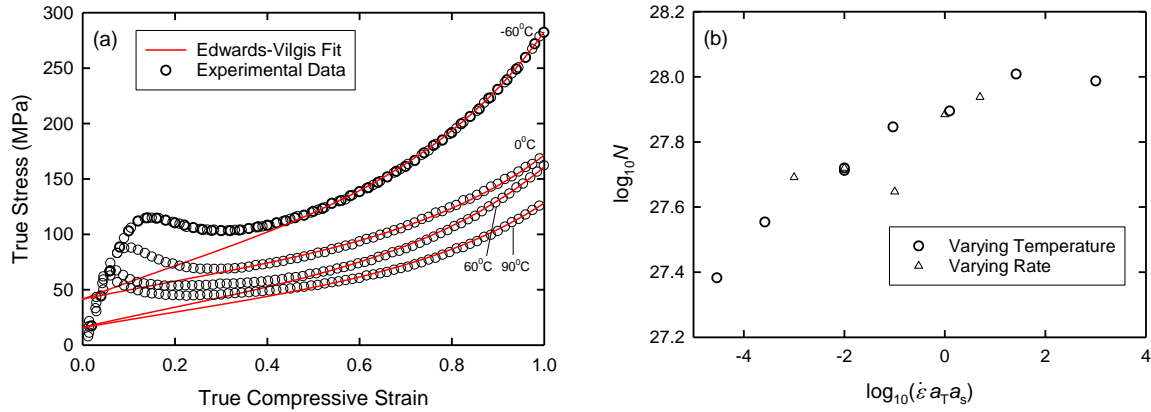
Figure 2 (a) Selected examples of compressive stress-strain data (circles) overlayed with simplified model simulations of an Edwards-Vilgis function with an added constant flow stress (lines); (b) the network density as a function of reduced rate obtained from a range of temperature and rate experiments.

### Structural evolution

To account for structural change within the polymer, the glass structure is defined in terms of the fictive temperature $T_f$. Previous implementations employed an approximate semi-empirical description of the evolution of $T_f$ [4]. In order for the model to be applicable to as broad a set of rates and temperatures as possible, the differential form of the structural evolution equations first proposed in [6] for the modelling of high strain rate deformations in epoxy resins and later implemented for polypropylene by [7,8] is used here,

$$\dot{T}_f = \frac{T_f - T}{\bar{\tau}^* a_s a_T} + \kappa \dot{\bar{\varepsilon}}_v$$

where $\bar{\tau}^*$ is the geometric mean reference relaxation time, $\dot{\bar{\varepsilon}}_v$ is the rate of effective viscous strain and $\kappa$ is a constant. This model produces a rise in $T_f$ with plastic strain, which leads to a stress drop after yield, and an eventual saturation of the rise in $T_f$ which depends on both rate and temperature.

### Adiabatic heating

At sufficiently high strain rates, and due to a high thermal diffusivity, polymer deformation occurs under adiabatic conditions. The energy input is transferred into four parts: a recoverable part stored as elastic strain energy in stretched bonds (both in shear and volumetric deformations), a non-recoverable part due to plastic deformation associated with viscous shearing of polymer segments, and two further parts, one associated with structural change and another with conformational change. Although plastic deformation accounts for the majority of the energy post-yield, there is expected to be a reduction in the temperature change due to the rise in fictive temperature, particularly in the proximity of yield. At sufficiently large stresses, where the conformational stress begins to dominate, it is important to consider the entropic nature of the entanglement network. Given sufficient time, the entropy-elasticity will contribute to a further temperature rise, but it is questionable whether this can really be the case at sufficiently high strain rates. Here it may be more reasonable to assume that, at least initially, further energy is stored elastically, and that this may transition to an entropic energy storage (and hence a temperature rise) over a given timescale. At present it is unclear what this timescale may be, but it is reasonable to consider that this may occur at a timescale associated with the Rouse relaxation time of an entanglement length, and thus, for the purpose of impact experiments be elastic rather than entropic [9]. We hope to be able to shed more light on this by careful comparison with experiments.

### The β-transition

It is apparent when looking at yield stresses as a function of rate at high strain rates, or by looking at the shift factors obtained at low temperatures in Figure 1b, that the β-transition plays an important role in determining properties at high rates and low temperatures. In polycarbonate, there is still debate in the literature as to the precise molecular origin of the β-transition [10] but there is agreement that it must be associated with segmental motions of parts of the monomer or with relationships between different parts of the monomer. As a means of attempting to capture this somewhat empirically, we propose the introduction of two distinct fictive temperatures, one associated with segmental motions of the entire monomer or Kuhn segment termed $T_{f\alpha}$, and another associated

with sub-segmental motions termed $T_{f\beta}$. We attribute the same meaning to these as the classical fictive temperature defines the structural state out of equilibrium as $T_f > T$. Thus, above the a-transition we have $T_{f\alpha} = T_{f\beta} = T$, below the b-transition both $T_{f\alpha} > T$ and $T_{f\beta} > T$, but in the intermediate region (at quasistatic rates this corresponds to temperatures between ~20 and ~120 °C), we have $T_{f\alpha} > T$ but $T_{f\beta} = T$. Using a similar approach to the Vogel-Tamman-Fulcher equation, we introduce two structural shift factor terms, each with their own constants defined as,

$$a_{s\alpha} = \exp\left[\frac{C_\alpha}{T_{f\alpha} - T_{\infty\alpha}} - \frac{C_\alpha}{T_{f\alpha}^* - T_{\infty\alpha}}\right] \quad \text{and} \quad a_{s\beta} = \exp\left[\frac{C_\beta}{T_{f\beta} - T_{\infty\beta}} - \frac{C_\beta}{T_{f\beta}^* - T_{\infty\beta}}\right]$$

and apply this together with an Arrhenius temperature shift factor to the experimental data. As shown in Figure 1b, this approach can provide a convincing representation to the shift factors below the $\beta$-transition whilst maintaining the behaviour above the transition. A full implementation will require some form of evolution equation for $T_{f\beta}$, and it is clear that this should occur over a much shorter timescale than that associated with $T_{f\alpha}$, which is currently approximated as the mechanical relaxation time in the absence of stress.

## Conclusions

This work has presented developments in a physically based constitutive model for glassy polymers focusing on the requirements of high strain rate simulations. Structural evolution is modelled using a differential equation for the evolution of the fictive temperature, and considerations have been made for the inclusion of adiabatic heating and for the presence of the $\beta$-transition. There are still many unanswered questions concerning the behaviour of glassy polymers at high strain rates, but it is hoped that the model will enable progress in this area by careful comparison with forthcoming experimental data at high rates of strain.

## References

[1]  Buckley C.P.; Jones D.C., Glass-rubber constitutive model for amorphous polymers near the glass transition. *Polymer (Guildf)* **1995**, *36(17)*, 3301–12.
[2]  Haward R.; Thackray G., The use of a mathematical model to describe isothermal stress-strain curves in glassy thermoplastics. *Proceedings of the Royal Society of London. Series A, Mathematical and Physical Sciences* **1968**, *302*, 453–72.
[3]  Dooling P.J.; Buckley C.P.; Rostami S.; Zahlan N., Hot-drawing of poly ( methyl methacrylate ) and simulation using a glass-rubber constitutive model. *Polymer* **2002**, *43*, 2451–65.
[4]  Wu J.J.; Buckley C.P., Plastic deformation of glassy polystyrene: A unified model of yield and the role of chain length. *Journal of Polymer Science Part B Polymer Physics* **2004**, *42(11)*, 2027–40.
[5]  Edwards S.F.; Vilgis T., The effects of entanglements in rubber elasticity. *Polymer (Guildf)* **1986**, *27*, 483–492.
[6]  Buckley C.P.; Dooling P.J.; Harding J.; Ruiz C., Deformation of thermosetting resins at impact rates of strain. Part 2: Constitutive model with rejuvenation. *Journal of the Mechanics and Physics of Solids* **2004**, *52(10)*, 2355–77.
[7]  Okereke M.I.; Akpoyomare A.I., Two-process constitutive model for semicrystalline polymers across a wide range of strain rates. *Polymer (Guildf)* **2019**, *183*, 121818.
[8]  Okereke M.I.; Le C.H.; Buckley C.P., A new constitutive model for prediction of impact rates response of polypropylene. *DYMAT 2012 - 10th International Conference on the Mechanical and Physical Behaviour of Materials under Dynamic Loading, EPJ Web Conferences* **2012**, *26*, 04031.
[9]  De Focatiis D.S.A.; Embery J.; Buckley C.P., Large deformations in oriented polymer glasses: Experimental study and a new glass-melt constitutive model. *Journal of Polymer Science Part B Polymer Physics* **2010**, *48(13)*, 1449-1463.
[10] Quinson R.; Perez J.; Germain Y.; Murraciole J.M., $\beta$- and $\alpha$-relaxations in poly(methyl methacrylate) and polycarbonate: non-linear anelasticity studies by antistress relaxation. *Polymer* **1995**, *36(4)*, 743-752.

# Failure in Long Glass Fiber Reinforced Thermoplastics: Key structural features and how they affect performance

S.J.J. van den Broek, T.A.P. Engels, L.E. Govaert

*Eindhoven University of Technology, Eindhoven, The Netherlands*

Long Fiber Thermoplastic (LFT) composites are an important class of materials combining the processability of thermoplastics with the excellent specific modulus and strength of highly reinforced systems. They enable replacement of metallic semi-structural parts and where allowable structural parts, supporting fuel reduction and vehicle range extension in automotive applications. Their main use is in load-bearing applications, where structural integrity and long-term reliability are of utmost importance and hence the required ability to predict their mechanical performance is evident. A major problem in their practical use is that the fibers orient in flow, leading to anisotropy in the mechanical response, resulting in strong spatial variation over the product.

For a short fiber reinforced composite this is also the case but due to reduced complexity it is often sufficient to measure the fiber orientation, volume fraction and aspect ratio (distribution) in order to describe the microstructure and hence predict the mechanical performance. The microstructure of a LFT system shows however more complexity due to the higher aspect ratios of the fibers. Consequently, the fibers tend to show curvature resulting in a fiber orientation varying over the fiber centerline itself. On top of that this is often accompanied with clustering of the fibers.

Current tools are not able to describe such microstructures in much detail. Therefore, a method is developed which is able to extract these microstructural parameters, i.e. local orientations and curvatures, clustering and aspect ratio distributions, and hence to allow the comparison between different LFT systems based on quantifiable information rather than for example µCT images. This method uses 2D images obtained from µCT measurements which are at first processed in the commercial software package GeoDict in order to make a 3D reconstruction and to identify each individual fiber subsequently as is shown in Figure 1. The obtained individual fibers are then approximated with a set of continuous parametrization functions which allows for the complete orientation and curvature analysis on both a local and macroscopic scale.

With simulations on representative volume elements it is possible to separate and vary these microstructural features separately in contrast to real-life experiments on injection moulded LFT systems. As a result, it is possible to observe the influence of these microstructural features on the performance of the composite.
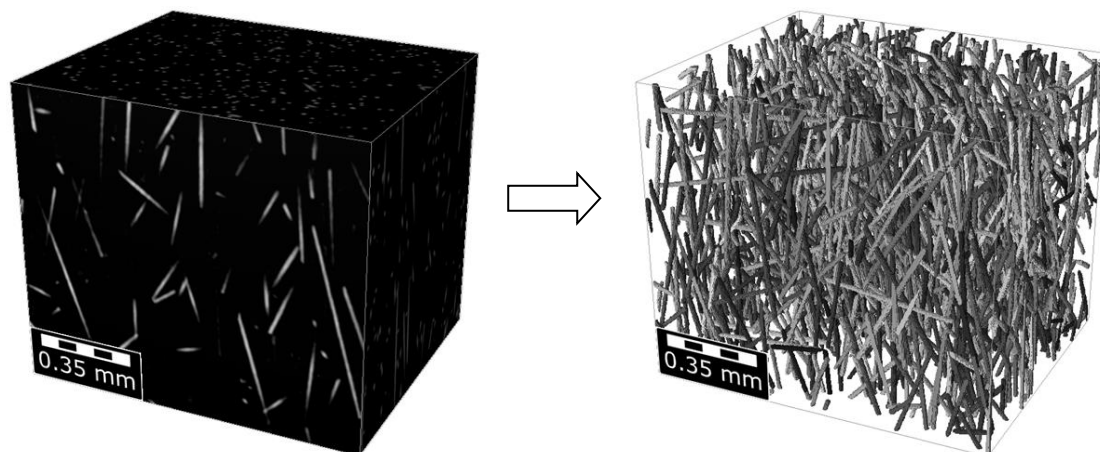


Figure 1: Visualization of the conversion of µCT images into segmented fibers using the GeoDict software.

# Damage mechanisms of amorphous and low semi-crystalline polymers under tensile deformation studied by Ultra Small Angles X-ray Scattering: from the initiation of cavitation to final breaking

Stéphanie Djukic[1], Anthony Bocahut[2][1], Jérôme Bikard[2], <u>Didier R. Long</u>[1]

[1] LPMA, Laboratoire des polymères et Matériaux Avancés, UMR 5268 Solvay/CNRS, Solvay in Axel'One, 87 avenue des Frères Perret CS 70061 69192 Cedex, France
[2] Solvay Research and Innovation Center, 87 avenue des Frères Perret 69192 St-Fons Cedex, France

## Abstract

We investigate the damage mechanisms of amorphous and low semi-crystalline semi-aromatic polyamides, polyphthalamides (PPA) and two other amorphous polymers, polycarbonate (PC) and poly(metyl)methacrylate (PMMA) under tensile deformation [1]. Ultra-Small Angles X-ray Scattering (USAXS) experiments permit to describe the beginning of the damage when cavities are about 10 nm in diameter, and the growth of crazes. Interpreting the results allows to measure the volume fractions of damages, as well as their distribution of sizes at different stages of tensile deformation. Different modes of damage are observed. They are initiated by the nucleation of nanometric crazes around pre-existing defects for PC, PMMA and the amorphous polyamide. Then the growth of these crazes is blocked by the strain hardening at the local level when cavities are about 50 nm in diameter. By increasing the strain further, the growth of a second family of large crazes is observed for these three polymers before the yielding which leads to fracture for PC and PMMA far in the macroscopic strain hardening regime, but not for the amorphous polyamide for which damaged is stabilized after the stress softening and in the ensuing necking regime for which strain hardening is also observed. We show that the growth of cavities and then crazes is the consequence of homogeneous nucleation of new cavities just ahead of them where the stress is the highest. It provides in particular an explanation for the appearance of fibrils. The same mechanisms have also been observed in cellulose acetate [2].
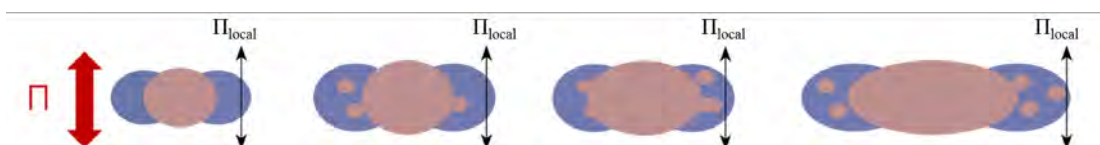
*Schematic representation of the growth crazes by nucleation of cavities followed by a coalescence mechanism. The blue region is the one where the stress is the highest. Once the local stress is sufficiently high in the vicinity of a cavity, homogeneous nucleations which take place as parallel events allows for crazes growth.*

## References

[1] Djukic, S.; Bocahut, A.; Bikard, J.; Long, D.R. Damage mechanisms of amorphous and low semi-crystalline polymers under tensile deformation studied by Ultra Small Angles X-ray Scattering. *Macromolecules* **2020**, *52* (17), 6613–6632.

[2] Charvet, A.; Vergelati, C.; Sotta, P.; Long, D. R. Damage Mechanisms of Plasticized Cellulose Acetate under Tensile Deformation Studied by Ultrasmall-Angle X-Ray Scattering. *Macromolecules* **2019**, *52* (17), 6613–6632.

# Nanocavitation distribution and morphology evolution in deformed High Density PolyEthylene (HDPE)

Ovalle, C.[1]; Cloetens, P.[2]; Proudhon , H.[1]; Morgeneyer, T.F.[1]; Laiarinandrasana, L.[1]

[1]*MINES ParisTech, PSL University, Centre des Matériaux (CMAT), CNRS UMR 7633, BP 87 91003, Evry, France*

[2]*European Synchrotron Radiation Facility, BP 220, F-38043, Grenoble Cedex, France*

## Abstract

The observation of cavitation in polymers depends on the resolution of the involved experimental technique. Addressing the void nucleation requires resolution able to reach the nanometric scale: SAXS, WAXS, SEM, TEM were commonly used to obtain the best resolution. 3D observations like tomography is limited to micro-scale. Furthermore, the size and the morphology of voids are dependent on the spherulitic microstructure characteristic length.

This study deals with the examination of the nanocavitation distribution in deformed High Density PolyEthylene (HDPE), for which the average diameter of the spherulite was about 2-3 µm. The motivation of this work is therefore to show that the cavitation mechanisms are the same as in other semicrystalline polymers but at a lower scale.

A flat notched sample of semicrystalline HDPE was deformed under steady crosshead speed up to the end of the stress softening. The microstructure and the voiding state in the unloaded sample was ex-situ observed in 3D at the European Synchrotron Radiation Facility (ESRF). Two parallel regions were studied: four locations of interest near the notch edge and three locations of interest centred on the longitudinal axis, through the necked zone up to the un-necked zone with a particular focus on the neck shoulder, by classical synchrotron parallel beam microtomography and magnified holotomography with a true spatial resolution of 0.7 µm ($HDPE_{0.7}$) and 0.05 µm ($HDPE_{0.05}$), respectively.  A qualitative study on the evolution of the distribution and morphology of cavities along the longitudinal axis was first carried out. The results of both $HDPE_{0.7}$ and $HDPE_{0.05}$ were compared with the axial evolution of the microstructure in PA6, from previous works [1, 2]. The qualitative study showed that the cavitation mechanisms in HDPE are the same as in the PA6 but at a lower scale. Then, thanks to 3D image segmentation and 2D-Fast Fourier Transform,  quantification of void volume fraction and void morphology was performed.

It was found that the nanovoid morphology and spatial distribution in HDPE revealed to be similar to those of other semicrystalline polymers, but at a different scale. While a slight decrease of the void diameter was seen, from the end of the neck shoulder to the extended neck region, a significant increment of the height was evidenced. Furthermore, the results provide compelling evidence of morphology transition of cavities within the test sample from an oblate to a prolate geometry [3].

## References

[1] Cayzac, H.-A.; Saï, K.; Laiarinandrasana, L., *International Journal of Plasticity* **2013**, *51*, 4372-7383.

[2] Laiarinandrasana, L.; Klinkova, O.; Nguyen, F.; Proudhon, H.; Morgeneyer, T.F.; Ludwig, W., *International Journal of Plasticity* **2016**, *83*, 19-36.

[3] Ovalle, C.; Cloetens, P.; Proudhon, H.; Morgeneyer, T.F.; Laiarinandrasana, L., *Polymer* **2021**, *229*, 123959.

# Modelling load sharing capabilities of UHMWPE ropes for floating offshore wind turbines

Tom A.P. Engels, Marc J.W. Kanters, Rigo L.M. Bosman

*DSM Protective Materials, Urmonderbaan 22, 6167 RD Geleen, The Netherlands*

Ultra-High Molecular Weight Polyethylene (UHMWPE) fibers, such as Dyneema® or Spectra®, are introduced in synthetic ropes as an alternative to steel or polyester because of their lower weight (ease of handling), smaller diameter (easier storage and transportation), higher stiffness (better station keeping) and excellent long-term properties (tension and bending fatigue, UV and chemical resistance). As a result of these benefits, they also are starting to find their use in the innovative and emerging market of offshore floating wind. Synthetic ropes can for example be applied as mooring lines to anchor a platform to the seabed or as tendons to connect counterweights to the floating vessel. However, during the design process of such solutions for offshore floating wind, the engineers often rely on experience based models for solutions on steel, and there remains a gap in experience and confidence in accurate modelling of synthetic ropes, hindering their use at full potential.

Just like all polymeric fibers, UHMWPE fibers display typical features such as viscoelasticity and viscoplasticity. These phenomena can be properly described as a function of time, temperature and loading conditions using a constitutive model developed in the nineteen-eighties at the Eindhoven University of Technology in close collaboration with DSM [1,2,3]. The model decomposes the total strain additively into a visco-elastic contribution (VE) and a visco-plastic contribution (VP), where the visco-elastic part is reversible and the visco-plastic part is irreversible. Both contributions are placed in series meaning that the stresses on both are equal, but are assumed to act independently. The VE contribution can be modelled according to the classical theory of linear visco-elasticity by means of the Boltzmann superposition principle and the stress and temperature dependence of the VP contribution by a double powerlaw or a Ree-Eyring flow rule [4]. This constitutive model allows to estimate the performance of the material in various load cases, such as dynamic loads, creep, and stress relaxation.

This model is applied to a design called Hexafloat for Floating Offshore Wind by SAIPEM. In this design, a 3000 tons counterweight is added to counteract the momentum induced on the system by the turbine and to ensure good hydrodynamics of the floater prototype to make it withstand extremely harsh environments. The counterweight is suspended by six 60 meter long tendons consisting of UHMWPE ropes and the model can help to guide design. Because next to being a statically overdetermined system, practical limitations on rigging will always cause a slight mismatch in absolute length. As a result, some tendons will be loaded more severe than others and the load is unevenly distributed over the six tendons. And due to the high modulus, this can result in very large differences in force. For illustration, with a modulus of 80GPa, a mismatch of only 30 cm on 60 meters (only 0.5% pre-strain) between the shortest and longest tendon corresponds to a preload of approx. 500 tons.

In the case of steel wires, such mismatch in length and load needs to be overcome by putting in place expensive subsea tensioners. However in UHMWPE ropes, due to the viscoelastic material behavior, the modulus changes in time and forces re-adjust in each tendon. So by the creep in the tendons that are loaded less, and a combination of stress relaxation and creep in the tendons that carry more load, a process of load sharing takes place, allowing one to refrain from the expensive subsea tensioners and still benefit from the reduced maximum load in the ropes.

This concept is tested and demonstrated in a small(er) scale prototype, in which a 5 tons counter weight is lifted by six 12 meter long tendons consisting of UHMWPE ropes with 7 mm diameter. The forces in each tendon for specific variations in rigging are predicted by the model. The results of the model will be compared to actual measurements of the tendon force of this specific design, demonstrating that these models can guide design and that peak loads reduce in a relatively short time.

## References

[1] Govaert, L.E.; PhD thesis, Eindhoven University of Technology, **1990**
[2] Leblans, P.J.R.; Bastiaansen, C.W.M.; Govaert, L.E., *J. Polym. Sci, B, Pol. Phys.,* **1989**, 27, 1009
[3] Govaert, L.E.; Bastiaansen, C.W.M.; Leblans, P.J.R., *Polymer,* **1993**, 34, 534
[4] Jacobs, M.J.N., PhD thesis, , Eindhoven University of Technology, **1999**

# Effect of die temperature on the fatigue behaviour of PLA produced by means of fused filament fabrication

S. Petersmann[1], A. Primetzhofer[2], M. Habicher[2], J. Leßlhumer[3], H. Lammer[3], F. Arbeiter[1,*]

[1]*Materials Science and Testing of Polymers, Montanuniversitaet Leoben, Otto Gloeckel-Straße 2, 8700, Leoben, Austria (sandra.petersmann@unileoben.ac.at; florian.arbeiter@unileoben.ac.at)*
[2]*Polymer Competence Center Leoben GmbH (PCCL), Roseggerstraße 12, 8700, Leoben, Austria*
[3]*Kompetenzzentrum Holz GmbH (Wood K plus), Altenbergerstraße 69, 4040, Linz, Austria*

Additively manufactured components often suffer from process-induced weld lines and insufficient bonding between adjacent layers. A well-known additive manufacturing process for thermoplastics is fused filament fabrication, in which different processing conditions, such as the use of various die temperatures, change the welding behaviour and thus often also the mechanical behaviour.

## Introduction

Additive manufacturing, often termed 3D printing, facilitates the fabrication of industrial applications with different materials and complex structures. In terms of polymers, fused filament fabrication (FFF) is the most widespread 3D printing process. Due to the layer-wise deposition of the thermoplastic material, the manufacturing process induces several weld lines in the parts, which significantly affect the resulting mechanical properties. These weld lines mostly represent the weak spots of additively manufactured components. Subsequently, the resulting mechanical properties strongly depend on the bonding or welding quality between individual layers. Furthermore, components for industrial applications often have to withstand continuously loading and unloading cycles. Consequently, understanding the fatigue behaviour of process-related welds is vital.

In this study the behaviour of weld lines under tensile and fatigue loads was investigated. Hence, one strand thick boxes were printed with varying die temperature, as previous studies showed that this processing parameter significantly effects the interdiffusion depth between adjacent strands [1-3]. Polylactide (PLA) was chosen as the material of choice because it is easy to process using 3D printing and is also a bio-based polymer. The test specimens were prepared from the boxes in a way that the load acts perpendicular to the strands. In this way, the quality of the weld is examined. Fatigue tests were carried out in tension on different force levels and the respective fracture surfaces were measured under a microscope to evaluate the resulting stresses. Finally, correlations between the manufacturing process, tensile and fatigue results were made.

## Materials and methods

### Material and processing

The investigated PLA was Luminy® L175 (TotalEnergies Corbion, The Netherlands), a homopolymer generally used for film extrusion and fibre spinning. The material was provided in form of filaments with a diameter of approx. 1.75 mm by Wood K Plus.

Boxes, consisting of a single deposited strand per layer, with dimensions of (180x180x80) mm$^3$ (Fig. 1a) were printed on an Original Prusa i3 MK3S (Prusa Research, Czech Republic) equipped with a steel nozzle with a diameter of 0.6 mm. The slicing was performed with the PrusaSlicer 2.1.0 (Prusa Research, Czech Republic) using spiral vase mode. One part was fabricated per print. An extrusion width of 0.675 mm and an extrusion multiplier of 1.0 were applied. The PEI-coated build platform was heated to 60°C. The

printing speed was 40 mm·s$^{-1}$, and 20 mm·s$^{-1}$ for the first layer. The layer thickness was set to 0.25 mm and the first layer thickness to 0.2 mm. Four different die temperatures were utilised: 190, 210, 230 and 250°C. The subsequent characterisations were performed on cut-out dumbbell specimens, which were prepared in a way that the load acts perpendicular to the strands. This way the weld strength can directly be investigated.
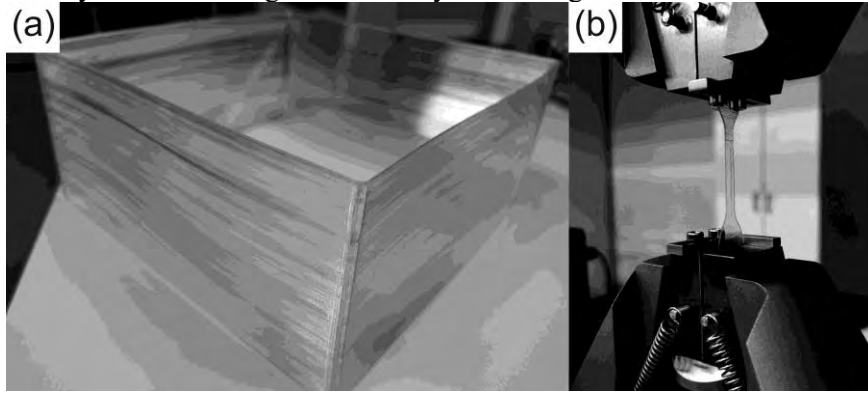


Figure 1: (a) 3D-printed one strand thick PLA boxes and (b) setup for fatigue experiments.

*Tensile tests*

The tensile tests were performed on the universal testing machine Zwick Z001 (Zwick Roell Gruppe, Germany) equipped with a 1 kN load cell. The testing speed was set to 1 mm·min$^{-1}$ for the evaluation of the Young´s modulus ($E$) and 50 mm·min$^{-1}$ afterwards. Pneumatic clamps (6 bar pressure) with serrated grip inserts were used. The clamping length was 42 mm. Four samples were tested per die temperature. The Young´s modulus and tensile strength ($\sigma_M$) were evaluated according to DIN EN ISO 527-2. However, the cross-head displacement was used to determine the Young's modulus, as a measurement with an extensometer was not possible due to the corrugated structure of the samples and an optical measurement did not provide meaningful results.

*Fatigue tests*

The fatigue tests were performed on the electrodynamic testing machine ElectroPlus$^{TM}$ E3000 Linear-Torsion (Instron, US) equipped with a 3 kN load cell (Fig. 1b). A cyclic load with a sinusoidal shape and a load ratio ($R = F_{min}/F_{max}$, wherein $F_{min}$ and $F_{max}$ are the minimum and maximum applied force, respectively) of 0.1 were used. The clamping length was 42 mm. A proper loading frequency was selected in order to avoid excessive hysteretic heating (f = 5 Hz). The stress levels were set to reach cycles to failure in the range of 10$^3$ to 10$^6$. Therefore, $F_{max}$ in the range of 16–24 N were applied during a cycle. Before testing, the width and the thickness of the samples were measured by calliper, whereby the smallest measured values were used to evaluate the cross-section of the component ($A_{component}$), which was further used to calculate the maximum stress of the component: $\sigma_{max,\ component} = F_{max}/A_{component}$. After fatigue testing, the respective fracture surfaces ($A_{real}$) were measured under a SZX12 (Olympus, Germany) stereo-microscope under reflected light to evaluate the real maximum stress: $\sigma_{max,\ real} = F_{max}/A_{real}$. The evaluated maximum stresses were plotted against the cycles to failure ($N_f$) and a Woehler line is fitted using a power law fit.

## Results and discussion

*Tensile tests*

Figure 2a shows the obtained stress-strain curves for the for different die temperatures. Overall 3D-printed PLA shows a characteristic brittle fracture behaviour, reaching very low levels of strain and showing no signs of yielding. There seems to be no clear trend between the Young´s modulus ($E$) and the die temperature ($T_N$). At this point it has to be mentioned, that the punched samples were curved due to residual stresses caused by the printing process

(Figure 2b). The degree of curvature was highest for the specimens printed at 210°C followed by the specimens printed at 230°C. For the other two die temperatures, the samples were only marginally curved. Due to the curvature, the specimens are first pulled straight before being pulled apart. This distorts the values for stiffness and subsequently also for strength. The "real" stiffness and strength values would therefore be higher. An increasing tensile strength with increasing $T_N$ was also found by Spoerk et al. [1]. The higher temperature leads to lower viscosity values and therefore higher interdiffusion depth between adjacent layers. Hsueh et al. [4] showed both an increasing $E$ as well as $\sigma_M$ with increasing printing temperature. Ahmed and Susmel [5] stated that the effect of most processing parameters on Young´s modulus and tensile strength can be neglected with little loss of accuracy in terms of engineering static assessment, and 3D-printed PLA can be simplified as a homogenous, isotropic and linear-elastic material for design purposes.
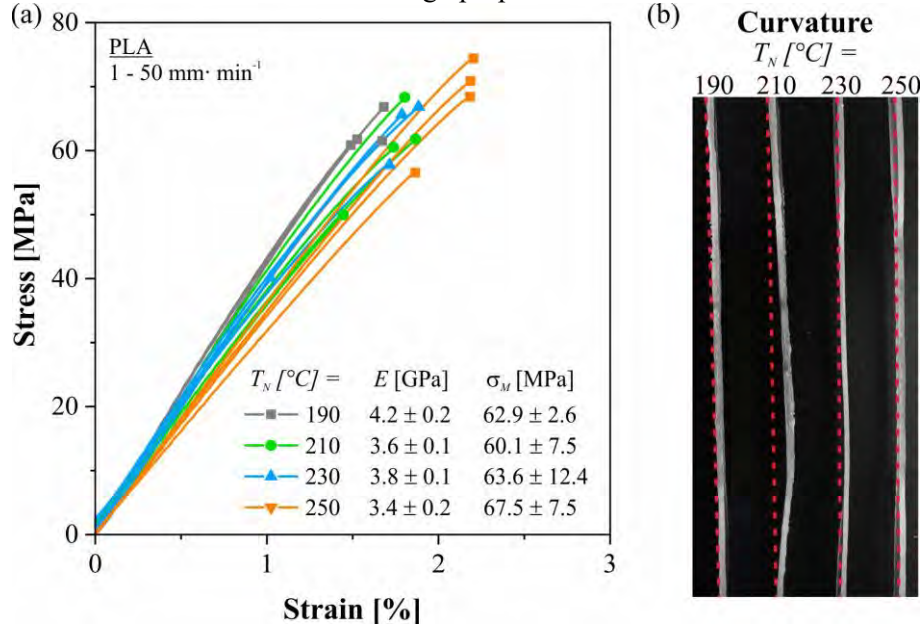


Figure 2: Stress-strain curves of PLA specimens prepared from 3D-printed one strand thick boxes in a way that the strands are oriented perpendicular to the load direction (a). The boxes were manufactured with four different die temperatures ($T_N$): 190, 210, 230 and 250°C. The mean and standard deviation for the Young´s modulus ($E$) and tensile strength ($\sigma_M$) of four samples are given on the right. In (b) the curvature of the samples is demonstrated.

*Fatigue tests*

It was found that the Woehler lines considering $\sigma_{max,\,component}$ start highest in the range of low cycle fatigue for the highest die temperature and decrease with decreasing temperature (Figure 3a). On the other hand, the slope of the curve is highest for $T_N = 230$°C, followed by 250, 210 and 190°C, respectively. When considering $\sigma_{max,\,real}$, all curves were shifted to higher stress values (Figure 3b), since the fracture surfaces are smaller than the area measured by calliper (Figure 3c and d). In this case, similar slopes were observed for the three higher die temperatures and a much flatter curve for $T_N = 190$°C. This may be explained by the curvature of the samples, which was weakest at the lowest die temperature. This warpage of the samples (Figure 2b) led to additional bending stresses during the test, resulting in reduced fatigue life. Dadashi and Azadi [6] also found that decreasing the die temperature increased the fatigue lifetime of 3D-printed PLA, without providing a cause. On the other hand, an increased printing speed reduced the slope of the Woehler lines. This is reasonable, since at higher printing speeds the time for diffusion between adjacent strands is reduced, and therefore the weld strength is reduced as well.
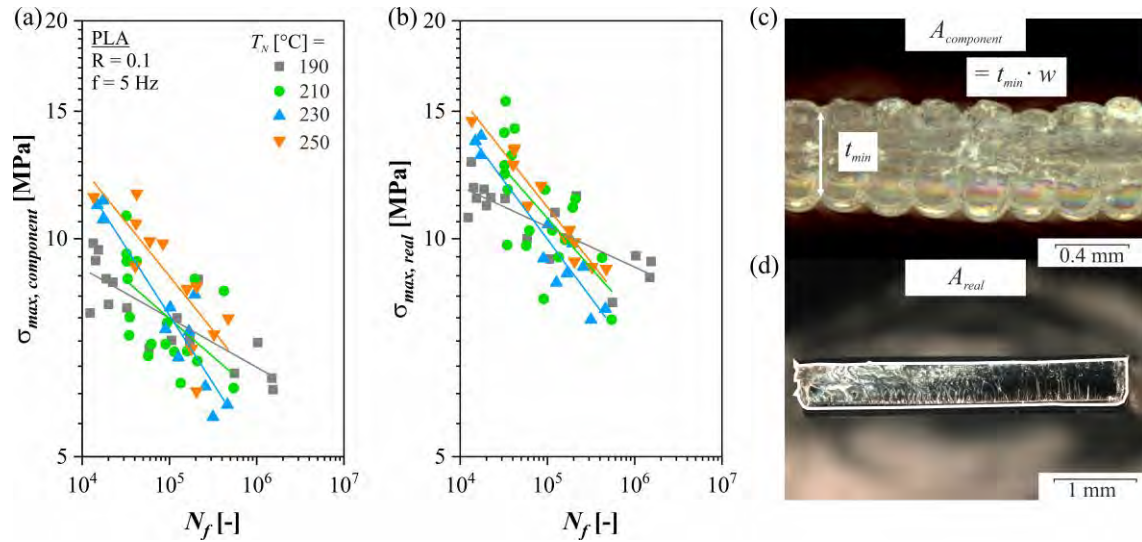
Figure 3: Full logarithmic plot of maximum stress over cycles to failure ($N_f$) measured for PLA specimens prepared from 3D-printed one strand thick boxes in a way that the strands are oriented perpendicular to the load direction. $\sigma_{max,\ component}$ (a) was calculated from the minimal cross-sectional area measured by calliper ($A_{component\ =\ t_{min}\ \cdot\ w}$, with $t_{min}$ is the minimal thickness and $w$ is the specimen width) (c) and $\sigma_{max,\ real}$ (b) from the fracture area determined via optical microscope ($A_{real}$) (d). The boxes were manufactured with four different die temperatures ($T_N$): 190, 210, 230 and 250°C.

## Conclusions

The die temperature has an influence on the fatigue properties of 3D-printed PLA; a significant influence on the tensile properties was not observed. A higher temperature resulted in higher slopes of the Woehler lines. This was not to be expected, as higher temperatures generally lead to higher inter-diffusion between adjacent strands, and therefore enhance the fatigue life. However, the die temperature affected the residual stresses within 3D-printed PLA boxes, developing different degrees of warpage for punched samples. This warpage resulted not only in tensile stresses during fatigue testing, but also in bending stresses, which falsified the results. Further tests for a more thorough explanation are currently under investigation.

## Acknowledgements

## References

[1] Spoerk, M.; Arbeiter, F.; Cajner, H.; Sapkota, J.; Holzer, C.; *J. Appl. Polym. Sci.* **2017**, 1*34*, 45401.
[2] Seppala, J. E.; Hoon Han, S.; Hillgartner, K. E.; Davis, C. S.; Migler, K. B.; *Soft Matter* **2017**, 13(38), 6761–6769.
[3] Petersmann, S; Spoerk-Erdely, P.; Feuchter, M.; Wieme, T.; Arbeiter, F.; *Addit. Manuf.* **2020**, 101384.
[4] Hsueh, M.-H.; Lai, C.-J.; Wang, S.-H.; Zeng, Y.-S.; Hsieh, C.-H.; Pan, C.-Y.; Huang, W.-C.; *Polymers* **2021**, 1*3*, 1758.
[5] Ahmed, A. A.; Susmel, L.; *Frattura ed Integrità Strutturale* **2017**, 11(41), 252-259.
[6] Dadashi, A.; Azadi, M.; *Preprints* **2022**, 2022010252.

# The influence of recyclates on the mechanical and long-term properties of virgin materials

Jessica Hinczica[1], Jutta Geier[1], Ulrike Kirschnick[2], Clemens Holzer[3], Andreas Frank[1], Gerald Pinter[4]

1    Polymer Competence Center Leoben GmbH, Leoben, Austria
*jessica.hinczica@pccl.at, jutta.geier@pccl.at, andreas.frank@pccl.at*
2    Institutes of Processing of Composites, Montanuniversitaet Leoben, Leoben, Austria
*ulrike.kirschnick@unileoben.ac.at*
3    Institutes of Polymer Processing, Montanuniversitaet Leoben, Leoben, Austria
*clemens.holzer@unileoben.ac.at*
4    Institutes of Polymer Engineering and Science, Montanuniversitaet Leoben, Leoben, Austria
*gerald.pinter@pccl.at*

Recently, the recycling of polymers in particular gained increasing attention in the scientific, industrial and commercial community as well as the wider public. One the one hand, due to the materials economic and technical relevance, and on the other hand to the environmental and social challenges connected with the waste perspective and circular economy of plastic products [1–3]. Currently, in Europe only 13 % of all plastic waste is processed into recyclates and used in new products [4]. By adding virgin material, the mechanical properties of the recyclate can be improved and a higher amount of recyclates can be processed into new products [5]. In order to analyse the influence of the recyclate on the rheological, mechanical and long term properties, two virgin/recyclate blends with different weight fractions 10 % and 40 % of recyclates were compounded and compared with the properties of the pure materials (virgin and recyclate). A clear influence of the recyclate content on the material properties is identifiable. The melt flow rate (MFR) of the virgin material is 30 % lower compared to the recyclate, and by blending these materials, the MFR increases continuously with higher recyclate content. For the determination of the mechanical properties, tensile tests and Charpy impact tests were performed. All mechanical measurements demonstrate the same trend, as high recyclate content yields to lower mechanical performance. A linear correlation between the mechanical properties and the MFR was observed. Linear Elastic Fracture Mechanics was used to determine the slow crack growth (SCG) resistance of these blends. There is a clear non-linear correlation of the SCG resistance depending on the recyclate content.

## References

[1] C. Aumnate, N. Rudolph, M. Sarmadi, Recycling of Polypropylene/Polyethylene Blends: Effect of Chain Structure on the Crystallization Behaviors, Polymers (Basel) 11 (2019). https://doi.org/10.3390/polym11091456.

[2] A. Reichel, M. de Schienmakere, J. Gillabel, Circular economy in Europe: developing the knowledge base, Publications Office, Luxembourg, 2016.

[3] S. Rajendran, A. Hodzic, L. Scelsi, S. Hayes, C. Soutis, M. AlMa'adeed, R. Kahraman, Plastics recycling: insights into life cycle impact assessment methods, Plastics, Rubber and Composites 42 (2013) 1–10. https://doi.org/10.1179/1743289812Y.0000000002.

[4] PlasticsEurope AISBL, The Circular Economy for Plastics: A European Overview (2019).

[5] L.A. Utracki, C.A. Wilkie (Eds.), Polymer blends handbook, 2nd ed., Springer, Dordrecht, 2014.

# Influence of hydrogen bonds on the slow crack growth resistance of polyamide 12

Mario Messiha [1],*, Andreas Frank [1], Florian Arbeiter [2], Gerald Pinter [2]

[1] *PCCL GmbH, Leoben, AT*
[2] *Montanuniversitaet, Leoben, AT*
\* *Presenting author*

## Abstract

Crack initiation and subsequent Slow Crack Growth (SCG) are considered to be the most critical failure mode for a variety of long-term applications [1-2]. In case of polyamide 12 (PA12), however, hydrogen (H) bonds and their influence must be considered, as they are well-known to affect the mechanical properties of plastics [3]. Therefore, a Sequential Debonding Fracture (SDF) model [4] was applied to estimate the amount of fracture energy, which must be additionally supplied to break the additional physical cross-links between PA12 chains compared to a non-cross-linked material, such as polyethylene. With the aid of a fracture mechanical test – the so-called Cracked Round Bar (CRB) test standardized in ISO18489 – conducted at different temperatures, as well as the time temperature superposition using the Arrhenius' equation, the activation energy for SCG was approximated. Therefore, the total fracture energy $G_f$ of PA12 was divided into a pure chain disentanglement fracture energy, driven by creep processes during SCG ($G_{dis,f}$), and the additional energy needed to dissociate effective H-bonds that are actively resisting SCG ($G_{H,f}$) within PA12. It could be demonstrated for the selected PA12 grade, that $G_{H,f}$ becomes the dominating source of energy which has to be overcome, if at least 45 % of all H-bonds crossing the crack plane engage in the fracture process.

## References

[1] C.J.G. Plummer and H. H. Kausch, "Semicrystalline Polymers: Fracture Properties," in *Reference Module in Materials Science and Materials Engineering*, Elsevier, 2016.
[2] T. L. Anderson, *Fracture Mechanics*: *Fundamentals and Applications, Fourth Edition*, Chapman and Hall/CRC, Boca Raton, 2017.
[3] S.-W. Kuo, *Hydrogen bonding in Polymeric Materials*, John Wiley and Sons Inc, Weinheim, Germany, 2018.
[4] H. Xin, F. Oveissi, S. Naficy et al., "A Sequential Debonding Fracture Model for Hydrogen-Bonded Hydrogels," *Journal of Polymer Science: Part B: Polymer Physics*, vol. 56, no. 19, pp. 1287–1293, 2018.

# Integrative lifetime estimation method for short fibre reinforced polymers

Andreas Primetzhofer[1], Gabriel Stadler[2], Gerald Pinter[1,3], Florian Grün[2]

1. Polymer Competence Center Leoben, Rosseggerstraße 12, A-8700 Leoben
2. Montanuniversity of Leoben, Chair of Materials Science and Testing of Polymers,
3. Montanuniversity of Leoben, Chair of Mechanical Engineering, Franz-Josef-Straße 18, A-8700 Leoben

In order to use parts made of short fibre reinforced polymers in rough conditions it is indispensable to consider their anisotropic behaviour along the whole value chain. Especially the consideration of the service time in an early stage of the development is key. To take into account anisotropic behaviour in lifetime prediction of parts made of short fibre reinforced polymers, an integrative simulation method is presented in this work.

In the first step, a process simulation delivers the local fibre orientation (FO) and if necessary as well as information about weld lines and initial stresses. By homogenizing the inhomogeneous structure (fibre/matrix) and the application of constitutive laws, orientation-dependent material properties can be calculated. Element based mechanical properties are then used to calculate the inhomogeneous stress field. However, special attention hast to be paid on an appropriate modelling, due to a great influence on the result of a downstream service life calculation. The derived stress field and the local FO from the process simulation can then be directly used in the service life calculation. The local fatigue lifetime (or damage) is calculated from the local stress and strength which is calculated from a test data based dataset [2].
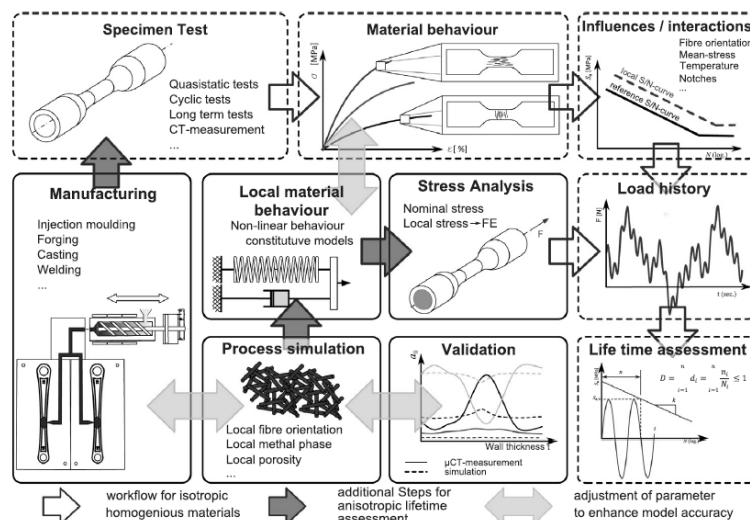


**Figure 1 Scheme of life time estimation for short fibre reinforced polymers [1]**

Combining different simulation techniques and technologies allows an efficient service life determination of fibre-reinforced plastics. Beside the determination of the material parameters, an appropriate modelling and the accurate use of the model parameters are of particular importance. In order to detect errors at an early stage, validation of the results is useful at each step.

## References

[1] Primetzhofer, A.; Stadler, G.; Pinter, G.; Grün, F. In International Journal of fatigue **2018**, *120*, 294–302.
[2] Primetzhofer, A.; Stadler, G.; Pinter, G.; Grün, F. In *Journal of Plastics Technology*; **2019,** 15

# Estimation of local mechanical amorphous modulus evolution in HDPE materials submitted to oligo-cyclic loading conditions by in-situ SAXS/WAXS characterizations

Hang GUO[1] Renaud G. RINALDI[1], Sourour TAYAKOUT[2], Morgane BROUDIN[3], Olivier LAME[1]

1) Université de Lyon, CNRS, INSA-Lyon, MATEIS, UMR5510, 69621, Villeurbanne, France
2) EDF-DIPNN-Direction Technique, 19 rue Pierre Bourdeix, F-69007, LYON, France
3) EDF-R&D Lab Les Renardières, Avenue des Renardières-Ecuelles, F-77250, Moret-Loing-et-Orvanne, France

## Abstract

HDPE is known to be an excellent material to absorb the deformation induced by an earthquake. Yet the physical understanding needs to be deepened and is pursued in this work by evaluating the microstructure evolution under oligocyclic tensile loadings which mimic seismic events. In particular, the local amorphous modulus embedded in the crystalline stacks is evaluated before and after oligo cyclic testing. Thanks to tensile tests and simultaneous in-situ small- and wide- angle X-ray scattering (SAXS/WAXS) measurements, both local stress and strain can be evaluated. At microscale, the crystallites can be considered as stress gauges so that the local stress estimation is obtained *via* the measurement of the displacement of the crystallographic planes (as previously done in [1]). For the spherulitic structure, the local stress is found to be large in the polar region ($2<\sigma_{local}/\sigma_{macro}<3.5$) and limited in the equatorial region ($\sigma_{local}/\sigma_{macro}<1$). For the fibrillary structure resulting from the oligo-cyclic loading, even larger local-macro stress ratio ($5<\sigma_{local}/\sigma_{macro}<8$) are measured suggesting that the stress is highly concentrated in the intra-fibrillary region probably due to their higher stiffness compared to interfibrillar regions. With the local strain being evaluated simultaneously by in-situ SAXS measurements, an evaluation of the amorphous modulus is obtained and the results are presented in figure 1 below for HDPE with initial various microstructures.
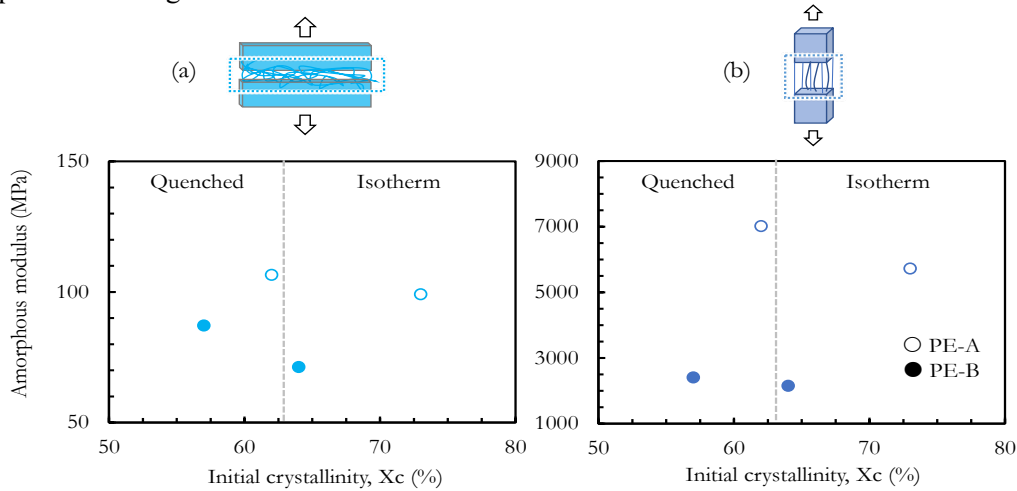
Figure 1: Indirect estimate of the local amorphous modulus within: (a) the spherulitic structure, (b) the fibrillar structure

The amorphous modulus was found to vary from 71-106 MPa in the equatorial region of spherulite structure to 2000-7000 MPa in the intra-fibrillary region. These strong variations will be discussed in relation with the thermal history and molecular structure of the materials.

## References

[1] B Xiong, O Lame, JM Chenal, C Rochas, R Seguela, G Vigier, Macromolecules 48 (7), **2015**, 2149-2160

# An engineering approach to predict the long-term strength of thermoplastics: Rupture dome tests

Alpay Aydemir

*Wavin Technology & Innovation B.V., alpay.aydemir@wavin.com*

## Abstract

Designing plastic parts with a defined long-term strength (LTS) has been a cutthroat competition. The difficulty lies mainly in the time necessary to generate the experimental data for LTS prediction. Many tried to accelerate the LTS test procedure and only a few test methods have been accepted by the plastics industry [1-3]. The most used *hydrostatic pipe test* [4], for example, requires more than a year testing time, which is not affordable anymore by companies. Moreover, the sustainability and environmental concerns compel the plastics industry and plastic part producers to review their current material and product testing methods. The industry is still tirelessly looking for a practical and quick method suitable for both the materials and product testing.

It is well known that as the stress state changes from compression to tension, the failure type also changes from ductile to brittle [5]. In this investigation, an internally pressurized; semi-sphere-shaped sample has been used to produce brittle failure in thermoplastic. Injection moulding process is used to produce the so-called "rupture dome" test samples. Few *Polyvinyl chloride* (PVC), *Polypropylene* (PP) and *Polyethylene* (PE) materials are tested. The rupture dome test data is used to generate the regression curves per tested material. The results show that the rupture dome test seems very suitable for investigating the LTS of PVC-like glassy thermoplastics, see figure below. Experimental results from PE and PP materials are also presented. Although the test method offers a quick way of ranking the materials according to their brittleness, more investigations are still needed to see if the test method is ever suitable for testing PP/PE-like rubbery thermoplastics.
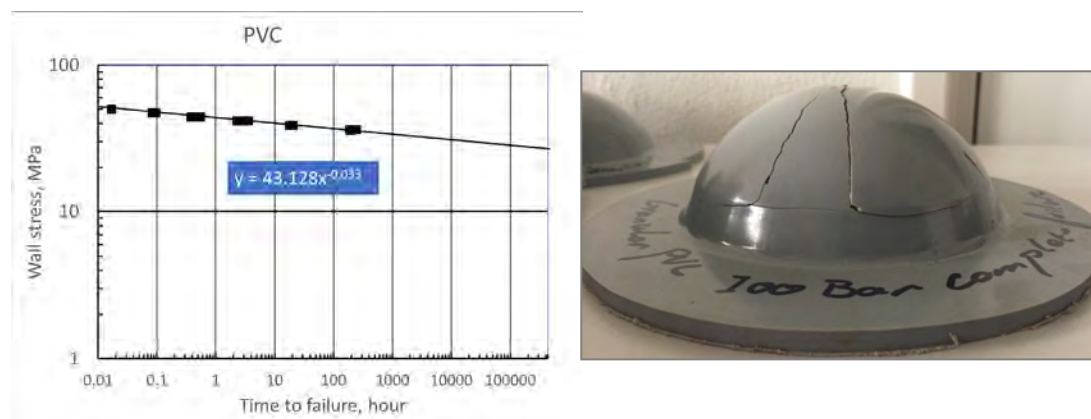
## References

[1] Erartsin, O.; A. J. J. Arntz, S.; Troisi, E. M.; Pastukhov, L. V.; van Drongelen, M.; Warnet, L.; Govaert, L. E., Journal of applied polymer science **2021**, *138(35)*, 50878.

[2] Kanters, M. J. W.; van Erp, T. B.; van Drongelen, M.; Engels, T. A. P.; Govaert, L. E., Polymer Testing **2017**, *59*, 177–184.

[3] Frank, A.; Arbeiter, F. J.; Berger, I. J.; Huta, P.; Náhlík, L.; Pinter, G., Journal of Pipeline Systems Engineering and Practice **2019**, *10(1)*, 04018030.

[4] ISO 9080:2012, Plastics piping and ducting systems — Determination of the long-term hydrostatic strength of thermoplastics materials in pipe form by extrapolation

[5] Christensen, R. M., *Journal of Applied Mechanics* **2015**, *83(2)*, 021011.

# Influence of production on the slow crack growth resistance of polyethylene parts

Britta Gerets, Kurt Engelsing

*SKZ – German Plastics Center, Friedrich-Bergius-Ring 22, 97076 Würzburg, Germany*
*b.gerets@skz.de*

## Abstract

In polyethylene three main failure mechanisms can be observed: First ductile failure due to locally exceeding the yield stress, second failure basing on slow crack growth and third brittle failure evoked by thermo-oxidative degradation. While ductile failure and degradation during service can be prevented by a proper product design and an adequate material stabilization, slow crack growth is correlated to the molecular structure [1]. Therefore, polyethylene materials for long-term application have been optimized with focus on their slow crack growth resistance. Going ahead with this development conventional material test methods, provoking a craze-crack-process faster than in real life application through raised temperatures, notching and the use of detergents (e. g. Full-Notch Creep Test), had to be modified. Additionally, new test methods (e. g. Strain Hardening Test) were developed and shown to correlate with the established ones [2]. Hence, adequate tests to quantitatively characterize highly stress crack resistant polyethylene materials are available. But as in application parts are used the influence of production on the slow crack growth resistance must be considered.

Therefore, injection molded sheets as well as extruded pipes were produced from a commercial high-density polyethylene material. In all production techniques, temperatures respectively cooling rates were varied to generate different morphologies. Pipe extrusion offered the opportunity to vary the orientational state through different extrusion rates. Differential scanning calorimetry allowed for a morphological characterization, whereas the slow crack growth resistance was measured in Strain Hardening Tests. Comparing the results of the injection molded and extruded parts to those of the material test of the same batch, the influence of the production became measurable. The specimen for these investigations were prepared from parts directly as well as from annealed (relaxation of internal stresses) and regranulated (erasure of molecular orientations) parts. Validation of the main findings were done by correlations with Full-Notch Creep Test results and tests of several commercially available polyethylene geosynthetic barriers, extruded sheets (exemplarily shown in Figure **1**) and pipes. Especially the molecular orientation state, resulting from the production process, showed to have a distinct influence on the results.
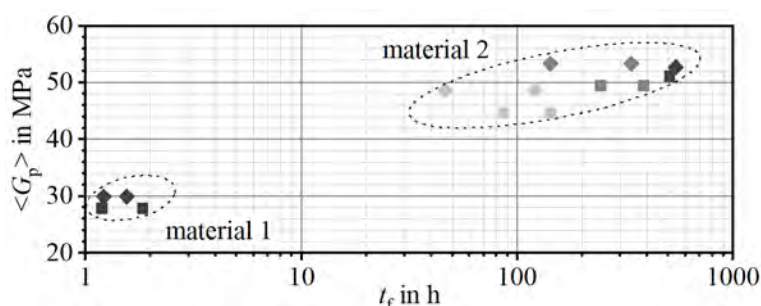
Figure 1: Strain hardening modulus $<G_\mathrm{p}>$ in relation to the time to failure $t_\mathrm{f}$
in Full-Notch Creep Tests (performed in Disponil® LDBS25 at 90 °C and 5 MPa)
for commercial extruded sheets of different thicknesses

## References

[1] Strobl, G., *The Physics of Polymers*, Springer-Verlag: Berlin, Heidelberg, 2007.
[2] Deblieck, R.; Gerets, B.; Boerakker, M.; Caelers, H.; Wilbers, A.; Boonen, T., Relation between Life Time, Failure Stress and Craze Microstructure in Polyethylene as evidenced by Fracture Surface Texture Analysis after an Accelerated Full-Notch Creep Test, *Polymer* **2019** *176*, 264-273.

# Influence of post-processing on the mechanical behavior of selective laser-sintered polyamide 12 parts

Britta Gerets, Malte Nebel, Kurt Engelsing

*SKZ – German Plastics Center, Friedrich-Bergius-Ring 22, 97076 Würzburg, Germany*
*b.gerets@skz.de*

## Abstract

Laser sintering is gaining increasingly importance as a production process for additive manufacturing of functional parts made of plastics. For a successful application – meaning a reliable behavior over the hole service lifetime – an adequate design is needed [1, 2]. Hence, in addition to the desired optical and haptic appearance, the functional requirements must be met. In terms of component dimensioning, the focus is habitually on strength and toughness, including notch or impact sensitivity. To which extent these properties are changed by post-processing, such as smoothing, coloring and infiltration, was systematically investigated.

Therefore, specimen made of a standard polyamide 12 laser sintering material were thoroughly mechanically characterized before and after post-processing. For multi-stage post-processing the intermediate stage was captured also. Tensile tests at 23 °C, using a DIN EN ISO 527-2 type 1A geometry either of the standard 4 mm as well as of 1 mm thickness, provided strength and toughness values whereas sensitivity to impact loading was measured via ISO 179 tests. The specimen used were laser-sintered in three different building directions: horizontal (x-y direction), vertical (z direction) and diagonal (45°).

Changes in mechanical behavior due to the significant changes of the surfaces by post-processing of the specimen were expected. Surprisingly within measurement accuracy in many cases only minor changes were observed although e. g. surface roughness was significantly reduced. In Figure 1 exemplarily the stress-strain behavior of the 4 mm thick specimen is shown before and after smoothing of the surface by vibratory finishing; fivefold tested each. A small decrease in measurement scattering is visible, but the basic mechanical behavior remains unchanged; only the diagonal specimen shows a slight strength improvement.

For all post-processing methods investigated, it seems that the intrinsic material properties combined with the 3D printing typic orientation influences dominate the mechanical properties.
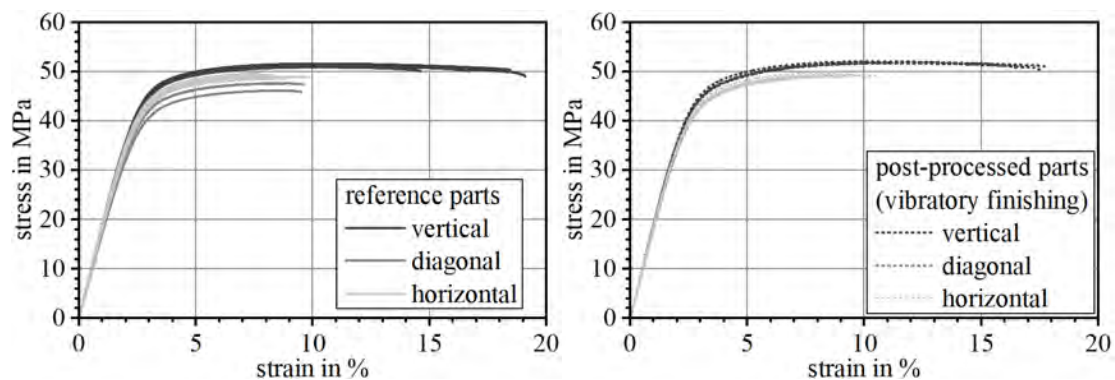
Figure 1: Stress-strain-behavior of laser-sintered polyamide 12 parts before (left) and after (right) post-processing by vibratory finishing.

## References

[1] Gebhardt, A. *Understanding Additive Manufacturing*; Carl Hanser Verlag: Munich, 2012.
[2] Gebhardt, A.; Hötter, J.-S., *Additve Manufacturing – 3D Printing for Prototyping and Manufacturing*; Carl Hanser Verlag: Munich, 2016.

# Impact of nanoparticles on the printability and properties of acrylate-based resin in M-SLA 3D printing

Martina Korčušková, Petr Lepcio, Veronika Sevriugina, František Ondreáš

*Brno University of Technology, Central European Institute of Technology, Purkyňova 656/123, Brno, 612 00, Czech Republic*
*Corresponding author's email address: Martina.Korcuskova@ceitec.vutbr.cz*

Summary: The impact of bare zinc oxide and alumina-doped zinc oxide nanoparticles on the kinetics of the free radical photopolymerization reaction during 3D printing was studied. The reinforcement effect of the nanoparticles present was considered, and the thermomechanical properties of the 3D printed samples were compared with the effect of the post-curing process.

## Introduction

3D printing techniques have recently become popular, due to their ability to fabricate complex shapes, while maintaining good mechanical properties. Above that, Vat 3D printing techniques, such as masked stereolithography (M-SLA), are bringing further advancement of 3D printing, employing the photopolymerization reaction. Vat 3D printing process is also ideal for the introduction of nanoparticles (NPs), as the polymer precursors represent a good low-molecular and low-viscosity dispersing medium for NPs [1]. However, the presence of NPs affects the photopolymerization from both a physical and a chemical point of view. The physical effect is based on the fact that NPs in monomer mixture can absorb or scatter curing light, on the other hand, the chemical effect is caused by the chemical interaction between present NPs and the photopolymerizable resin.

Certain types of NPs, such as semiconductive metal oxides (ZnO, TiO$_2$ or Fe$_3$O$_4$) [2–4] reportedly provide a photo-initiating effect and can act as a free-radical photo-initiators for vinyl monomers, such as acrylates. However, the influence of photo-initiating NPs on the printability in low-power UV printers such as M-SLA has not yet been fully characterized. Recent study [5] has revealed that the low-power UV curing employed by most of the entry-level 3D printers may struggle with the complete conversion of the resin beyond the vitrification point, that is, when the $T_g$ of the growing photopolymer network exceeds the processing temperature. Accelerated photo-kinetics combined with the reinforcement effect of the NPs [6] is expected to shift the vitrification point to lower conversion and, thus, promote this adverse effect.

In this study, we have investigated how the incorporation of selected NPs, bare zinc oxide (ZnO) and alumina-doped zinc oxide (AZO), influence the kinetics of the photopolymerization reaction and the 3D printing of nanocomposite resins. Specifically, we have compared the effect of ZnO and AZO nanoparticles on the photocuring kinetics of a common free radical photopolymer matrix and the final properties of the nanocomposites.

## Materials and Methods

A commercial UV photosensitive acrylate-based resin (Shenzhen Yongchanghe Technology Co., Ltd.) with 6 % of the diphenyl (2,4,6-trimethylbenzoyl)-phosphine oxide (TPO) photoinitiator was used as a matrix. Dry zinc oxide (ZnO, 20 nm) and zinc oxide doped with 2 wt. % of alumina (AZO, 20-40 nm) NPs were obtained from IOLITEC Ionic Liquids Technologies GmbH and used as received with no further purification or modification.
Samples were 3D printed with the Original Prusa SL1 printer (Prusa, Czech Republic) equipped with a 405 nm UV LED source (0.661 mW·cm$^{-2}$) and further analysed either

without additional curing or post-cured at 35 °C for 10 or 60 min using the Original Prusa CW1 curing and washing unit (Prusa, Czech Republic) with the irradiation intensity of 10 mW·cm$^{-2}$.

Photo-DSC measurements were conducted by a Discovery DSC (TA Instruments, USA) under isothermal conditions at 25 °C. Appropriate sample mixtures (15 µl) were irradiated in uncovered aluminum pans by the continual non-pulsing light from 405 nm LED matrix with a light density of 0.661 mW·cm$^{-2}$. For the formation of Jacobs working curves, square geometries (10×10 mm) of samples were printed with a curing time varying from 10 s to 60 s for the corresponding samples. The thickness of single layers was measured with a micrometer.

Hybrid dynamic mechanical analysis (DMA) combined with measurement of heat deflection temperature (HDT) was performed according to Štaffová, et al. [5] in three-point bending setup using RSA-G2 (TA Instruments, USA). Three regular specimens (3.5×5×48.5 mm) were analyzed for each of the following samples: 3D printed with no post-curing, post-cured for 10 and 60 minutes. All measurement were performed at a controlled heating rate of 2 °C/min from 30 °C to 160 °C at an oscillatory frequency of 1 Hz and an oscillation dynamic strain of 0.002 % superimposed with small a static stress of 0.455 MPa. The heat deflection temperature (HDT) was defined as the temperature at which the sample bar deflected by 0.25 mm (equals to 0.195 % flexural strain).

## Results and discussion

To describe the effect of semiconductive nanoparticles on the photopolymerization reaction and the 3D printing process, ZnO and AZO NPs were selected. The used NPs have a significant photocatalytic effect on the photopolymerization process, as verified by photo-DSC (Fig. 1). The presence of two exothermic peaks in the curing curves is consistent with previous reports on photocuring of two-monomer resins at relatively low light intensity [5]. It documents the heterogenous character of the cure reaction, where the second peak is related to the reaction of the oligomer or generally the heavier monomer in the resin [7]. This change in curing behavior is an important technological parameter with a large impact on the post-processing and final mechanical performance of the prints [5].

Nanocomposites containing ZnO NP show a higher first exothermic peak and a faster overall reaction compared to AZO NPs. According to photolysis analysis, the ZnO NPs showed a surface plasmon resonance and irradiation of such species can cause a localized photothermal effect, which affects the kinetics of photopolymerization [8]. The heat produced by ZnO NPs caused higher heat flow values on the DSC curve and led to a faster curing reaction. On the other hand, AZO NPs show only low absorbance, without a surface plasmon resonance band, in the wavelength range of the used light, and, according to the DSC curves, AZO NPs did not increase the heat flow during the curing reaction of the monomers.
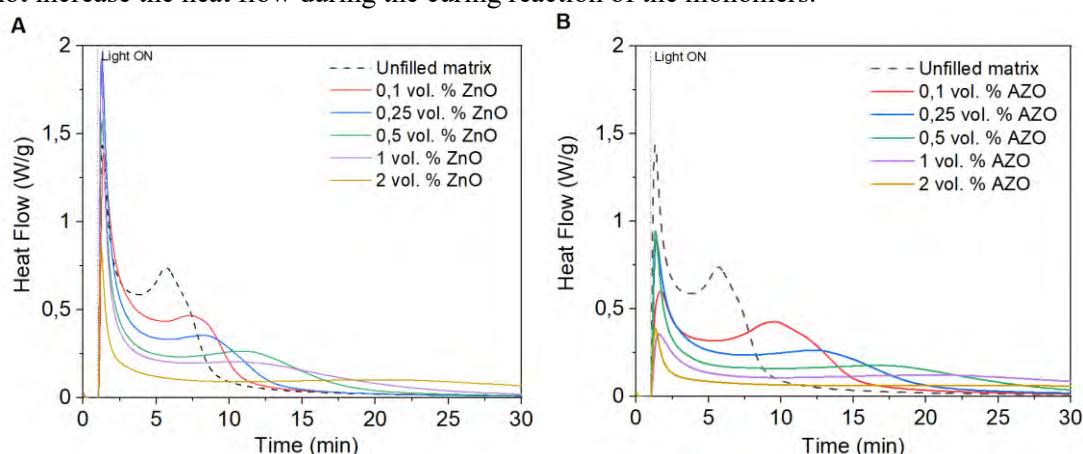


Fig. 1: Curing kinetic analysis of unfilled resin and resin reinforced with (A) ZnO and (B) AZO nanoparticles with various content

The effect of the NP presence on the printing parameters was evaluated using Jacobs working curves (Fig. 2). Jacobs working curves were created as a dependence of the linear-logarithmic plot of the curing depth of the single layer ($C_d$) and the cure energy ($E_0$), which is determined by the irradiation intensity of the 3D printer and the curing time. The intersection of the Jacobs working curve with the x-axis gives the critical energy ($E_c$), required to initiate the polymerization.

The course of the Jacobs working curves corresponded to the photo-DSC results described above. The initial course of the reaction showed a logarithmic fit, and at certain point, a transition to a second logarithmic fit with higher $C_d$ and $E_0$ is observed as a result of the two-step curing mechanism. Both ZnO and AZO NPs reduce the initial values of $E_c$ in most cases, which assumes an increase in the kinetics of the reaction compared to the unfilled matrix. ZnO NPs show even lower values of the initial $E_c$ as a result of the photothermal effect, which accelerates the curing reaction.
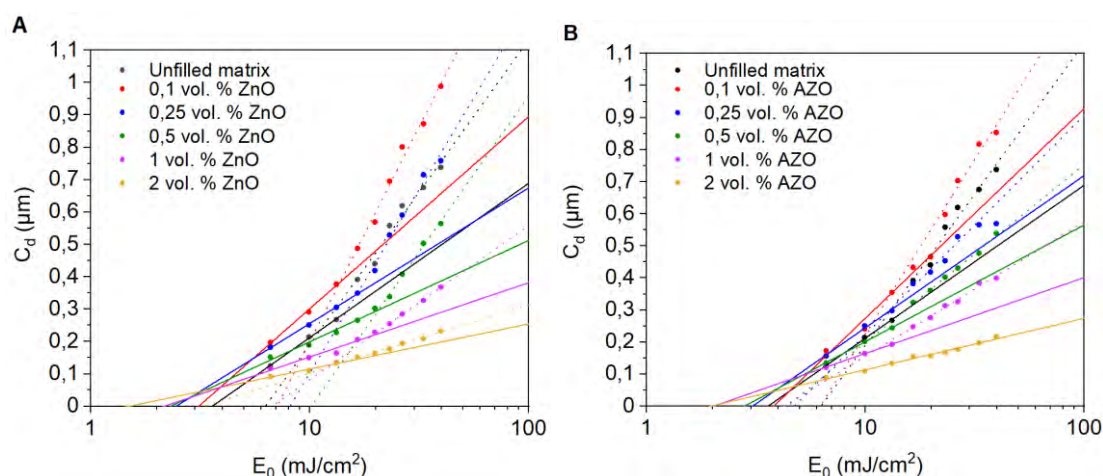


Fig. 2: Jacobs working curves for the tested nanocomposites. The initial logarithmic fit is marked with a solid line and the subsequent logarithmic fit with a dotted line

As previously described, ZnO and AZO NPs affected the kinetics of photopolymerization differently. However, the presence of photocatalytic NPs not only affected the photopolymerization reaction but also brought about a reinforcement effect of NPs in the resin, thus affecting the final properties of the nanocomposites. To study this effect, the thermomechanical properties of 3D printed samples were evaluated. Since NPs also affected the post-curing process, samples post-cured for 0, 10 and 60 minutes were compared.

Using the combined DMA-HDT measurement, the storage modulus ($E'$), loss modulus ($E''$), and loss tangent ($\tan \delta = E''/E'$) were obtained as a function of temperature. All samples exhibited the glassy behaviour at low temperatures, with low $\tan \delta$ values and weak dependence of the storage modulus on the temperature, followed by the glass transition region, characteristic by the drop in storage modulus and the peak of $\tan \delta$. At temperatures above glass transition temperature ($T_g$), rubbery behaviour continued with rubbery plateau of storage modulus and low $\tan \delta$ values. To compare the effect of different concentrations and NPs used, the initial storage modulus measured at 35 °C, representing the stiffness of the material, $T_g$ and HDT were evaluated (Fig. 3).

By comparing samples without additional post-curing, nanocomposites with more than 0.25 vol. % load of AZO NPs showed a higher initial storage modulus and comparable HDT than the unfilled matrix. On the other hand, nanocomposites reinforced with ZnO NPs show in almost all cases lower values of storage modulus, HDT and also $T_g$. From these values, it is clear that the presence of AZO or ZnO NPs has an evident effect on the mechanical response of 3D printed samples. However, the post-curing process has a greater effect on thermomechanical properties, than the NPs reinforcement itself. As evident from Fig. 3, the unfilled matrix post-cured for 10 min showed a significant increase in storage modulus

(3140 GPa), while the unfilled matrix cured for 60 minutes shows only slightly higher value (3308 GPa). At both post-curing times (10 and 60 min) samples with NPs show lower values of initial storage modulus and HDT, while nanocomposites with ZNO NPs generally show even lower values than nanocomposites prepared with AZO NPs. As the content of nanoparticles in the post-cured samples increases, the storage modulus and HDT decrease, because of the absorbance and scattering of cured light on the present NPs, which prevents the curing of the resin.
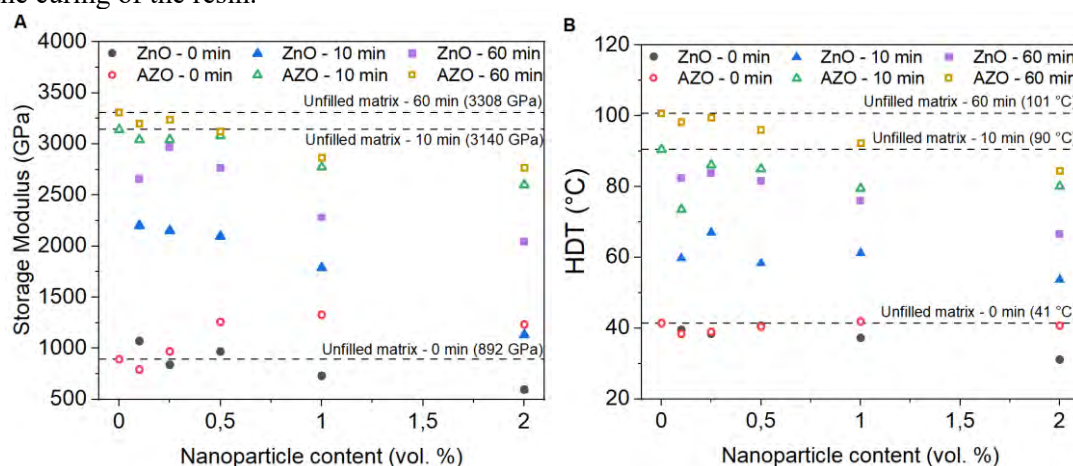


Fig. 3: (A) Initial storage modulus and (B) heat deflection temperature (HDT) as a function of nanoparticle content with 0, 10 or 60 min of post-curing time

## Conclusion

In this study, nanocomposites containing ZnO and AZO NP in different contents were prepared, and their photocatalytic properties were evaluated by photolysis, photo-DSC and Jacobs working curves. ZnO NPs were found to exhibit surface plasmon resonance and a subsequent photothermal effect after irradiation, thereby accelerating the kinetics of photopolymerization. AZO NPs also increase reaction kinetics, but to a lesser extent. The presence of NP in the matrix also causes a reinforcement effect, which is observable, for example, in thermomechanical properties. In samples without additional post-curing, the presence of AZO NP caused an increase in values such as initial storage modulus, $T_g$ or HDT. However, the post-curing process of 3D printed samples has a more significant effect than the presence of nanoparticles on the thermomechanical properties.

## Acknowledgements

## References

[1] Manapat, J. Z.; Chen, Q.; Ye, P.; Advincula, R. C.; Wood-Adams, P. M., *Macromolecular Materials and Engineering* **2017**, *302* (9), 2875-2880.
[2] Nakatani, A. I.; Chen, W.; Schmidt, R. G.; Gordon, G. V.; Han, C. C. *Polymer* **2001**, *42* (8), 3713-3722.
[3] Riad, K. B.; Arnold, A. A.; Claverie, J. P.; Hoa, S. V.; Wood-Adams, P. M., *ACS Applied Nano Materials* **2020**, *3* (3), 2875-2880.
[4] Check, C.; Chartoff, R.; Chang, S.; Advincula, R. C.; Wood-Adams, P. M. *European Polymer Journal* **2015**, *70* (9), 166-172.
[5] Štaffová, M.; Ondreáš, F.; Svatík, J.; Zbončák, M.; Jančář, J.; Lepcio, P. *Polymer Testing* **2022**, 108.
[6] Ondreas, F.; Lepcio, P.; Zboncak, M.; Zarybnicka, K.; Govaert, L. E.; Jancar, J. *Macromolecules* **2019**, *52* (16), 6250-6259.
[7] Jancar, J., Wang, W., & Dibenedetto, A. *Journal of Materials Science: Materials in Medicine*, *11*(11), 675-682.
[8] Neelgund, G. M.; Oki, A. *Materials Chemistry Frontiers* **2018**, *2* (1), 64-75.

# Anisotropic solid-state $CO_2$ foaming of 3D printed poly(lactic acid) and its impact on mechanical properties

Juraj Svatík, Petr Lepcio, Ema Režnáková, František Ondreáš, Josef Jančář

*Brno University of Technology, Central European Institute of Technology, Purkyňova 656/123, 612 00 Brno, Czech Republic.*
*Corresponding author's email address: xcsvatik@vutbr.cz*

Summary: A two-level hierarchical structure with multiple anisotropic microcellular channels inside a single printing line was created using 3D printing of semicrystalline poly(lactic acid), its saturation in subcritical carbon dioxide, and solid-state foaming in a heated silicon-oil bath.

## Introduction

The desire to create even better materials directed the effort towards structural control of a material from macro- to nano-level creating hierarchy in the system [1]. The hierarchy has developed in biological systems for thousands of years, and these materials have extraordinary properties (mechanical or functional) considering the rather narrow palette of elements used, unlike artificially made materials [2]. The focus of research in natural materials is also due to the attempts to create structures similar to those present, for example, in bone. That means to provide not only mechanical support but also biocompatible material and structure that are capable of nourishing bone and other parts of body [3]. In this complex task, we put in attention the canals in the bone, which are transport roads for nutrients through the bone reaching sizes of 50-600 nm based on the specific type and function in the system [4]. To reach such a precise structure, it is necessary to have control over the distribution of the material.

Control of material distribution to a certain amount is possible thanks to additive manufacturing (AM). Material extrusion 3D printing (a type of AM) utilizes polymer filament extruded at high temperatures through a die with usual diameter between 0.25-1.0 mm, which determines the smallest voxel possible to print. However, the fabrication of micro- or smaller cells requires the use of other techniques, such as solid-state foaming [5] or freeze drying [6]. A few researchers focused on the combination of 3D printing with physical foaming using $CO_2$ as foaming agent. Some studies [7] prepared porous scaffolds using 3D printing, which were then saturated with $CO_2$ gas and foamed creating a hierarchical structure with differently sized pores. Another study [8] saturated the polymer filament prior to 3D printing, so foaming occurred during 3D printing. Saturation was also performed with supercritical $CO_2$ [9], although the issue of low printing accuracy was caused by different foamability over time. Nevertheless, no specific orientation of pores within the structure was reported because of the semicrystalline template. Manufacturing of macropores is controlled, but microporosity due to foaming is randomly distributed, considering distribution and cell shape. A certain orientation of the cell shape can be achieved via external confinement, though this is concentrated at the borders of the confinement vessel, and other parts of the material remain untouched.

The focus of this work is on the preparation and characterization of anisotropically foamed PLA specimens prepared via 3D printing. The preparation process is characterized step by step, from initial crystal pre-orientation during 3D printing towards larger crystal orientation during saturation resulting in so-called microchannels after the foaming process – highly oriented micro pores with one large dimension.

## Materials and methods

Poly(lactic acid) (PLA) as a 'PLA natural' filament (*Gembird, NL*) with diameter of 1.75 mm and molecular weight of 128 000 g·mol$^{-1}$ (measured by DLS analyser – *DynaPro NanoStar,*

*Wyatt Technology, USA*), and $CO_2$ gas (*SIAD, CZ*) with a purity level of $\geq 99.5$ % and relative density of 1.529 were used to 3D print and saturate testing specimens, respectively. The PLA filament (dried at 40 °C for 24 h) was 3D printed using 0.25 mm nozzle with Original MK3S 3D printer (Prusa, CZ) in various shapes – a dogbone of $(35 \times 10 \times 1)$ mm$^3$ for the tensile test, a cube of $(8 \times 8 \times 8)$ mm$^3$ for the compression test, a rectangular beam of $(8 \times 8 \times 80)$ mm$^3$ and $(2 \times 8 \times 80$ mm$^3)$ for the impact test and the characterization of the specimen, respectively. The infill density was set at 100 % with 0.1 mm layer height and a printing rate of 45 mm·s$^{-1}$, and the infill orientation was parallel or perpendicular to the longest side of the specimen.

The printed specimens were separated with thin aluminum foil prior to placement in the cylindrical pressure chamber to avoid face-to-face contact. The saturation conditions were established at 15 °C, 72 h, and 5 MPa. After the saturation period ended, the pressured gas was slowly released and the specimens were confined between two thick aluminum spacers and immediately foamed in a silicon-oil bath heated to 130 °C. After the foaming period of 1 min, the foamed specimens were let to cool freely.

## Results and discussion

Oriented microchannels were created within foamed 3D printed PLA specimens (fig. 1) using a material extrusion 3D printer, $CO_2$ saturation, foaming in a silicon-oil bath, and cryo-shrinkage in liquid nitrogen ($N_2$(l)). Two levels of hierarchy were reported – one at submicrometer size consisting of channels formed due to crystal pre-orientation of PLA and foaming, the other at hundreds of micrometers size consisting of defects (gaps) between adjacent printing lines.
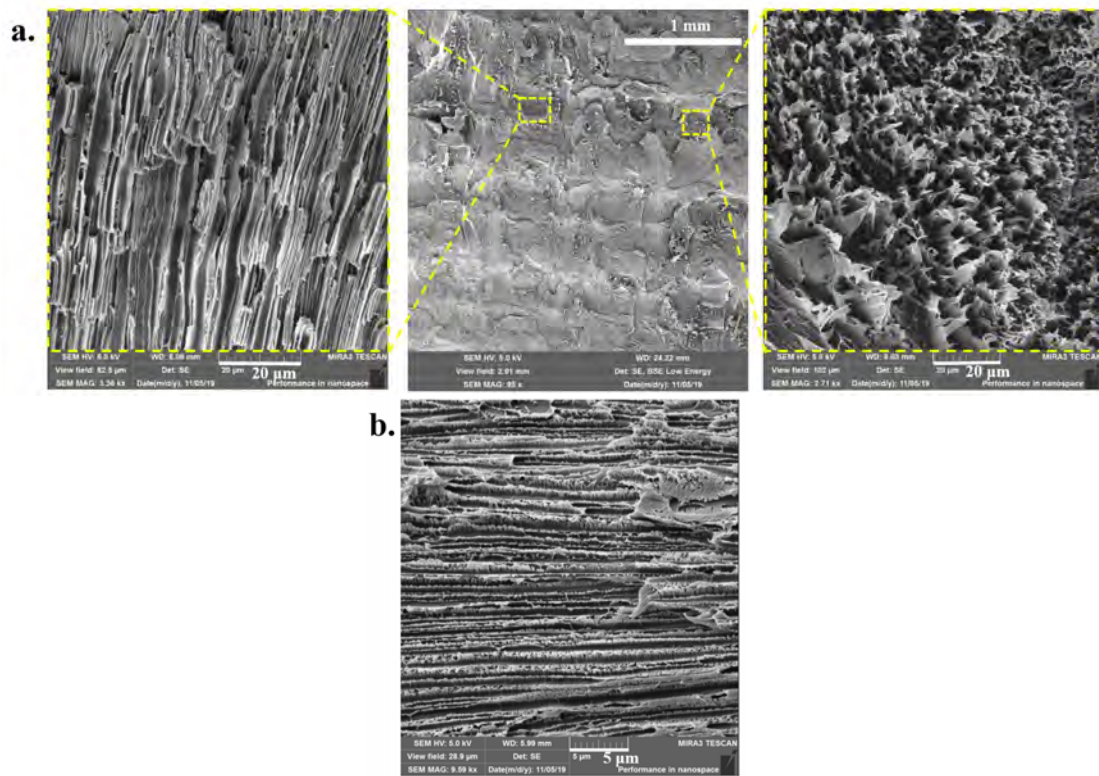


Figure 1: Microcellular channels within a 3D printing line in the longitudinal (left a.) and perpendicular direction (right a.) to the printing direction; b. a detail of the microchannels in the longitudinal direction

The process started with 3D printing during which small crystals of PLA were formed creating pre-orientation within the specimen, which was further enhanced during the $CO_2$ saturation forming complex PLA/$CO_2$ crystals. Crystallinity was investigated by wide-angle X-ray scattering (WAXS), differential scanning calorimetry (DSC), and Fourier-transformed infrared spectroscopy (FTIR). The 3D printed specimen has shown an almost completely

amorphous structure, both with WAXS and DSC, containing only about 0.9 % crystallinity, while the 3D printed specimens saturated in $CO_2$ showed complex PLA/$CO_2$ crystals with crystallinity around 22.3 %. Well-developed crystallites in $CO_2$ saturated specimen were confirmed by a single melting peak of PLA, whereas usually two peaks occur because of the presence of polymorph phases. The low amount of crystallinity after 3D printing seems to be the reason for the large crystals in PLA/$CO_2$ system building on small primary crystals pre-oriented during 3D printing. Furthermore, the PLA/$CO_2$ crystals were compared to the most abundant crystal phases in PLA [10] (α, α', and β) based on the peaks' positions in the WAXS diffractogram and the peaks of the PLA/$CO_2$ crystals were shifted, resulting in a different crystal phase. The theoretical enthalpy of the 100 % crystalline PLA/$CO_2$ specimen determined combining WAXS and DSC data has shown higher values than that of α-PLA and α'-PLA, too.

FTIR measurement was used to characterize the amount of orientation within the specimen through the dichroic ratio, which is determined as a ratio of polarized IR light absorbance with polarizers set to 90° and 0°, in this case for peaks at 918 and 956 cm$^{-1}$ corresponding to the crystalline and amorphous phase of PLA [10], respectively. The orientation of the crystalline phase in the perpendicular (90°) direction was reported in the 3D printed specimen, which was partially preserved in the saturated specimen and finally diminished during the foaming process while the α-PLA recrystallization occurred. These three analyses confirmed the growth of oriented PLA/$CO_2$ crystallites based on the small pre-oriented crystals created during 3D printing, which were used as a template for the fabrication of fine microporous channels' (diameter of $0.4 \pm 0.2$ μm) by solid-state foaming. The length of the channels ($> 20$ μm) was not measured due to the stretching beyond the view field of the scanning electron microscopy (SEM) imaging, although the observed length would yield an aspect ratio of at least 50.

The density of the printed and foamed specimens varied only slightly (about 13 %) due to gaps between adjacent printing lines as a direct effect of the 3D printing process as well as their extinction during the foaming and formation of highly dense crystalline phase. The microcellular channels were formed within the printing line, in the core, and thus surrounded by a dense, unfoamed region, a shell. The shell is a characteristic feature of solid-state foaming where the dissolved gas escapes from the material upon desaturation. This usually occurs only at the borders of the specimen, but due to the gaps between the adjacent printing lines, the shell is formed around each of them, occupying approximately 50-70 % of the total volume, leaving the remaining 30–50 % for the microcellular channels. We note that the microchannels were not observed in the 3D printed, heated, or reference specimen from PMMA. The oriented microcellular structure was also observed in unconfined specimens, proving that the origin was not affected by the external confinement.

Oriented microchannels create inhomogeneity in the material and affect multiple properties that become directionally dependent. The direction of the laid 3D printing line was directly responsible for the orientation of the microcellular channel after foaming. This was confirmed by SEM and a simple dying test, where the dye could only permeate through the specimen if the microchannels were aligned perpendicular to the dyed surface. The dye spread mainly through the 3D printing gaps, although the fine microchannels helped the dye permeation into the bulk of the PLA (confirmed by optical microscopy). Therefore, mechanical performance was investigated in two directions – longitudinal (parallel to the printing lines) and transverse (perpendicular to the printing lines), while the microchannels are oriented parallel to the direction of printing line. 3D printed, saturated, heated (3D printed specimen put in silicon oil at 130 °C for 1 min to simulate foaming conditions), and foamed specimens were investigated while loaded in compressive, tensile, or impact test (fig. 2). The longitudinal loading direction always yielded properties better than the transverse one for each kind of mechanical test, which was caused mainly by the printing direction and the crystal growth influenced by the printing direction. The directional influence was pronounced the most during the impact test, therefore when the load was applied the fastest. However, the mechanical properties (strength, elastic modulus) of the foamed specimens were always diminished compared to the 3D

printed specimens due to additional porosity. The foamed specimens reached higher deformation values in both tested directions compared to the 3D printed specimens during the tensile test and the foamed specimens also missed the plateau region during the compression test directly proceeding to the densification state. Both phenomena were ascribed to the crystalline phase evolved during the foaming step.
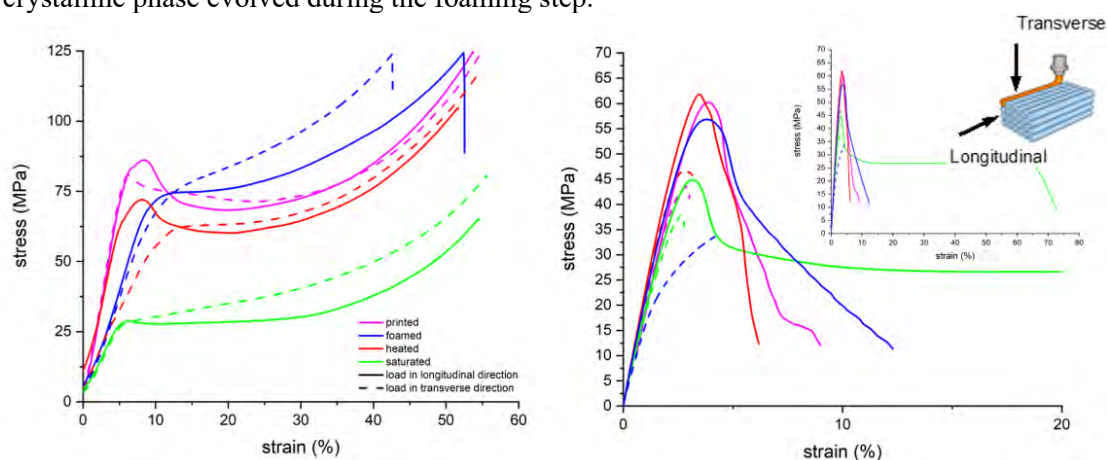


Figure 2: Stress-strain response of 3D printed, saturated, heated, and foamed specimens in compression (left) and tension (right) based on the load direction

## Conclusion

A two-level hierarchical porous structure with highly oriented cells was prepared using a material extrusion 3D printer and PLA filament. Tiny pre-oriented crystals of PLA during 3D printing served as a template for the growth of complex $PLA/CO_2$ crystals while saturating PLA with $CO_2$ gas. Anisotropic cellular structure with small cells and long channels perpendicularly and parallel to the printing direction, respectively, was achieved during the foaming. Based on the direction of laid 3D printed filament, the direction of the microchannels could be controlled, thus not needing any external confinement to create oriented cellular structure. Mechanical testing showed diminished performance of foamed specimens compared to 3D printed ones, but a pronounced effect of the loading direction was observed with respect to the printing and microchannel orientation yielding better properties in the parallel loading direction to the printing.

## Acknowledgement

## References

[1]   Weinkamer, R.; Fratzl, P. *Materials Science and Engineering: C* **2011**, *31*, 6, p. 1164-1173.
[2]   Liu, Z.; Zhang, Z.; Ritchie, R. *Advanced Functional Materials* **2020**, *4*, 5, p. 626-657.
[3]   Mudassir, M.; Tarlochan, F.; Mansour, M. *Applied Sciences* **2020**, *10*, 13.
[4]   Yu, B.; Pacureanu, A.; Olivier, C.; Cloetens, P.; Peyrin, F. *Scientific Reports* **2020**, *10*, 1-12.
[5]   Kanbargi, N.; Erp, M.; Lesser, A. *Journal of Polymer Science* **2020**, *58*, 23, p. 3311-3321.
[6]   Zeng, Z.; Jin, H.; Chen, N.; Li, W.; Zhou, L.; Zhang, Z. *Adv. Funct. Mater.* **2016**, *26*, 303-310.
[7]   Zhou, Ch.; Yang, K.; Wang, K.; Pei, X.; Dong, Z.; Hong, Y.; Zhang, X. *Materials&Design* **2016**, *109,* 415-424.
[8]   Li, M.; Jiang, J.; Hu, B.; Zhai, W. *Composites Science and Technology* **2020**, *200,* 108454.
[9]   Morascio, M. G. M.; Antons, J.; Pioletti, D. P.; Bourban, P.-E. *Adv. Mater. Tech.* **2017**, *2*, 1700145.
[10]  Xu, R.; Xie, J.; Lei, C. *RSC Advances* **2017**, *7*, 39914-39921.

# 3D printing with focused ultrasound

Frank P.A. van Berlo, Patrick D. Anderson and Lambert C.A. van Breemen

*Polymer Technology, Eindhoven University of Technology, The Netherlands*
*Email: f.p.a.v.berlo@tue.nl*

# 3D Printing of autonomous self-healing elastomers for soft robotics

S. Menasce, R. Libanori, F. Coulter, A. R. Studart

*Complex Materials, ETH Zürich, Zürich Switzerland*
*e-mail: stefano.menasce@mat.ethz.ch*

The increasing demand for robots that can carry out complex tasks in natural environments and safely interact with humans and other fragile objects has stimulated the development of multifunctional compliant materials for soft robotics. Given the demanding loading conditions required in these applications, the lifetime of materials that are typically used in soft robotics can be strongly reduced due to fatigue, wear, and cuts caused by sharp objects. To extend the lifetime of these materials and reduce the maintenance costs of soft robots, one potential solution is to employ materials that exhibit an autonomous self-healing behavior [1]. Despite exhibiting a remarkable self-healing efficiency, rubbery polymer networks crosslinked by dioxaborolane groups are also strongly prone to creep due to the dynamic nature of covalent bonds present in their molecular structure [2]. The large plastic deformation experienced by these dynamic polymers upon mechanical loading prevents the damaged surfaces to get in contact with each other, resulting in a significant reduction of their autonomous self-healing behavior. In this work, we present a strategy to improve the autonomous self-healing behavior of rubbery dynamic networks to enable their use for soft robotics. To achieve this, we synthesize chemically-compatible polymers with different autonomous self-healing efficiency and elastic recovery. Our experiments show that the synthesized polymers are able to self-repair its damaged surface at room temperature in only 5 minutes. We envision that autonomous self-healing soft robotic parts exhibiting complex geometries, tailored elasticity and autonomous healing efficiency can be manufactured by shaping the proposed polymers using 5-axis 3D printing technologies.

[1] Terryn, S.; Lagenbach, J. *et Al., Materials Today* **2021**, *47,* 187-205
[2] Breuillac, A.; Kassalias, A.; Nicolaÿ, R., *Macromolecules* **2019**, *52*, 7102-7113

# Structure-property relations for semi-crystalline PEEK

R.A.M. Geveling, L.E. Govaert, J.A.W. van Dommelen

*Department of Mechanical Engineering, Eindhoven University of Technology,*
*P.O. Box 513, 5600 MB Eindhoven, The Netherlands.*

# Material Extrusion Additive Manufacturing of PLA and ABS: deformation-dependent Eyring rate constant or activation volume?

Wilco M.H. Verbeeten, Miriam Lorenzo-Bañuelos

*Structural Integrity Group, Universidad de Burgos, Avenida Cantabria s/n, E-09006 Burgos, Spain*
*Email: wverbeeten@ubu.es*

Material Extrusion Additive Manufacturing (ME-AM) is a rapidly upcoming production process, which has gained increasing interest from both industry as well as academics. Its popularity is due to a combination of low investment costs, availability of a wide range of materials, and ease for manufacturing. Furthermore, components with good and near-bulk mechanical properties can be obtained, if proper processing parameters are chosen [1-3].

Products fabricated using ME-AM have a laminate composite structure consisting of stacked layers of partially bonded filaments with interstitial voids [4]. During ME-AM processing, the extruded material elements experience *local* time-strain and time-temperature profiles, which are influenced by the chosen ME-AM parameters [3]. Due to the initial fast cooling combined with successive heating cycles, these profiles are significantly different from more conventional processing methods, e.g. injection or compression molding. Hence, ME-AM products undergo a complex processing step, resulting in (local) anisotropy and heterogeneous mechanical properties along its dimensions. This leads to specific macroscopic deformation behavior as measured in macroscopic characterization tests (*e.g.* tensile, compression, shear, torsion, bending, creep, fatigue, impact).

In the present research, the strain-rate dependence of the yield stress is quantified and analyzed for both acrylonitrile-butadiene-styrene (ABS) and polylactide (PLA) materials, using samples fabricated via material extrusion additve manufacturing with different printing parameters. Apparent densities of the ME-AM processed tensile test specimens were measured and taken into account in order to study the effects of the ME-AM parameters and processing step on the material behavior.

The ABS material manifested thermorheollogically simple behavior that can correctly be described by an Eyring flow rule [5,6]. PLA, on the other hand, showed thermorheollogically complex behavior. The Ree-Eyring modification of the Eyring flow rule was applied to analyze the PLA yield kinetics, taking two molecular deformation processes into account [3].

Anisotropy was detected not only for the yield stresses but also for its strain-rate dependence for both materials [3,5,6]. Results also showed a lower strain-rate dependence manifested by ME-AM PLA samples compared to compression molded samples [3]. Furthermore, for PLA, some ME-AM sample sets demonstrated semi-ductile behavior, while compression molded samples were brittle. These remarkable results were attributed to the processing phase [3].

By changing infill orientation angles and print velocities, anisotropy effects could be attained. Sample sets were obtained with different levels of polymer chain orientation and stretch, as determined from thermal shrinkage measurements [3,4,6]. Experimental results suggest that PLA shows a deformation-dependent Eyring rate constant, while ME-AM processed ABS manifests a deformation-dependent activation volume.

## References

[1] Spoerk, M.; Arbeiter, F.; Cajner, H.; Sapkota, J.; Holzer, C.; *J. Appl. Polym. Sci.* **2017**, *134*, 45401.
[2] Song, Y.; Li, Y.; Song, W.; Yee, K.; Lee, K.-Y.; Tagarielli, V.; *Mater. Des.* **2017** *123*, 154–164.
[3] Verbeeten, W.M.H.; Lorenzo-Bañuelos, M.; Arribas-Subiñas, P.J.; *Addit. Manuf.* **2020**, *31*, 100968.
[4] Rodríguez, J.; Thomas, J.; Renaud, J.; *Rapid Prototyp. J.* **2001**, *7*(3), 148-158.
[5] Verbeeten, W.M.H.; Lorenzo-Bañuelos, M.; Saiz-Ortiz, R.; González, R.; *Rapid Prototyp. J.* **2020**, *26*(10), 1701-1712.
[6] Verbeeten, W.M.H.; Arnold-Bik, R.J.; Lorenzo-Bañuelos, M.; *Polymers*, **2021**, *13*, 149.

# Challenges in additively manufactured thermoset continuously reinforced composites

Jevan Furmanski[1,2], Andrew Abbott[1,2], G. P. Tandon[1,2], Mark Flores[1], Jeffery Baur[1]

[1] *Air Force Research Laboratory, Wright Patterson Air Force Base, OH, USA*
[2] *University of Dayton Research Institute, Dayton, OH, USA*

Additive manufacturing (AM) has realized tremendous gains in structural applications. Many of the achievements of AM in primary load-bearing structure has been limited to powdered metal consolidation processes. Polymers are often not suited for structural applications. Polymer matrix composites (PMC) have mostly been limited to short-fiber extrudable formulations with limited fiber volume fractions [1]. AM of continuously reinforced PMCs (CR-PMCs) has emerged as a viable manufacturing process recently. While many providers of thermoplastic continuous fiber additive printing are currently available, as-manufactured mechanical properties have not reached their theoretical expectations due to poor filament inter-diffusion, porosity, and low fiber-resin interface strength [2]. In comparison, thermoset continuous fiber printed composites, specifically those with snap-cure capability through UV or other means, have been addressed commercially and have performance approaching that of conventional PMCs. The extreme strength-to-weight ratios achievable with continuously reinforced PMCs, with a high volume fraction of carbon fiber is especially attractive for flight structures. The present work explores opportunities and challenges in AM of CR-PMCs and their mechanical performance and manufacturability.

One of the most promising aspects of AM is the ability to fabricate structures with complex geometries that cannot reasonably be manufactured by conventional means, such as topologically-optimized (TO) structures. TO algorithms generally operate by adding/subtracting material point-wise, which is nominally sufficient for AM because these processes also add material in a point-wise manner. However, AM of CR-PMC structures comes with the constraint that the continuity of the fibers must be maximally respected (and tow overlapping disallowed), along with other geometric limitations on manufacturability that are not easily accounted for in TO. The impact of these manufacturability constraints for TO of structures can be highlighted by the problem of topological intersections (i.e., joints). When four structural members come together in an intersection (an "X-joint"), it is not generally possible to pass the fibers continuously across the joint in both directions without overlapping the tows. As a result, one can either steer tows to adjacent arms of the joint, or cut the tows in one direction just outside the joint – however, both of these tactics result in the loss of over 70% of the expected strength of the material. The failure mechanism inside such joints (loaded in tension along the member direction) is dominated by the transverse strength of the matrix and fiber-matrix interface due to multiaxial stresses that occur near fiber ends, or delamination-type fracture along steered fibers. This work presents results illuminating performance-limiting aspects of AM CR-PMCs, exploring the origins of their performance, and probing potential future avenues for improved performance via material design.

The PMCs explored in the present work employed an initial UV snap-cured thermoset resin applied to a 12k carbon fiber tow to fix shape, followed by a thermal cure to achieve full cure while maintaining printed shape. Some of the incident UV radiation is absorbed by the fibers, resulting in a cure gradient where the bottom of the tow is the least cured region, affecting the adhesion of the printed layer. While the composite is fully cured after the build is complete, the difference in cure kinetics may result in a heterogeneous, non-ideal network structure. Further, inhibited UV curing presents a concern for manufacturability, potentially limiting the stresses that can be supported during printing of tight radii or overhanging structures. This work presents results demonstrating the cure gradient from UV light extinction and its impact on manufacturability in UV-cured AM CR-PMCs.

## References
[1] van de Werken, N., Tekinalp, H., et al. *Additive Manufacturing* **2020**, *31*
[2] Brenken, B., Barocio, E., et al. *Additive Manufacturing* **2018**, *21*

# Multiscale modelling of the glass transition in Nafion membranes for perspective flow and fuel batteries

Soumyadipta Sengupta[1], Rakesh Pant[3], Arun Venkatnathan[3]
and **Alexey V. Lyulin**[1,2]

[1]*Soft Matter and Biological Physics, Department of Applied Physics, Technische Universiteit Eindhoven, 5600 MB, Eindhoven, The Netherlands.*
[2]*Center for Computational Energy Research, Department of Applied Physics, Technische Universiteit Eindhoven, 5600 MB, Eindhoven, The Netherlands.*
[3]*Department of Chemistry and Center for Energy Science, Indian Institute of Science Education and Research, Dr. Homi Bhabha Road, Pashan, Pune 411008, Maharashtra, India*

Nafion is a commonly used polyelectrolyte membrane (PEM) in fuel cells and flow batteries. The properties of hydrated membranes, and the water influence on Nafion glassy behavior is very important. We report molecular-dynamics simulations of Nafion films of different thicknesses between two potential walls of variable wettability We also discuss the modelling of the annealing effects on both structure, dynamics and electric conductivity of the membranes. We observe strong antiplasticization and increase in the glass-transition temperature upon hydration. The hydrophilic channels evolution upon annealing and associated changes in ion diffusion and electric conductivity will be discussed.

## Introduction

Polyelectrolyte membranes (PEMs) are key components to be used in fuel cells and flow batteries. They provide a pathway for proton transport and separate gases/electrolytes from mixing. PE membranes absorb water on contact, and connected water pathways, necessary for charge transport, are formed inside. Nafion, see **FIGURE 1a**, which has a polytetrafluoroethylene (PTFE) hydrophobic backbone and a slightly hydrophilic (due to the presence of a sulfonic acid group) side chain, is a widely used membrane for both flow batteries[1] and PEM fuels cells (PEMFCs)[2]. It has good conductivity and mechanical stability at room temperature, but it loses water at high temperatures. Due to the loss of water upon heating, the conductivity of Nafion degrades[2,3], and the behaviour of Nafion upon thermal annealing attracts attention; the recent experiments[4,5] show significant conductivity decrease upon annealing.

Different nanoparticles like silica, zirconia, and modified carbon nanotubes have been used in Nafion nanocomposites, to increase water retention and proton conductivity. In addition, Nafion can also exist in catalyst layers between carbon support and platinum nanoparticles. The filler nanoparticles and supports have varying levels of hydrophilicity. Therefore, the model of Nafion capped between substrates of varying hydrophilicity will be effective to provide insights into the importance of the interfacial interactions in Nafion nanocomposites.

In the present manuscript, using classical molecular-dynamics (MD) technique, the glass transition of Nafion bulk was simulated for samples with different hydration levels, and cooled down with different cooling rates. Nafion films capped between walls of different hydrophilicity were simulated across a range of thicknesses and walls hydrophilicity levels.

## Simulated Models

The Nafion chains were initially constructed using Materials Studio[6]. The *pcff* (Polymer Consistent Force Field)[7] and LAMMPS software were used for simulating the Nafion matrices, water and hydronium ions. Partial charges for all the atoms were assigned using *COMPASS* (Condensed-phase Optimized Molecular Potentials for Atomistic Simulation Studies) force field. To investigate annealing, the bulk Nafion samples, **FIGURE 1b**, were initially equilibrated at T=600K and cooled down to 200K with different cooling rates. To simulate capped films, **FIGURE 1c**, Nafion chains were confined between structureless potential walls of tuneable hydrophilicity[8-10].

Nafion with an equivalent weight (EW) of 1100 has been chosen for this study. In films, Nafion was simulated at one hydration level ($\lambda = 15$); the hydration was varied from $\lambda = 0$ to $\lambda = 20$ in Nafion bulk studies.



a)          b)          c)
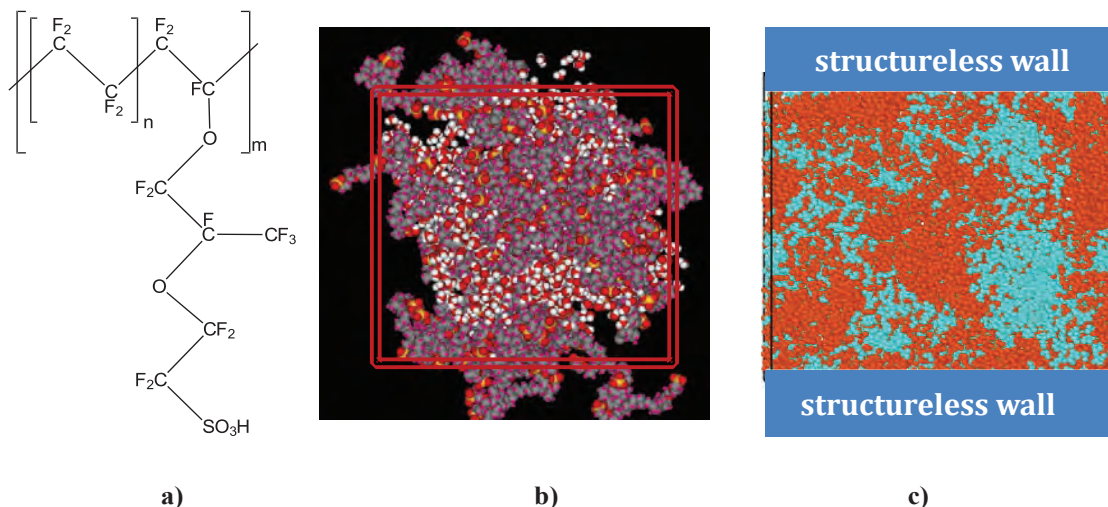
**FIGURE 1. a)** Chemical structure of a single Nafion chain of the present study. **b)** Nafion bulk samples made of 20 chains, hydration level is 5, light spheres indicate water molecules and hydronium ions. The central simulation box is also shown. **c)** Nafion capped film confined between two structureless walls of varied hydrophilicity

## Results and Discussion



a)          b)          c)
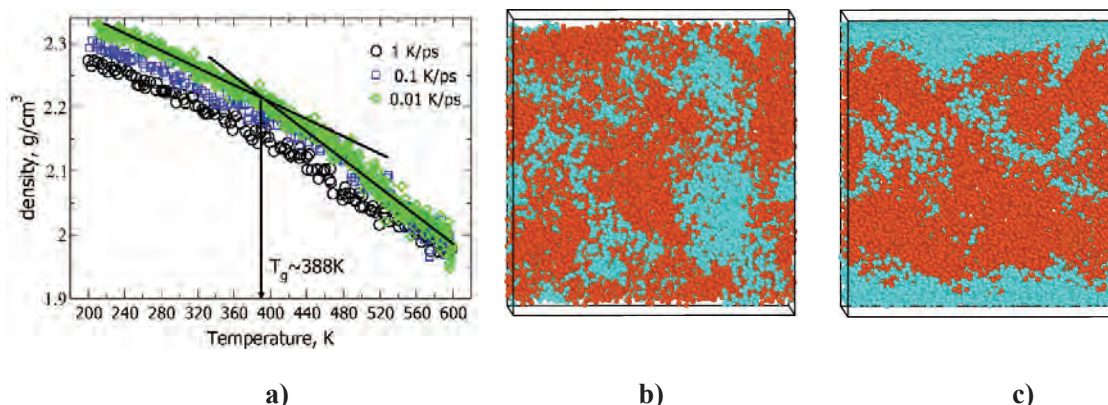
**FIGURE 2. a)** Glass transition MD simulation for dry Nafion bulk. Snapshots for capped hydrated Nafion films between very hydrophobic (**b**) and very hydrophilic (**c**) walls where blue color shows the water molecules and hydronium ions, and orange color shows the Nafion atoms.

The **FIGURE 2a)** shows the typical N$p$T molecular-dynamics results for dry Nafion density evolution upon cooling using different cooling rates. The samples cooled down slower show higher density, as an effect of ageing below $T_g$.

**a)**                                                                            **b)**
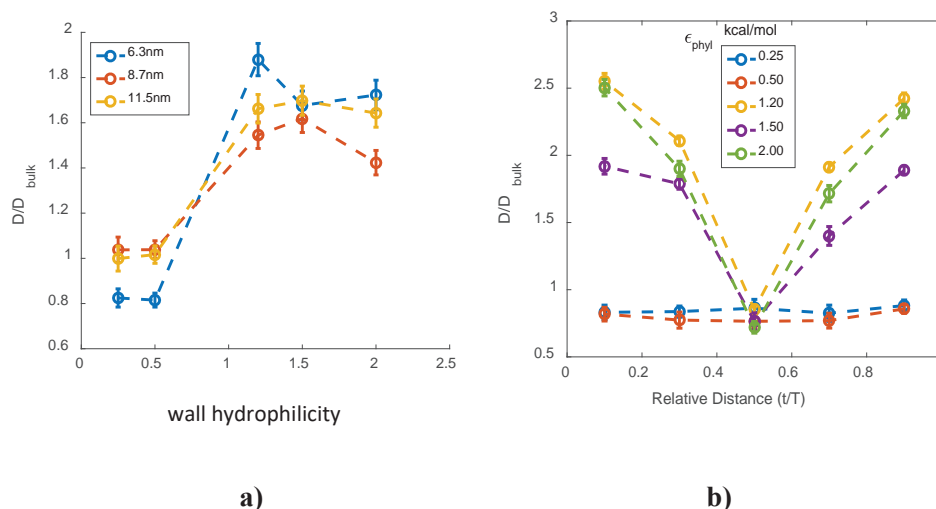
**FIGURE 3. a)** Film averaged (a) in-plane water diffusion constants (D) normalized by the corresponding two-dimensional water diffusion ($D_{bulk}$) constant at $\lambda$=15 for bulk Nafion.
**b)** Layer resolved in-plane water diffusion constants (D) in Nafion capped film normalized by the two-dimensional water diffusion constant ($D_{bulk}$) at $\lambda$=15 for bulk Nafion. Results are shown for the 6.3 nm film for varying wall hydrophilicity.

The glass-transition temperature, $T_g \sim$ 388 K, produced by the slowest cooling, is not very far from the experimental value, ~370K.

In capped Nafion films, the water and hydronium atoms can be seen to form large clusters close to the confining walls, as the wall hydrophilicity increases, **FIGURE 2b,c**. Water clusters become more disconnected through the center of Nafion film for highly hydrophilic walls. This leads to the lower average cluster sizes, which explains the experimentally observable low crossover of methanol for composite membranes with highly hydrophilic nanoparticles[11]. For highly wettable walls clusters grow significantly in thick films, because in this case the confinement effect weakens.

In Nafion films the in-plane water diffusion constant ($D$) has been computed using the Einstein relation, averaged over the film and resolved in 5 equal layers in the Z-direction. **FIGURE 3a** shows the in-plane water diffusion, normalized by the bulk water diffusion constant for different wall hydrophilicity values and for the different film thicknesses. The in-plane water diffusion is noticeably higher for the hydrophilic walls. **FIGURE 3b** shows the layer resolved in-plane water diffusion constant, normalized by the bulk two-dimensional water diffusion constant, for the 6.3 nm film. The water diffusion constants are slightly smaller than bulk values for the hydrophobic walls. For the hydrophilic walls, the diffusion constant near the centre of the film is close to that for the bulk, but the diffusion increases considerably on moving closer to the walls. It is the presence of such highly mobile water layers near both the walls in a capped Nafion film that can explain the noticeably high film averaged in-plane water diffusion constant for the hydrophilic walls. Previously simulated supported Nafion films were shown to have considerably less in-plane water diffusion near the free interface as compared to that near the highly hydrophilic substrates[8]. In contrast, we observe occurrence of highly mobile layers at both hydrophilic walls across all the film thicknesses. This fact can explain the considerably higher film averaged in-plane diffusion for the capped Nafion films confined by hydrophilic walls.

## Conclusions

Using fully atomistic MD modeling, we have simulated Nafion at four different hydration levels of $\lambda$ = 5, 10, 15, and 20 and three different cooling velocities of 1, 0.1, and 0.01 K/ps, corresponding to annealing from T = 600 to 200 K. The simulated glass-transition temperature $T_g$ of Nafion increased with increasing hydration. This was due to the compression of the hydrophobic Nafion domains by larger water clusters with increasing hydration. Interestingly, a second lower $T_g$ was observed for the simulated systems which indicated the glass transition temperature of confined water. The sulfur–sulfur close range structure remained largely unaffected by annealing. The water cluster sizes increased with lower cooling rates. This was explained by the extra time

which these water clusters had to agglomerate into larger clusters at lower cooling rates. This agglomeration into larger clusters with lower cooling rates reduced their connectedness and charge mobility. This reduction in connectedness was evident from the reduced diffusivity of the water molecules and hydronium ions with reduced cooling rates. Previous experiments have also shown a noticeable decrease in proton conductivity with longer annealing/lower cooling rates, in qualitative agreement with the presented simulations.

The reported molecular-dynamics simulations show that
- the atomistic molecular dynamics can be used to study thermal annealing effects in Nafion;
- the hydrophilic substrates can drastically reduce the water cluster sizes and enhance in-plane water diffusion;
- the film thickness, which is representative of nanoparticle loading, can be used to control cluster connectivity.

## Acknowledgements

## References

1. B. Huskinson, M. P. Marshak, C. Suh, S. Er, M. R. Gerhardt, C. J. Galvin, X. Chen, A. Aspuru-Guzik, R. G. Gordon and M. J. Aziz, *Nature*, 2014, **505**, 195-198.
2. S. Bhadra, N. H. Kim, J. S. Choi, K. Y. Rhee and J. H. Lee, *J. Power Sources*, 2010, **195**, 2470-2477.
3. M. A. Ilhan and E. Spohr, *J. Electroanalyt. Chem.*, 2011, **660**, 347-351.
4. D.K. Paul, K. Karan, *J. Phys. Chem. C*, 2014, **118**, 1828-1835.
5. O. Kwon, S. Wu, D.-M. Zhu, *J. Phys. Chem. B*, 2010, **114**, 14989-14994.
6. *Accelrys Inc., San Diego, CA*, 2013.
7. H. Sun, S. J. Mumby, J. R. Maple and A. T. Hagler, *J. Am. Chem. Soc.*, 1994, **116**, 2978-2987.
8. D. Damasceno Borges, A. Franco, K. Malek, G. Gebel, S. Mossa, *ACS Nano* 2013, **7**, 6767–6773.
9. D. Damasceno Borges, G. Gebel, A. Franco, K. Malek, S. Mossa, *J. Phys. Chem. C* 2015, **119**, 1201–1216.
10. S. Sengupta, A. V. Lyulin, *J. Phys. Chem. B*, 2018, **122**, 6107-6119.
11. R. Gosalawit, S. Chirachanchai, S. Shishatskiy, S. Nunes, *Solid State Ionics*, 2007, **178**, 1627−1635.

# MOLECULAR MODELLING OF STRETCH-INDUCED CRYSTALLIZATION IN POLYPROPYLENE LAYERS

Sigalas I. Nikolaos and Alexey V. Lyulin

*Eindhoven University of Technology, TU/e*

Nowadays, in the modern circular economy, there is a trend towards designing easily recyclable and energy-efficient products. One growing segment of such products is the packaging industry. Polypropylene is widely used for this purpose and its performance in packaging applications is a strong function of its semicrystalline morphology that develops during processing. So our project aims at developing a multiscale computational approach to address the structure-property-processing-performance relations in the polypropylene-based nanocomposites and unraveling the mechanisms controlling crystallization.

In order to understand the crystallization mechanisms, we have performed molecular-dynamics computer simulations of both pure bulk isotactic polypropylene (iPP) and of polypropylene confined between talcum surfaces (Figure 1). Such a molecular approach is feasible as computational power has dramatically increased and Molecular Dynamics has been established as a powerful method. Of course, crystallization is still a really slow process, even for the most powerful computers, and, for this reason, we employ two strategies: stretch-induced crystallization and coarse-graining. It is a fact that elongational flow accelerates crystallization significantly and recent simulations confirm this [1]. Regarding the latter strategy, the coarse-grained models have been widely used over the years. Specifically, a number of atoms are regarded as one interaction center, decreasing the time needed for a simulation. Given these two powerful approaches, crystallization can be observed on both spatial and temporal scales accessible to molecular simulations.

Till now, in our project, some significant steps have been accomplished towards the multiscale modeling of polypropylene. First of all, the mimicking of the Machine Direction Orientation process, the process that is used for making films, is essential. To simulate it, we bring the sample to the desired orientation temperature, then stretch it and at the end perform annealing at a specific temperature. Following this process, a small system of pure isotactic polypropylene of 50 monomers per chain at the united-atom level was crystallized successfully (Figure 2). Crystallization has also been achieved for larger systems, up to 2000 monomers per chain. Subsequently, we discuss the role of the iPP helicity during the ordering in lamellae. Finally, we have reproduced an IPP helical structure at a coarse-grained level and we propose a methodology for developing a coarse-grained force field that can effectively capture this helical behavior.
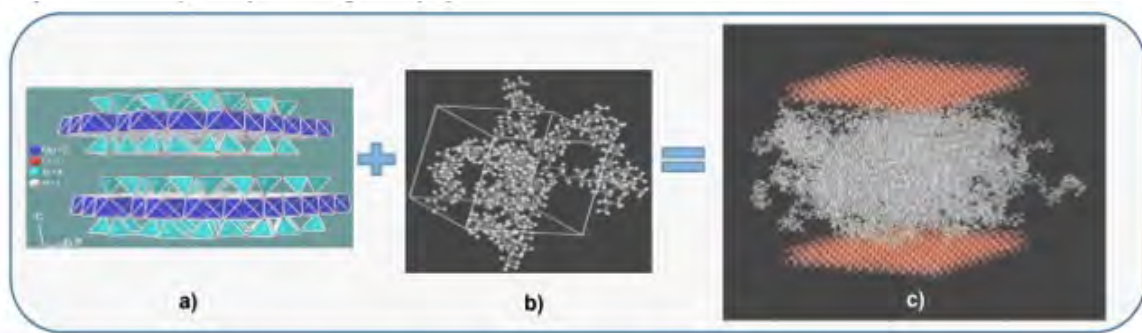
[1] Yamamoto, T., Macromolecules, 2014, 47, 3192–3202
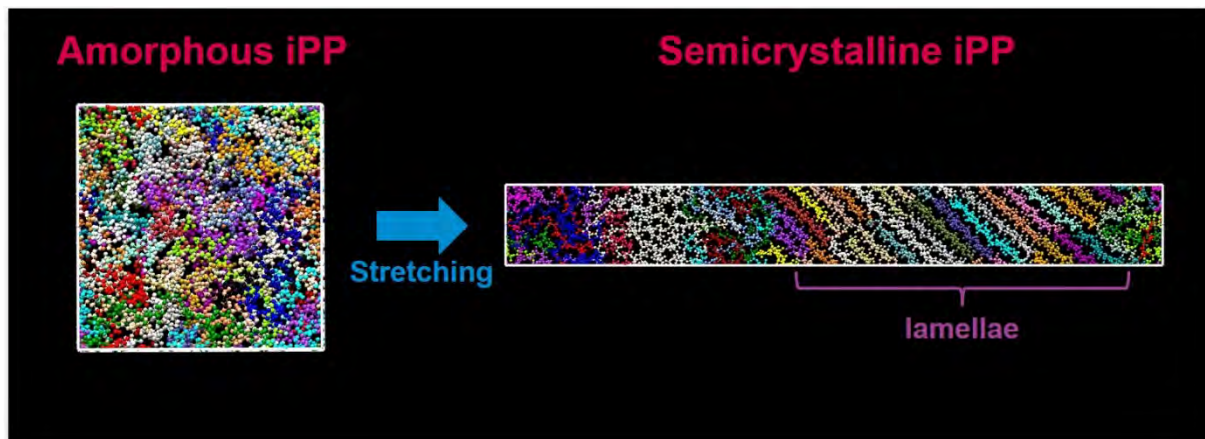
**Figure 1**



**Figure 2**

# A data-driven study of the large deformation behaviour of triblock copolymers

Aravinthen Rajkumar [1,2], Peter Brommer [1, 3], Łukasz Figiel [1, 2]

1. EPSRC Centre for Doctoral Training in Modelling of Heterogeneous Systems (HetSys), University of Warwick, Coventry CV4 7AL, UK
2. International Institute for Nanocomposites Manufacturing (IINM), WMG, University of Warwick, Coventry, CV4 7AL, UK
3. School of Engineering, University of Warwick, Coventry, CV4 7AL, UK

Corresponding emails:   arre.rajkumar@warwick.ac.uk,   L.W.Figiel@warwick.ac.uk

## Abstract

As inherently heterogeneous materials, block copolymers can demonstrate non-trivial mechanical properties such as hyperelasticity, viscoplasticity and hysteresis. Whilst there exist a range of continuum approaches to modelling block copolymer response [1-2], models that encompass the full detail of the underlying polymer physics have been missing.

In this work, we employ molecular simulations to capture the mechanical response of an ABA triblock copolymer system at various block sizes. The stress-strain curves of the system in the loading/unloading stage are then predicted as a function of block size via a data-driven surrogate model. From here, an analysis of the relation between block size and mechanical response is conducted in which all quantities specifically originate from the microstructural detail.

Data acquisition is primarily performed through coarse-grained molecular dynamics simulations. An equilibrium structure is generated by first obtaining the copolymer segment distribution via field-theoretic simulations, the results of which are subsequently used to generate biased random walks to build a particle-based molecular model [3-4]. After a short equilibration in which the initial soft-core potentials between the beads are gradually modified into hard excluded volume interactions [5], the system is quenched. This leads to the formation of glassy phases within the system alongside a softer rubbery phase. After inducing deformation, we then train a Gaussian process regression model using the stress-strain data at different strain rates and temperatures as a function of the size of the blocks that compose each copolymer chain within the system. The subsequent data-driven model can serve as a bridge between the microscopic physics of a block copolymer and the macroscopic description of the system's large deformation behaviour.

## Acknowledgements

## References

[1] Buckley, C.P.;  De Focatiis, D.S.A.; Prisacariu, C.; In *Constitutive Models for Rubber VII; 1st Ed.; Jerrams, S; Murphy, N;* CRC Press: London, 2011; pp. 3-10.
[2] Cho, H.; Mayer, S.; Pöselt, E.; Susoff, M.; Boyce, M. C., Polymer **2017** 128, 5
[3] Terzis, A. F.; Theodorou, D. N.; Stroeks, A., Macromolecules **2000** 33, 1397
[4] Aoyagi, T.; Honda, T.; Doi, M., J. Chem. Phys. **2002** 117, 8153
[5] Parker, A. J.; Rottler J., Macromol. Theory Simul. **2014** 23, 401

# Control of the Final Morphology of Epoxy-Thermoplastic Blends and Mechanical Properties

Anne Coloigner [1,2*], Marie-Laure Michon [2], Claude Billaud [2], Didier Long [1]

[1] Matériaux, Ingénierie et Sciences (MATEIS), UMR 5510 CNRS - INSA de Lyon, Villeurbanne, France
(*anne.coloigner-ext@solvay.com PhD student)
[2] Solvay Research and Innovation Center, 85 avenue des Frères Perret 69192 St Fons Cedex, France

Thermosetting epoxy resins are used to lighten materials weight in the aerospace and automotive industries. High performance resins exhibit excellent physical properties like stiffness and strength with high temperature performance and chemical resistance. Nevertheless, a high crosslink density makes the resins brittle. To improve the mechanical properties of the materials, thermosets can be toughened by the dissolution of thermoplastic polymer into resin monomers followed by a phase separation during the curing cycle [1]. By controlling the final morphology of the resin, mechanical properties can be enhanced for composite applications.

The main parameters that control the final morphology have to be determined. The associated length scale is a key parameter regarding the mechanical properties and toughness of the materials. Previous thesis [2] has allowed to identify two key parameters for controlling the morphology. The solubility parameters between constituents control the onset of the phase separation and the corresponding conversion stage. The glass transition temperature of the blend at phase separation controls the rate of growth of the morphology. The smaller the difference between the process temperature and glass transition temperature of the blend at which phase separation takes place, the smaller the size of the morphologies can achieve a few tens of nanometres.

Thermoplastic-modified epoxy resins are considered. They consist of different epoxy monomer structures modified with a fixed amount of commercial thermoplastic and cured with different curing agents. The mechanism of phase separation process which takes place during curing of epoxy-thermoplastic blends has been studied. Also, synthesizing thermoplastic copolymers from different monomers will give access to a broader range of thermoplastic glass transition temperatures and solubility parameters.

The characterisation of the different morphologies are realized by electron microscopy. Rheology analysis allows to identify the phase separation onset by a sudden variation of viscosity. For systems containing a commercial thermoplastic, it has been demonstrated that the scale of the morphologies depends on the initial solubility parameters of each component. For large values of solubility parameters, an early phase separation and micron-scaled morphology were observed. With more compatible curing agents, late phase separation occurs and morphologies of a few hundred nanometers have been observed. Moreover, curing of the resins at lower temperatures involves small morphologies as expected by decreasing the temperature difference at phase separation.

## References

[1] Pascault J.-P ; Sautereau H. ; Verdu J. ; Williams R. J. J., Thermosetting polymers, **2002**.
[2] Mathis E., Thermoplastic toughened thermoset composites: control of morphology, in relation with applicative properties, **2020**.

# In-situ time-resolved study of the effects of thermal history on stereocomplexation of a PLLA/PDLA racemic blend

Hamid Ahmadi[1], Ruth Cardinaels[1] and Patrick D. Anderson[1]

[1] *Department of Mechanical Engineering, Eindhoven University of Technology, P.O. Box 513, 5600 MB Eindhoven, The Netherlands.*

## Abstract

Poly(lactic acid) (PLA) is a promising biodegradable thermoplastic that has received considerable attention in recent decades. It shows excellent performance in terms of biodegradability, renewability, biocompatibility and applicable mechanical properties [1]. Unfortunately, its low crystallisation rate and lack of thermal, mechanical and hydrolysis stability limits the possible applications. To improve these properties, the two enantiomers of PLA, i.e. poly(L-lactide) (PLLA) and poly(D-lactide) (PDLA), can simultaneously be packed into one unit cell. The result is stereocomplex (SC) crystallisation between PLLA and PDLA [1]. Compared to PLLA or PDLA homo-crystals (107 helical conformation), Stereocomplex crystals (31 helical conformation) with a compact side-by-side helical structure shows unique properties such as higher melting temperature (Tm ~ 220-230°C) and higher thermal stability [1]. Hence, increasing the fraction of SC crystals in processed PLA products is crucial for improving their properties. It has been demonstrated that two main mechanisms can lead to the formation of stereocomplex crystals. SC crystals can originate from PLLA/PDLA helix pairs that cluster into a mesophase. Besides, α and α' type of homo-crystals can transform into stereocomplex crystals through melting and recrystallization at an elevated temperature below the melting point of SC-crystals (Fig. 1) [2-3].

In this work, we use synchrotron wide and small angle X-ray diffraction (WAXD & SAXS) techniques in combination with a custom-designed setup that allows quick temperature jumps to perform high-frequency structure characterization. Thereby, we generate a systematic understanding of the crystal growth and homocrystal transformation in PLLA/PDLA stereocomplex forming mixtures. Moreover, the melting behavior of stereocomplex crystals after isothermal crystallization is studied using differential scanning calorimetry (DSC) and small-angle X-ray diffraction (SAXD) techniques. The results indicate that using melt-recrystallization of homocrystals to form stereocomplex crystals is a quite promising method to achieve improved stereocomplex crystallization rates and to expand the application areas of PLA (see Fig. 2).
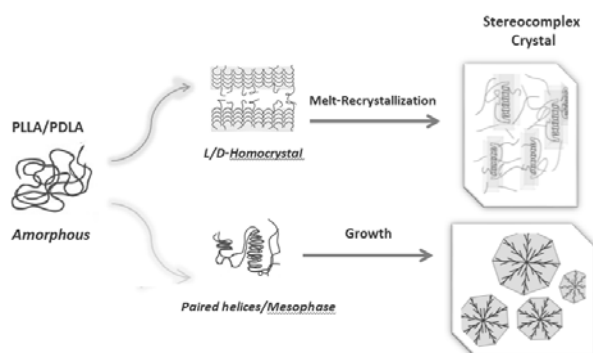
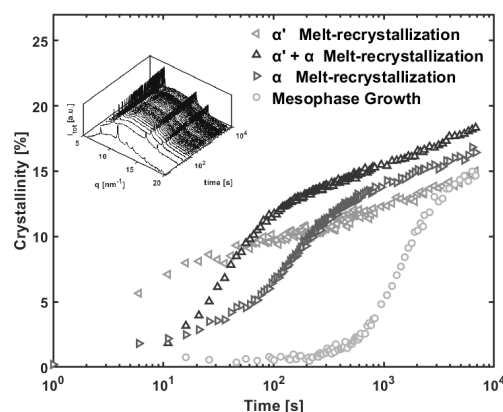*Figure 1:* Schematic of stereocomplex crystallization through different mechanisms



*Figure 2:* Results of time-resolved XRD analysis during isothermal crystallization of SC crystals

[1] Bai, Hongwei, et al. "Recent advances in processing of stereocomplex-type polylactide." *Macromolecular rapid communications* 38.23 (2017): 1700454.

[2] Na, Bing, et al. "Stereocomplex formation in enantiomeric polylactides by melting recrystallization of homocrystals: crystallization kinetics and crystal morphology." *Macromolecules* 47.1 (2014): 347-352.

[3] Yang, Ching-Feng, et al. "Extensive development of precursory helical pairs prior to formation of stereocomplex crystals in racemic polylactide melt mixture." *Macromolecules* 45.2 (2012): 872-878

# Predicting the rate- and temperature dependent behaviour of polyvinylidene-fluoride (PVDF)

T. (Tom) Lenders, T. (Tommaso) Pini, J.J.C. (Joris) Remmers, M.G.D. (Marc) Geers, L.E. (Leon) Govaert

*Department of Mechanical Engineering, Eindhoven University of Technology*
*email: t.lenders@tue.nl*

The application of fiber reinforced plastics is increasing in the oil and gas industry. Carbon fiber reinforced polyvinylidene fluoride (PVDF) may be a viable option to be used in offshore applications, due to the favourable chemical and thermal properties of the PVDF matrix combined with the mechanical properties of carbon fiber. To predict the long- and short-term behaviour of the composite under extreme offshore conditions, the behaviour of its constituents must be well understood. The matrix is responsible for a great deal of the deformation and failure response of the composite. In this study the rate- and temperature dependent behaviour of the matrix PVDF is modelled and compared to experimentally observed behaviour.

To model the PVDF matrix, the Eindhoven Glassy Polymer (EGP) model is used as it can capture the nonlinear viscoelastic pre-yield response and the viscoplastic post-yield response of many solid polymers [1]. The mechanical analogue of the EGP model is represented by a series of parallel linked Maxwell spring-dashpot elements connected in parallel to a spring. The Maxwell elements allow for describing the intrinsic response of the polymer by defining the viscosity of the dashpots. The hardening behaviour of the polymer is described by the spring that is linked to the Maxwell elements.

The viscosity of the dashpots is described by an Eyring-type flow rule that incorporates rate-, temperature- and pressure dependence. It is defined by a reference viscosity and a number of Eyring equation parameters. These parameters of the Eyring equation are characterized in [2] using the deformation behaviour of PVDF that is obtained from a set of uniaxial compression and tensile tests. The experimental study described in [2] shows that the yield kinetics of PVDF are rate- and temperature dependent due to presence of at least two molecular mechanisms. In the EGP model this is modelled as two series of Maxwell elements connected in parallel. Each mechanism is described by its own set of Eyring equation parameters. The reference viscosities are determined from the pre-yield response of a single uniaxial compression test at a prescribed strain rate and temperature. The pressure dependence is determined by combining the response of a compression and tensile test at the same prescribed strain rate and temperature. This concludes the characterization of the material parameters.

Finally, the material parameters are validated on a set of experimental compression and tensile tests performed at various prescribed strain rates and temperatures. These testing conditions are different from the one used for the characterization. Furthermore, the parameters are validated by performing creep simulations and comparing the plastic flow rate and the time-to-failure to experimental results obtained from [2].

## References

[1] Breemen, van, L. C. A.; Engels, T. A. P.; Klompen, E. T. J.; Senden, D. J. A.; Govaert, L. E., *J. Polym. Sci. Part B: Polym. Phys.* **2012**, *50*, 1757-1771.

[2] Pini, T.; Van Drongelen, M.; Remmers, J. J. C.; Geers, M. G. D.; Govaert, L. E., *J. Polym. Sci.* **2021**, *59*, 1209-1220.

# Design of polymeric nanocomposite multilayers for efficient EMI shielding

F. Van Loock[1], P. D. Anderson[1], R. Cardinaels[1]

[1]*Polymer Technology group, Eindhoven University of Technology, PO Box 513, 5600, MB, Eindhoven, the Netherlands*

## Abstract

Electronic devices emit local electromagnetic (EM) waves. These secondary EM waves may interfere with the operation of neighbouring electronic components or the wireless EM networks that connect them; a phenomenon known as EM interference (EMI). Devices can be protected from harmful electromagnetic radiation by a layer of shielding material where the incident power is reflected by and/or absorbed throughout the shield. Metals are conventionally used as EMI shielding materials. These exhibit high shielding effectiveness values, yet most of the incident power is reflected to the environment due to the metal's high electrical conductivity. To reduce this secondary EM pollution, one can make use of polymer-based shielding materials, which can partially absorb the incident EM power via conductive dissipation [1]. Polymer-based shielding materials also offer improved mass-rationalised mechanical properties, corrosion resistance and flexibility in shape design with respect to their metallic counterparts. Typical polymer-based shielding materials are particulate composites comprising a non-conductive polymer matrix and conductive fillers such as carbon nanotubes (CNTs).

The challenge is to produce polymer composite-based shields exhibiting sufficiently high shielding effectiveness where shielding is dominated by absorption instead of reflection. Multi-layered material concepts have been explored for this purpose. In addition, polymer multilayers may exhibit enhanced ductility and toughness compared to mono-layers made from identical materials [2]. An attractive design strategy for EMI shielding is the stacking of layers with alternating electromagnetic properties. In this way, wave absorption can be enhanced via multiple wave reflections between the layers. This principle has been explored experimentally in the recent literature, yet some outstanding questions remain on how the interplay between the electromagnetic properties, geometry and stacking order of the composite layers dictate the multilayer's shielding properties [3]. The aim of this work is to make use of an analytical transfer-matrix method and finite element calculations to predict shielding properties of polymer composite multilayers. Model predictions are validated via shielding effectiveness measurements on PMMA-CNT multilayers. Design maps are constructed to reveal regimes of interest to produce absorbent-dominated multilayers of high shielding effectiveness.

## References

[1] Thomassin, J.M.; Jerome, C.; Pardoen, T., Bailly, C., Huynen, I., Detrembleur, C. Polymer/carbon based composites as electromagnetic interference (EMI) shielding materials. *Materials Science and Engineering: R: Reports*, **2013**, 74 (7), pp. 211-232

[2] Wiener, J.; Kaineder, H.; Kolednik, O.; Arbeiter, F. Optimization of mechanical properties and damage tolerance in polymer-mineral multilayer composites. *Materials* **2021**, 14, 725.

[3] Gaoui, B.; Hadjadj, A.; Kio, M. Enhancement of the shielding effectiveness of multilayer materials by gradient thickness in the stacked layers, *J Mater Sci: Mater Electron* **2017** 28 (15), pp. 1-8.

# Composite performance from fiber-matrix interactions: the effect of MAH-g-PP compatibilizer on interphase structure and properties

Stan F.S.P. Looijmans[1,2,*], Dario Cavallo[3], Patrick D. Anderson[1] & Lambèrt C.A. van Breemen[1]

[1] *Polymer Technology, Eindhoven University of Technology, P.O. Box 513, 5600MB Eindhoven, The Netherlands*
[2] *DPI, P.O. Box 902, 5600AX Eindhoven, The Netherlands*
[3] *Department of Chemistry and Industrial Chemistry, University of Genova, Via Dodecaneso 31 – 16146 Genova, Italy*

[*] corresponding author: s.f.s.p.looijmans@tue.nl

Despite the extensive literature on i-PP/fiber composites crystallization, the effect of transcrystalline layers at the fiber/polymer interface on the composite's mechanical properties is controversial [1-3]. Conflicting results have been obtained on the variations of fiber/matrix adhesion due to the occurrence of transcrystalization. Typically, fiber pull-out experiments are employed on ill-defined prepreg composite materials, without considering the local morphology. In this work we show the influence of the addition of a compatibilization agent on the crystallizing structure, phase composition and crystal orientation at a single-fiber level. It is found that by the addition of MAH-g-PP the highly oriented, transcrystalline β-phase layer has no time to develop due to the rapid and abundant nucleation of small α-phase spherulites, see Figure 1a. For various shear rates and temperatures the phase composition is quantified using WAXD and while in neat iPP the sample may consist of nearly 40% β-phase, no trace of this modification is found when the compatibilizer is added (Figure 1b).
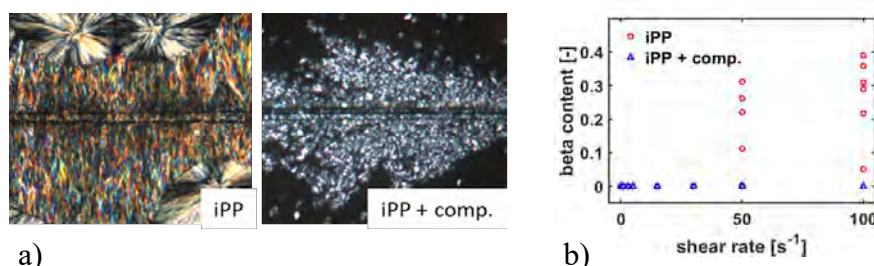


Figure 1: Comparison between neat and compatibilized iPP in terms of a) structure and morphology (POM micrographs) and b) β-phase content measured by WAXD.

From a mechanistic point of view, β-PP has preferred intrinsic properties. i.e. less strain softening, more strain hardening, compared to α-PP [4]. Besides that, the profound crystal orientation in neat iPP composites will contribute to a higher stiffness and strength. In-situ SAXS/WAXD characterization upon tensile deformation of our well-defined morphologies allows an adequate determination of the matrix/fiber interaction, an example is shown in Figure 2. These experiments indicate that the role of local phase composition and morphology on the deformation kinetics and subsequent failure mechanisms is much more pronounced than the increased adhesion between fiber and matrix by compatibilization or sizing effects.
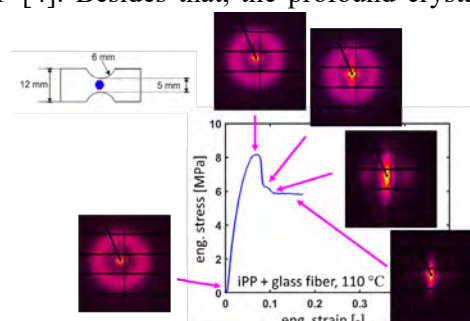


Figure 2: Example of an in-situ XRD measurement during tensile testing.

[1] Quan, H.; Li, Z.-M.; Yang, M.-B.; Huang, R., *Compos. Sci. Tech.* **2005**, 65, 999-1021.
[2] Folkes, M. J.; Wong, W. K., *Polymer* **1987**, 28, 1309-1314.
[3] Gati, A.; Wagner, H. D., *Macromolecules* **1997**, 30, 3933-3935.
[4] Caelers, H. J. M.; Troisi, E. M.; Govaert, L. E.; Peters, G. W. M., *Polymers* **2017**, 9, 547-586.

# Crystallization and structure-function relationship of melt-processed (dis)entangled ultrahigh molecular weight polyolefins

Roel H.M. Bröker[1,2], Dario Romano[3], Catharina S.J. van Hooy-Corstjens[1], Sanjay Rastogi[2,3], Jules A.W. Harings[2]

[1]*Zuyd University of Applied Sciences, P.O. Box 413, 6200 AK, Heerlen, The Netherlands (roel.broker@zuyd.nl). [2]Aachen-Maastricht Institute for Biobased Materials, Maastricht University, P.O. Box 616, 6200 MD, Maastricht, The Netherlands. [3] King Abdullah University of Science and Technology, Thuwal 23955-6900, Kingdom of Saudi Arabia.*

Entanglements are the folklore of polymer science and play an important role in controlling the mechanical properties of polymeric materials. Conventionally, on melting of the crystalline domains the heterogeneously distributed entanglements distribute homogeneously leading to a thermodynamically equilibrated polymer melt. With the advance of disentangled Ultrahigh-Molecular-Weight PolyEthylene (UHMWPE) and corresponding non-equilibrium melt state [1,2], the questions rise how these concepts translate to other polymers and how the dis- or re-entangled state alter crystallization and in turn the structure-function relationship after melt processing. Crystallization and the resulting mechanical properties strongly depend on the disengagement of polymer chains. It is hypothesized that the differences in the entangled state of an equilibrated and non-equilibrated polymer melt, influence crystallization and the resulting mechanical properties that is most expressive for high molar masses.

By controlled polymerization a unique set of entangled and disentangled ultrahigh and low molecular weight polyolefins have been synthesized. Based on compression and tensile tests in combination with differential scanning calorimetry, and small and wide-angle scattering, the mechanical properties and particularly strain hardening of disentangled and entangled isotactic polypropylenes and polyethylenes in the range of 200 – 1,000 kg/mol and 400 – 5,000 kg/mol respectively have been studied upon crystallization under different cooling rates, Figure 1. High molecular weights and a relatively disentangled state provide novel opportunities in controlling the mechanical properties of semi-crystalline polymers.
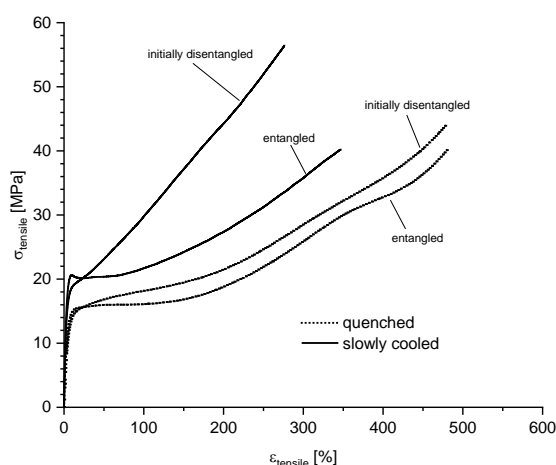


Figure 1. Tensile stress- strain diagram of (initially) disentangled and entangled UHMWPE of ~5,000 and ~4,400 kg/mol respectively crystallized upon quenching and slow cooling to room temperature after being kept in the melt at 180°C for 180 minutes.

[1] Rastogi, S.; Lippits, D. R.; Peters, G. W. M.; Graf, R.; Yao, Y.; Spiess, H. W. Heterogeneity in polymer melts from melting of polymer crystals. *Nat. Mater.* **2005**, *4*, 635−641.
[2] Hawke, L. G. D; Romano, D; Rastogi, S; Nonequilibrium melt state of ultra-high-molecular-weight polyethylene: A theoretical approach on the equilibrium process. *Macromolecules* **2019**, *52 (22)*, 8849-8866.

# Effect of water inclusion in polyamide crystals on structural refinement and mechanical properties of polyamide 6

Milo Gardeniers[1], Mohan-Raj Mani[1], Robert Graf[2], Sanjay Rastogi[1,3], Jules A.W Harings[1]

[1]Aachen-Maastricht Institute of Biobased Materials, [1]Aachen-Maastricht Institute for Biobased Materials, Maastricht University, P.O. Box 616, 6200 MD, Maastricht, The Netherlands
milo.gardeniers@maastrichtuniversity.nl, Jules.harings@maastrichtuniversity.nl
[2]Max-Planck-Institute für Polymerforschung, Ackermannweg 10, D-55128 Mainz, Germany
[3]King Abdullah University of Science and Technology, 4700 KAUST, Thuwal, 23955-6900 (Saudi Arabia)

Polyamide 6 is known for its polymorphism that influences product performance. It is also known for its water sensitivity expressed by water induced plasticization of the amorphous phase [1]. Conventional extrusion processes challenge the formation of the thermodynamically most favourable crystal packing, crystal perfection and ultimate stiffness. In its superheated state, water strongly influences hydrogen bonding in the polyamide crystals, inducing melt suppression and even dissolution at elevated temperature and corresponding vapour pressure [2]. Mediation of hydrogen bonding by water molecules leads to the formation of the thermodynamically most stable monoclinic ($\alpha_1$) phase upon recrystallization. At milder conditions, water also induces structural transitions and refinement of thermodynamically less stable crystal forms such as the defected monoclinic ($\alpha_2$) and pseudohexagonal ($\beta$) phase (Figure 1 a,b). Despite the structural advances, water molecules are entrapped within the polyamide crystals. To understand process-structure-function relationships, the role and structural location of water molecules during dissolution, phase transitions and (re)crystallization of different polyamide 6 polymorphs were in-situ studied by high-resolution solid-state $^1$H NMR spectroscopy, and small and wide-angle X-ray scattering. Correlation of these results to tensile and compression tests, Figure 1c, provide a molecular and structural understanding of water molecules in the polyamide crystals and the effect on mechanical properties. The controlled shielding and deshielding of hydrogen bonding in polyamide crystals accompanied by crystal refinement assists in enhanced control of polyamide process-structure-function relationships.
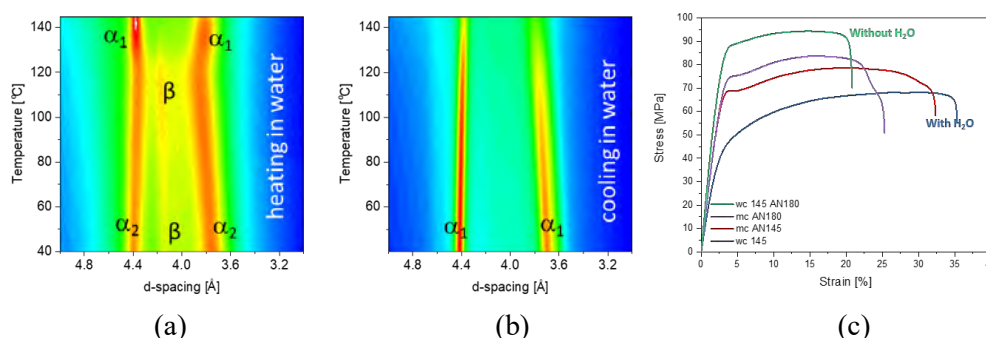


**Figure 1:** a) Dissolution, recrystallization and structural refinement of defected crystal phases $\alpha_2$ and $\beta$ in the superheated state of water, which perfections to the $\alpha_1$-phase. b) Cooling from after structural refinement. c) Stress-strain response of water-crystallization/reorganized samples (wc) made at 145 °C and annealed at 180 °C to remove water. In comparison, melt-crystallized (mc) samples were annealed at identical temperatures.

# References

[1] Parodi, E.; Peters, G. W. M.; Govaert, L. E., Prediction of plasticity-controlled failure in polyamide 6: Influence of temperature and relative humidity. *Journal of Applied Polymer Science* **2018,** *135* (11).

[2] Vinken, E.;  Terry, A. E.;  van Asselen, O.;  Spoelstra, A. B.;  Graf, R.; Rastogi, S., Role of superheated water in the dissolution and perturbation of hydrogen bonding in the crystalline lattice of polyamide 4, 6. *Langmuir* **2008,** *24* (12), 6313-6326

# Rheological investigation of partially crystallized polymer melts

Marat Andreev[1], Anthony Kotula[2], Jonathan Moore[3], Jaap den Doelder[4], Gregory C. Rutledge[1]

[1]Department of Chemical Engineering, Massachusetts Institute of Technology, Cambridge, MA
[2]National Institute of Standards and Technology, Gaithersburg, MD
[3]The Dow Chemical Company, Midland, MI,
[4]Dow Benelux BV, Terneuzen, The Netherlands

## Abstract

Deformation and flow of polymers is important for industrial processing and product fabrication. For scientific and engineering purposes, a significant effort has been invested in developing rheological models for entangled polymer melts. Currently, these models can predict mechanical response of fully molten polymers just from knowledge of the molecular weight distribution (MWD), long-chain branching distribution, and/or other molecular-level material characterization information. Unfortunately, much less is known about the relation between the rheology of partially crystallized polymers and the molecular details of constituting chains. Although, this knowledge is certainly applicable for industrial processing since many of the final products are semi-crystalline.

On the other hand, it is well known that the arrangement of crystalline and amorphous domains is primarily responsible for the unique mechanical properties of plastic goods. For decades, crystallite size, shape, and orientation have been altered through molecular structure and processing conditions. Presently, MWD and short-chain branching distribution (SCBD) are manipulated as well to tailor industrial resins to specific applications. Indeed, MWD and SCBD affect the development of morphology along with the material's rheology as it crystallizes.

In this work, we seek to uncover the relationships between molecular details, crystallite/amorphous domain arrangement, and rheology of partially crystallized polymers. In a collaboration between Dow, NIST, and MIT, we combine industrially synthesized and characterized Linear Low Density Polyethylenes (LLDPEs) with a novel rheological model using slip-links[1] and high-resolution rheo-Raman measurements[2] to probe dynamic modulus over two decades of frequency. Within the slip-link model, the differences in the dynamic modulus are interpreted as different fractions of bridging and dangling chains in the amorphous domains of a semi-crystalline material. Moreover, we show that SCB variations, usually implicit in the dynamic modulus of the melt, manifest strongly in the structure of the network formed from crystallites and polymer chains participating in both amorphous and crystalline domains [3]. Furthermore, the information from this dataset is used to parametrize a multi-scale modeling framework connecting SCBD and MWD to the rheology of semi-crystalline polymers. The monomer-level model uses ethylene/comonomer content to calculate bridging and dangling chain distribution. The entanglement-level model is based on slip-links and can calculate the stresses of the material in complex flows and arbitrary deformations and can be targeted at industrial processes under various conditions.

## References

[1] Andreev, M.; Rutledge, G. C., *Journal of Rheology* **2020**, *64*, 213-222.
[2] Kotula, A. P.; Meyer, M. W.; De Vito, F.; Plog, J.; Hight Walker A. R.; Migler K. B., *Review of Scientific Instruments* **2016**, *87*, 105105.
[3] Andreev, M.; Nicholson D. A.; Kotula A.; Moore J. D.; den Doelder J.; Rutledge G. C., *Journal of Rheology* **2020,** *64*, 1379–1389.

# Morphological analysis of Polyoxymethylene specimens produced under standard and industrial-near injection molding conditions by X-ray scattering and diffraction

Theresia Schrank[1], Michael Berer[1], Eric Helfer[1], Michael Feuchter[2], Gerald Pinter[2]

[1]*Polymer Competence Center Leoben (Leoben)*
[2]*Chair of Materials Science and Testing of Polymers, Montanuniveristaet Leoben (Austria)*

## Abstract

Polyoxymethylene (POM) is a semi-crystalline engineering thermoplastic, which is widely used in structural applications that yield high requirements regarding the performance of the part. The mechanical properties of the final component are strongly dependent on the inner structure of the part, which is determined by the processing. X-ray measurement methods, such as small angle X-ray scattering (SAXS) and wide angle X-ray diffraction (WAXD), are powerful tools to examine the morphological features of polymers [1,2].

This study is investigating POM homopolymer components, which were injection molded at different processing conditions, regarding their morphological features. A study on this material processed under moderate conditions was already done by [3]. Contrary, this study focuses on standard injection molding conditions and industrial-near injection molding conditions of selected specimen geometries. Morphological features will be discussed by analyzing the characteristic SAXS and WAXD measurements (Figure 1). For SAXS, the volumetric degree of crystallinity, the lamellar thickness and the long period were determined by the so-called 1D-correlation. The mass degree of crystallinity was determined from the WAXD measurements by peak fitting. The orientation of the lamellae was characterized by analyzing the azimuthal plots of the SAXS patterns. For the quantification, the so-called $\rho$-parameter was used. Furthermore, the orientation of the crystal lattice planes was assessed from the azimuthal plots of the WAXD patterns. A suggestion for the preferred orientations of the structures within the samples was derived. Additionally, mechanical testing was carried out to rank the different processing conditions. The possibilities of X-ray measurements to examine the structure of POM and corresponding results will be focused in the discussion.
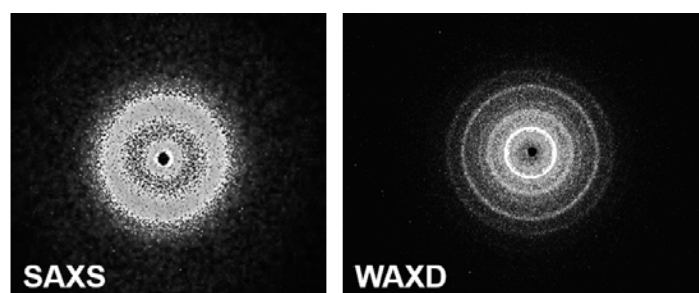
**Figure 1: Characteristic scattering and diffraction patterns of Polyoxymethylene**

## References

[1] Alexander, L. E.: X-ray diffraction methods in polymer science. New York: Wiley-Interscience (Wiley series on the science and technology of materials) (1969).

[2] Stribeck, N.: X-Ray Scattering of Soft Matter. 1. Aufl. s.l.: Springer-Verlag (Springer Laboratory S) (2007).

[3] Berer, M.; Halb, M.; Feuchter, M.; Pacher, G.; Pinter, G.: Fatigue Fracture Properties and Morphology of Polyoxymethylene (POM) Plates Produced under Moderate Processing Conditions. In: International Journal of Polymer Science (2018), S. 1–18.

# Distribution of the Composition in

# Semicrystalline/Amorphous Miscible Blends of PEKK/PEI and effect on the mechanical properties

Romain Martin-Faure[1], Aude Belguise [1,2,3],2, Sabine Cantournet[1], François Lequeux[2], Helene Montes[2]

*1 PSL University, Mines ParisTech, Centre des Matériaux, CNRS 7633 BP 87, F-91003 Evry,*
*2 UMR 7615, SIMM, ESPCI PSLCNRS UPMC, 10 Rue Vauquelin, 75005 Paris, France France*
*3 present adress : Saint-Gobain Recherche, 39 Quai Lucien Lefranc, 93300 Aubervilliers, France*

Semi-crystalline materials exhibit complex relation between their morphology and their structure. We study the semi-crystalline materials of a PEKK/PEI polymer blend, where PEKK and PEI are completely miscible when amorphous but phase separate when the PEKK crystallizes – while the PEI is always amorphous. We combine X-ray scattering and calorimetry to estimate the spatial distribution of the mixture. It appears that three phases are observed, crystalline PEKK, amorphous inter-lamellar PEKK/PEI mixtures and inter-fibrillar PEKK/PEI mixtures. We discuss the role of this complex structure on the linear viscoelastic properties of the materials, under different annealing.
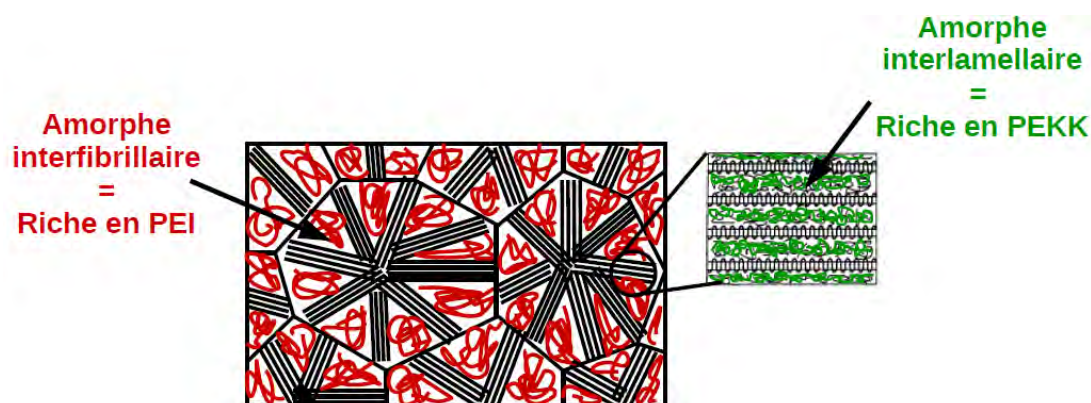
# References

[1] Belguise A, Cantournet S, Lequeux F, Montes H, *Macromolecules* (2021), 54, 7364−7376

# Prediction of rate and temperature dependent deformation of isotactic polypropylene

Senem Aktas Celik, Ismet Baran, Leon Govaert, Remko Akkerman

*Department of Mechanics of Solids, Surfaces and Systems, University of Twente.*
*Email: s.aktas@utwente.nl*

## Abstract

A polymer is described by its intrinsic stress-strain responses under homogeneous deformation. In intrinsic behavior, a nonlinear viscoelastic response is followed by the yield point where the deformation becomes irreversible. Then, strain softening takes place due to the plastic flow. It is established that yield kinetics and the softening behavior of many polymers display a significant change in particular strain rate and temperature intervals [1]. It is crucial to predict intrinsic response under varying conditions to design and optimize these polymer structures more efficiently.

For all polymers, there are certain strain rate and temperature ranges that cover the deformation response with one molecular process. However, isotactic polypropylene (iPP) as a semi-crystalline polymer has three processes representing the main chain segment motion and the partial chains mobility [2]. Stress contribution of these processes to the yield kinetics can be described by the Ree-Eyring rule additively. Hence, an increase in the slope of rate-dependent yield kinetics is observed by the activation of another molecular process as seen in Figure 1. The onset of a second process can be observed at a strain rate $10^{-3}$ s$^{-1}$ at 50°C and a third process is also evident at 5°C since the slope at 5°C is higher than the slope at 23°C.
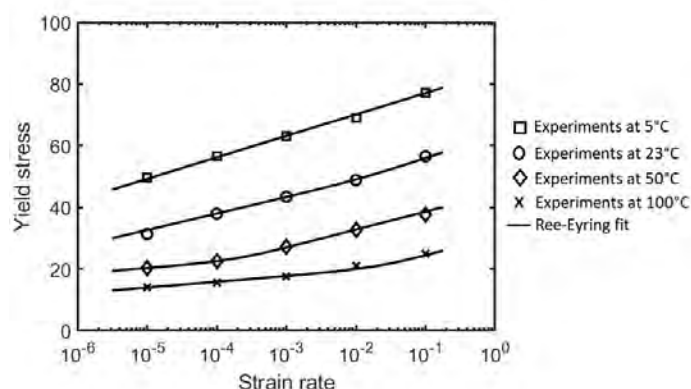
**Figure 1.  Strain rate dependence of the yield stress of iPP at different temperatures.**

The objective of this study to develop a methodology that could capture the contribution of each process separately and to develop a phenomenological model to capture the complex deformation mechanism. For this aim, a viscoelastic Eindhoven Glassy Polymer (EGP) model, developed by the Polymer Technology group at TU Eindhoven, The Netherlands has been extended to three processes. Pressure dependence, intrinsic softening and ageing terms are used to describe the nonlinear viscosity. An outstanding benefit of EGP is its capability to capture both pre-yield and post-yield very accurately.

## References

[1]     T. B. Van Erp, D. Cavallo, G. W. M. Peters, and L. E. Govaert, "Rate-, temperature-, and structure-dependent yield kinetics of isotactic polypropylene," *J. Polym. Sci. Part B Polym. Phys.*, vol. 50, no. 20, pp. 1438–1451, 2012.

[2]     L. C. A. Van Breemen, T. A. P. Engels, E. T. J. Klompen, D. J. A. Senden, and L. E. Govaert, "Rate- and temperature-dependent strain softening in solid polymers," *J. Polym. Sci. Part B Polym. Phys.*, vol. 50, no. 24, pp. 1757–1771, 2012.

# Deformation in Semi-Crystalline Polymers from a Heterogeneous Spherulitic Microstructure

Marc Cornu[1], Mohamed El Bachir Seck[2], Julien Boisse[3] et Stéphane André[4]

*[1,2,3] Laboratoire Energies et Mécanique Théorique et Appliquée, UMR 7563 - Université de Lorraine, CNRS, 2, avenue de la Forêt de Haye, 54504 VANDOEUVRE-lès-NANCY*

[1] marc.cornu@univ-lorraine.fr    [2] mohamed-el-bachir.seck@univ-lorraine.fr

[3] julien.boisse@univ-lorraine.fr  [4] stephane.andre@univ-lorraine.fr

**Keywords:** semi-crystalline polymers; spherulitic structure; viscoelastic behavior; DLR model; FFT code

During a mechanical solicitation, the microstructure of semi-crystalline polymers (PSCs) such as High Density Polyethylene, which have a spherulitic structure, evolves. Our objective is to understand the micro-mechanisms of deformation when the solicitation remains in the low deformation range but takes into account the viscoelastic character of the amorphous phase. We will use a code based on the resolution of the Lippman-Schwinger equations by Fourier transform [1] (AMITEX code [2] developed at CEA Saclay).

To describe the pure mechanical behavior of PSCs seen as two-phase crystalline-amorphous domains, we have implemented an isotropic transverse viscoelastic law (in UMAT format) based on the DLR approach [3]. This law allows to account for the homogenized behavior of lamellar arrangements distributed under different radial orientations. These lamellae are composed of an isotropic viscoelastic amorphous phase and an orthotropic elastic crystalline phase.

Several typical spherulitic microstructures were then generated in VTK format, on a mesh of cubic voxels, with periodic boundary conditions, by varying several parameters such as:
− The size distribution of spherulites;
− The quantity of spherulites ;
− The number of angular sectors: each spherulite has been decomposed into a finite number of equivalent solid angle sectors. Within an angular sector, each voxel will then have a transverse isotropic viscoelastic behavior of the same isotropy axis. The number of angular sectors per spherulite can be varied;
− The thickness or the volume fraction of the inter-spherulitic zones which were modeled by an amorphous phase of isotropic viscoelastic behavior.

A parametric study was then conducted, based on the panel of microstructures thus generated. Virtual DMA simulations [4] were also carried out on these same microstructures and compared to the experimental DMA results in order to calibrate the parameters of the transverse isotropic law and the global micromechanical behavior in order to refine the simulations in time.

## References

[1] H. Moulinec, P. Suquet, A numerical method for computing the overall response of nonlinear composites with complex microstructure, Computers Methods in Applied Mechanics and Engineering, Vol. 157 pp. 69-94, 1998
[2] L. Gélébart, http://www.maisondelasimulation.fr/projects/amitex/general/_build/html/index.html
[3] S. Andre, Y. Mashaka, C. Cunat, Rheological constitutive equation of solids: a link between models based on irreversible thermodynamics and on fractional order derivative equations, Rheol. Acta, Vol. 42 pp. 500-515, 2003
[4] S. André, J. Boisse, and C. Noûs, An FFT solver used for virtual Dynamic Mechanical Analysis experiments: Application to a glassy/amorphous system and to a particulate composite Journal of Theoretical, Computational and Applied Mechanics (JTCAM - https://jtcam.episciences.org/) 2021 [https://doi.org/10.46298/jtcam.6450]

# Thermomechanical characterisation of viscoelastic ETFE membranes

## A. Comitti[1], L. Seixas[1], F. Bosi[1]

[1] Department of Mechanical Engineering, University College London, London, UK

E-mail: a.comitti@ucl.ac.uk, luis.seixas.20@ucl.ac.uk, f.bosi@ucl.ac.uk,

ETFE (ethylene-tetra-fluoroethylene) is a polymer used in the construction industry for membrane structures as a tensioned foil or shaped into inflated cushions. Its relevance arises from its exceptional features, namely high strength, ductility, durability, light transmission, self-cleaning and self-extinguishing properties, and full recyclability.

The mechanical properties of the material strongly depend on both time and temperature effects. The lack of a global understanding of the mutual influence of these variables in the material response results in the absence of a unified nonlinear thermo-visco-elasto-plastic consitutive model. This prevents an extensive use of ETFE, especially in sustainable and lightweight buildings. Therefore, the aim of our research is to fill this gap by providing experimental results and insights on the mechanical behaviour in order to build a comprehensive material model. In the first phase of the study, an experimental characterisation was performed through quasi-static universal electromechanical machine coupled with digital image correlation, and Dynamic Mechanical Analyser (DMA).

Uniaxial properties were investigated across a range of temperatures spanning from -20 to 60° C, at different displacement rates. Tests at different sample orientations enabled the assessment of material anisotropy . ETFE revealed a peculiar response, showing a nonlinear response with two localised inflexion points, the first being identified as the yield point. The effect of time and temperature on the mechanical response and onset of plasticity will be highlighted..

DMA tests proved that the material is mainly in a glassy phase in the range of temperature of interest, even if secondary transitions occur at higher temperatures. Additionally, creep tests on the DMA were performed to build a compliance master curve through the time-temperature superposition principle. Through these tests, it is shown that the shift factor does not follow the Arrhenius law, and deviation from it must be incorporated to correctly model the linear viscoelastic response.

The experimental results obtained and additional ones planned will be employed in the definition of a mathematical model that captures the complex nonlinear thermoviscoelastic behaviour and the yield criterion of ETFE, thus improving the material response prediction and structural design.

# Visco-elastic properties of silica-filled and silver-filled silicone elastomers and impact of confined aging

Martin Avila Torrado, Andrei Constantinescu

*Laboratoire de Mécanique des Solides, CNRS École Polytechnique, Institut Polytechnique de Paris, 91120 Palaiseau, France*
*Email : martin.avila-torrado@polytechnique.edu*

This work focuses on the visco-elastic behavior of filler reinforced silicone elastomers, and the influence of thermal aging in confined environment in their properties. It presents a series of experimental results and integrates them in an aging-dependent thermodynamic model inspired by [1]. The materials under scrutiny are three different silicone-based composites, two of them filled with silica in different proportions (14% and 24% w/w), and one filled with silver particles at approximately 80% w/w.

These materials were submitted to specific aging conditions: high temperatures during different times in an initially inert, confined environment. Compounds outgassed during aging were quantified through mass spectrometry. The presence of $C_6H_{18}O_3Si_3$ in the atmosphere of silica-filled silicone is a marker of degradation through Si-O bond scission, a procedure described in literature for PDMS [2]. For the silver-filled silicone, the most abundant outgassed product is $C_4H_8O_2$, which is an indicator of crosslink scission.

Mechanical behavior of the materials in their unaged and aged states was evaluated through DMA tests in torsion mode. In order to evaluate the dependence of the measured properties as a function of the applied strain (known as Payne effect [3]), amplitude sweep tests were performed in the unaged state. Strains from $10^{-3}$% to 10% were tested at a frequency of 1 Hz and a temperature of 25°C. Results show a clear decrease of the amplitude of the complex modulus as well as a change in the loss factor when the strain amplitude is above a limit value ($10^{-1}$% for the silica-filled silicone, $10^{-2}$% for the silver-filled silicone). The intensity of this effect is in correlation with the proportion of fillers that reinforce the silicone matrix.

Temperature sweep tests were also performed, for temperatures ranging from -140°C to 210°C. The mechanical response of the materials as a function of temperature allows the identification of two transitions: the glass transition occurring at around -125°C, and the fusion of crystalline phase at -42°C [4]. The crystal fusion temperature and the percentage of crystallinity were also assessed with DSC measurements, for unaged and aged samples. The results show a decrease of the crystal fusion temperature with aging, as a result of the increased molecular mobility in the aged materials.

The impact of aging on the visco-elastic behavior of silicones was quantified through frequency sweep tests. These experiments allowed measuring an aging-dependent softening of the filled-silicones. As aging progresses, the storage modulus of the materials decreases, and a light increase of the loss factor is observed. These considerations lead to concluding that chain scissions are the main driver of the material behavior change after aging.

## References

[1] Jalocha, D.; Constantinescu, A.; Neviere, R.; *Mechanics of Time-Dependent Materials,* **2015***,19(3),* 243-262.
[2] Camino, G.; Lomakin, S.M.; Lageard M., *Polymer*, **2002**, *43*, 2011-2015.
[3] Clément, F; Bokobza, L.; Monnerie, L.; *Rubber Chemistry and Technology*, **2005**, *78*, 211-231.
[4] Bosq, N.; Guigo, N; Persello, J.; Sbirrazzuoli, N.; *Physical Chemistry Chemical Physics,* **2014**, *16*, 7830-7840

# Strain-induced crystallization in natural rubber: is there time-strain superposition?

P. Sotta[1], P.-A. Albouy[2]

[1]*Ingénierie des Matériaux Polymères, CNRS/INSA Lyon UMR 5223, Villeurbanne, France*
[2]*Laboratoire de Physique des Solides, Université Paris-Sud, 91405 Orsay, France*

Stretching polymer chains promotes crystallization. This idea, rationalized by Flory as early as 1947, is one basic concept in polymer physics and is relevant in a vast majority of polymer manufacturing processes. In natural rubber (NR), strain-induced crystallization (SIC) is a key feature which underlies its exceptional performances as an elastomer material. In many, if not most, practical situations, the behavior is actually controlled by the kinetics of SIC. In particular, understanding crystallization kinetics is essential for explaining the hysteretic behavior observed in dynamic conditions.

In this talk we shall show that, under the strong assumption that, in crosslinked materials, SIC is mainly driven by nucleation processes, an explicit kinetic equation can be established to describe the evolution of the crystallinity index (Figure 1). This is based on the dependence of the nucleation rate on the overstretching of the amorphous phase. Indeed, while in thermal polymer crystallization the driving force is the overcooling, in SIC it is the overstretching. According to a lever rule, in contrast to thermal crystallization in which the overcooling may be controlled, overstretching relaxes as crystallization proceeds, which makes the kinetic equation a little bit more complex [1,2].

It follows that a general time-strain superposition principle cannot be rigorously established for the general time evolution of the crystallinity index at various initial overstretching values.
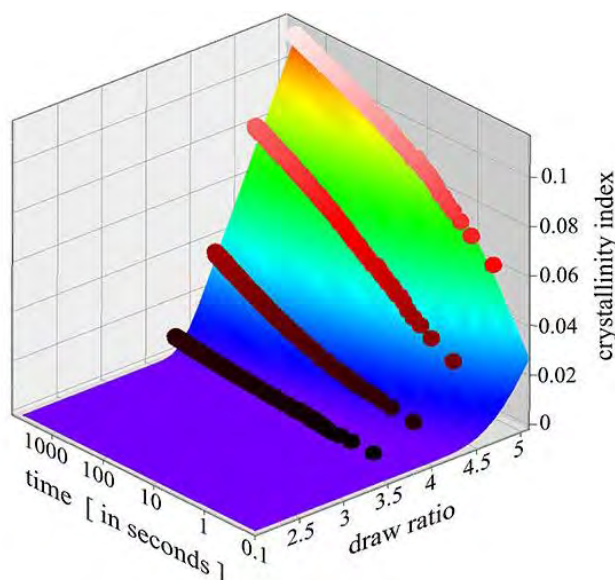


**Figure 1** : The surface in this figure illustrates how the crystallinity index evolves as a function of draw ratio and time in natural rubber. Dot curves are measurements in which samples are stretched to various, fixed draw ratios and the crystallinity indices are then measured as a function of time.

## References

[1] Albouy, P.-A.; Sotta, P., *Macromolecules* **2020**, *53*, 992-1000.
[2] Sotta, P.; Albouy, P.-A., *Macromolecules* **2020**, *53*, 3097-3109.

# Investigating the influence of network architecture and mechanical properties on the resistance to cavitation in soft elastomeric layers.

Flora-Maud Le Menn[1], Guido Hensen[2], Etienne Barthel[1], Costantino Creton[1]

*1: SIMM, ESPCI Paris, Université PSL, CNRS, Sorbonne Université, 10 Rue Vauquelin, 75005 Paris, France, flora-maud.le-menn@espci.fr*
*2: Covestro Resins B.V.,Science & Technology group, Brightlands Chemelot Campus, Urmonderbaan 22, 6167 RD Sittard Geleen, The Netherlands*

Every second, 29 Tb of data are produced on the internet, stocked and exchanged between continents. The vast majority of that data transits via optical fibres, consisting of thin glass fibres which carry light over hundreds of kilometres by total internal reflection. Being exposed to extreme conditions, these fibres are protected by several layers of polymers and metal. The first layer of protection consists of a soft elastomeric acrylate resin. This thin coating is under variable hydrostatic pressures created for example during manufacturing and during use. This may lead over time to the formation of cavities and ultimately to fibre blindness. The mechanisms ruling the nucleation and growth of cavities depend on various material parameters. Several models have been proposed, suggesting that the cavitation resistance is directly linked to the Young modulus[1] or that it depends on the initial defect size[2]. Experimental studies[3] however suggest a more complex cavitation behaviour where the network's fracture toughness and the strain hardening both play a role.

By UV polymerizing thin films consisting of a mix of di-acrylate-functionalized PPG8000 and 2 acrylate monomers (2-ethylhexyl acrylate and 2-phenoxy ethyl acrylate), and testing their behaviour under hydrostatic stress, the link between mechanical properties and cavitation resistance can be investigated. Through changes of oligomer functionalization and monomer ratios, different network architectures and properties can be achieved. The cavitation process is observed in a sphere against flat confinement (Figure 1). The opening of cavities in the thin layer is recognized by sudden drops of the force during the loading, while the end of the curve shows the final fracture of the sample.
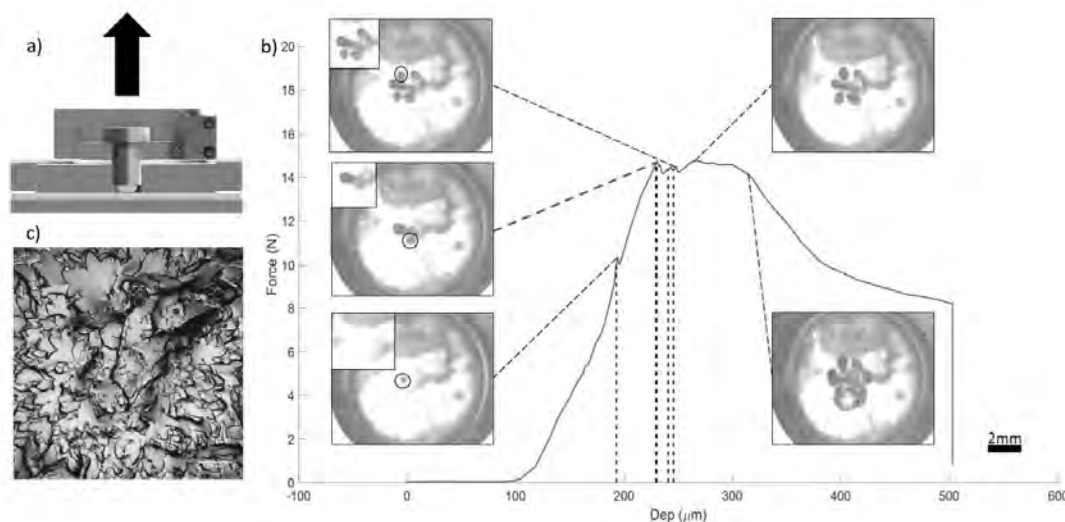


**Figure 1** – Inducing hydrostatic pressure in elastomer layers. a) Sphere against flat confinement of a 100um thick elastomer layer b) Force versus displacement in a traction experiment. Each cavitation event is circled; the upper left insert is the network 50ms before the cavity opening. c) Final fracture state of the sample (scale 0.5mm).

## References

[1] Gent, A.N.; Lindley, P.B.; *Proceedings of the Royal Society of London,* **1958**, volume 249 plate 19
[2] Gent, A.N.; Wang, C., *Journal of Materials Science* 1991, 26, 3392-3395
[3] Cristiano, A.; Marcellan, A.; Long, R.; Hui, C-Y.; Stolk, J.; Creton, C.; *Journal of Polymer Science: Part B: Polymer Physics,* **2010**, Vol. 48, 1409-1422

# Puncture mechanics of ultra-soft hydrogels at the elastocapillary length scale

Yuanyuan Wei[1], Costantino Creton[1,2,] and Tetsuharu Narita[1, 2]

[1]*Sciences et Ingénierie de la Matière Molle, CNRS UMR 7615, ESPCI Paris, PSL University, Paris, France*
[2]*Global Station for Soft Matter, Global Institution for Collaborative Research and Education, Hokkaido University, Sapporo, Japan*

Though the mechanical properties of hydrogels have been intensively studied worldwide, the surface properties of them are much less studied despite academic and industrial importance. The surface tension can play an important role in mechanics when the elastocapillary length (ratio of the surface tension to the modulus) is large. Fracture (initiation) properties can be affected by surface tension since the creation of new surfaces by fracture becomes energetically expensive. In this project, poly(vinyl alcohol)-glutaraldehyde chemical hydrogels with an elastic modulus ranging from 80 to 2000 Pa were prepared and used as a model soft hydrogel system. By puncture experiment, fracture behavior of ultra-soft PVA hydrogel will be systematically studies at the elastocapillary length scale.

With the neo-Hookean model, we analyzed the mechanical response of model gels to deep indentation. In the small contact region, Young's modulus of the hydrogels was determined. The values of the modulus were found identical to those of the modulus measured by shear rheometry. In the large deformation region, fracture of the gel was identified as a peak of the indentation force. Interestingly, we found the critical load displacement decreases with the gel modulus when the elastic modulus is less than 400 Pa, suggesting that the softer gels are more resistant to puncture failure. The normalized critical nominal stress by elastic modulus $\sigma_c/G'$, is plotted as a function of normalized indenter radius by elastocapillary length $RG'/\Upsilon$. We assume there are two distinct fracture regions when the elastocapillary length normalizes the indenter radius. Above the characteristic size, the nominal stress over $G'$ is almost constant while it sharply increases below the length, indicating different fracture mechanisms, namely elastic fracture and capillary fracture, respectively. To further characterize the local fracture behaviors, a birefringence setup was coupled to the mechanical test, allowing us to study the chain orientation and stress distribution during puncture process. We found a fracture precursor marginally above the indenter tip appears depicted as a dark point emerging from the intensity-increasing light, before the peak of the puncture force.
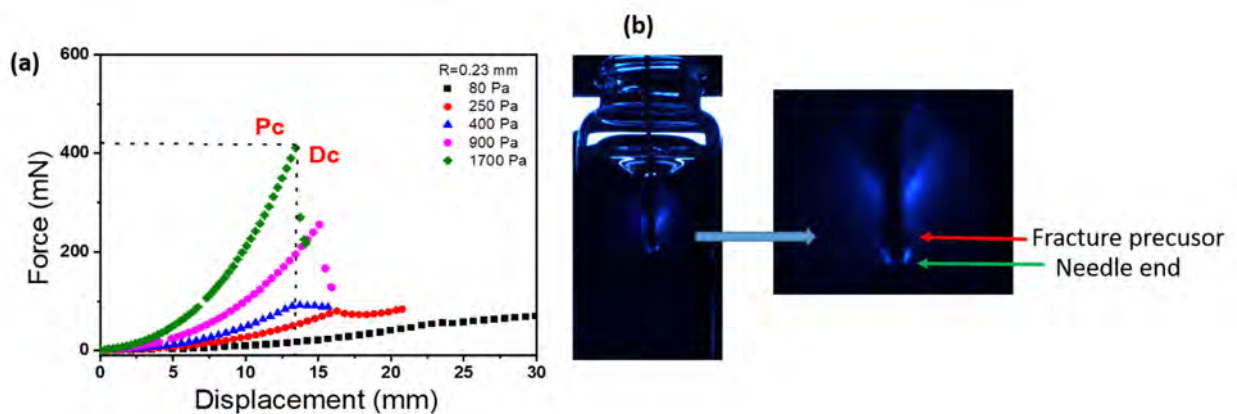


Figure 1. (A) Representative puncture loading curve: puncture force as a function of puncture displacement (Critical puncture force Pc is the peak force in the loading curve, and the corresponding displacement is marked as critical displacement Dc). (B) Fracture observation of PVA under birefringence.

# Hydroelastomers: soft, tough, highly swelling composites

Simon Moser[1], Yanxia Feng[1], Oncay Yasa[2], Stefanie Heyden[1], Michael Kessler[3], Esther Amstad[3], Eric R. Dufresne[1], Robert Katzschmann[2], Robert W. Style[1]

*1.Department of Materials, ETH Zurich, CH*
*2.Department of Mechanical and Process Engineering, ETH Zurich, CH*
*3Institute of Materials,EPFL, CH*

## Abstract

Most biological tissue is incredibly tough, while maintaining a high water content. By contrast, synthetic water-swellable materials (i.e. hydrogels) are typically very brittle. A number of strategies have emerged to make tough hydrogels, but the processing for these materials can be tricky. In this project, we demonstrate a novel approach for making tough, highly water-swelling materials with a very simple synthesis based on common commercial materials. Composites are made by embedding sodium polyacrylate (NaPA) particles in a range of soft elastomers including silicones and polyurethanes. The resulting material have a high swelling potential inherited from the hydrogel and high stiffness and toughness inherited from the elastomer matrix. This enables us to easily make complex shapes, for example with extrusion printing.

# Highly stretchable hydrogels and their retraction behavior

Santanu Kundu, Anandavalli Varadarajan, Rosa Maria Badani Prado, Satish Mishra

*Dave C Swalm School of Chemical Engineering, Mississippi State University, MS State, MS, USA.*
*santanukundu@che.msstate.edu*

Biological elastomeric proteins such as resilin display high stretchability and resilience, and such properties lead to power amplified activities in biological species necessary for locomotion, feeding, and defense.[1] High stretchability and resilience in these biological proteins have been attributed to the balanced combination of entropic and enthalpic elasticity originated from the presence of hydrophilic and hydrophobic segments. Inspired by these biopolymers, hydrogels with hydrophilic and hydrophobic contents have been obtained using a simple free-radical copolymerization of acrylic acid (AAc), methacrylamide (MAM), and poly(propylene glycol) diacrylate (PPGDA). Gels with elastic modulus as high as 100 kPa, and stretchability up to 800% have been obtained.[2] These properties enable the synthesized gels to catapult projectiles with very little dissipation. Further, when released from a stretched state, these gels achieve a retraction velocity of 16 m s$^{-1}$ with an acceleration of $4 \times 10^3$ m s$^{-2}$. These values are comparable to those observed in many biological species during the power amplification process (e.g., appendage strike by Mantis shrimp, frog jump). The gel stretcability and retraction velocity can be varied by changing overall monomers and PPGDA contents. By varying the monomer compistion and the environmental conditions, we are developing a fundamental structure-property relationship for synthesizing stretchable and resilient hydrogels from synthetic polymers. The potential applications of these materials will be in artificial muscles, prosthetic devices to assist an individual with limited mobility.
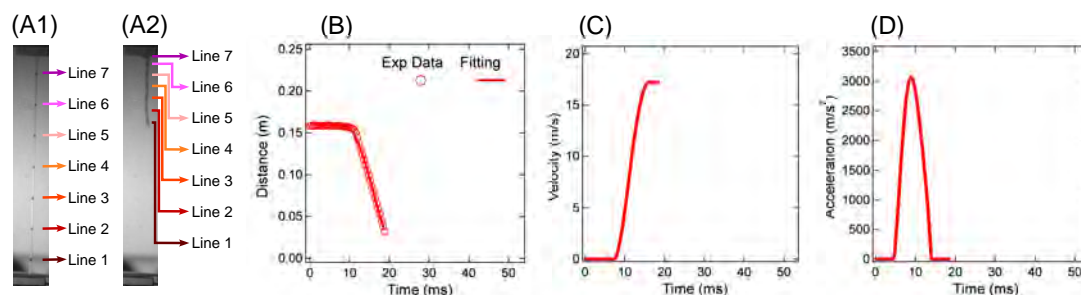


Figure 1: Retraction behavior of a gel stretched to a stretch-ratio of 6. (A) Capturing retraction of a gel strip. The positions of seven lines at different locations of the strip as a function of time have been tracked. (B) The displacement of Line 1 as a function of time. (C) Velocity of Line 1 as a function of time. Velocity reached a constant value after initial acceleration (D) Acceleration as a function of time. The acceleration became zero after velocity reached a constant value.

## References

(1) Ilton, M.; Bhamla, M. S.; Ma, X.; Cox, S. M.; Fitchett, L. L.; Kim, Y.; Koh, J.; Krishnamurthy, D.; Kuo, C.-Y.; Temel, F. Z.; Crosby, A. J.; Prakash, M.; Sutton, G. P.; Wood, R. J.; Azizi, E.; Bergbreiter, S.; Patek, S. N. *Science* **2018**, *360* (6387), eaao1082.

(2) Badani Prado, R. M.; Mishra, S.; Morgan, B.; Wijayapala, R.; Hashemnejad, S. M.; Kundu, S. *ACS Appl. Mater. Interfaces* **2020**, *12* (36), 40719–40727.

# A study on the mechanical behaviour of carbon black filled HNBRs

Isabella Denora [(*)], Claudia Marano

*Dipartimento di Chimica, Materiali e Ingegneria Chimica "Giulio Natta", Politecnico di Milano, Piazza Leonardo da Vinci, 32, 20133 Milano MI, Italia*

(*) *E-mail: isabella.denora@polimi.it*

A study on the mechanical behaviour of two HNBR rubber grades is reported. Quasi-static tensile tests have been performed in different loading conditions and dissipated and stored energies components of the deformation energy have been also evaluated. Fracture tests have been carried out and material toughness has been evaluated using an energy-based fracture mechanics approach.

## Introduction

Our research is part of a major project which has the aim to develop polymeric materials, suitable for working in extreme conditions of pressure and temperature within the hydrogen infrastructure. Our investigation is focused on elastomers, widely used in this kind of application as O-rings, gaskets, seals and hoses [1]. The objective is to find a correlation between the materials fracture behaviour and their tendency to fail when a rapid gas decompression (RGD) occurs from a high pressure value, a process usually referred to as "RGD failure". For this purpose, several rubber compounds will be studied in relation to modifications of matrix and filler, provided to improve RGD resistance.

In this work, a study on the mechanical behaviour of two carbon black filled hydrogenated nitrile butadiene rubbers (HNBR) is reported. A mechanical characterization of the two materials has been performed by quasi-static tests in different loading conditions: uniaxial/equibiaxial tensile and pure shear tests. The effect of the strain rate has been tested for a first evaluation of their viscoelastic behaviour. Moreover, fracture toughness at the crack onset was determined by using the *J-integral*-based fracture mechanics approach. With the purpose of studying fracture aspects, in which dissipative behaviour plays an important role, also deformation energy has been considered by performing cyclic tests to evaluate its dissipated and stored energy components.

## Materials and methods

Two HNBR-based compounds provided by Arlanxeo have been investigated. They consist in two fully hydrogenated rubbers with 21% of acrylonitrile content and peroxide as curing agent. They present the same amount of filler: the first compound (HNBR_1) is filled with carbon black while the second one (HNBR_2) with carbon black and a small quantity of a thermoplastic polyamide, added with the aim to increase the material RGD resistance by reducing the $H_2$ permeability of the material. The compounds have been compression moulded and cured at 170°C and at a pressure of 10 MPa for 20 minutes, as suggested by Arlanxeo. Specimens for pure shear and equibiaxial tests have been directly produced with proper home-made moulds, while dumbbell specimens have been punching die-cut from sheets obtained with a 170x200 mm rectangular mould. A post curing treatment has been applied (at 160°C for 4 hours) in order to complete the vulcanization process. By preliminary tests it was verified that post curing makes the material stiffer and its mechanical response does not change in time for specimens stored at 23°C up to 7 days.

Uniaxial tensile tests and pure shear tests have been performed with an Instron 5967 dynamometer while equibiaxial tests with the CLUSTex Biaxial tester. Tests were carried out at a temperature of 23°C and at a strain rate of 0.3, 3 and 30 min$^{-1}$. They have been

videorecorded for strain measurement through "*digital image correlation*" analysis (subset size=33 pixel, step size=3 pixel).

## Results and discussion
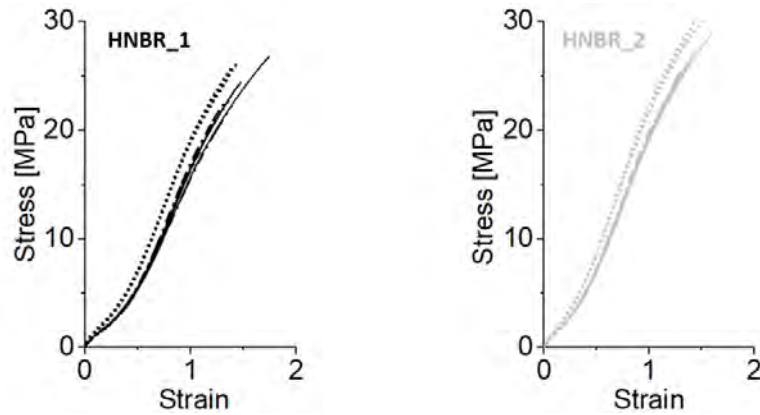


*Figure 1: Strain rate effect on mechanical behaviour of the two studied HNBRs.*

— · — *: 0.3 min-1;* ——— *: 3 min-1;* •••••• *: 30 min-1.*

Tensile uniaxial tests have been performed as a first evaluation of the two materials mechanical response and in order to evaluate the effect of the strain rate. Values of rates at three different orders of magnitude have been chosen (0.3, 3 and 30 min^{-1}).  As shown in *Figure 1*, for both the two rubbers there is no difference between the curves recorded at 3 min^{-1} and 0.3 min^{-1} while at 30 min^{-1} both materials appear stiffer, as an effect of their viscoelastic behaviour.
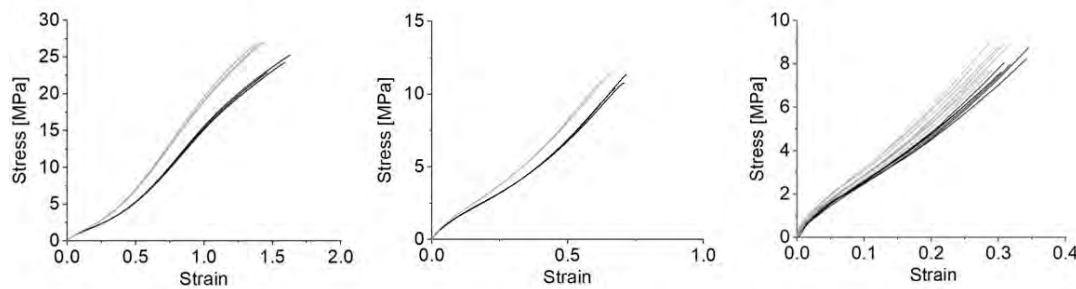


*Figure 2: Stress-strain curves for the two materials investigated (HNBR_1 in black and HNBR_2 in grey) for three loading conditions. From left to right: uniaxial tensile, pure shear and equibiaxial tensile tests.*

With the aim of defining a constitutive model for the materials, a mechanical characterization in different homogeneous states of deformation is necessary[2]. For this purpose, tests in pure shear and equibiaxial tensile loading conditions have been also performed at a strain rate of about 3 min^{-1}. In *Figure 2* the relevant stress-strain curves have been reported: it can be observed that, as expected, the two HNBRs show a similar behaviour but HNBR_2 exhibits higher stresses than HNBR_1.

In addition, the material fracture behaviour has been evaluated performing fracture tests in pure shear loading conditions. Specimens have a height/width ratio of 5, that is the minimum ratio in order to obtain a state of deformation close to pure shear in the centre of the specimen[3]. An initial notch length $a_0$ of about 15 mm was used. By using the fracture mechanics approach based on the *J-integral*, originally introduced by Rice in 1968[4] to determine the toughness of non-linear elastic materials, the fracture toughness was evaluated as $J= \eta \frac{U}{B(w-a_0)}$, where $\eta$ is a dimensionless factor which depends on specimen geometry, equal to 1 for pure shear loading conditions, *U* is the total input energy at crack onset calculated as the area under the

force-displacement curve up to the fracture onset, $B$ the thickness of specimen, $w$ the specimen width and $a_0$ is the initial notch length.
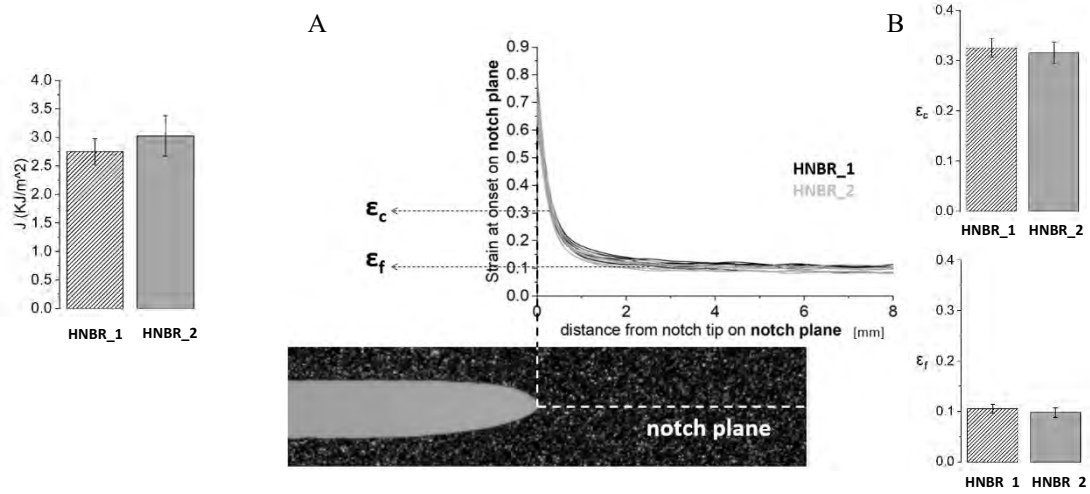


Figure 3: J-integral at crack onset for the two materials.

Figure 4,A: Trend of strains on the notch plane for the two materials (HNBR_1 in black and HNBR_2 in grey). $\varepsilon_c$: strain close to the crack tip; $\varepsilon_f$: strain far from the crack tip. Figure 4,B: Values of strains for the two materials.

Fracture tests results are showed in *Figure 3* and *Figure 4*. It can be noticed that HNBR_2 exhibits a higher value of *J-integral* at crack onset, that is its fracture toughness is higher than HNBR_1. In *Figure 4, A* the values of deformations measured at crack onset on the initial notch plane are plotted versus the distance from the notch tip. A frame reproducing a HNBR_1 specimen at crack onset is also shown as an example. The values of the strain close to the crack tip (at a distance of 0.32 mm), $\varepsilon_c$, and of the strain measured on the initial notch plane far from the crack tip, $\varepsilon_f$, are also reported for the two materials (*Figure 4, B*). Despite the difference in fracture toughness, the strain values at fracture onset are comparable for the two materials.
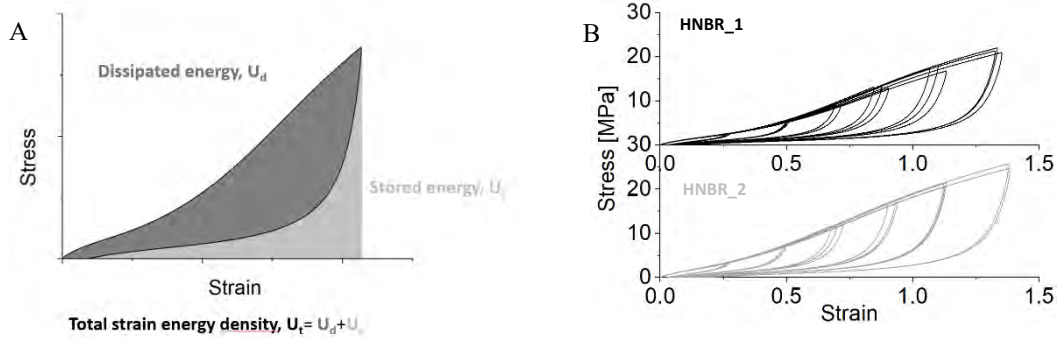


Figure 5, A: Total strain energy density ($U_t$) and its components stored and dissipated (respectively $U_s$ in light grey and $U_d$ in dark grey) calculated on one cycle.

Figure 5, B: Experimental curves for the two materials.

In order to explore the energy involved in the fracture process, a preliminary study on strain energy dissipation has been performed. Cyclic uniaxial tensile tests have been carried out at a strain rate of 3 min$^{-1}$: specimens were loaded up to a fixed value of strain and then unloaded up to zero force. For each cycle the total strain energy density and its stored and dissipated components have been calculated (see *Figure 5, A*). In *Figure 5,B*, experimental stress-strain curves of cyclic tests differing in the strain applied are reported for the two materials. As shown in *Figure 6,A*, HNBR_2 resulted to have a higher energy density than HNBR_1, due to a larger value of dissipated energy component, because stored energies of the two compounds are quite

comparable. In *Figure 6,B*, the elastically stored and dissipated energies are reported as a percentage of the total strain energy to highlight that HNBR_2 is a more dissipative material than HNBR_1. Further it can be noted that HNBR_1 has a larger strain range where the elastic behaviour of the material is dominant on its dissipative behaviour. These results justify the larger fracture toughness evaluated for HNBR_2 with respect to HNBR_1 and can be related to the deformation mechanism of the thermoplastic polyamide present in HNBR_2.
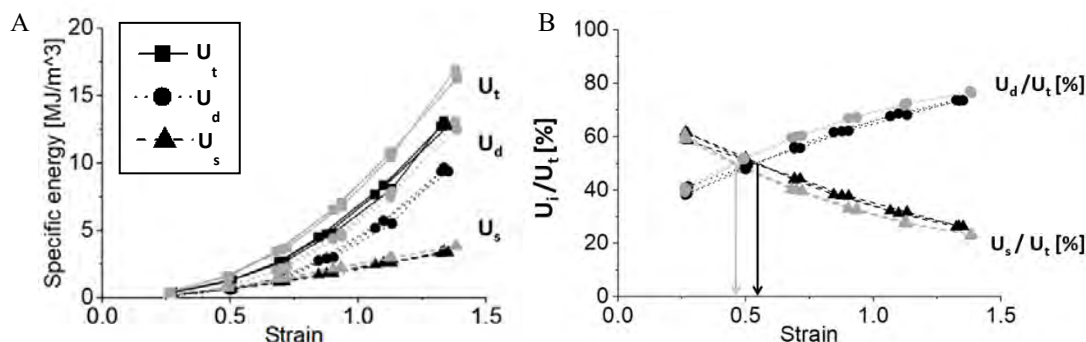


*Figure 6, A: Total strain energy density ($U_t$), dissipated energy ($U_d$) and stored energy ($U_s$). HNBR_1 is in black, HNBR_2 in grey.*
*Figure 6, B: Dissipated ($U_d$) and stored energy ($U_s$) components as percentage of the total energy for the two materials (HNBR_1 in black and HNBR_2 in grey).*

## Conclusions and future work

A mechanical characterization of two HNBRs reinforced with carbon black has been performed. HNBR_2 contains a small quantity of a thermoplastic polyamide, not present in HNBR_1. For all the test performed, the stress-strain curves of HNBR_2 result to have higher stresses than HNBR_1. As regards the materials fracture behaviour, HNBR_2 exhibits higher toughness, but strains reached at fracture onset are comparable to HNBR_1. PA containing HNBR shows also a higher quantity of dissipated strain energy component. All these results can be explained by the deformation process of the polyamide, added to increase material RGD resistance. Looking for the development of this work, the results of tests performed in three different loading conditions (uniaxial, pure shear and equibiaxial) will be used to define the constitutive equations for the two studied materials.

## References

[1]     Barth, R. R.; Simmons, K. L.; San Marchi, C. W. *Polymers for Hydrogen Infrastructure and Vehicle Fuel Systems :*; SAND2013-8904, 1104755; 2013; pp SAND2013-8904, 1104755. https://doi.org/10.2172/1104755.
[2]     Treloar. *THE PHYSICS OF RUBBER ELASTICITY*; 1975.
[3]     Yeoh, O. H. Analysis of Deformation and Fracture of 'Pure Shear' Rubber Testpiece. *Plastics, Rubber and Composites* **2001**, *30*, 389–397. https://doi.org/10.1179/146580101101541787.
[4]     Rice, J. A Path Integral and the Approximate Analysis of Strain Concentration by Notches and Cracks. *Journal of Applied Mechanics* **1968**, *35*, 379–386. https://doi.org/10.1115/1.3601206.

# Improving the thermomechanical resistance of a fluoroelastomer by adding POSS nanoparticules

Adrien Simon[1,2], Julie Pepin[1], Marie-Pierre Deffarges[1], Stéphane Méo[1]

*[1] Laboratoire de Mécanique Gabriel Lamé, Université de Tours, Université d'Orléans, INSA Centre Val de Loire, Polytech Tours, 7 avenue Marcel Dassault BP40, 37004 Tours, France*
*[2] SAFRAN ELECTRICAL COMPONENTS, 20 avenue Georges Pompidou, 37600 Loches, France*
*julie.pepin@univ-tours.fr*

Fluoroelastomers are commonly used in aeronautical industry where a thermo-chemo mechanical resistance is needed. Usually, for high temperatures applications, peroxide crosslinking combined with a coagent, is chosen. Nonetheless, even if the thermal resistance is improved, the coagent has revealed to be the main thermal weakness of this system [1]. This limitation could be overcome by adding POSS nanoparticules [2]. The way these nanoparticles act to improve the mechanical behaviour at high temperature or after thermal aging has not yet being fully understood. The main goal of this work was to understand the relationship between the structural organization of a FKM reinforced by various amount of POSS nanoparticules and its mechanical response. In this study, the POSS used displays a functionality equal to eight as illustrated in Figure 1. This configuration provides three types of possible interactions for the nanoparticule: be inert, react with the matrix or react with itself.
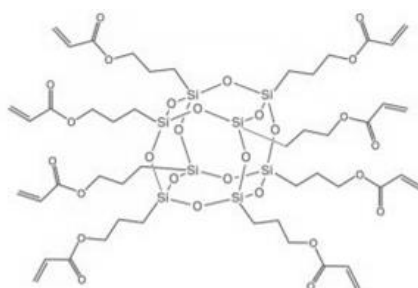


*Figure 1: Structure of POSS-A with eight functional groups*

After curing, thermomechanical analyses have revealed that the Tg is not impacted by different amounts of nanoparticules. Furthermore, swelling experiments combined with uniaxial tensile tests have shown that the crosslinking density is unchanged whatever the POSS content is. This indicates that these nanoparticules do not act as crosslinker for FKM. Nonetheless, the storage modulus in the rubbery plateau increases with POSS content which suggest a classical reinforcing effect of the nanoparticules. The most interesting observation regarding POSS, is its ability to react with itself to form a second network. This has been highlighted by the presence of a second relaxation in the rubbery phase observed by DMTA. Tan δ of this relaxation shifts to higher temperature with the increase of POSS.

Regarding the thermal resistance of these nanocomposites, thermogravimetric analyses have shown that increasing POSS concentration leads to the thermal degradation delay of the weak point. The link between structure and mechanical properties at high temperature and after thermal aging will enable us to understand how the POSS network could delays the thermal degradation of the weak point.

# References

[1] Liu, Q.; Li, J.; Cong, C.; Cui, H.; *Polymer Degradation and Stability* **2020**, *177*, 109180.
[2] Liu, Y.; Shi, Y.; Zhang, D.; Li, J.; Huang, G., *Polymer* **2013**, *54*, 6140-6149.

# Numerical modelling of fibrillation and cavitation in PSA

K. Patel [1], M. Ciccotti [1], E. Barthel [1]

[1]*Sciences Et Ingénierie De La Matière Molle - Paris (France),*
[1]*École supérieure de physique et de chimie industrielles de la Ville de Paris - Paris (France),*
[1]*PSL Université – Paris (France),*
[1]*Sorbonne Université- Paris (France),*
[1]*CNRS- Paris (France)*
*Email id: krupalpatel12@hotmail.com*

In a pressure-sensitive adhesive (PSA) tape, adhesion rupture is accompanied by fibrillation and cavitation of the adhesive layer. In this study, we propose a multiscale picture of adhesion rupture, involving a better understanding of fibrillation. Numerically, a single fibril is modelled using the Finite element method using axis-symmetric boundary conditions. An Arruda Boyce, hyper-elastic constitutive law is employed to tackle the large strains associated with the computer modelling of the layer of adhesive. Apart from Arruda Boyce, we are using other relevant constitutive relations like the Yeoh model, as well. We found that peeling a single fibril from a bulk of adhesive requires more energy than the uniaxial extension of the fibril for the same patch diameter in the numerical study, which is true for peeling experiments previously done at the SIMM lab. [1] In addition to that, we are also studying Cavity expansion along with the fibril extension and we want to connect these two phenomena happening in PSAs by numerical study. Our final aim is to connect the macroscopic work of fracture and the dissipative properties of the PSA material through a proper description of the large strain deformation of the interface.
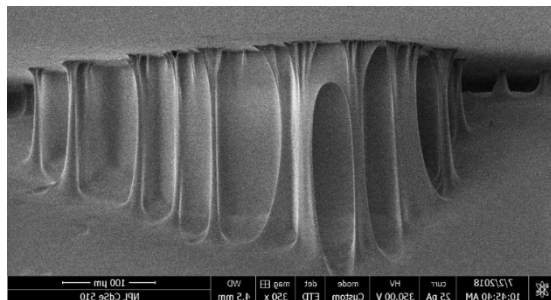


Fig. 1: SEM view of adhesion rupture of a PSA, fibrillation (X. Morelle & B. Bresson)
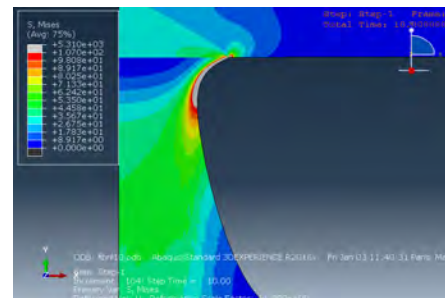


Fig. 2: FEM simulation of a fibril (axisymmetric)

## Acknowledgement

## References

[1] *Chopin J.; Villey R.; Yarusso D.; Barthel E.; Creton C.; Ciccotti M., Macromolecules 2018, 51, 21, 8605–8610*

# Adhesion mechanisms of silane terminated polymers on glass

Gabriel Santos[1], Jérémie Lacombe[2], Paul Fourton[2], Marie Savonnet[2],
Costantino Creton[1], Matteo Ciccotti[1] and Yvette Tran[1]

[1]*Soft Matter Sciences and Engineering, ESPCI Paris, PSL University, CNRS, Sorbonne Université,
75005 Paris, France*
[2]*Saint-Gobain Research Paris – Aubervilliers, France*
*Email: gabriel.mello@espci.psl.eu*

Silane Terminated Polymers (STPs) were developed to be used mainly in adhesives and sealants for construction. The STP molecule is composed of three different parts (Figure 1): an organic backbone, at least two coupling groups and at least two silane functions. The silane moieties are condensable alkoxy silane groups that can crosslink at room temperature upon contact with air moisture and a catalyst. This type of system provides health advantages for not containing noxious components like traditional polyurethane (PUR) adhesives. The objective of the project is to understand the adhesion mechanisms of such polymers on controlled glass surfaces. To do so, model polymers are synthesized with polyols, diisocyanates and silanes. The achievement and completion of the reaction (Figure 2) was assessed with Fourier Transform Infrared spectroscopy (FTIR-ATR).

Then, the adhesion of the STP polymer to glass was measured in 90° peeling tests. This apparatus allows us to capture the profile images of the peeling process (Figure 3), which can be used to calculate the polymer strain through the curvature of the backing[1].

Finally, the present work aims at investigating the composition at the interface along with the bonds that are formed between the polymer and substrate. The ability to detect and distinguish siloxane bonds in the polymer and at the interface is a particular challenge in this project.
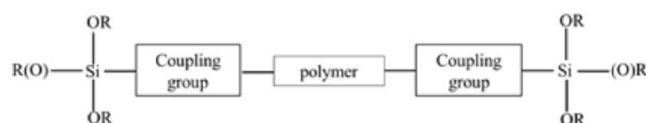


Figure 1: Basic structure of a silane terminated polymer.
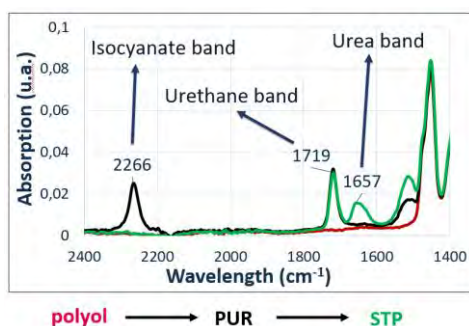


Figure 2: FTIR-ATR spectra of different steps in the STP synthesis.
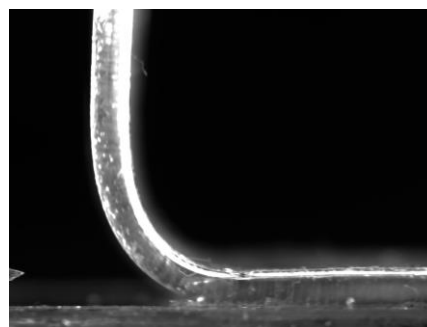


Figure 3: Profile image of peeling stripe.

## References

[1] Villey, R.; Cortet, P.-P.; Creton, C.; Ciccotti, M., Int J Fact **2017**, 204, 175-190.

# Using mechanophores to characterize damage in the sub-surface during wear of elastomers

Ombeline Taisne, Côme Thillaye du Boullay, Jean Comtet, Costantino Creton

*SIMM laboratory ESPCI Paris, France*

Tire wear due to friction is a major issue for tire manufacturers. Beyond economic aspects, increasing the lifetime of tires has an impact on road safety, use of resources and environmental pollution. It is therefore necessary to understand the mechanisms of tire wear. During wear by fatigue of tyre tread materials [1][2][3], the material at the surface of the tyre tread undergoes cycles of mechanical solicitation each time the wheel turns. These loads (in particular slippage at the road-tyre interface) induce progressive damage and structural modifications at the surface of the filled elastomer, leading ultimately to erosion through mass loss and wear.

However, a mechanistic understanding of elastomer wear by fatigue is still incomplete, due to the difficulty in accessing the local damage field at the surface of the material following mild frictional events. Here, we take advantage of recently developed mechanophore molecules to characterize molecular damage gradients in the sub-surface. Once chemically incorporated in known quantities in the elastomer network as crosslinkers, these molecules can be used to probe molecular scission events damaging the integrity of the network [5][6]. The activation of a fluorescent moiety upon covalent breakage of the molecule allows a 3D spatial characterization of the extent of chain breakage in the elastomer network, using confocal microscopy [5].

Specifically, we use this strategy to characterize and quantify the damage gradient at a molecular scale in multiple networks elastomers made of poly (ethyl acrylate). Confocal microscopy observations of the fluorescence of mechanophores after mild friction cycles against glass shows a localized damage under the surface of the elastomer and suggest a 2-step damage mechanism of damage accumulation in the sub-surface, followed by erosion of the material. Our observations shed new light on the underlying mechanisms of frictional wear in tough multiple network elastomers.
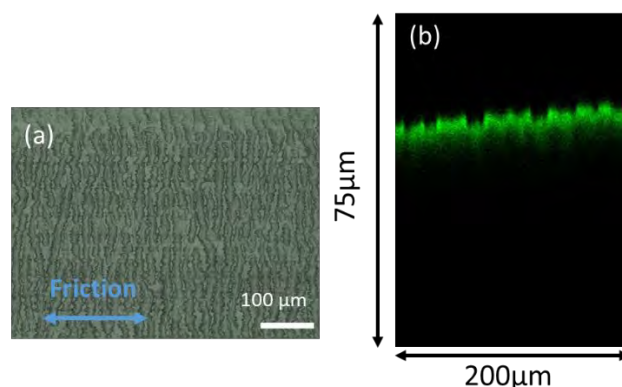


Figure 1 : Formation of wear ridges : (a) microscope picture of a triple network wear mark for FN=15mN after 1000 cycles (b) Cross-section picture reconstructed from a scan with the confocal microscope, on a triple network wear mark for FN = 21 mN and after 1000 cycles

## References

[1] D.F. Moore, *Wear*, 61 (2), 980, 273-282, **1980**
[2] G. Petitet et al., *Rubber Chemistry and Technology,* 78, (2), 312-320, **2005**
[3] A. Schallamach, *J. Appl. Polym. Sci*., 12, (2), 281–293, **1968**
[4] K.L. Johnson*, Contact Mechanics*, Cambridge University Press, **1985**
[5] J. Slootman et al., *Phys. Rev. X* 10, 041045, **2020**
[6] Y. Zhang et al, Macromol. *Rapid. Commun*., 2000359 **2020**

# Micromechanical characterisation of interphase and local matrix properties in a glass fibre-reinforced thermoplastic composite

S. F. Gayot[1,2], N. Klavzer[2], C. Bailly[1], T. Pardoen[2], P. Gérard[3] and B. Nysten[1]

[1]*Institute of Condensed Matter and Nanosciences, UCLouvain, Louvain-la-Neuve, Belgium,*
*sarah.gayot@uclouvain.be, christian.bailly@uclouvain.be, bernard.nysten@uclouvain.be*
[2]*Institute of Mechanics, Materials and Civil Engineering (IMMC), UCLouvain, Louvain-la-Neuve,*
*Belgium, nathan.klavzer@uclouvain.be, thomas.pardoen@uclouvain.be*
[3]*Groupement de Recherche de Lacq, Arkema, Lacq, France, pierre.gerard@arkema.com*

## Abstract

The recyclability of fibre-reinforced polymer composites can be improved by making use of thermoplastic instead of thermoset matrices. In this perspective, a range of methyl methacrylate (MMA)-based resins has recently been formulated to allow the production of long-fibre thermoplastic composites via liquid moulding techniques (e.g. vacuum infusion) followed by in-situ reactive polymerisation [1].

The failure mechanisms in thermoplastic composite specimens ultimately result from localised inter-fibre deformations at the micron scale, leading to large stress transfer to the fibres and interfaces, and finally damage. Numerical frameworks used to study the micro-scale stress and strain distributions in the matrix of thermoplastic composites generally assume that the material in the matrix pockets involves uniform constitutive properties equal to those measured on bulk samples of the same polymer. Yet, the thermochemical history and mechanical behaviour of the polymer matrix are strongly influenced by the presence of fibres and by the formation of a fibre-matrix interphase during in-situ polymerisation.

In this work, micro-scale mechanical analysis of a thermoplastic MMA-based composite matrix is performed on pseudo-unidirectional (UD) glass fibre reinforced composite samples. In particular, the thickness and mechanical behaviour of the interphase region are determined by atomic force microscopy (AFM). The mechanical properties of the matrix outside the interphase region are also measured by nanoindentation and AFM, as described in Fig. 1. The mechanical properties (e.g. stiffness) of the matrix in intra and inter-tow pockets are compared for different levels of physical ageing. Finally, transverse compression tests of UD specimens are performed in a scanning electron microscope, relying on digital image correlation to map the strain fields and localisation process in the matrix at the fibre scale.
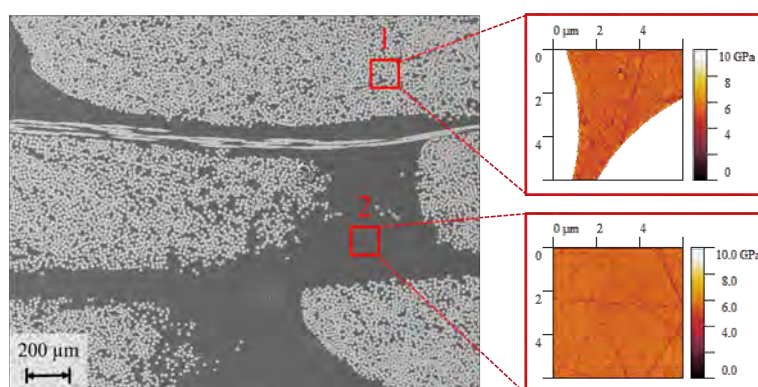
**Figure 1 -** Examples of AFM measurement locations for the local characterisation of Young's modulus in the composite matrix: (1) intra-tow vs. (2) inter-tow resin pockets.

## References

[1]  Gayot, S. F.; Bailly, C.; Pardoen, T.; Gérard, P.; Van Loock, F., *Materials & Design* **2020**, *196*, 109170.

# Multiscale characterisation of the spherulitic microstructure of iPP polymer by nanoindentation

Olga Smerdova, Jeremy Grondin, Sylvie Castagnet, Christophe Tromas

*Institut Pprime, CNRS, ISAE-ENSMA, Université de Poitiers, Futuroscope Chasseneuil F-86962, France*

Nanoindentation is a non-destructive experimental technique of choice when mechanical properties of a material need to be characterized at very small scale either because of the lack of material or due to the confinement of the material in a multiphase composite. However, the small scale mechanical response is highly dependent on the macromolecular organization when it comes to polymers. The state of the surface is another important factor that influences the result, since the test consists in a penetration of a hard indenter of a known shape into the polymer surface, and the properties are obtained through analytical contact models. Moreover, the methods of analysis usually used for nanoindentation data were developed for a homogeneous solid, so the properties obtained on a heterogeneous material are homogenized and dependent on the morphology of the tested volume.

In this work, we aim to test the nanoindentation response of a semi crystalline polymer with spherulitic microstructure at several scales with respect to the size of a spherulite and the size and local organization of crystal lamellae. The experiments were done on an isotactic polypropylene provided by GoodFellow in form of pellets. The samples were melted and recrystallized to form nice spherulites of several tens of microns in diameter. A particular care was taken to obtain surfaces as flat as possible. An X-ray diffractometry study revealed that the sample was mostly composed of the α phase, which gives spherulites with a cross-hatched lamella pattern between the branches. This morphology was confirmed by Atomic Force Microscope (AFM) measurements (see Fig.1), which also provided the topography of the spherulites at the nanoscopic scale. Finally, several nanoindentation grids with a size of imprint between hundreds of nanometers to dozens of microns in diameter were realized in quasi-static mode. The results were compared in terms of elastic modulus and hardness obtained by Oliver&Pharr method.
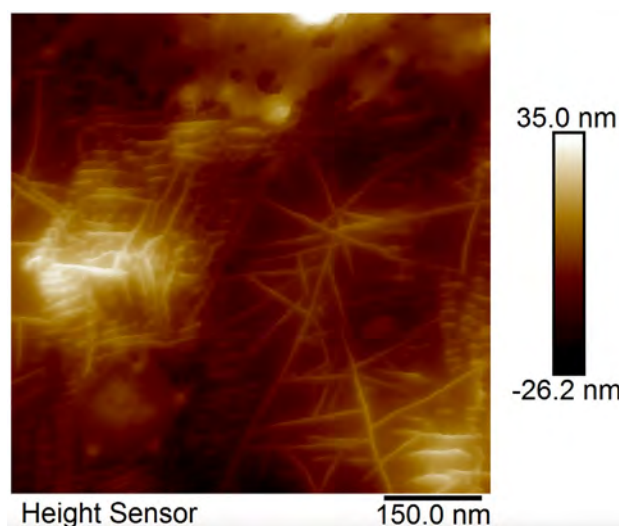


Fig 1. Typical topography of the α phase spherulite measured on the surface of iPP sample by AFM.

# Experimental investigation on the effect of beta transition temperature on the recovery of indentation prints on amorphous polymers

Marina Pecora, Candy Mitia Ramarosaona, Christian Gauthier

*Université de Strasbourg, CNRS, INSA Strasbourg, Institut Charles Sadron, F-67000 Strasbourg, France*

In this work, the effect of lateral chain mobility (enabled by beta transition) of an amorphous polymer (PMMA) on the recovery of indentation imprints has been experimentally investigated. The beta transition temperature, identified on tanδ *vs* temperature thermogram obtained through DMA compression tests at 0.2Hz, is of about 10°C. Indentation tests have been performed with a 250μm radius spherical tip and a three sided pyramid (Berkovich) tip on a load controlled micro indentation device allowing the *in-situ* observation of contact surfaces [1]. The indentations were performed at -40°C and 30°C, temperatures respectively lower and higher than beta transition. The load on spherical tip has been adjusted in order to lead a representative strain equivalent to that of the Berkovich tip ($\varepsilon \approx 7\%$). Loading phase was followed by a 100s creep and a 1000s recovery at the testing temperature in order to reach a steady state of the imprint geometry. Once the indentation imprints stabilised, the temperature in the chamber has been increased and the evolution of the residual imprints with temperature followed, thanks to an *in-situ* interferometric set-up. Figure 1 presents the recovery with increasing temperature of spherical (a) and Berkovich (b) indentation imprints performed at -40°C.
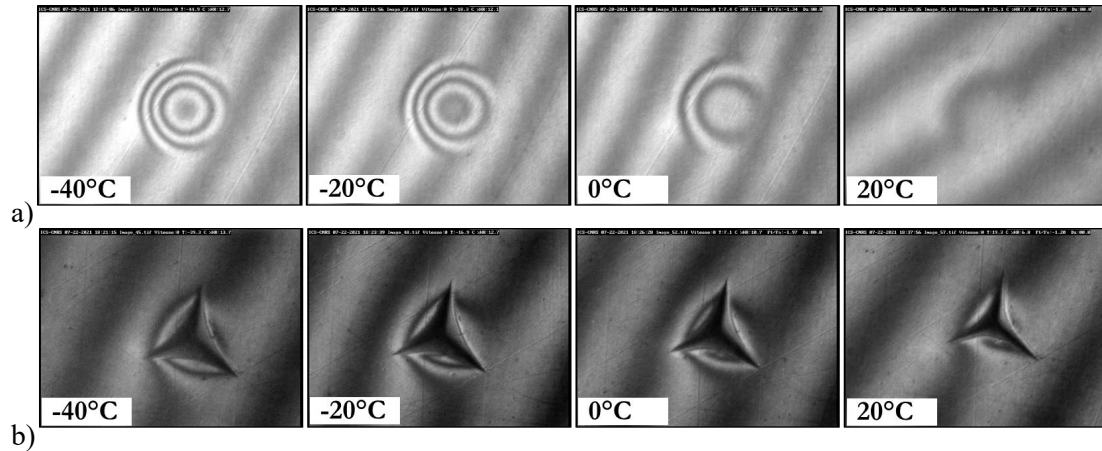


Figure 1. Recovery of spherical (a) and Berkovich (b) micro indentation prints with temperature

Figure 1a shows that crossing the beta transition peak enhanced chains mobility and thus allowed a complete recovery of the spherical impression. Contrariwise, because of the geometrical singularities of the sharp Berkovich tip, plastic deformations are induced and no complete recovery is therefore observed on Figure 1b: these geometric singularities slow down the recovery of the three faces of the imprint which bulge with recovery time. Current work of modelling will try to take into account nonlinear viscoelasticity at small and intermediate strains.

## References

[1] Chatel, T.; Gauthier, C.; Pelletier, H.; Le Houerou, V.; Favier, D.; Schirrer, R., *Journal of Physics D :Applied Physics* **2011**, *44*, 375403.

# Experiments and Numerics on the scratch behaviour of pre-oriented polycarbonate depicting a weak anisotropy in its plasticity behavior

M. Solar[1,3], M. Pecora[1,2], L. Stalter[1], A. Egele[1], D. Favier[1] and C. Gauthier[1,3]

[1] Institut Charles Sadron, 23 rue du Loess, 67200 Strasbourg (France)
[2] Université de Strasbourg, UFR de Physique, 3-5 Rue de l'Université, 67000 Strasbourg (France)
[3] INSA Strasbourg, 24 Boulevard de la Victoire, 67000 Strasbourg (France)
mathieu.solar@insa-strasbourg.fr, marina.pecora@ics-cnrs.unistra.fr

**Summary:** the scratch behaviour (i.e., plastic flow on the surroundings of the indenter) of Polycarbonate is investigated through experimental tests and numerical simulations. Anisotropic plasticity apparition has been obtained through tensile orientation. Numerical simulations of scratch have been calibrated on compression tests using Hill plasticity. Scratch tests have been performed on a device allowing *in-situ* recording of the true contact area.

## Introduction

From previous works performed in the laboratory [1][2], the basis for the experimental study and the analysis of the surface behaviour of different stretched semi-crystalline polymers was established. Scratch tests performed on thin films of polypropylene (iPP) and oriented High Density Polyethylene (HDPE), allowed *in-situ* observations of the frontal plastic bulges around the contact and, *post-mortem* lateral plastic bulges of the grooves (at the rear contact). These bulges present very often dissymmetry of geometry according to the direction of
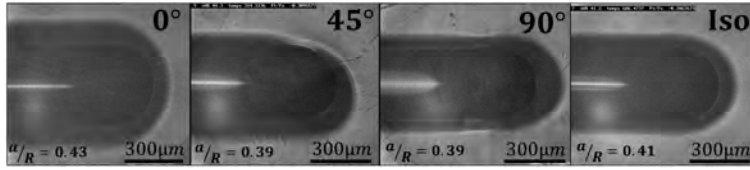


**Figure 1:** in-situ observations of scratch grooves for a normal force of 15N obtained on isotropic (λ=1) and anisotropic (λ=1.8) polycarbonate (PC) at different orientation angles with respect to the drawing direction.

scratching, with respect to the stretching direction. Furthermore, scratch tests on thin films can confine the material under the contact and, may disturb the yielding of polymers under and around the contact. Nevertheless, it is not possible to measure the compressive behaviour of thin films and, to implement this response (by inverse analysis) in a numerical scratch modelling. This work presents the first results on a thick solid polycarbonate sample, see Figure 1. PC was chosen for its ability to be stretched at room temperature and, its transparency for *in-situ* scratching observations on samples.

## Scratching experiments, plastic rheology and numerical simulations

The material used in this study is a commercial grade of Polycarbonate (PC). Anisotropic samples have been obtained through tensile orientation at a stretch ratio λ=1.8. Non-oriented isotropic reference samples (λ=1) have been tested as well.

### Compression tests

Compression tests have been performed on isotropic and anisotropic PC cylindrical samples (D=5mm; L=10mm) in order to evaluate the effect of pre-orientation on Young's modulus and yield stress. Anisotropic samples have been machined from stretched plates at different angles from the stretch direction: 0°, 30°, 45°, 60° and 90°. Three samples for each configuration have been tested at a strain rate of 0.004 s⁻¹. Nominal stress-strain curves, depicted in Figure 2, clearly show that pre-orientation induced anisotropy on plastic behaviour, namely yield stress and strain hardening. Nevertheless, the anisotropy on strain hardening will be neglected
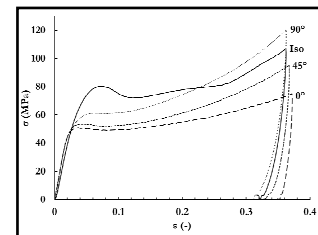


**Figure 2:** compression stress-strain curves for isotropic and anisotropic PC tested at 0°, 45° and 90° from stretching direction.

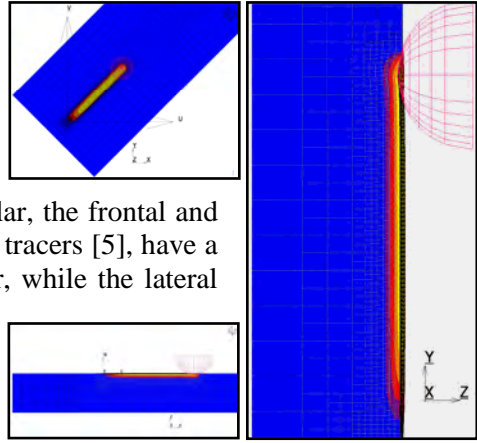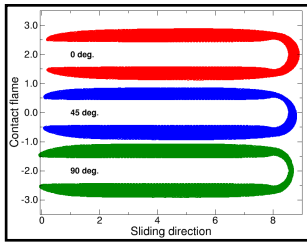as it occurs at higher strain level than the range covered by scratch tests (i.e., $\varepsilon_r \approx 0.2a/R \approx 4/50 \approx 8\%$). In that range, (0-15%) the material behaviour is approximated by an elastic-perfectly plastic law. The yield stress for each orientation angle was evaluated from the strain energy equivalence (up to 15% of strain). The elastic properties are, however, independent of orientation angle and no appreciable difference on Young's modulus (2.2 GPa) has been observed for pre-oriented samples. Moreover, the intrinsic softening due to physical ageing visible on stress-strain curve of non-oriented sample (named Iso), is no longer appreciable on oriented one, proving a rejuvenation of the material induced by stretching [3].



**Figure 3:** evolution of the contact radius "*a*" as a function of the normal force for isotropic and anisotropic PC sample scratched at different angles. The square root fitting function (continuous red line) is also reported.

## Scratch tests

Scratch tests have been performed on our device allowing to record *in-situ* the true contact area [4] with a 500μm radius spherical tip and an increasing normal load from 0.5N to 15N at different orientation with respect to the drawing direction: 0°, 45° and 90°. The *in-situ* images of the corresponding scratches with contact areas for a normal force of 15N are represented in Figure 1. The scratch obtained on an isotropic sample (λ=1) is reported as well. Figure 1 reveals that anisotropy affects the yielding around the sliding tip. In particular, the frontal and lateral plastic bulges, that are the plastic deformation tracers [5], have a different shape for each orientation angle. Moreover, while the lateral bulges of the groove are symmetrical with respect to the scratch axis for the scratch directions parallel and normal to the drawing direction, an asymmetry is observed on the scratch obtained at 45°. However, no appreciable effect of the anisotropy on the contact area has been remarked as it can be observed in Figure 3 in which, the evolution of the contact radius "*a*" in the plastic regime is plotted against the normal force for anisotropic and isotropic PC. This result can be explained by a physical rejuvenation of polymer surface induced by plasticity during scratching. A similar conclusion was drawn in work [6] in which, the effect of physical ageing on friction has been explored.



**Figure 5:** contact flames (i.e., transversal cuttings at z=0), where the reader may remark the dissymmetry of plastic flow in front and around the tip.



**Figure 6:** illustration of a scratch simulation tilted to 45 degrees, where local adaptivity refinement was used to refine meshing around the sliding tip. Direction X (resp. Y) corresponds to 0 degrees (lowest plasticity), whereas direction Y corresponds to 90 degrees (highest plasticity).
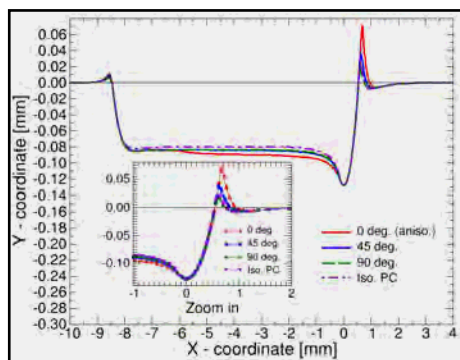


**Figure 4:** Hill's plasticity description [7] calibrated on compression experiments. Parameters: Yield Stress = 82 [MPa], Yrdir1 = 0.6226, Yrdir2 = 0.7313, Yrdir3 = 1, Yrshr1 = 0.5923, Yrshr2 = 1 and Yrshr3 = 1. Material parameters were calibrated on experimental compression tests (till 15% of deformation), that is: Young's modulus is E = 2.2 [GPa], Poisson ratio ν=0.35. The yield stress was calculated using the accumulated strain energy equivalence for specific orientation angles with respect to the pre-orientation direction.

## Numerics

Scratch test simulations have been performed using Marc/Mentat by MSC Software, using a spherical tip of radius 1.2 [mm], the local friction coefficient being set to $\mu_{loc} = 0.1$. The rheology implemented was elastic-perfectly plastic, using the Hill's flow rule to model anisotropy in plasticity apparition. Thus, the plastic behaviour of the pre-oriented PC is modelized in the (x;y) plane, whereas it was assumed that the plasticity in the z-direction remains identical to the threshold

observed for tests on non-preoriented PC (i.e., 82 MPa as a peak value indicating first plastic events on the compression curve). Results are illustrated in Figure 4 and, material constants for simulations are given as well. The details of the FEA analysis are not discussed here in details, but one used weak formulation of contact algorithms to allow the simulation to converge, since one took δ/R=0.107, so that $(a/R)_{th}=[1-(1-δ/R)^2]^{0.5}≈0.45$ (considering the plastic bulge, the real value should be approximatively equal). Some snapshots are given in Figure 6. Figure 5 illustrates contact flames (i.e., transversal cuttings at z=0): the reader may remark the dissymmetry of plastic flow in front and around the tip.

## Analysis of contact geometries and plastic behaviour around the sliding tip

Since the plastic yield surface does not obey von Mises criterion, the plastic flow around the indenter would be non-symmetric back and forth the sagittal plane (i.e., the plane lying on the sliding direction and cutting the tip in two identical half-spheres). Since there exist many possibilities to analyse the asphericity of stresses and strains in the surroundings of the moving tip, it was decided to observe evolutions of the total equivalent plastic strain (TEPS) first. This quantity is defined from the plastic strain tensor and, provides an indication of plastic yielding intensity, but also is a indicator to evaluate plastic zone, specially 90 region beneath the contact where plastic deformations set in.
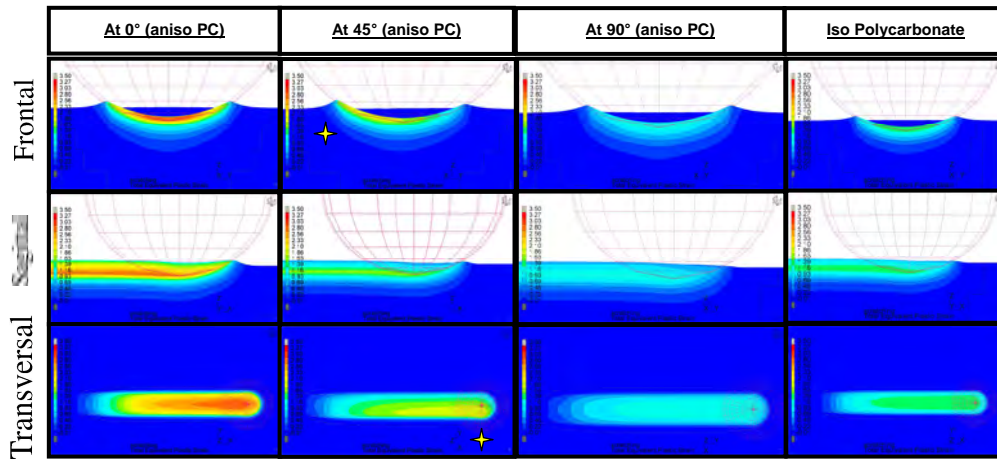


**Figure 7:** contour bands for the TEPS depicted in three fashions (frontal, sagittal and transversal cuts). The scale ranges from 0 to 3.5 for each snapshot. The reader may observe, that the plasticized volume is similar between all situations, but the peak intensity is stronger for the scratch at 0 degrees on anisotropic PC (for which the yield stress is the lowest one) and, that the spatial distribution of this same quantity is non-symmetric back and forth from the sagittal plane for the scratch at 45 degrees.

Figure 7 depicts contour bands for the TEPS in three fashions (frontal, sagittal and transversal cuts). The scale ranges from 0 to 3.5 for each snapshot. The reader may observe, that the plastic volume is similar between all situations, but the peak intensity is stronger for the scratch at 0 degrees on anisotropic PC (for which the yield stress is the lowest one). In addition, the spatial distribution of this same quantity is non-symmetric back and forth from the sagittal plane for the scratch at 45 degrees. To illustrate how the plastic flow sets in for all situations investigated, scratch profiles lying on the sagittal plane are shown in Figure 8. In this figure, it is evident that the plastic bulge is larger for the scratch at 0 degrees, since plastic events occurs more rapidly according to Figure 4. A similar conclusion for the scratch at 45 degrees may be drawn, in comparison to the scratch at 90 degrees and to the isotropic PC. For these two-last cases, the frontal plastic bulges are very similar. In order to further investigate the plasticity around the indenter considering frontal cuts observed during the contact process, see Figure 9. In this



**Figure 8:** scratch profiles lying on the sagittal plane (i.e., in the sliding direction), which cuts the indenter in two identical half spheres. The tip slides from the left to the right. All length units are in [mm]. The reader may observe (a), how the plastic bulge sets in at the frontal domain of the contact and (b), how the elastic recovery at the rear contact takes place. As usual all situations simulated are presented.

figure, it is magnified that the plastic bulge is more extensive for the scratch at 0 degrees but also, that the plastic bulge is non-symmetric from both sides of the contact. This last result is particularly interesting and, it is gratifying to notice that it matches with experimental *in-situ* observations of the contact and the groove. Furthermore if one looks at the TEPS resolved from the top of the tip to 0.5 [mm] apart and below from it, one remarks that plasticity is stronger for the scratch at 0 degrees. Nevertheless, the latter spreads on approximatively 0.32 [mm] for all situations investigated. Figure 10 confirms then these last conclusions, since it provides the magnitude of the TEPS from both sides of the indenter, still during the contact. Plasticity is still stronger for the scratch at 0 degrees, but scratches at 45 and 90 degrees surrounds the case for the isotropic polycarbonate, which is a quite surprising result. If the reader pays attention to this figure,



**Figure 9:** frontal cuts for all situations, to illustrate the non-symmetrical plastic bulges around the sliding tip. The reader may keep in mind that this frontal cut is performed just through the top of the tip: it is the so-called *agendo* contact (by opposition to *post-mortem* groove). All length units are in [mm]. On the right, the TEPS beneath the top of the indenter is given, sampled along the depth under this indenter.

he may observe that the TEPS is weakly non-symmetric apart (i.e., tilted to the left) from the vertical axis (still for the scratch at 45 degrees). Finally, we were also interested in the evolution of the TEPS from the front of the contact to the rear contact. The results are presented in Figure 11, where one observes the decrease of plastic deformations as the distance from the tip increases (in the region of rear contact). Furthermore, one remarks that master curves may be eventually extracted, as evolutions look similar when scaled to their respective maximum value.



**Figure 10:** TEPS from both sides of the indenter at 0.1926 [mm] below the free surface (but not from the top of the tip). One still considers the frontal plane for the contact. The small panel illustrates the same evolutions, but scaled to their maximum values: it illustrates that the spreading is very similar between all situations.

## Conclusion and outlooks

Numerical simulations of the scratch test on polycarbonate surface were achieved. The rheology was calibrated directly from experimental data and, the local friction was set to a value for low friction intensity on polymer surfaces. The plastic flow around the indenter and, the cartography of the Total Equivalent Plastic Strain (TEPS) under the contact were considered. The results for various scratching angles with respect to the pre-orientation direction were of study and, allow us to highlight the influence of this parameter on plastic spatial evolutions. We would like to address the influence of local friction magnitude and, to investigate stress / strain triaxiality ratio and plastic strain tensor sphericity under the contact, to build a mapping with respect to "macro" contact response.



**Figure 11:** TEPS in the sagittal plane at 0.1926 [mm] below the free surface (but not from the top of the tip). One distinguishes between the frontal and the rear contact. The small panel illustrates the same evolutions, but scaled to their maximum values. The reader may discern a master curve, expect for the scratch at 0 degrees.

## References

[1] Nan Yi, "Influence of the molecular orientation of HDPE by mechanical drawing on the surface mechanical behaviors" Phd 09 July 2019 Strasbourg University France.
[2] Pepin J.; Rubin A.; Favier D.; Gauthier C. "Influence of macromolecular orientation and environmental conditions on contact creep of semi-crystalline polymers surfaces", 11th International Conference on the Mechanics of Time Dependent Materials, MDTM 2018, sept 2018, Milan.
[3] Govaert, L. E.; Timmermans, P. H. M; Brekelmans, W. A. M, *Journal of Engineering Materials and Technology,* **2000**, *122*, 177-185.
[4] Gauthier, C.; Durier, A L.; Fond, C.; Schirrer, R., *Tribology International.* **2006**, 39, 88-98.
[5] Pelletier, H.; Gauthier, C.; Schirrer, R., *Journal of Materials research.* **2009**, *24*, 1169-1181.
[6] Charrault, E.; Gauthier, C.; Marie, P.; Schirrer, R., *Journal of Polymer Science: Part B: Polymer Physics.* **2008**, *46,* 1337-1347.
[7] Hill, R., *Proceedings of the Royal Society of London.* **1948**, *A193*, 281-297.
*Remark:* references [1] and [2] were funded by a DPI project between University of Strasbourg (FRANCE) and TU Eindhoven (The Netherlands), under the reference Project #783t **CONFINEd SURFACES,** COntact mechaNics, FrictIon and coNtact fatiguE on polymeric SURFACES.

# Replicating the material inhomogeneity effect of biological materials to increase the fracture toughness in polymers

Johannes Wiener[1], Florian Arbeiter[1], Otmar Kolednik[2], Gerald Pinter[1]

[1] *Materials Science and Testing of Polymers, Montanuniversitaet Leoben, 8700 Leoben, Austria*
[2] *Erich-Schmid-Institute of Materials Science, Austrian Academy of Science, 8700 Leoben, Austria*

Biological composites are often known for their outstanding toughness despite being composed of a seemingly brittle base material. In some cases, the fracture toughness is increased through mechanisms caused by a specific microstructure. A well-known example is nacre [1], where hexagonal platelets made of brittle aragonite are conjoined by thin layers of protein. The resulting brick-and-mortar structure causes crack deflection as well as an enlarged fracture area through platelet pull-out. In other examples, the right combination of hard and soft phase is enough to enhance the mechanical properties. Skeletons of deep-sea sponges are built in such a way [2]: The load bearing rods are composed of alternating, concentric rings of bio-glass and a ductile protein. In this structure, crack deflection and pull-out effects are not likely. Nonetheless, the material exhibits high toughness and excellent damage tolerance. Closer investigation reveals that growing cracks are stopped at the soft interlayers (IL), thus providing increased toughness and damage tolerance.

An explanation for this phenomenon can be found in elastic plastic fracture mechanics, where the crack driving force at the crack tip can be expressed as a local *J*-integral. However, the original definition of *J* by Rice [3] cannot be used for inhomogeneous bodies. An additional term has to be introduced in order to describe inhomogeneous materials [4]. This inhomogeneity term describes the influence of the IL on the crack driving force, which is caused by the difference in the stress-strain fields. As a result, the crack driving force is increased when a crack grows from a hard to a soft material (crack tip anti-shielding effect) and equally decreased by the transition from soft to hard (shielding effect). These phenomena are also called material inhomogeneity effect. Shielding and anti-shielding effect appear in conjunction at soft IL and lead to a minimum in crack driving force directly at the IL. The minimum causes growing cracks to be stopped at the soft IL due to the material inhomogeneity effect.

In this contribution, biological structures are mimicked using an IL of soft polypropylene within a brittle matrix of mineral reinforced polypropylene. The effects on fracture toughness are measured using the experimental *J*-integral, $J_{exp}$. Fracture mechanical experiments on single edge notch bending specimens are able to illustrate the benefits of soft IL for polymeric materials. On the one hand, $J_{exp}$ is increased significantly at the position of the IL. On the other hand, the damage mechanism is changed due to a crack arrest at the IL. Specimen failure progresses as slow crack growth at first, starting at the initial notch. The failure mode is then transformed to a bending fracture of the remaining ligament. After crack arrest the load must be increased until final fracture of the remaining ligament occurs. While a minimum IL thickness is required to achieve the inhomogeneity effect, further increases of thickness and numbers of ILs is not advisable. It is shown, that the increase in fracture toughness in such cases is negligible, while the specimen stiffness is unnecessarily reduced. Ongoing research focuses on exploiting these effects for industrial applications as well as offering guidelines on how to design effective layer architectures.

## References

[1] Barthelat, F.; Espinosa, H.D., *Exp. Mech.* **2007**, *47*, 311–324, doi:10.1007/s11340-007-9040-1.
[2] Aizenberg, J.; Weaver, J.C.; Thanawala, M.S.; Sundar, V.C.; Morse, D.E.; Fratzl, P., *Science* **2005**, *309*, 275–278, doi:10.1126/science.1112255.
[3] Rice, J.R., *J. Appl. Mech.* **1968**, *35*, 379, doi:10.1115/1.3601206.
[4] Sistaninia, M.; Kolednik, O., *Eng. Fract. Mech.* **2014**, *130*, 21–41, doi:10.1016/j.engfracmech.2014.02.026.

# Osmosis-driven deformation of non-vascular-plant-inspired soft composites

Amrita Kataruka[1], Alexandra Spitzer[2], and <u>Shelby Hutchens[2,3*]</u>

[1]*Dept. of Civil and Environmental Engineering, University of Illinois Urbana-Champaign*
[2]*Dept. of Material Science and Engineering, University of Illinois Urbana-Champaign*
[3]*Dept. of Mechanical Science and Engineering, University of Illinois Urbana-Champaign*
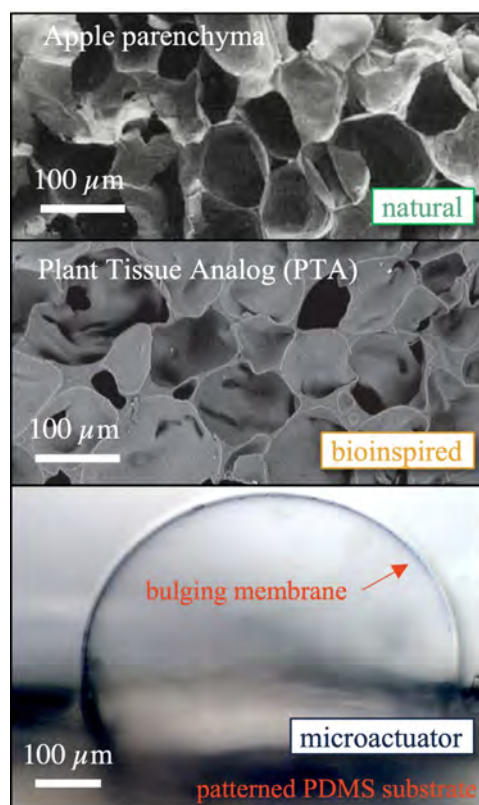[*]*email: hutchs@illinois.edu*

## Abstract

Even without the aid of muscle, plant tissue drives large, forceful motion via osmosis-driven fluid flow. In this work, we demonstrate that a synthetic, plant tissue analog (PTA) can mimic the closed-cell structure and osmotic actuation of non-vascular plant tissue (Figure 1), enabling the emergence of turgor-pressure-induced stiffness and leading to more forceful swelling deformations. We present data from two geometries. The first, are PTAs that consist of micron-sized saltwater droplets embedded within thin, highly stretchable, selectively-permeable polydimethylsiloxane PDMS walls. When immersed in water, these PTAs reach a state of equilibrium governed by the initial osmolyte concentration (higher produces more swelling) and cell wall mechanical response (stiffer and less stretchable yields less swelling). The second, are individual osmotic microactuators, which we leverage to understand the details of the material parameters that mediate to the time-dependent response of the more foam-like PTAs. Capturing the time-dependent response of these individual actuators provides estimates for PDMSs' permselectivity properties and for the improved performance of PEO-PDMS composites. Both structures represent an alternate class of aqueous, autonomous synthetic materials that, like hydrogels, may benefit biomedical applications.

**Figure 1.** Osmotically active soft composites. (top) and (middle) SEM images showing the similarity of non-vascular plant tissue and PTA microstructure. (bottom) A microscope image of an osmotic microactuator at equilibrium.

## Materials and Methods

To fabricate materials with closed pores having thin, selectively permeable walls and a readily varied inner phase, we recently developed an emulsion templating process that yields tightly packed, aqueous-filled, microcavity inclusions (>80% volume fraction) in an elastomeric matrix [1]. Individual osmotic actuator microwells are fabricated by adhering patterned PDMS and thin PDMS or PEO-PDMS films (Figure 1, bottom) in a saltwater environment. Both samples are placed in pure water and monitored over time until they reach equilibrium.

[1] Kataruka, A. and Hutchens, S. B., *Soft Matter* **2019**, 15, 9665–75.

# Polymeric materials and processes for the fabrication of Soft Dielectric Actuators

Ivan Raguž [a)], Mathias Fleisch [a)], Gerald Meier [a)], Sandra Schlögl [a)], Clemens Holzer[b)], Michael Berer[a)]

[a)] Polymer Competence Center Leoben GmbH, Roseggerstrasse 12, 8700 Leoben, Austria
e-mail: ivan.raguz@pccl.at
[b)] Department of Polymer Engineering and Science, Montanuniversitaet Leoben, Otto-Gloeckel Strasse 2, 8700 Leoben, Austria

Soft Dielectric Actuator (DEA) is a type of an actuator, where the movement is caused by high Columbo's forces, which are the consequence of the high electric field. The electric field is appearing in the insulator of the actuator. This insulator is located between two electrodes, which are connected to high voltage. The insulator is also called the membrane. The working principle of Dielectric Actuators is deeper described in [1].

Despite the fact that Soft Dielectric Actuators are already known, there is still a lot of space for improvements. The technical characteristics, such as actuation displacement and actuation force were not sufficient for real practical use of DEA. These facts were an inspiration for this work.

The important task of our work is also to find proper dielectric materials and as well as to find proper electrode materials. Looking for the proper materials is not an easy task, since the materials sometimes need to have contradictory properties, like high filler content for good electrical conductivity and simultaneously a low stiffness. The requirements for an electrode materials are listed in [2].
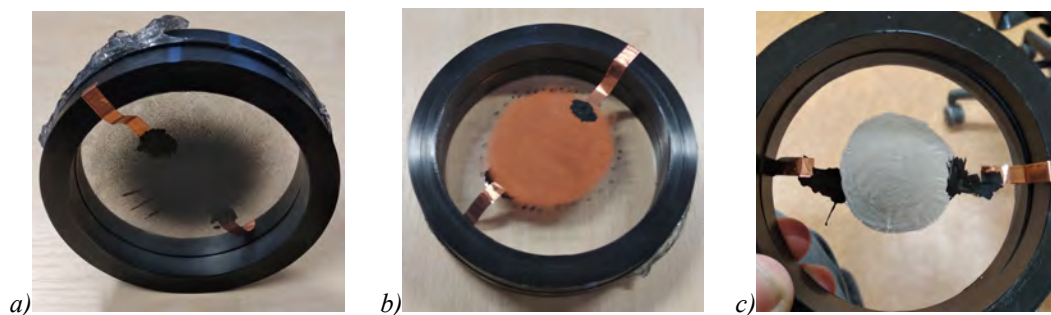


*Figure 1. Testing different electrode materials: a) carbon powder; b) copper powder; c) silver paint*

Figure 1. shows different electrode materials during testing. As already mentioned, some materials have good electrical conductivity, while other have low stiffness. Since these two properties are often contradictory, the focus of this work is also based on finding a good compromise, which will make possible the improved fabrication of DEAs.

## References

[1] R. Pelrine, R. Kornbluh, G. Kofod, High-Strain Actuator Materials Based on Dielectric Elastomers, Adv. Mater. 12 (2000) 1223–1225. https://doi.org/10.1002/1521-4095(200008)12:16<1223:AID-ADMA1223>3.0.CO;2-2.
[2] S. Rosset, H.R. Shea, Flexible and stretchable electrodes for dielectric elastomer actuators, Appl. Phys. A 110 (2013) 281–307. https://doi.org/10.1007/s00339-012-7402-8.

# Experimental fracture analysis of oriented polyethylene films using digital image correlation and full-field mechanics post-processing

Jevan Furmanski[1,2] and Jorgen Bergstrom[3]

*[1] Air Force Research Laboratory, Wright Patterson Air Force Base, OH, USA*
*[2] University of Dayton Research Institute, Dayton, OH, USA*
*[3] PolymerFEM LLC, Dover, MA, USA*

The tearing resistance of blown polyethylene films is one of their most important performance characteristics, and yet remains one of the least understood. Experimental approaches to calculating fracture driving force (J-integral) and crack growth resistance curves are available [1], but these lack detail about the mechanics in the fracture process zone. Finite element (FE) simulations of tearing can be conducted with a suitably complex and calibrated constitutive model, but these are prone to model error and numerical instability, especially for anisotropic, semi-crystalline strain-hardening polymeric materials. Further, FE simulation of tearing also requires the *a priori* imposition of a local material failure law, which tends to be empirical, and the parameterization of which is better served as an outcome of rather than an input to fracture analysis. The present work concerns the development of a new approach to measuring tearing resistance *in-situ* while also quantifying the material mechanics underlying tearing for polymer films with a complex deformation response.

Digital image correlation (DIC) was used to obtain the strain field during planar tearing of linear-low density polyethylene (LLDPE) blown films with either a high or low extent of locked-in processing-induced microstructural pre-orientation. The homogeneous deformation response of the films was calibrated to a fully-anisotropic, hyperelastic-viscoplastic 3D constitutive model with the PolyUMod material model library (PolymerFEM, [2]). The stress tensor and energy density fields were then calculated from the time-resolved deformation gradient history by running the PolyUMod engine at each material point from the DIC result. J-integral was computed at each time point for an integral contour in the far-field region of the specimen. Crack advance was measured in the reference configuration, and used to compute the crack growth resistance curve. The analysis flow appears in Figure 1.

Crack growth resistance curves revealed that the initial tearing resistance of the highly-oriented (HO) film was approximately an order of magnitude greater than the low-orientation (LO) film, while its tearing resistance for large tearing was about twice that of the LO film. A transition from blunted tearing to complete crack arrest was also captured some cases for the HO film. High-resolution mapping of the stress at the crack tip revealed a focused fracture process zone (FPZ) in the HO film, while a reduced intensity focused stress field embedded within a Dugdale plastic zone was observed for the LO film. Material reorientation from crack blunting and extreme anisotropy are thought to enable crack arrest.

The present work computed the crack growth resistance and fracture process zone mechanics in situ during tearing for a highly constitutive response, without recourse to FE simulation. Ongoing work is exploring the thermodynamic fracture driving force for a rigorous accounting of the energy consumed at the crack tip and globally in the structure [3].
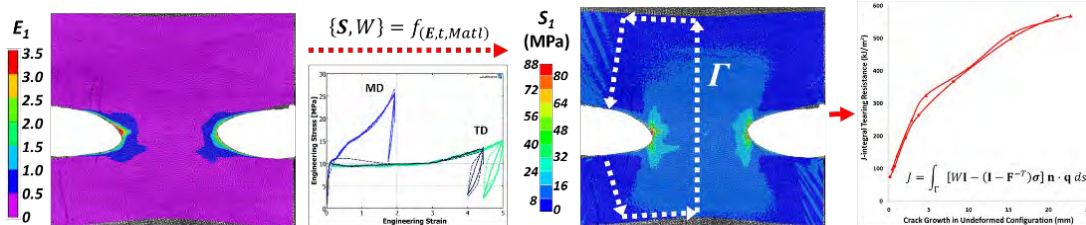


Figure 1. DIC strain fields during planar tearing are converted to stress and energy density fields via a point-wise incremental calculation via an advanced 3D constitutive model. The resulting fields are then operated on to calculate the J-integral and crack growth resistance curve.

## References

[1] Tielking, JT, *Polymer Testing* **1993**, *12*
[2] Bergstrom, JS *Mechanics of Solid Polymers: Theory and Computational Modeling. Elsevier* **2015**
[3] Kolednik, O, Schoengrundner, R, Fischer, FD, *Int J Fracture* **2014**, *187*

# Glass reinforced plastic pipelines: are they durable or not?

Soheyl Khajehpour-Tadavani[1*], Fatemeh Nikpour[1], Amanda L. T. Brandão[2]

[1]*Faculty of Engineering, Department of Polymerization Engineering, Iran Polymer and Petrochemical Institute, Tehran, Iran (E-Mail: s.khajehpour@ippi.ac.ir)*
[2]*Chemical and Materials Engineering Department, Pontifical Catholic University of Rio de Janeiro, Rio de Janeiro, Brazil*
*Senior Engineer of the Process Department, Zagros Petrochemical Company, Bushehr Province, Asalouyeh Port, Iran*

## Abstract:

Glass Reinforced Plastic (GRP) pipes are widely used for water transmission due to their light weight, high strength, and corrosion resistant characteristics. These composite materials are exploiting in the gas and oil industries for transporting sea cooling water.[1] Moreover, their unique corrosion resistant characteristic provides a longer lifetime rather than carbon steel pipelines. [2] There are various categories of requirements in the pipe systems which the most prominent of them are mechanical stability, serviceability, environment, and durability. Nevertheless, in relation with the failure analysis, one may define the failure event as the phenomenon in which one or several of such requirements are no longer fulfilled. Failure of pipelines especially GRP pipes may have some causes in a probabilistic medium in which they have known as types of failure. Furthermore, ageing of the polymeric and composite materials is defined as the irreversible physical or also chemical changes in the material and the material system. There are lots of factors which they influence on the ageing of polymers and composites such as GRP buried pipelines. Underground GRP pipelines are the most favourable pipes for conveying sea cooling water to the petrochemical plants. They could transfer high pressure cooling water to the plants in the long-term behaviour which is crucial for many practical purposes in the petrochemical industry. [3] However, they could be disposed toward fracture in combination with ageing and failure modes. Not only static and dynamic loadings in the short- and long-term performance could impose them lots of stress, but also thermal condition in the hot and humid regions is another main reason which could force GRP pipelines in the deterioration condition. Throttling action on the main block valves of the sea cooling water heat exchangers for tuning cooling water flow that could be attained a better performance in the long hot season is a suitable and convenient idea. Nevertheless, whenever GRP header pipelines are under block valves throttling situation, it could lead these composite materials to put under lots of stress and finally fracture takes place. Hence, using glass flake epoxy coating which is a protective layer in the inner side of carbon steel pipelines may be an appropriate solution for separating from failure and fracture. This polymeric strategy increases the short- and long-term efficiency of the sea cooling water pipeline headers. It seems in comparison with the GRP pipelines, glass flake epoxy coating lines are more durable and could tolerate much more stress under block valves throttling condition at the hot and humid regions. Current work proposes a literature review of the GRP pipelines and their glass flake epoxy alternatives.

## References

[1] Rafiee, R., *Composites Part B: Engineering* **2013,** 45.1, 257–267.
[2] Thomas, N.; Sajimol, G.; George, S., *AJAME* **2014**, 4, 435-440.
[3] Farshad, M. *Plastic Pipe Systems: Failure Investigation and Diagnosis,* 1st ed; Elsevier: UK, 2011; Vol. 1, p 12-35.

# Fibre induced crystallisation in elongational flows

Paul M.H. van Heugten; Stan F.S.P. Looijmans;
Lambèrt C.A. van Breemen; Patrick D. Anderson

*Eindhoven university of technology, p.m.h.v.heugten@student.tue.nl*

Polymers can be reinforced with fibres to improve mechanical properties. Nowadays, the crystallisation of thermoplastics around fibres in elongational flow conditions is still underexposed. The developed microstructure can be related to the mechanical and physical properties of the product, such as modulus or strength. [1] Isotactic polypropylene (iPP) is studied, which is commonly reinforced with fibres and extruded into tapes. During the process of producing polymer composite tapes, a strong elongational flow is experienced by the material between the slit-die and the water-cooled roller, where it is collected. The molecular orientation, which develops when undergoing these uniaxial conditions, are frozen-in when the material is cooled down. [2,3] In this study, the morphology and kinetics of the polymer matrix around a single fibre are characterised via in- and ex-situ X-ray experiments. A uniaxial extensional flow is applied using an in-house built filament stretching extensional rheometer (FiSER), which design allows for in-situ experiments. [4]
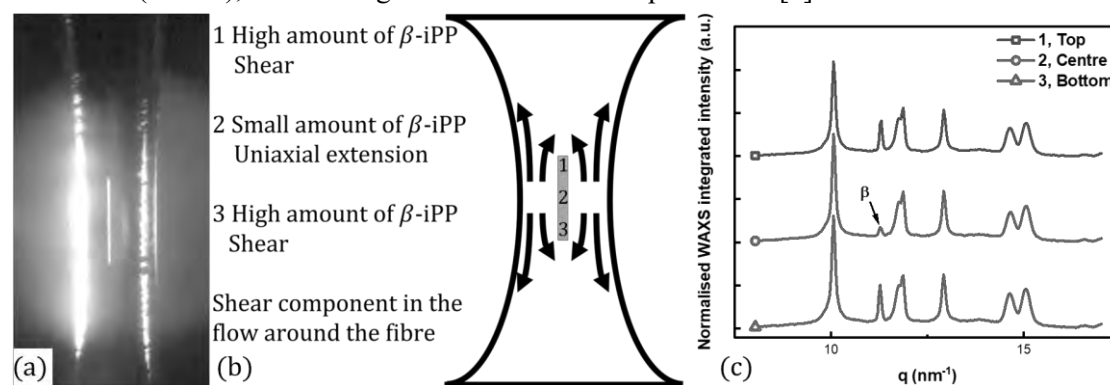


**Figure 1 (a) Photo of a single glass fibre after stretching the filament. (b) Schematic representation of the flow around a single fibre in a stretched filament. (c) Ex-situ WAXS pattern at 3 different positions around the fibre.**

In Figure 1a, it is shown that the glass fibre remains in the centre of the filament during stretching. The flow field, displayed in Figure 1b, relates the development of β-iPP to the position along with the fibre. The shear contribution increases and therefore the alignment of α-iPP enlarges when moving from the centre to the tip of the fibre. Aligned α-iPP is essential for the nucleation of β-iPP and hence the number of β-crystals also increases moving to the tip of the fibre as visible in Figure 1c. α- and β-iPP differ in their mechanical response. Figure 2 shows that β-iPP has a less pronounced contribution to strain softening and a higher amount of strain hardening. Consequently, the mechanical properties vary along the fibre resulting in more stabilisation of strain localisation towards the tip.
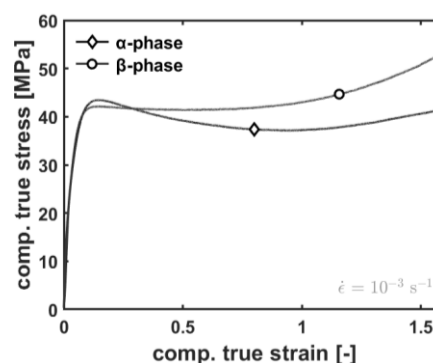


**Figure 2 Comparison of the intrinsic deformation behaviour between α- and β-iPP.**

## References

[1]   Koscher, E.; Fulchiron, R., *Polymer* **2002**, 43, 6391-6942.
[2]   Hisham, A. M., *American Journal of Polymer Science* **2016**, 6, 1-11.
[3]   Philips, K. J.; Ghosh, T. K., *Textile Progress* **2003**, 33, 1-53.
[4]   Pepe, J.; Cleven, L. C.; Suijkerbuijk, E. J.; Dekkers, E. C.; Hermida-Merino, D.; Cardinaels, R.; Peters, G. W.; Anderson, P. D., *Review of Scientific Instruments* **2020**, 91, 073903.

# Material model fitness evaluation using full-field digital image correlation measurements based on equilibrium gap indicator and reconstructed axial force

A. Peshave[1], F. Pierron[2], P. Lava[2], D. Moens[1], D. Vandepitte[1]

[1]Department of Mechanical Engineering, LMSD group, KU Leuven, 3001 Belgium
[2]MatchID NV, 9000 Ghent, Belgium

Mechanical design methodologies can significantly benefit from an accurate material characterisation. Conventional material identification techniques normally rely on a test sample under a simple state of stress, often requiring multiple tests in order to activate all the parameters driving the material behaviour. Recent developments in the field of digital cameras have brought full-field measurement techniques such as digital image correlation (DIC) to the forefront. DIC can measure full-field displacements (from which strains and stresses can be calculated) meaning that the test data set is information rich and can handle complex states of stress. This makes it possible to identify multiple material model parameters based on a single test using inverse identification techniques such as the virtual fields method (VFM) (1). The advantage of the VFM is that it does not require the knowledge of accurate boundary conditions and relies solely on the total applied load. If the material model is not known *a priori*, it is necessary to fit different material models to the same full field data and evaluate their fitness. In this work, the authors propose a methodology to do just this based on full field stresses calculated using DIC strain field and an assumed material model. A uniaxial tensile test on a double notched test sample made of high density polyethylene (HDPE) is used as a test case. The VFM is used to identify material parameters corresponding to the following hyperelastic material models: Neo-Hookean, two parameter Mooney-Rivlin and Yeoh. Two metrics are used to evaluate the material model fitness: reconstructed axial force ratio (RAFR) and equilibrium gap indicator (EGI). In the existing literature, EGI has been used for detection of material heterogeneity (2) and damage (3) in case of transverse bending. We adapt this concept to in-plane (membrane) situations. EGI evaluates the static admissibility of stresses by calculating equilibrium of different stress components in a small window. The EGI window can be swept over the entire measured domain in order to generate EGI maps. Ideally, EGI should be zero all over the measured domain. EGI is very sensitive to discrepancies such as damage, material heterogeneity, inaccurate material model, inaccurate material model parameters etc. The axial stress at each cross section along the length of the test specimen can be integrated over the width to calculate the total axial force ($F_c$) acting at that cross section. This can be compared to the actual total force ($F_a$) known from the loadcell of the tensile test bench. RAFR is then defined as the ratio $\frac{F_c}{F_a}$. RAFR should ideally be equal to 1 and constant over the length of the test specimen. Based on the RAFR metric, the hyperelastic material models are found to fail at capturing the material behaviour at low strain levels. At moderately high strains, Yeoh material model is found to be superior in terms of both metrics. In order to further improve material model behaviour, piecewise linear elastic and hyperelastic material model is implemented. The transition between the two behaviours is defined in terms of the von Mises stress. An additional parameter needs to be identified, corresponding to the von Mises stress threshold defining the transition between linear elasticity and hyperelasticity. The piecewise hyperelastic material models (linear elastic – Neo-Hookean, linear elastic – Mooney-Rivlin, linear elastic - Yeoh) are found to generally outperform their pure hyperelastic counterparts in terms of both metrics, except in the vicinity of the transition phase between the two behaviours. This means that an improvement in the way linear elastic – hyperelastic threshold is formulated is needed. This improvement is envisioned in the future scope for this work.

## References

1. **Pierron, F and Grédiac, M.** *The Virtual Fields Method.* s.l. : Springer, 2012.

2. *Smoothly varying in-plane stiffness heterogeneity evaluated under uniaxial tensile stress.* **Considine, JM, et al.** 2017, Strain, Vol. 53.

3. *Impact damage detection in composite plates using deflectometry.* **Devivier, C, Pierron, F and Wisnom, MR.** 2013, Composites Part A: Applied Science and Manufacturing, Vol. 48, pp. 201-218.

# List of (referenced) authors